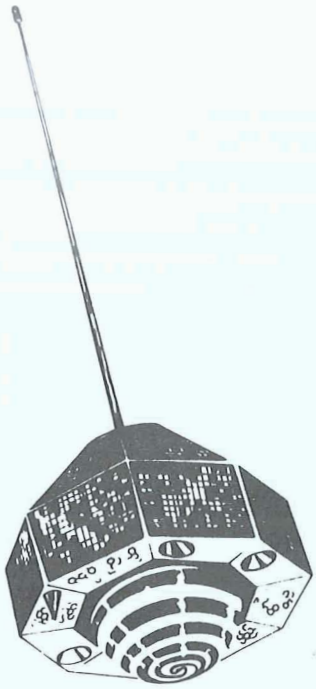

NOVEMBER 1970

PROCEEDINGS OF THE GEOS-2 PROGRAM REVIEW MEETING 22-24 JUNE 1970

VOLUME IV

GENERAL

EDITED BY:

CSC

COMPUTER SCIENCES CORPORATION

6565 ARLINGTON BOULEVARD POST OFFICE BOX [illegible] FALLS CHURCH VA [illegible]

NATIONAL AERONAUTICS AND SPACE ADMINISTRATION

NASA

PROCEEDINGS OF THE GEOS-2 PROGRAM REVIEW MEETING

22-24 June 1970
NASA Goddard Space Flight Center
Greenbelt, Maryland

Volume IV

GENERAL

Edited by Computer Sciences Corporation
6565 Arlington Boulevard, Falls Church, Virginia

November 1970

TABLE OF CONTENTS

TABLE OF CONTENTS (Continued)

FOREWORD

This volume contains a number of papers of general interest to the geodetic program as well as a series of papers relating to GEOS-C. This satellite will be the third active satellite in the National Geodetic Satellite Program and is planned for a launch in calendar year 1973.

The general interest papers are presented in Section I of this volume and those relating to GEOS-C are presented in Section II.

SECTION I

General

Perturbation of GEOS-1 Orbit by Solar Radiation Pressure

L. Wong
R. Prislin

Aerospace Corporation
El Segundo, California

June 15, 1970

Prepared for

National Aeronautics and Space Administration

Perturbation of the GEOS-I Orbit by Solar Radiation Pressure

The geometry of solar illumination on the GEOS-I orbit for January 2, 1966 is illustrated in figures 1a, b, and c. For this date the pertinent parameters for calculating the perturbations due to radiation pressure are given in table 1.

Table 1 Eclipse Elements

GEOS Elements	Equatorial	Ecliptic
semi-major axis (a)	= 8067 km	
eccentricity (e)	= .071	
inclination (i)	= 59.3°	39.6°
ascending node (Ω)	= 332°	-39°
argument of perigee (ω)	= 187°	204°
Position of Sun		
right ascension (α)	= -78°	
obliquity of ecliptic (ϵ)	= 23.4°	
longitude (λ)	= -85°	
Angles (refer to figure 1)		
a_1 = 46°	$\beta \triangleq \widehat{JQ}$ = 243°	
a_2 = 27°		
a_3 = 39°		

	at entrance into shadow	at exit from shadow
ecliptic longitude	105.4°	195.9°
true anomaly (θ)	-104.6°	.3°
$\odot + \theta$	138.4°	243.3°

Radiation pressure produces both periodic and secular perturbations on the GEOS orbit. In figure 1c, the solid arc over which the element of work, $dW = F \cdot ds$, is positive exceeds the dashed part over which dW is negative. Hence energy is added to the orbit and there is a net change in the semi-major axis, a. The rate of change of a is given by Moulton (1914)

$$\frac{da}{dt} = \frac{P}{\pi\sqrt{1-e^2}}[e \sin\theta\, R + (1+e\cos\theta)\, S]$$

where P is the period, R and S are respectively the accelerations along and perpendicular to the radius in the orbit plane, e is the eccentricity, and θ the true anomaly. Wyatt (1963) has shown that the change in period is given by

$$\frac{\Delta P}{P} = 1.40 \times 10^{-7} D_s K^2 \frac{(1+e)}{(1-e)} \sin i' \left[\frac{\cos(\beta+\theta)}{1+e\cos\theta}\right]_{\theta_{enter}}^{\theta_{exit}} \quad (1)$$

where for the GEOS satellite:

D_S = area/mass = 1.23 m^2/175kg = .07 cm^2/gm

K = a(1-e)/earth radius = 1.17, K^2 = 1.38

(1+e)/(1-e) = 1.15

sin i' = sin $(90-a_2)$ = .89

$$\left[\frac{\cos(\beta+\theta)}{1+e\cos\theta}\right]_{\theta_{enter}}^{\theta_{exit}} = .34$$

Substituting into (1) results in the dimensionless ratio

$$\frac{\Delta P}{P} = 1.4 \times 10^{-7} (.07) \cdot 1.38 (1.15) (.892) (.34) = 4.75 \times 10^{-9} \quad (2)$$

Comparison with Numerical Integration

Figure 2 shows the perturbations inthe osculating semi-major axis obtained by numerically integrating the variational equations (for $\gamma = 10^{-8}$, dimensionless)

$$\ddot{\Delta\vec{r}} = \gamma g \vec{e} + \Delta\vec{G}; \quad \gamma = \frac{C_p \cdot D_S}{g} \tag{3}$$

where $\vec{G}$ is the graviational acceleration and $\vec{e}$ is a unit vector away from the sun, C_p the radiation pressure constant at the earth, and g the conversion factor from mass to weight. A large periodic oscillation superimposed on a much smaller secular change of .036 meters per revolution is observed. The secular change in period is

$$\frac{\delta P}{P} = \frac{3}{2} \frac{\delta a}{a} = 1.5\ (.042\text{m})/8 \times 10^6 \simeq 7.9 \times 10^{-9} \tag{4}$$

The value of γ corresponding to $D_S = .07\ \text{cm}^2/\text{gm}$ is 5.8×10^{-9} and not 10^{-8} as had been assumed in the integration of equation (3). Taking .58 times the right side of (4) gives the value from numerical integration

$$\frac{\delta P}{P} = .58 \times 7.9 \times 10^{-9} = 4.6 \times 10^{-9} \qquad (5)$$

which should be compared with the result of equation (2).

As a further comparison, the along track perturbation, η, from numerical integration (again with $\gamma = 10^{-8}$) for the last 3 revolutions of a 6-day interval is shown in figure 3. The secular change over one period is seen to be approximately 26 meters/revolution. From (4) the expected change is

$$\Delta\eta = N\frac{dP}{dN} v$$

where N is the total number of revolutions in 6 days, v is the orbital velocity. Using v = 6600 m/sec, N = 70, and $\frac{dP}{dN} = 7.9 \times 10^{-9}$ (7200 sec) one obtains $\Delta\eta \simeq 26.3$ meters/rev which agrees rather well with the graphical results.

Conclusions

It appears that the perturbation calculation agrees with the numerical integration to within 5 or 10 percent which is quite good. It is interesting that the periodic effects on the major axis are much larger than the secular effects per revolution.

GEOMETRY OF SOLAR ILLUMINATION FOR GEOS-I

JAN 2, 1966

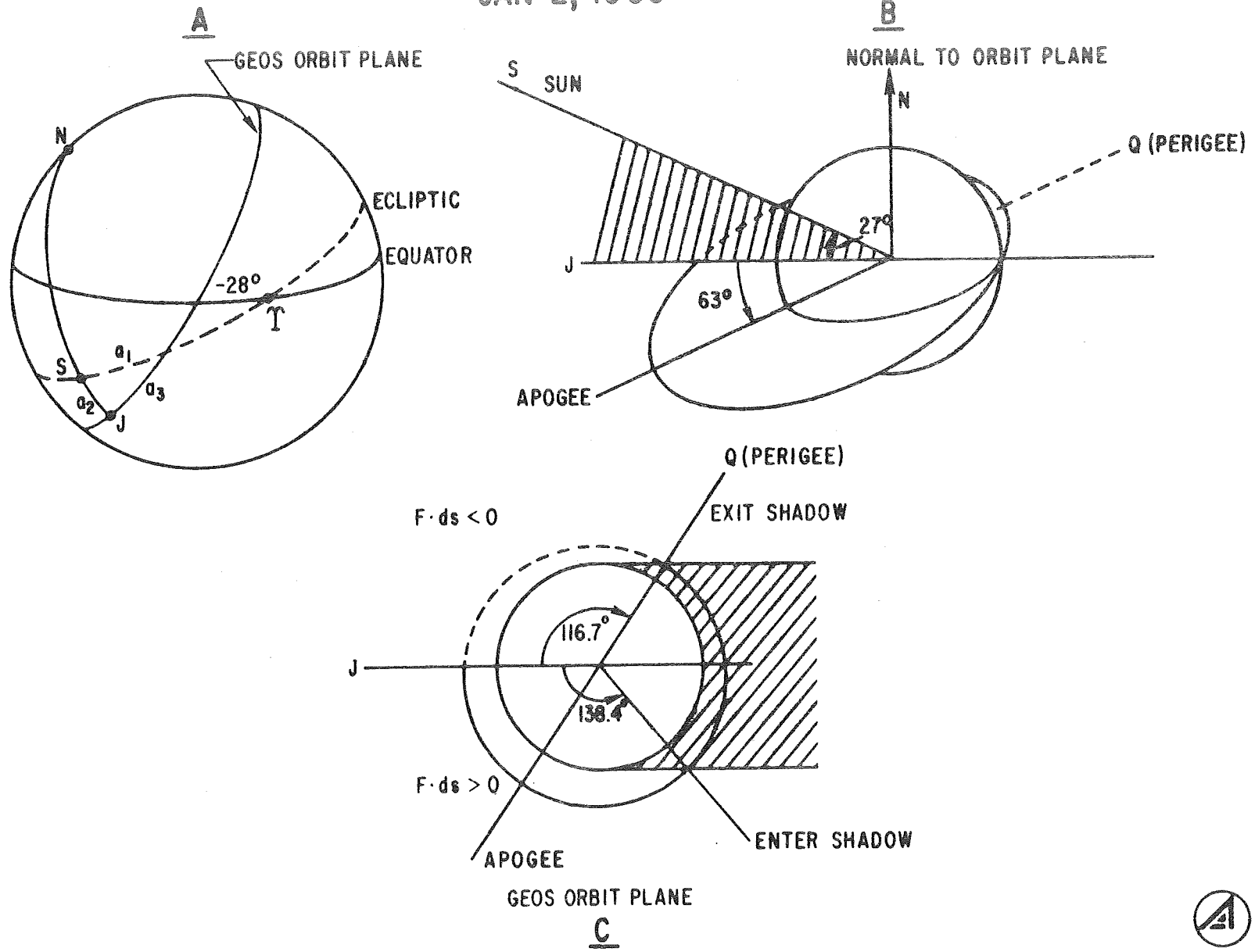

Figure 1

PERTURBATIONS IN SEMI MAJOR AXIS FOR $\gamma = 10^{-8}$

$0 < t < 360$ min

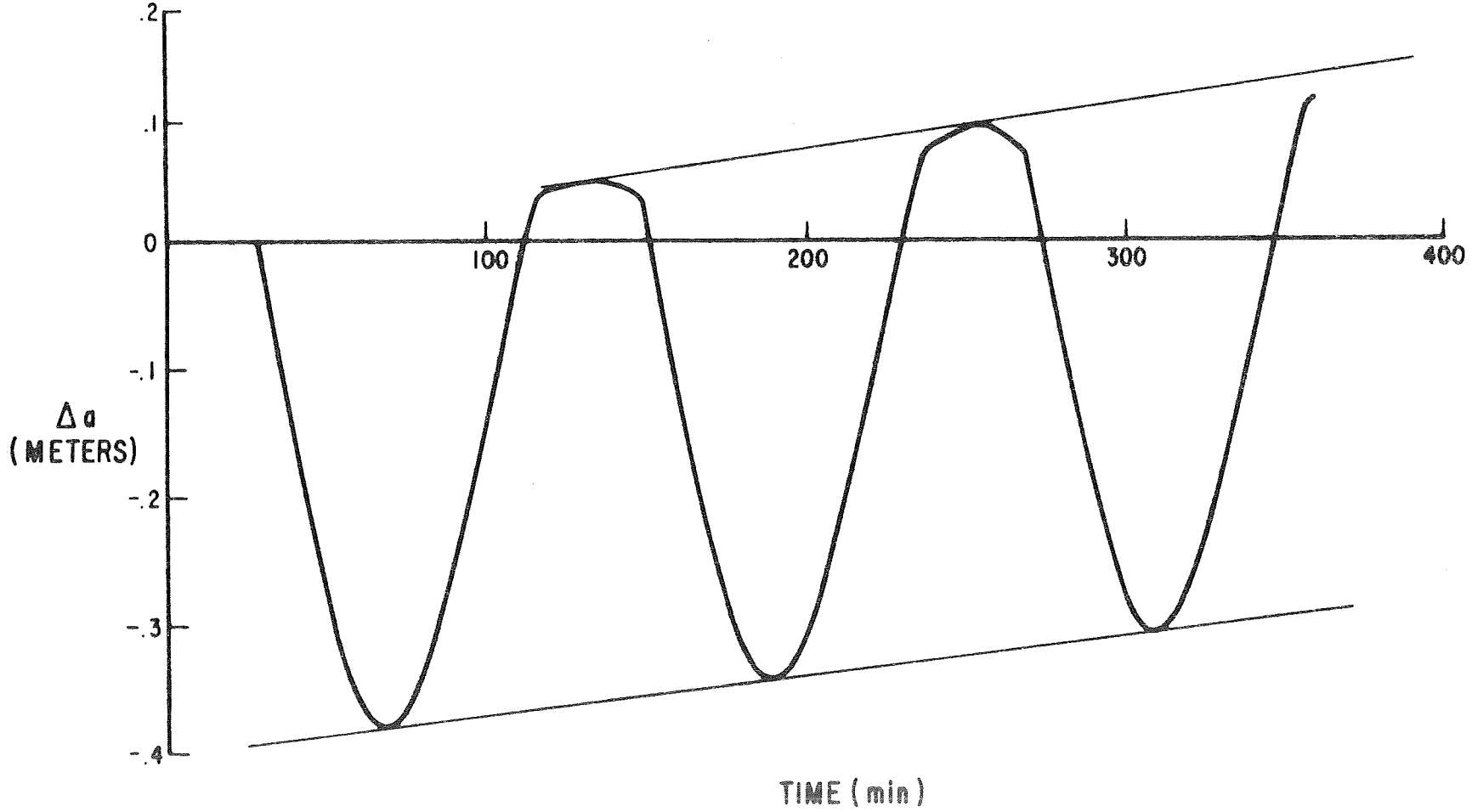

Figure 2

INTRACK PERTURBATIONS FOR $\gamma = 10^{-8}$

$8280 < t < 8640$ minutes

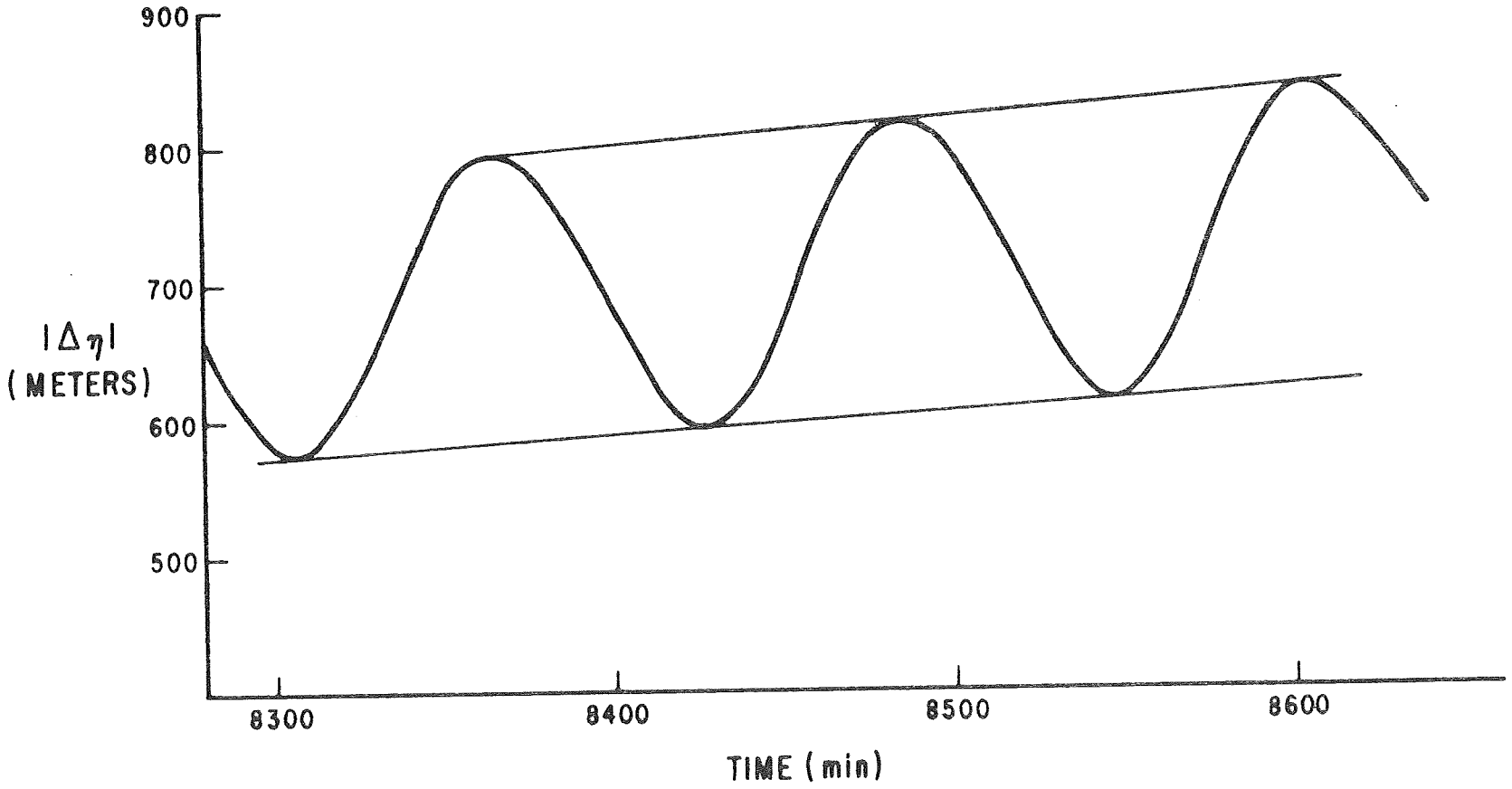

Figure 3

The Orbit of Pageos through March 1970

B. Chovitz
J. Lucas

ESSA - C&GS
Rockville, Maryland 20852

Presented to the GEOS-2 Review Conference, NASA Goddard Space Flight Center, Greenbelt, Maryland, June 22 - 24, 1970

The Orbit of Pageos through March 1970

B. Chovitz
J. Lucas

ESSA - C&GS

1. This study was motivated by the need for precise predictions for Pageos. Geodetically, Pageos has served as a target for concurrent observations by cameras placed at stations in the geometric worldwide satellite triangulation network. To point the cameras correctly, the stations require orbital predictions which, for logistical reasons, must be computed 14 to 21 days in advance. The difficult part of a prediction is the determination of the position of the satellite along its orbit--that is, the timing of the predictions. Because the Earth is rotating, an error of 1 minute in time moves a station by an arc of (15') $\cos\phi$, or about 10' of arc for a station at 45° latitude. On a photograph taken by a 450mm camera, this would cause the trail of the satellite to miss the center of the plate by 1.3 mm--a non-negligible amount. For this reason, it is important to obtain the time of the satellite's predicted position to within a few seconds. For a satellite like Geos this is a fairly trivial problem, but for a 100 ft. diameter balloon it is not.

The Keplerian element which is crucial in determining the prediction of the satellite's position is the semi-major axis, a. This study has therefore concentrated on this particular element. The history of a is, of course, equivalent to that of the period P, or the mean motion n, since they are constrained together by Kepler's third law. If this history can be explained satisfactorily by physical mechanisms, then twofold benefits will accrue: predictions can be made more accurate, and knowledge of the satellite's environment will be augmented.

2. Pageos was launched on June 24, 1966 in an almost circular orbit at an inclination of 87°. Its semi-major axis, starting at 10615 km, has reached a minimum of 10545 km and is currently (1 June 1970) 10558 km. A near zero initial eccentricity built up to about 0.2, and is now 0.14.

The chief influence on the semi-major axis of Pageos is direct solar radiation pressure (s.r.p.). If the satellite is sunlit during an entire revolution, the perturbation is short-periodic with no buildup--thus effectively zero. However, if the satellite is in the Earth's shadow part of the time, the perturbation will build up at a rate depending on the eccentricity, the orientation of the sun's rays to the orbital plane, and the assymmetry of perigee with respect to the shadow interval. Because of the regularity of change

of these conditions, the part-shadow and total-sunlit revolutions fall exclusively within well-defined intervals. Pageos was launched within an all-sunlit interval, and has gone through 9 complete cycles of all-sun and part-shadow. On June 3, 1970, it entered its 10th part-shadow interval.

The above remarks on the effect of direct solar radiation pressure on a hold under the assumptions that the solar force is constant, and acts on a surface whose characteristics do not change--in particular the cross-sectional area perpendicular to the sun's rays. It is now fairly well established [1] that Pageos has the form of a prolate ellipsoid which is not only rotating but wobbling as well.

3. Empirical determinations of the Pageos orbit have been performed weekly by the Coast and Geodetic Survey since December 1966, using optical observations provided by the SAO Baker-Nunn, C&GS BC-4, and the NASA MOTS cameras. These seven-day arcs are internally consistent to about 1 minute of arc topocentric, but in many instances adjacent arcs failed to meet. Therefore, it was necessary to readjust the available data in longer arcs using a more complicated empirical model.

The available tracking data consisted of 61,572 optical observations of the so-called "field-reduced" type covering the period from 16 July 1966 through 3 April 1970. Of these

29,822 were obtained by the NASA cameras, 16,834 came from SAO, and 14,916 from C&GS. These data were divided into tractable segments, 89 in all, covering time spans which varied from 15 to 35 days with at least seven days overlap between adjacent segments.

A differential orbit improvement program similar to that of SAO was used to obtain 25 polynomial parameters which describe the variations in the orbital elements ω, Ω, e, i, and M in order to obtain the best fit, in the least squares sense, to the tracking data. The mean motion n results from extracting the derivative of M, and the semi-major axis was then computed from Kozai's formula. Eight of the 25 parameters were allocated to M, this being the maximum number of parameters that the program will permit for any single element, so that the derived semi-major axis is expressed by a 6th degree polynomial in time. During intervals when the satellite was constantly in sunlight this representation was adequate to fit all observations over 35 day arcs, and longer arcs could probably have been used. Most of the part-shadow intervals were fitted in 21 day arcs, but the most recent shadow period, December 1969 to March 1970, showed such an increased frequency of variations in a that 15 day arcs had to be employed. The

mean of the standard deviations of all fits was 95 seconds of arc topocentric.

The semi-major axis obtained by this method is displayed in Fig. 1 .

4. The theoretical orbit (Fig. 2) is obtained by numerical integration from initial conditions without adjustment to observations. The orbit program employed is a revision and extension of ROPP (Rapid Orbit Prediction Program) prepared originally by TRW for NASA. ROPP computes by means of a variable step size Adams-Moulton integration technique which is very fast. For a stable orbit like Pageos step sizes are from 1/4 of a day to over 2 days. The ROPP physical models account for the following effects:

oblateness: J_2, J_2^2

other gravitational terms: J_3, J_4

sun and moon

s.r.p.

Although ROPP contains a drag model, the density values are assumed zero above 1000 km altitude, so any possible drag effect is not taken into account.

Only s.r.p. during the part-shadow periods causes any fluctuations in the semi-major axis.

The exact expression for the change in $\underline{a}$ over a satellite revolution is well-known (e.g. [2]) and can be expressed as:

$$\Delta a = K_1 \cos J \left[\cos\beta(\cos E_2 - \cos E_1) - (1 - e)^{1/2} \sin\beta \, (\sin E_2 - \sin E_1)\right] \qquad (1)$$

where K_1 is a constant (based on the previously stated assumptions of constancy of solar force, and isotropy of satellite), J is the angle between the sun's rays and the orbital plane, β is the angle between satellite perigee and the sun's rays projected on the orbital plane, and E_1 and E_2 are the eccentric anomalies of the satellite at shadow exit and entrance. This is the expression programmed into ROPP.

For a low eccentricity satellite (which includes Pageos) it is reasonable to develop (1) to the first-order in e, obtaining [3]

$$\Delta a = - K_2 \, e \sin\beta \, f(a,J) \qquad (2)$$

where K_2 is a positive constant, and f(a,J) a positive quantity based on the dependence of the shadow intersections on the scale of the orbit (i.e., $\underline{a}$) and on the inclination of the sun's rays to the orbital plane. (2) indicates that Δa has

its maximum decrease (increase) at $\beta = 90°$ (=270°). Furthermore [3] (with $\underline{a}$ expressed in units of earth radii)

$$f(a,J) = g(a)\ (1 - \frac{a^2 - 1}{a^2 \cos^2 J})^{1/2}$$

where J varies from some value J_o ($0 < J_o < 90°$) at shadow intersection to 0 when the sun's rays are parallel to the orbital plane. The essential point is that f(a,J) changes in the same direction as cos J as J decreases from J_o to 0, so that we can write

$$\Delta a = - h(a,J)\ e \sin\beta \cos J \qquad (3)$$

where h is a positive quantity.

5. Fig. 3 (the combination of Figs. 1 & 2) indicates emphatically the inadequacy of the theoretical model. The discrepancies are better displayed on Fig. 4 in which the long-term drift is eliminated by running independent theoretical models over a single shadow-sun cycle, assuming coincidence with reality at the start of each cycle. There are three main discrepancies of the real curve with respect to the theoretical curve:

(I). the downward slope of the real curve during the sunlit period.

(II). the "shrinkage" of the real curve during shadow, and height of the curve at shadow end.

(III). the bumps on the real curve during shadow (which show up better as high-frequency variations on the da/dt curve).

There are three possible causes for these discrepancies:

(a) Earth-reflected radiation pressure (e.r.p.)

(b) Atmospheric drag.

(c) Non-isotropy of the satellite with respect to s.r.p.

E.r.p. is very difficult to model adequately. Wyatt has given a formula [4] which can be written as:

$$\Delta a = - K_3 \, e \, \cos J \, \sin\beta \qquad (4)$$

and Prior [5] obtained similar results by employing an empirical expression. The correspondence of this formula with (3) should be noted. Both are in the same direction. Wyatt estimated that e.r.p. was about 10% of s.r.p. Prior has been the only one to try to explain observed orbital changes by e.r.p., but he did not attempt this for $\underline{a}$ because he feared contamination by drag.

The explication of a physical mechanism for drag at Pageos height is probably even more difficult than for e.r.p. Density variations with time are much more extreme than at lower altitudes, and whatever drag effect exists is undoubtedly

quite small compared to the unmodelled variations in s.r.p. The most exhaustive study carried out thus far on this subject [6] is pessimistic on obtaining an atmospheric density model at this altitude.

The consequences of the non-isotropy of Pageos have been discussed in detail by Smith and Fea [7]. In brief, the ellipticity of the balloon, its rotation, and the precession of the rotational axis all combine to make the quantity K_1 in (1) vary periodically with time.

Figure 4 begins a few days after launch at the start of the first shadow period. The shape of Δa in the shadow is basically determined by β. For each shadow period starting with the third, β begins larger than 180°, and decreases to a value less than 180° at the end of the shadow interval. The curve changes direction at $\beta = 180°$.

According to (4), during the sunlit periods e.r.p. should round out horizontal parts of the curve in accordance with the value of β, but the effect will be flattened somewhat due to J which attains a maximum in the middle of the sunlit period. During the shadow periods, comparison of (4) with (3) indicates that e.r.p. should manifest itself by augmenting the change in $\underline{a}$ due to s.r.p. Prior [5] has pointed out this should be equivalent to increasing K_1 in (1). Thus the effect of (4) can be simulated by increasing K_1.

The application of e.r.p., either by applying (4), or by increasing K_1, is not successful in explaining the bulk of discrepancies (I) and (II). For example, the first sunlit interval in Fig. 4 shows a convex shape which is exactly opposite the effect e.r.p. should produce over the first half of the interval in accordance with the current values of β. The type (II) discrepancies in the 6th, 8th, and 9th shadow intervals go counter to the expected e.r.p. effect; if K_1 is increased, the discrepancy becomes worse. In the 5th shadow interval, an increase in K_1 will cause the real and theoretical peaks to approach coincidence, but the difference at the end of the shadow period is increased.

E.r.p. apparently fails to deliver any help as a possible physical mechanism for either of the following reasons: the present application of e.r.p., either through (4) or by adjusting K_1 is not a sufficiently accurate model; or, e.r.p. is effectively masked by other perturbations. (4) is probably not a realistic model for e.r.p. because the Earth's albedo is treated there as a constant, and albedo varies with position and time. However, Wyatt [3] has shown that all of the various e.r.p. models he has drawn up tend to produce the same amplitude. Furthermore, Prior [5] has satisfactorily correlated discrepancies in argument of perigee and eccentricity of Pageos based on this e.r.p. model. Hence, it appears more natural

to blame the failure of e.r.p. in explaining the variations in a on the masking by either drag or non-isotropic s.r.p.

Of these, only drag acts in the sunlit intervals. In the large, that is, over the whole 3-1/2 year period, the separation of the real and theoretical curves (Fig. 3) points to drag. Some of this, however, may be ascribed to the influence of the changes in the other orbital elements. The fact that the two curves begin to diverge appreciably only after perigee height has lowered to about 2200 km would be a natural consequence of drag. On the other hand, over individual intervals, drag is even less successful as an explanation. Although the type (II) discrepancies of the 6th, 8th, and 9th shadow intervals could be ascribed to drag, the 2nd, 5th and 7th interval discrepancies reverse themselves in this respect. It is difficult to conceive of a mix of e.r.p. and drag mechanisms to account for these apparent contradictions.

The type (I) discrepancies, which at first glance might appear the easiest to explain by drag, are actually the ones which are most mystifying in this respect. The downward secular trend in each case would seem to be most naturally attributable to drag. But the slopes of the curve during the first and second sunlit intervals at perigee heights

3300 km and 2700 km, respectively, are much steeper than at later sunlit intervals with perigee heights at around 2200 km.

Finally, there remains consideration of the effect of non-isotropy of the satellite on s.r.p. Since s.r.p. is by far the predominant effect in the shadow intervals, it is plausible that variations in this model could effectively mask all other possible sources of perturbations in a. The theory of [7] has been proposed specifically in order to explain discrepancy (III). No definitive results have been obtained yet, but the proposed mechanism is ingenious, credible and promising. It is the only one of the three mechanisms which could possibly explain the apparent randomness of the separation between real and theoretical a at the end of the shadow period. The end of shadow is arbitrary with respect to the phase of the high-frequency perturbations due to the Smith-Fea mechanism, and cut off within a cycle will yield an addition or subtraction of energy in a rather random fashion. However, it is difficult to see how this mechanism can satisfy discrepancy (I) or the overall shrinkage in some cases of discrepancy (II).

6. At present, the behavior of the semi-major axis of Pageos cannot be analyzed well enough so that the orbit can be

precisely predicted. Drag and current models of e.r.p. do not answer satisfactorily any of the observed discrepancies. The theory of Smith and Fea [7] based on the assumption of non-isotropy of the balloon to the sun's rays seems to be the most promising vehicle for explaining the periodic variations in the shadow interval, and the total change of $\underline{a}$ over the shadow interval.

REFERENCES

[1] R. Vanderburgh and K. Kissell, Measurement of Deformation and Spin Dynamics of the Pageos Balloon Satellite by Photoelectric Photometry, presented to the Eleventh Astrodynamics Conference, Goddard Space Flight Center, April 1970.

[2] Y. Kozai, Smithsonian Contrib. to Astrophysics, Vol. 6, 1963, p. 110.

[3] S. Wyatt, ibid., p. 118.

[4] S. Wyatt, in Dynamics of Satellites, IUTAM Symposium May 1962, p. 189.

[5] E. Prior, Earth Albedo Effects on the Orbital Variations of Echo I and Pageos I, report presented to COSPAR, Prague, 1969.

[6] K. Fea and D. Smith, Some Further Studies of Perturbations of Satellites at Great Altitudes, Planetary and Space Science, in press.

[7] D. Smith and K. Fea, NASA Goddard Space Flight Center Report X-550-70-92, March 1970.

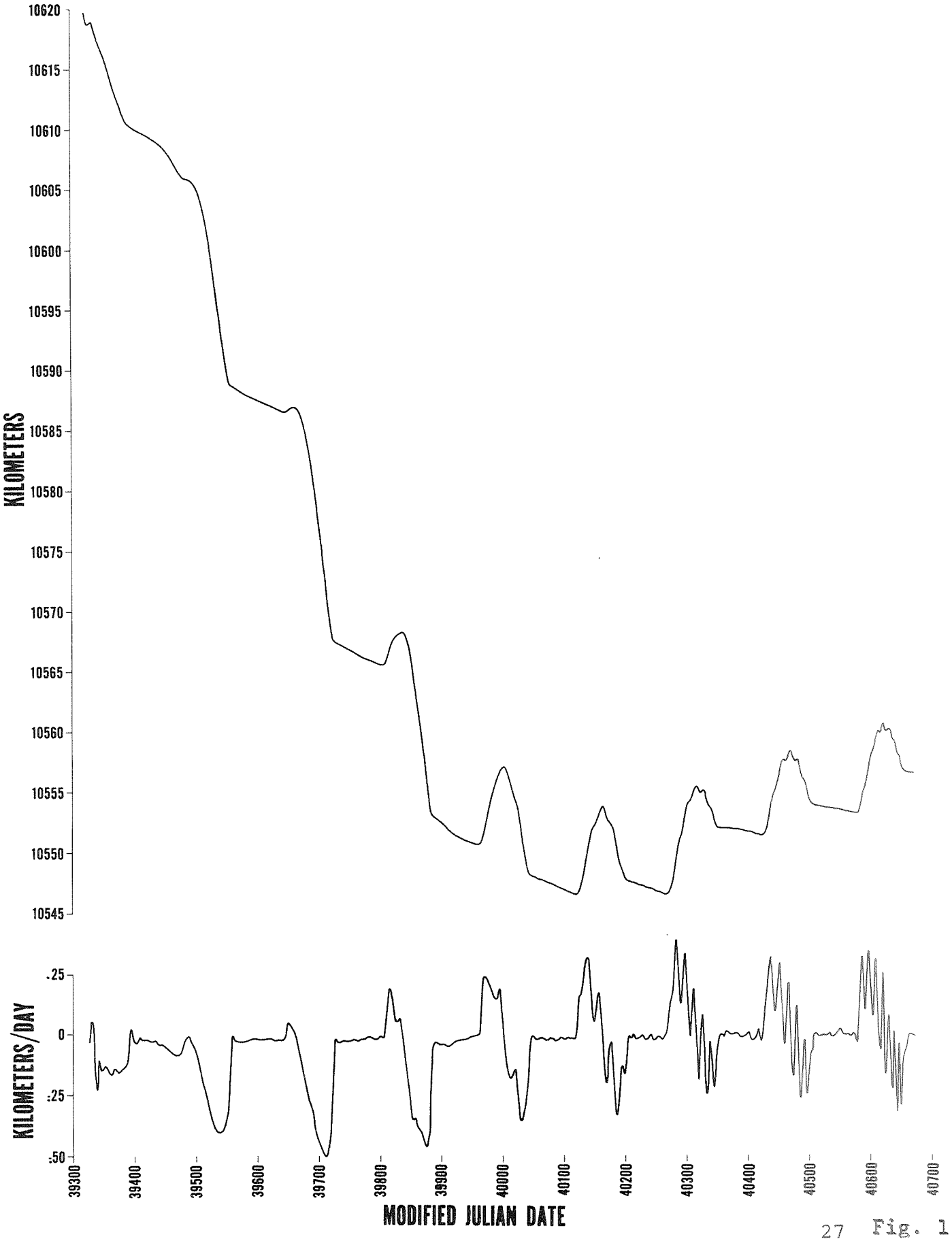
KILOMETERS
10620
10615
10610
10605
10600
10595
10590
10585
10580
10575
10570
10565
10560
10555
10550
10545
KILOMETERS/DAY
.25
0
-.25
-.50
39300
39400
39500
39600
39700
39800
39900
40000
40100
40200
40300
40400
40500
40600
40700
MODIFIED JULIAN DATE

Fig. 1

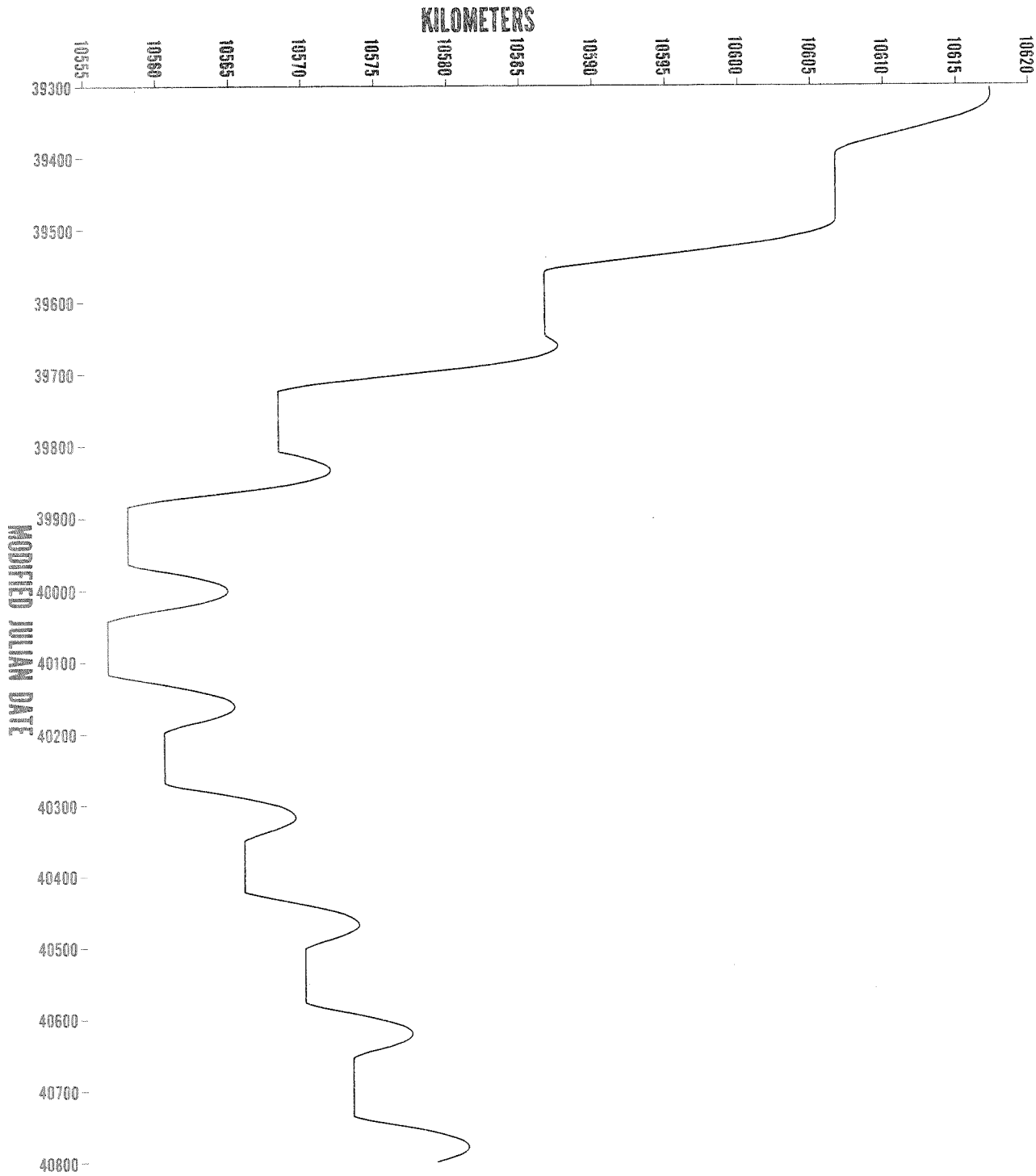
KILOMETERS
10555
10560
10565
10570
10575
10580
10585
10590
10595
10600
10605
10610
10615
10620
39300
39400
39500
39600
39700
39800
39900
40000
40100
40200
40300
40400
40500
40600
40700
40800
FEET

Fig. 2

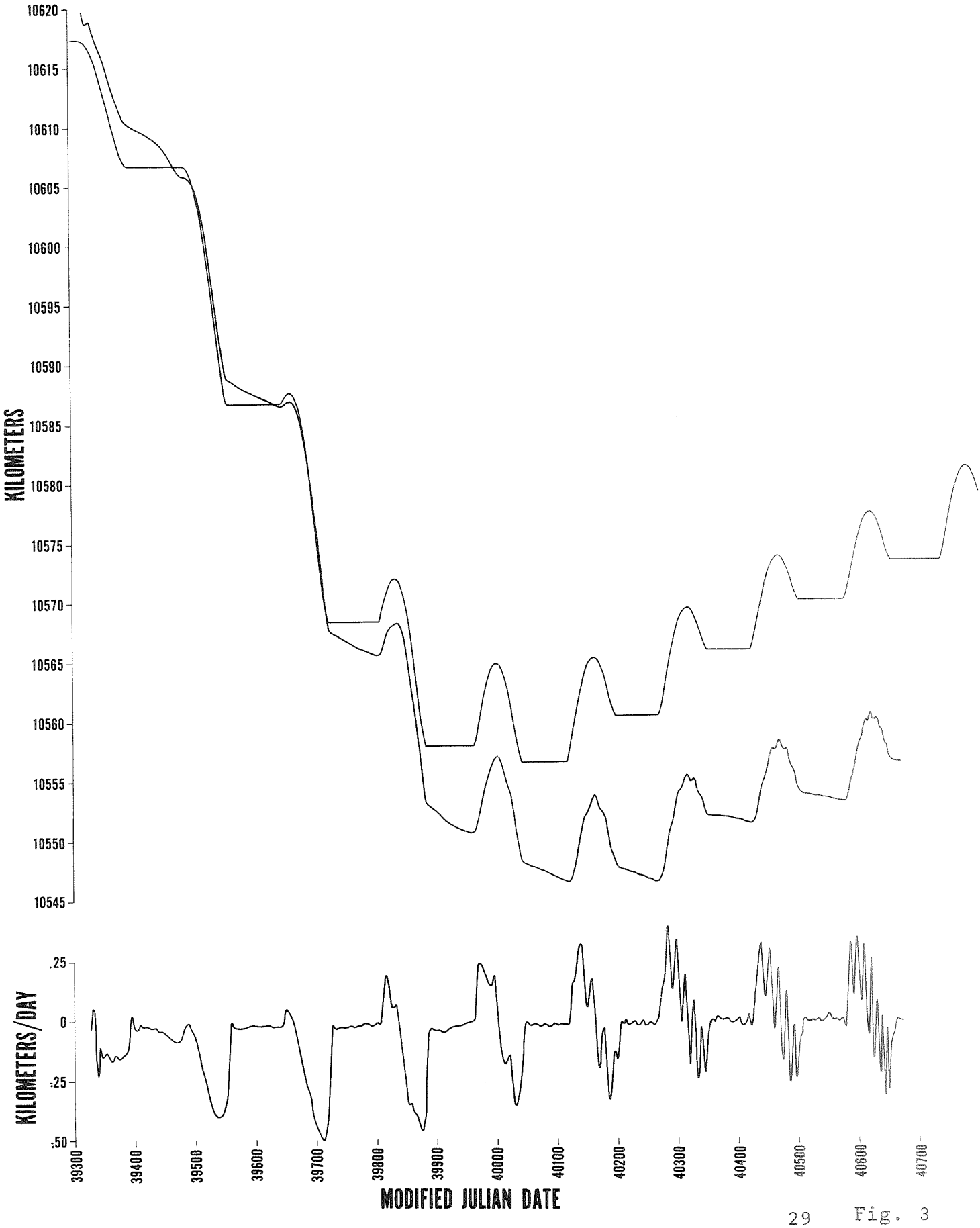
10620
10615
10610
10605
10600
10595
10590
10585
10580
10575
10570
10565
10560
10555
10550
10545
KILOMETERS
.25
0
-.25
-.50
KILOMETERS/DAY
39300
39400
39500
39600
39700
39800
39900
40000
40100
40200
40300
40400
40500
40600
40700
MODIFIED JULIAN DATE

Fig. 3

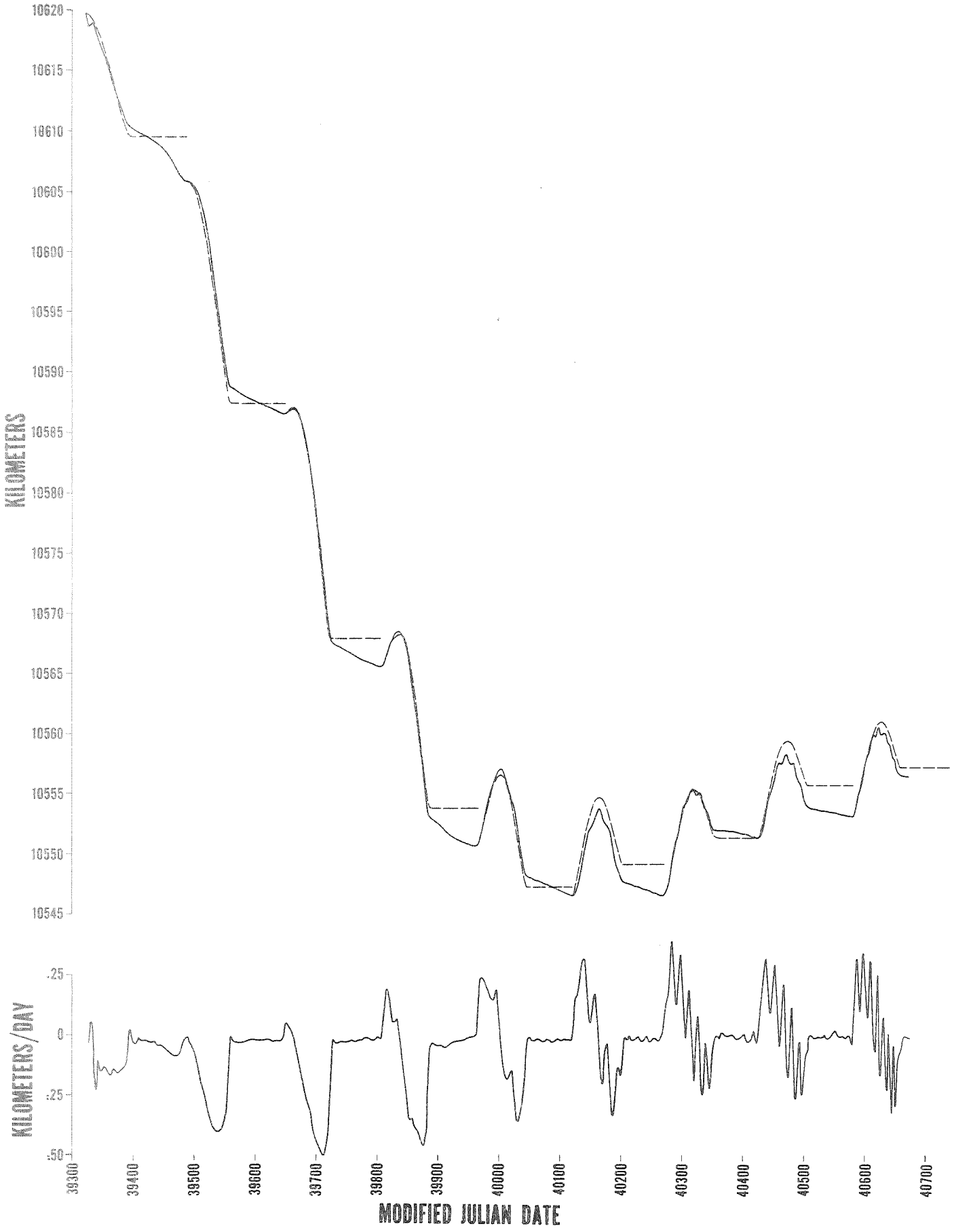
10620
10615
10610
10605
10600
10595
10590
10585
10580
10575
10570
10565
10560
10555
10550
10545
KILOMETERS
.25
0
-.25
-.50
KILOMETERS/DAY
39300
39400
39500
39600
39700
39800
39900
40000
40100
40200
40300
40400
40500
40600
40700
MODIFIED JULIAN DATE

Fig. 4

X-550-70-92

PREPRINT

RADIATION PRESSURE EFFECTS ON THE ACCELERATION OF HIGH ALTITUDE BALLOON SATELLITES

David E. Smith

Mission and Trajectory Analysis Division

Kenneth H. Fea

University of London

England

March 1970

GODDARD SPACE FLIGHT CENTER

Greenbelt, Maryland

RADIATION PRESSURE EFFECTS ON THE ACCELERATION OF HIGH ALTITUDE BALLOON SATELLITES

David E. Smith

Mission and Trajectory Analysis Division

Kenneth H. Fea

University of London

England

ABSTRACT

Previous studies of the orbital accelerations of the high altitude balloon satellites, Pageos and 1963-30D have shown the existence of perturbations that appear to be related to solar radiation pressure but of unknown mechanism. The normal method of computing the radiation perturbations assumes the effective shape of the spacecraft to be spherical but in the present paper an investigation is undertaken to assess the perturbations that may arise when the satellite has an ellipsoidal shape and the radiation scattered by the spacecraft is no longer symmetric about the line joining the satellite and the sun. Consideration is given to both diffuse and specular reflection. The study indicates that a slowly precessing rotation axis might explain the anomalous accelerations found in the earlier studies.

CONTENTS

RADIATION PRESSURE EFFECTS ON THE ACCELERATION OF HIGH ALTITUDE BALLOON SATELLITES

INTRODUCTION

Recent studies by Fea (Reference 1) and Fea and Smith (Reference 2) have shown the existence of an unexplained perturbation of the acceleration of two high altitude spacecraft. Both the spacecraft are balloon satellites of large area to mass ratio and in References 1 and 2 it was suggested that the unexplained acceleration might be associated with or caused by solar radiation pressure.

Figures 1 and 2, taken from References 1 and 2, show the predicted and observed accelerations of Pageos (1966-56A) and Dash 2 (1963-30D). The difference between the computed and observed accelerations is the unexplained perturbation. Inspection of Figures 1 and 2 indicates several important features of the perturbation. Firstly, the perturbation is periodic; secondly, the perturbation is only present when part of the orbit is in shadow (or the amplitude is considerably reduced), thirdly, the amplitude of the perturbation is comparable to the perturbation by solar radiation pressure, and fourthly, the period of the perturbation is decreasing.

There is evidence (References 3 and 4) that one of the satellites showing this anomalous acceleration (Pageos) is no longer spherical and that it is probably shaped like a prolate spheroid. If this is true, the major assumption made in calculating the radiation pressure perturbations, namely, that the

solar radiation scattered by the satellite is symmetrical about the satellite-sun line, no longer holds. In such circumstances it must be expected that additional perturbations of the orbit will arise.

In the present paper the perturbations to the semi-major axis of the orbit of a satellite having the shape of a prolate spheroid are developed. The satellite is assumed to be rotating about the major or a minor axis of the spheroid with a period considerably less than the period of revolution of the satellite about the Earth. Sunlight scattered by the satellite is assumed to be reflected both diffusely (according to Lambert's law) and specularly.

INCIDENT AND REFLECTED RADIATION

Let the satellite have the shape of a prolate spheroid whose surface is described by the equation

$$\frac{(x^2 + y^2)}{b_0^2} + \frac{z^2}{a_0^2} = 1 \qquad (1)$$

where a_0 is the semi-major axis (polar radius)

b_0 is the semi-minor axis (equatorial radius)

and the origin of the coordinate system is at the center of the spheroid with the z - axis corresponding to the polar radius and the x and y axes lying in the equator. Let the angle between the z - axis and the sun be θ, then the shape of the cross-section normal to the sun-satellite line is an ellipse of area $A(\theta)$ where

$$A(\theta) = \pi b_0 d \qquad (2)$$

where

$$\frac{1}{d^2} = \frac{\sin^2\theta}{a_0^2} + \frac{\cos^2\theta}{b_0^2} \tag{3}$$

If the satellite is spinning about its major axis then the average cross-sectional area over one revolution of the satellite is $A(\theta)$ and the incident solar flux, F_I, is given by

$$F_I = A(\theta)\frac{S}{c} \tag{4}$$

where S is the solar constant in erg cm^{-2} sec^{-1}

c is the velocity of light in cm sec^{-1}

If, however, the satellite is rotating about a minor axis making an angle θ' with the sun-satellite line then $A(\theta)$ is a function of time and we need its average value.

Let $A(\theta')$ be the average value of $A(\theta)$ then

$$A(\theta') = \frac{1}{2\pi}\int_0^{2\pi} A(\theta)\, d\omega \tag{5}$$

where ω is the angle between the sun-rotation axis plane and the major axis of the satellite-rotation axis plane (see Figure 3). From Figure 3 we obtain

$$\cos\theta = \sin\theta' \cos\omega \tag{6}$$

and hence

$$A(\theta') = \frac{b_0}{2} \int_0^{2\pi} [d] \, d\omega \tag{7}$$

Substituting for d from Equation 3 and for θ from Equation 6 leads to

$$A(\theta') = \frac{a_0 \, b_0}{2} \int_0^{2\pi} \frac{d\omega}{(1 - k \cos^2 \omega)^{1/2}} \tag{8}$$

where

$$k = \left(1 - \frac{a_0^2}{b_0^2}\right) \sin^2 \theta' \tag{9}$$

The solution to Equation (8) is a hypergeometric function, and can be written as

$$A(\theta') = \pi \, a_0 \, b_0 \, F\left(\frac{1}{2}, \frac{1}{2}, 1, k\right) \tag{10}$$

where

$$F\left(\frac{1}{2}, \frac{1}{2}, 1, k\right) = \sum_{n=0}^{\infty} \left[\frac{(2n)!}{2^{2n}(n!)^2}\right]^2 k^n \tag{11}$$

The average incident solar flux on a prolate spheroid rotating about a minor axis can therefore be written

$$F_I = A(\theta') \frac{S}{c} \tag{12}$$

If the satellite were spherical the solar radiation that is reflected specularly would be distributed evenly over the entire unit sphere surrounding the satellite. If, however, the satellite is prolate or oblate there will be a direction about which the specular reflection will be largely symmetric and which will be the effective direction of any forces arising from the specular reflection. This direction will, for reasons of symmetry, lie in the plane containing the rotation axis of the satellite and the sun. We now make the first major assumption; that the effective direction of reflection of the specular flux is determined by Snell's law on the incident ray that passes through the center of the satellite (see Figure 4). We also make the assumption that the magnitude of the flux reflected in this direction approximates to that which would be reflected by a sphere of surface area equal to that of the spheroid. Hence the specularly reflected flux, E_s, can be written

$$E_s = \alpha_s \frac{\bar{A}}{4\pi} \left(\frac{S}{c}\right) \tag{13}$$

where

$$\left.\begin{aligned} \bar{A} &= A(\theta) \quad \text{for rotation about the major axis} \\ \bar{A} &= A(\theta') \quad \text{for rotation about a minor axis} \end{aligned}\right\} \tag{14}$$

and α_s is the specular albedo of the satellite.

The assumption concerning the direction of the reflection holds for $\theta = 0$, $\pi/2$ and π (also θ'), and for $0 < \theta \lesssim \pi/2$ and $\pi/2 < \theta < \pi$ the direction of reflection is moved towards the minor axis direction as indicated by Snell's law. Thus the assumption is considered adequate for the present study.

Similar arguments can be applied to the magnitude of the reflection; the magnitude of the flux for $\theta = 0$ is probably overestimated but underestimated for $\theta = \pi/2$. An exact formulation of the magnitude and effective direction of the specular reflection is extremely complex and is, at present, believed to be unnecessary for the present study.

Diffusely reflected radiation is normally symmetric about the normal to the surface and this is the assumption made here (see Figure 4). The satellite is assumed to be a uniformly diffuse reflector (Lambert's law) and for the purposes of calculating the dependence of the magnitude on the phase (not the size) the satellite is assumed to be spherical.

In Reference 5 the author has derived an expression for diffusely reflected radiation falling on a unit area distant r from the satellite. By putting $r = 1$ this expression may be used to give the flux (E_D) reflected diffusely in the direction of the normal to the surface on the incident ray that passes through the center of the satellite. We therefore have

$$E_D = \frac{2}{3} \alpha_D \frac{\bar{A}}{\pi^2} \left(\frac{S}{c}\right) \left[(\pi - \epsilon) \cos \epsilon + \sin \epsilon\right] \qquad (15)$$

where α_D is the diffuse albedo of the satellite,

$$\epsilon = \frac{\pi}{2} - (\theta + \phi)$$

and (16)

$$\tan \phi = \left(\frac{b_0^2}{a_0^2}\right) \Big/ \tan \theta$$

for rotation about the major axis, or where

$$\epsilon = \theta' - \phi'$$

and (17)

$$\tan \phi' = \left(\frac{b_0^2}{a_0^2}\right) \tan \theta'$$

for rotation about a minor axis.

For convenience, we summarize the directions of the incident and emitted fluxes as follows:

(a) The incident flux, F_I, is directed radially from the sun through the center of the satellite; its magnitude is given by Equations 4 or 12;

(b) The specularly reflected flux, E_s, lies in the plane containing the sun and axis of rotation of the spacecraft and makes an angle 2ϵ with the

incident ray through the center of the satellite; the magnitude is given by Equation 13,

(c) The diffusely reflected flux, E_D, lies in the plane containing the sun and the axis of rotation of the spacecraft and makes an angle ϵ with the incident ray through the center of the satellite, the magnitude is given by Equation 15.

As a check on the effect of the approximations we have made we can integrate the specular and diffuse fluxes (Equations 13 and 15) over the entire unit sphere. This integration leads to

$$\text{total reflected flux} = \bar{A}\left(\frac{S}{c}\right)(\alpha_s + \alpha_D) \tag{18}$$

If $(\alpha_s + \alpha_D) = 1$, then the total reflected flux is equal to the total incident flux (Equation 4) which means that the approximations (on average) only affect the relative magnitudes of the specular and diffuse components and not the total flux. If $(\alpha_s + \alpha_D) < 1$, the satellite is absorbing some of the incident radiation and implies we are making the additional assumption that when the satellite re-emits the absorbed radiation it does so isotropically so that there is no change in momentium of the satellite.

PERTURBATIONS OF THE SEMI-MAJOR AXIS

The semi-major axis is a measure of the energy of the orbit and hence the perturbations to the semi-major axis are equal to the work done by the forces

of radiation pressure on the satellite. The perturbations to the semi-major axis can therefore be written as (Reference 6)

$$\Delta a = \frac{2F}{n^2 a m}\left[r \cos \phi\right]_{\text{shadow exit}}^{\text{shadow entry}} \tag{19}$$

where

Δa is the change in the semi-major axis per revolution

F is the flux of radiation (F is negative)

n is the mean motion

a is the semi-major axis

m is the mass of the satellite

r is the geocentric radial distance of the satellite

ϕ is the angle between the sun and the satellite (see Figure 5)

Applying equation 19 to the incident and reflected fluxes already derived we obtain

$$\Delta a = -\frac{2}{n^2 a m}\left[r\left\{F_I \cos \phi_0 + E_D \cos \phi_1 + E_s \cos \phi_2\right\}\right]_{\text{shadow exit}}^{\text{shadow entry}} \tag{20}$$

where ϕ_0, ϕ_1 and ϕ_2 are the angles between the satellite and the incident, diffuse and specularly reflected flux directions (see Figure 5).

Subsequently, we shall want to allow the spin axis to precess about another axis so we shall assume we know the direction of the precession axis $(\bar{\omega}, \bar{\theta})$

with respect to the sun (see Figure 5), the position of the sun (α, δ), the position of the spin axis (ω_s,θ_s) with respect to the precesson axis (see Figure 5) and the position of the satellite (α_0, δ_0).

With the aid of Figure 5 we can derive the right ascension ($\bar{\alpha}$) and declination ($\bar{\delta}$) of the precession axis from

$$\sin \bar{\delta} = \cos \bar{\theta} \sin \delta + \sin \bar{\theta} \cos \delta \cos \bar{\omega}$$

$$\sin (\bar{\alpha} - \alpha) = \frac{\sin \bar{\theta} \sin \bar{\omega}}{\cos \delta} \tag{21}$$

and the spin axis (α_s, δ_s) from

$$\sin \delta_s = \cos \theta_s \sin \bar{\delta} + \sin \bar{\theta}_s \cos \bar{\delta} \cos \omega_s$$

$$\sin (\alpha_s - \bar{\alpha}) = \frac{\sin \bar{\theta}_s \sin \omega_s}{\cos \delta_s} \tag{22}$$

We can also derive the position of the spin axis (ω_0, θ) with respect to the sun from

$$\cos \theta = \sin \delta \sin \delta_s + \cos \delta \cos \delta_s \cos (\alpha_s - \alpha)$$

$$\sin \omega_0 = \frac{\cos \delta_s \sin (\alpha_s - \alpha)}{\sin \theta} \tag{23}$$

and the right ascensions and declinations of the diffuse (α_1, δ_1) and specular (α_2, δ_2) reflections from

$$\sin \delta_1 = \sin \delta \cos (\theta + \epsilon) + \cos \delta \sin (\theta + \epsilon) \cos \omega_0$$

$$\sin (\alpha_1 - \alpha) = \frac{\sin (\theta + \epsilon) \sin \omega_0}{\cos \delta_1} \tag{24}$$

$$\sin \delta_2 = \sin \delta \cos (\theta + 2\epsilon) + \cos \delta \sin (\theta + 2\epsilon) \cos \omega_0$$

$$\sin (\alpha_2 - \alpha) = \frac{\sin (\theta + 2\epsilon)}{\cos \delta_2} \tag{25}$$

The above equations have been derived for rotation about the major axis of the satellite. For rotation about a minor axis we replace θ with θ' and ϵ with $-\epsilon$ in Equations 24 and 25.

We are now in a position to determine ϕ_1 and ϕ_2 from

$$\cos \phi_1 = \sin \delta_0 \sin \delta_1 + \cos \delta_0 \cos \delta_1 \cos (\alpha_0 - \alpha_1) \tag{26}$$

$$\cos \phi_2 = \sin \delta_0 \sin \delta_2 + \cos \delta_0 \cos \delta_2 \cos (\alpha_0 - \alpha_2) \tag{27}$$

which, together with,

$$\cos \phi_0 = \sin \delta_0 \sin \delta + \cos \delta_0 \cos \delta \cos (\alpha_0 - \alpha) \tag{28}$$

enables equation 20 to be evaluated. Equations 20 through 28 therefore represent the perturbation to the semi-major axis due to incident, diffuse and specular radiation.

EXAMPLE

The magnitude and form of the perturbation can best be demonstrated by an example. Let us assume we have a circular orbit with inclination 90 degrees, and the sun on the equator. Because the shadow entry and exit points are symmetric about the Earth-sun line Equation 20 reduces to

$$\Delta a = -\frac{2}{n^2 m}\left[E_D \cos\phi_1 + E_s \cos\phi_2\right]_{\text{shadow exit}}^{\text{shadow entry}} \qquad (29)$$

For this particular example it is preferable to use slightly different formulations for $\cos\phi_1$ and $\cos\phi_2$. Let ϕ_0' be the value of ϕ_0 at the point of entry and exit into the shadow, then we can write (see Figure 6)

$$\cos\phi_{1N} = \cos(\theta+\epsilon)\cos\phi_0' + \sin(\theta+\epsilon)\sin\phi_0'\cos(\omega_1+\omega_2) \qquad (30)$$

$$\cos\phi_{1X} = \cos(\theta+\epsilon)\cos\phi_0' + \sin(\theta+\epsilon)\sin\phi_0'\cos\omega_1 \qquad (31)$$

and

$$\cos\phi_{2N} = \cos(\theta+2\epsilon)\cos\phi_0' + \sin(\theta+2\epsilon)\sin\phi_0'\cos(\omega_1+\omega_2) \qquad (32)$$

$$\cos \phi_{2X} = \cos(\theta + 2\epsilon) \cos \phi_0' + \sin(\theta + 2\epsilon) \sin \phi_0' \cos \omega_1 \qquad (33)$$

where $\phi_{1N}, \phi_{1X}, \phi_{2N}, \phi_{2N}$ are the shadow entry and exit values of ϕ_1 and ϕ_2. The angles ω_1 and ω_2 are defined in Figure 6.

We can now write

$$\Delta a = \frac{4}{n^2 m} \sin \phi_0' \sin\left(\omega_1 + \frac{\omega_2}{2}\right) \sin \frac{\omega_2}{2} \left[E_D \sin(\theta + \epsilon) + E_s \sin(\theta + 2\epsilon)\right] \qquad (34)$$

The $\sin \phi_0'$ term changes slowly as the orbit moves with respect to the sun but its sign is always positive. The $\sin \omega_2/2$ term is zero when there is no shadow on the orbit and the perturbation vanishes. When non-zero, the term is always positive. The term containing E_D and E_s changes only slowly as the spin axis moves and is normally of constant sign. However, for an oblate satellite the sine terms can change sign if $2\epsilon > \theta'$. The $\sin(\omega_1 + \omega_2/2)$ is also positive unless ω_1 is negative, implying that the spin axis lies near the equatorial plane and between the sun and the shadow points on the orbit.

Let us further simplify our example by having the precession axis on the equator, so that $\bar{\omega} = \pi/2$ on $\bar{\delta} = 0$, and let the spin axis rotate slowly about the precession axis. The $\sin(\omega_1 + \omega_2/2)$ term in equation 34 will then oscillate about zero with a period equal to the precession period and produce a quasi-periodic perturbation about the mean value. This situation could have existed for the Pageos satellite in July 1968. Reference 4 indicates that the spin axis of Pageos was near the equator on July 4th and if the axis was precessing about

a point even nearer the equator we should expect to observe a quasi-periodic perturbation in the semi-major axis. The predicted maximum magnitude of this perturbation of Pageos, assuming a specular albedo of 0.86 (Reference 4) and negligible diffuse albedo, a mass of 55 kg, a mean motion of 8 revolutions/day is about 1 km/day or an acceleration of 8×10^{-4} revolutions/day^2 in mean anomaly. The observed amplitude of the acceleration shown in Figure 1 is about 1×10^{-4} revolutions/day^2. When account is taken of the trigonometric terms in equation 34 and of smoothing in the observational data; the amplitudes of the computed and observed perturbations are about equal.

CONCLUSIONS

Expressions have been developed for the perturbation of the semi-major axis of the orbit of a satellite with elliptical cross-section due to solar radiation pressure when both specular and diffuse reflections are taken into account. The theory has been applied to a very simplified example resembling the orbit of the Pageos satellite in July 1968 and it has been shown that if the spin axis is permitted to rotate about a fixed precession axis a perturbation of the semi-major axis is predicted which has approximately the same form and amplitude that is actually observed in the Pageos orbit.

The foregoing theory and example do not necessarily explain the perturbations in the Pageos and 1963-30D orbits but do suggest that a mechanism of the type described here could be the explanation. A more detailed examination of the theory and its application to these two satellites is being undertaken.

REFERENCES

1. Fea, K., "The Orbital Acceleration of High Balloon Satellites," presented at XIIth Plenary Meeting of COSPAR, Prague, May 1969.

2. Fea, Kenneth H. and Smith, David E. "Some Further Studies of Pertubation of Satellites at Great Altitude," accepted for Publication in Planetary and Space Science.

3. Vanderburgh, R. C., "Wide Band (Visual Spectrum) Photoelectric Photometry of PAGEOS During its First Fifteen Months in Orbit," Proceedings of University of Miami Symposium on Optical Properties of Orbiting Satellites, Edit. Duke, D., and Kissell, K. E., May 1969.

4. Vanderburgh, R. C., "ARL OPOS Photoelectric Photometry of PAGEOS on 4 July 1968," Aerospace Research Laboratories report ARL-MR-68-0004. Wright Patterson Air Force Base, Ohio, August 1968.

5. Smith, D. E., "An Approximate Method of Estimating the Reflection Characteristics of a Spherical Satellite," Proceedings of University of Miami Symposium on Optical Properties of Orbiting Satellites, Edit. Duke, D., and Kissell, K. E,, May 1969.

6. Cook, G. E., Geophys. J., Vol. 6, No. 3, April 1962.

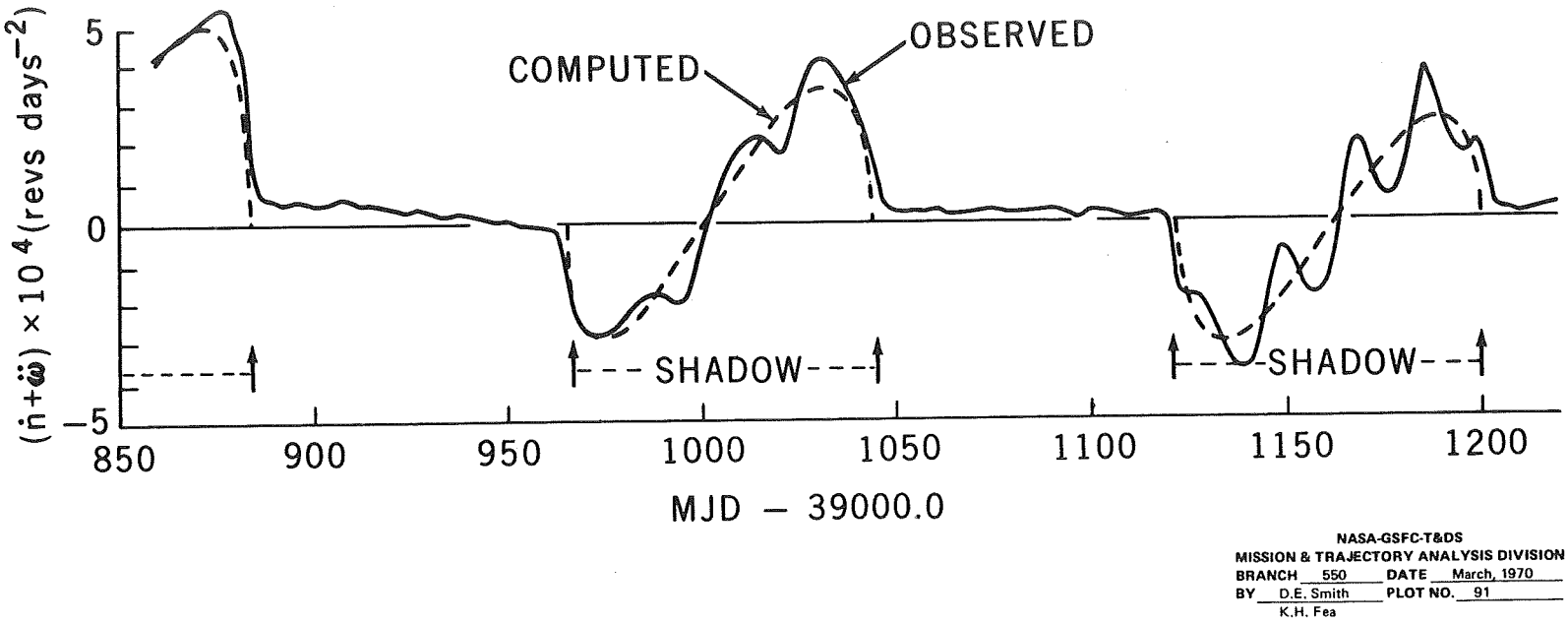

Figure 1. 1966 56A, Observed and Computed Orbital Acceleration v. Modified Julian Date (1968)
(after Fea, Reference 1)

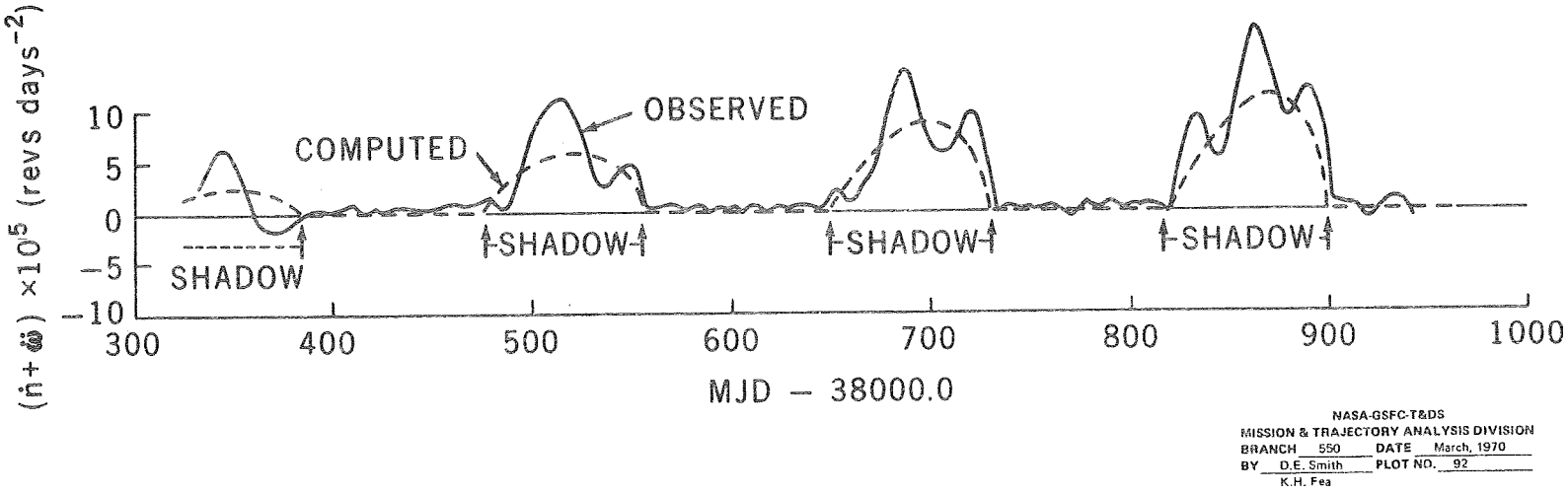

Figure 2. 1963 30D, Observed and Computed Orbital Acceleration v. Modified Julian Date (Nov. 1963 to Jun. 1965)
(after Fea and Smith, Reference 2)

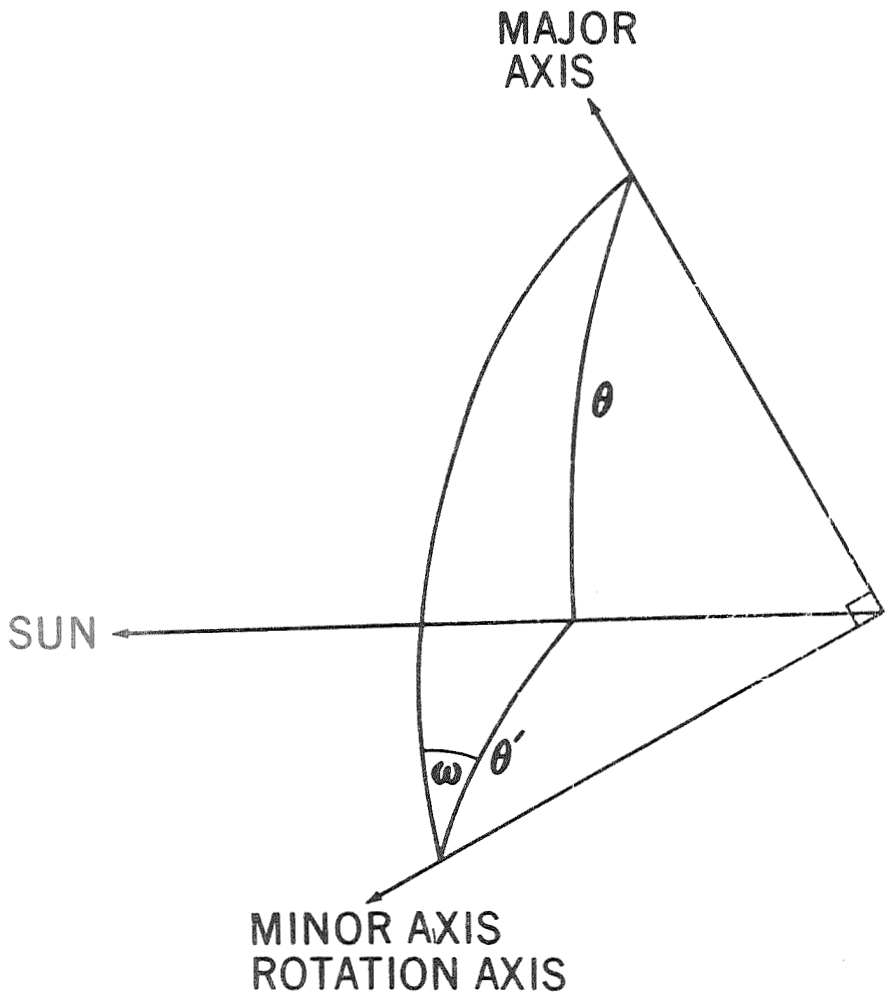

NASA-GSFC-T&DS
MISSION & TRAJECTORY ANALYSIS DIVISION
BRANCH 550 DATE March, 1970
BY D.E. Smith PLOT NO. 93
K.H. Fea

Figure 3. Rotation of Satellite About a Minor Axis.

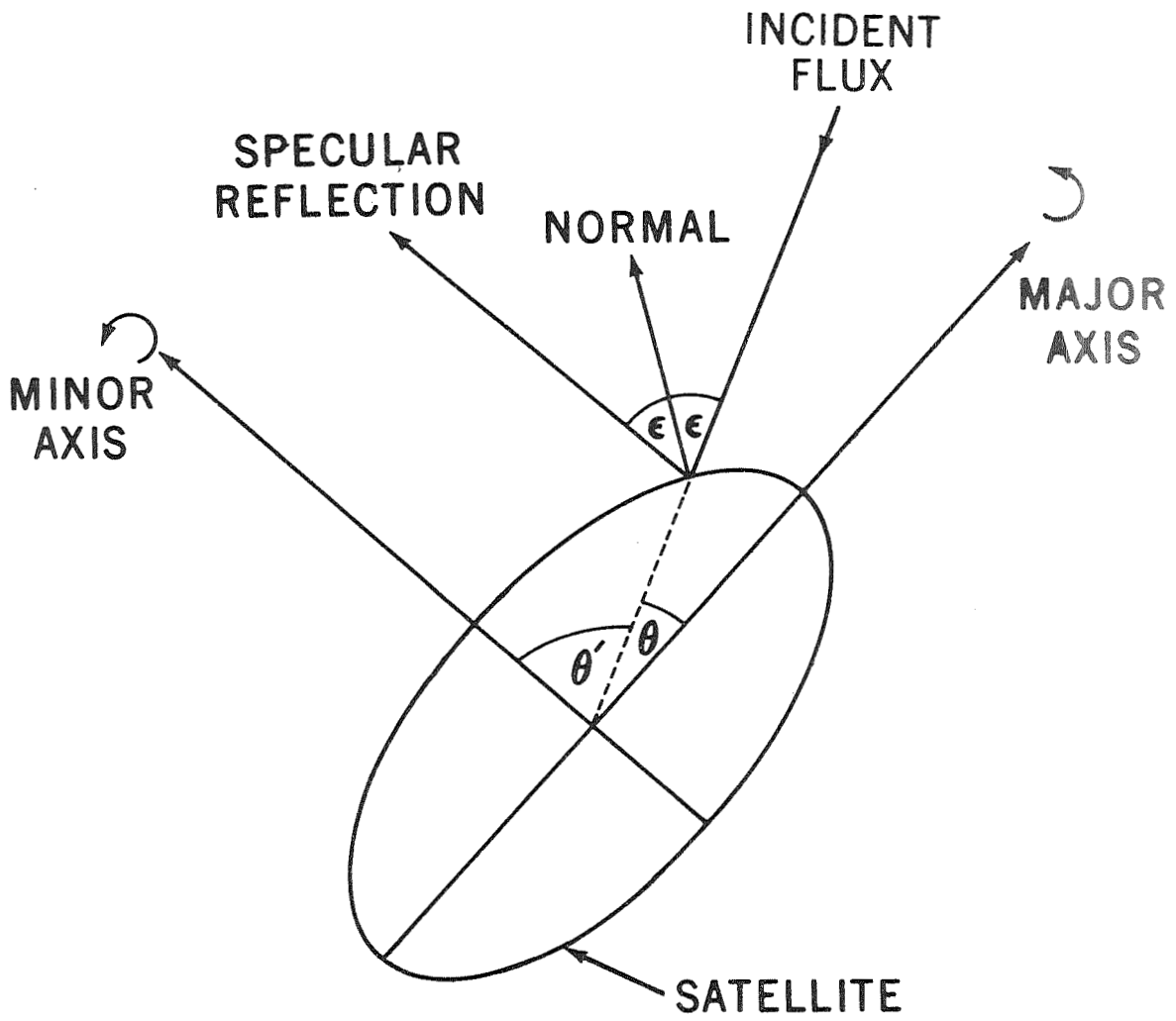

Figure 4. Incident and Reflected Radiation.

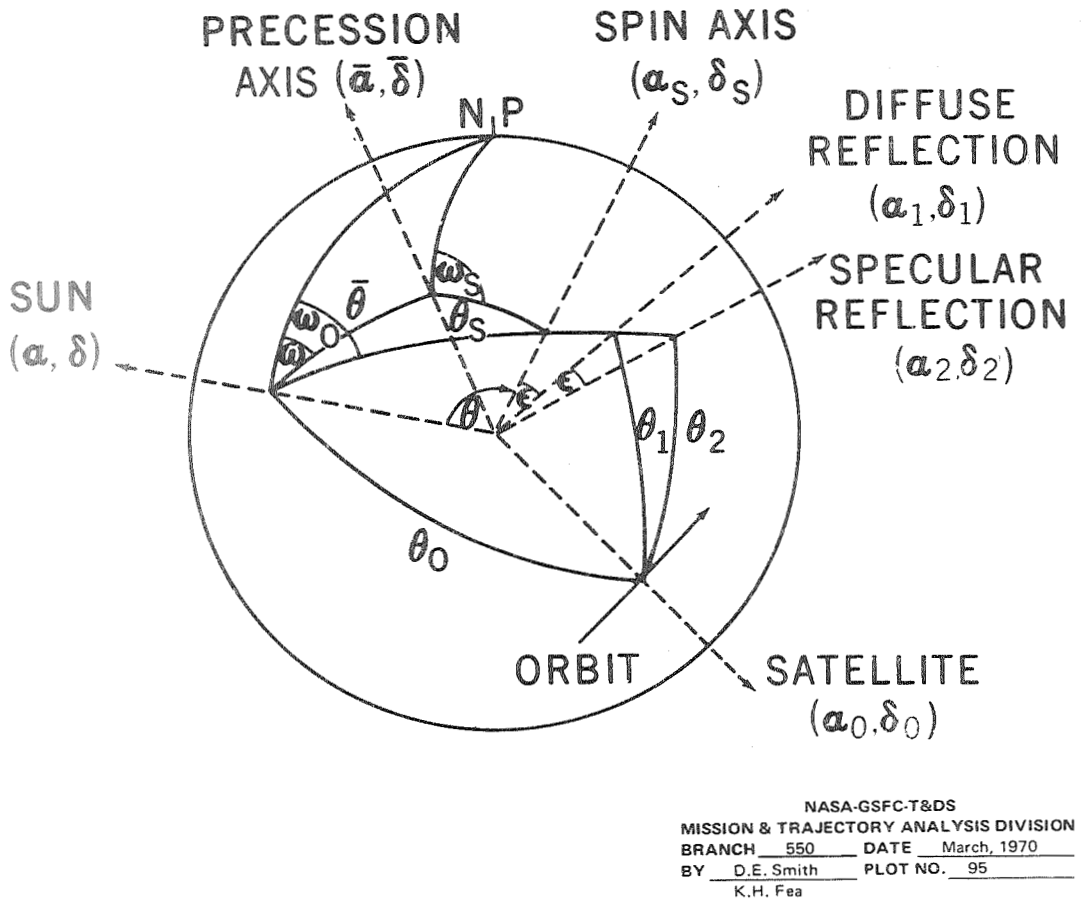

NASA-GSFC-T&DS
MISSION & TRAJECTORY ANALYSIS DIVISION
BRANCH 550 DATE March, 1970
BY D.E. Smith PLOT NO. 95
K.H. Fea

Figure 5. Relationship between Sun, Precession and Spin Axes, Diffuse and Specular Reflections, for Satellite Rotation about Major Axis.

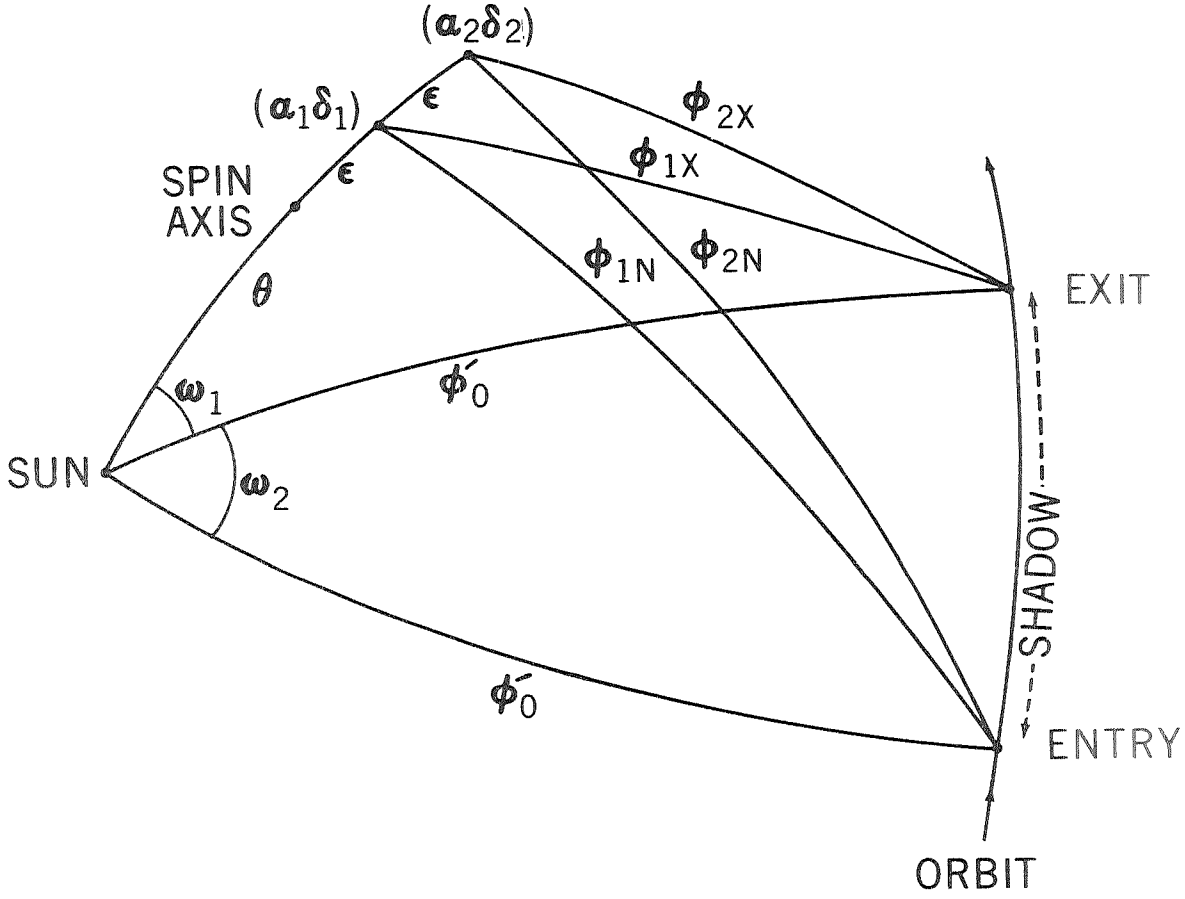

NASA-GSFC-T&DS
MISSION & TRAJECTORY ANALYSIS DIVISION
BRANCH 550 DATE March, 1970
BY D.E. Smith PLOT NO. 96
K.H. Fea

Figure 6. Shadow Entry and Exit Geometry for a Circular Orbit.

Air Force Use of Geodetic Satellite Data

H. Leroy Kuykendall

ACIC
St. Louis, Missouri

Presented at GEOS-2 Program Review Meeting, Goddard Space Flight Center, 22-24 June 1970

Air Force Use of Geodetic Satellite Data

The Aeronautical Chart and Information Center has been using the data obtained from the Geodetic Satellite Program (GSP) in a number of ways. Our investigations are divided into two separate categories which support the development of a World Geodetic System (WGS) both directly and indirectly. The geometric application of the data has been directed toward specific-point positioning on the Eastern Test Range (ETR), Bermuda, and Johnston Island using the AF PC-1000 camera systems. We have also undertaken the densification of the Passive Geodetic Satellite (PAGEOS) network in South America for the purpose of linking the single arcs of triangulation into a unified geodetic system. Observational data from ANNA 1B, GEOS I and II, ECHO I and II, and PAGEOS have been and are being used in these efforts. We are also working with data from other acquisition systems such as Baker-Nunn, STADAN (MOTS), BC-4, and SECOR.

The dynamic application of the GSP data is concerned primarily with the determination of an earth gravitational model and tracking station location from a combination of Baker-Nunn and Doppler data supplemented with existing surface gravity anomalies. To date, Kaula's analytic procedures, as outlined in ACIC Technical Report 112, have been used for computing an earth gravitational model.

1. Geometric Satellite Positioning

While observational data from active satellites can often be applied as it is received from the NASA Geodetic Satellite Data Center or other sources, the passive GSP data must be preprocessed for

geometric geodesy purposes. Details concerning our plate reduction procedure and processing techniques for both passive and active satellites are included in an ACIC report nearing completion. The Ohio State University (OSU) has already published two reports (No 82 and No 100) treating the preprocessing of optical and electronic satellite observations, respectively. Briefly, the procedures used in processing passive optical satellite data at ACIC involve:

1. A phase angle reduction which refers the observation to the geometric center of the satellite.

2. A propagation delay correction which accounts for the travel time of light reflected from the satellite to the camera.

3. A procedure of fitting third degree time series polynomials to produce computed "simultaneous" observations where shutters are not synchronized.

(For both active and passive satellite observations, ACIC applies a correction for parallactic refraction. This fact was omitted in the OSU Report No 82 noted above.)

Several computer programs are used at ACIC to determine the quality of reduced optical and electronic data. The principal ACIC program for screening simultaneous optical data computes satellite coordinates and the associated error estimates for each individual image. It will handle simultaneous data from two to six camera stations. The error estimates include the standard errors of the computed x, y, z coordinates and the spherical standard error of the satellite's spatial position. The slant ranges are determined from each observing station to the satellite. The

equivalent angular error, which is the relationship between the range and spherical standard error, is also computed.

Another program -- polynomial adjustment -- is used only for passive satellite data. Each residual from the adjustment indicates how well an observed Right Ascension (RA) or Declination (DEC) agrees with the RA or DEC computed from the respective polynomial for the same time. The relative magnitudes of the residuals indicate gross errors in individual points.

The goemetric triangulation adjustment program accomplishes a triangulation adjustment of the "unknown" and the constrained camera station positions. They are related to one or more camera positions already referenced to a particular geodetic datum.

The short arc program uses orbital constraints to adjust observations made by geodetic tracking nets. The input data includes both optical systems and electronic ranging systems such as LASERS, SECOR, Geoceiver, and C-Band Radar systems.

The computational processes just noted have been and are being used in connection with a variety of Air Force projects ranging from radar calibration to densification of geodetic control. The following tabulations represent current results for the ETR, Bermuda, Johnston Island, and South American densification effort. The items shown include stations, satellites observed, periods of observation, as well as the amount of data, adjusted coordinates, and the relative accuracy with respect to the North America Datum. In Table 1, the figures given under the heading "Observations Available" indicate the number of events observed. Each event may include as few as one or as many as nine satellite images, according to the type of satellite.

TABLE I

OBSERVATIONS

PROJECT	STATION	OBSERVATIONS AVAILABLE A	GI	EI	P	GII	PERIOD OF OBSERVATION
ETR (PC-1000)	Swan Is., U.S.	16	16				May 65 - Jun 66
	Grand Turk, U.K.	18	12				May 65 - Jun 66
	Curacao, Neth.	2	27		8		May 65 - Jun 66
	Antigua, U.K.	9	18				May 65 - Jun 66
	Trinidad	1	8		8		May 65 - Jun 66
	*Semmes, Ala.	2	9				May 65 - Jun 66
	*Hunter AFB, Ga.	2	6				May 65 - Jun 66
	*Homestead AFB, Fla.	14	20				May 65 - Jun 66
Bermuda (PC-1000)	Kindley AFB, Ber.			3	17		Oct 66 - Apr 67
	*Hunter AFB, Ga.			1	9		Oct 66 - Apr 67
	*Aberdeen, Md.			2	8		Oct 66 - Apr 67
Johnston Is. (PC-1000 and BC-4)	Johnston Is.			5	17		Jul 67 - Sep 67
	*Maui Is. (BC-4)			1	7		Jul 67 - Sep 67
	*Wake Is. (BC-4)			1	8		Jul 67 - Sep 67
	*Christmas Is. (BC-4)			4	9		Jul 67 - Sep 67
SAD (PC-1000 and BC-4)	Paramaribo, Sur.				34	3	Sep 67 - Feb 69
	Bogota, Col.				36	5	Nov 67 - Feb 69
	Manaus, Bra.				6		Nov 68 - Dec 68
	**Curacao, Neth.				60	1	Sep 67 - Feb 69
	**Trinidad				45	8	Sep 67 - Feb 69
	**Quito, Ecud.[1]				16	1	Sep 67 - Jan 69
	**Villa Dolores, Arg.[2]				21		Sep 67 - Dec 68
	*Beltsville, Md.[2]				10		Oct 67 - Dec 68
	**Paramaribo, Sur.[2]				29		Sep 67 - Dec 68

[1] BC-4, PC-1000

[2] BC-4

A - ANNA
GI - GEOS I
EI - ECHO I
P - PAGEOS
GII - GEOS II

*Stations held fixed in their respective adjustments.
**Station positions constrained.

Table 2 shows the horizontal and vertical coordinates and relative accuracies (one sigma) with respect to the fixed stations used in the adjustment.

TABLE 2

HORIZONTAL AND VERTICAL COORDINATES

STATION	LATITUDE	σ	LONGITUDE	σ	ELLIPSOID HEIGHT (Clarke 1866)	ASTROGEODETIC GEOID HEIGHT	σ	DATUM OF ADJUSTMENT
Swan Is.	17° 24' 16".669 N	0".166	83° 56' 29".866 W	0".069	60.4	20.0 m	3.5 m	NAD 27
Grand Turk	21 25 46.929 N	0.119	71 08 46.221 W	0.218	9.9	7.7	3.7	NAD 27
Curacao	12 05 22.244 N	0.290	68 50 17.385 W	0.263	36.6	31.0	4.4	NAD 27
Antigua	17 08 52.689 N	0.198	61 47 22.067 W	0.359	24.7	22.9	6.7	NAD 27
Trinidad	10 44 31.947 N	0.389	61 36 37.655 W	0.407	282.1	27.8	8.0	NAD 27
Bermuda	32 22 58.298 N	0.030	64 41 0.024 W	0.073	38.7	-12.0	1.0	NAD 27
(P) Johnston Is.	16 43 43.877 N	0.070	169 31 10.738 W	0.095	-83.5	-85.9	2.3	WN 84 (NAD 27)

(P) = preliminary

WN 84 = BC-4 World Net Adjustment 84, Mar 1969.

(It should be noted from Table 1 that only six observations were used to position Manaus.)

Table 3 is a tabulation of the data in the current short arc adjustment of the ETR project.

TABLE 3

SAGE READJUSTMENT OF ETR

STATION	OBSERVING SYSTEM	SATELLITE	OBSERVATIONS
Swan Is.	PC-1000	ANNA	17
	PC-1000	GEOS I	11
Grand Turk	PC-1000	ANNA	15
	PC-1000	GEOS I	12
Curacao	PC-1000	ANNA	3
	PC-1000	GEOS I	23
	PC-1000	PAGEOS	7
Antigua	PC-1000	ANNA	9
	PC-1000	GEOS I	14
Trinidad	PC-1000	ANNA	2
	PC-1000	GEOS I	5
	PC-1000	PAGEOS	7
Semmes	PC-1000	ANNA	6
	PC-1000	GEOS I	11
Hunter	PC-1000	ANNA	5
	PC-1000	GEOS I	3
	SECOR	GEOS I	7 (arcs)
Homestead	PC-1000	ANNA	15
	PC-1000	GEOS I	17
	SECOR	GEOS I	6 (arcs)
Ft. Meyers	MOTS	GEOS I	19
Herndon	SECOR	GEOS I	6 (arcs)
Greenville	SECOR	GEOS I	7 (arcs)

Table 4 lists other observation systems which may have observed in the same short arcs as the USAF PC-1000 cameras in South America from Sep 67 to Jan 70.

TABLE 4

OBSERVATION SYSTEMS

SYSTEM	NO. OF STATIONS
Doppler	9
NASA STADAN	6
C-Band Radar and Optical Calibration Stations	22
SECOR	3
BC-4	9
NASA Special Optical	9
SAO Optical	8
Total	66

2. Dynamic Satellite Positioning

During the past several years, ACIC has been engaged in Earth Gravitational Model (EGM) development from satellite orbital tracking data, surface gravity observations, and combinations of both data sources. Extensive studies have been made to determine the weighting schemes and the relative merits of combining Baker-Nunn and Doppler tracking data for EGM development from GSP satellites supplemented by other available tracking data (see Table 5). Current efforts are directed toward supplementing satellite tracking data with surface gravity anomalies to determine an expanded set of harmonic coefficients.

At present, tracking data is being processed for 15 satellites as contrasted with the twelve described in TR 112. The additional satellites are 1965-63A (SECOR 5), 1966-5A, and 1965-32A (Beacon-C), excluding Explorer 19. The arcs in the data set are 18 days in duration except for those from 1966-5A which are 15 days in length because of limited tracking data. While fewer arcs are being used in the current

solution, those selected are considered the best in terms of data distribution, etc. The satellites, orbital characteristics, and number of arcs are shown in Table 5.

Where both Baker-Nunn and Doppler data were available the two were merged as were ANNA and GEOS I data. Where merging was not possible, as with Beacon B (Explorer 22) and Beacon C (Explorer 27), the number of arcs was expanded so that both Baker-Nunn and Doppler data from the satellites would be included in the solution. A total of 350 geophysical parameters -- station latitude, longitude and height (above reference ellipsoid) for 31 Doppler and 13 Baker-Nunn stations; gravity model consisting of all tesseral terms through 13, 13; and 19 pairs of resonance terms -- will be determined in addition to the arc parameters. Since each set of arc parameters will be uncorrelated with the other sets, the normal equation matrix will be partitioned so that the maximum matrix to be inverted will be 350 x 350. Because a larger variety of orbits was used than would be available from either data type alone, we expect the solution will produce a consistent set of station locations for the Baker-Nunn and Doppler tracking networks and an improved EGM.

TABLE 5

SATELLITE ORBITAL CHARACTERISTICS

SATELLITE #	NAME	Semi-major axis (km)	e	inclination (deg)	Perigee (km)	Apogee (km)	# of ARCS
1960 13A	Courier 1B	7473	.017	28.3	977	1278	3
1961 31A	Transit 4B	7415	.010	32.4	970	1166	2
1959 1A	Vangd 2	8307	.164	32.9	560	3440	3
1965 32A	Beacon C	7512	.025	41.2	973	1365	6
1960 9B	Echo Rock	7977	.010	47.2	1500	1750	3
1962 60A	ANNA 1B	7514	.007	50.1	1080	1213	3
1965 89A	GEOS I	8079	.073	59.4	1153	1690	3
1961 15A	Tran 4A	7323	.008	66.8	880	1038	3
1965 63A	SECOR 5	8165	.080	69.2	1170	2508	1
1964 01A		7306	.004	69.7	938	963	3
1964 64A	Beacon B	7367	.012	79.7	915	1115	4
1966 5A		7422	.024	89.7	893	1260	2
1963 49B	63041	7477	.004	90.0	1108	1150	3
1961 28B	MIDAS	10008	.012	95.9	3500	3873	2
1968 02A	GEOS II	7708	.032	105.8	1084	1576	3

Determining an earth gravitational model from satellite tracking data requires that orbital perturbations resulting from a particular harmonic coefficient be greater than the noise level (observational error) of the tracking data. Computations have been made with current estimates of the coefficients to estimate the magnitude of the perturbations through degree and order 24. The results indicate that most perturbations are less than 10 meters for coefficients from degree 14 through 24 except for the resonance terms. Consequently, if the higher degree and order coefficients are to be determined, extreme precision will be necessary in future tracking data and/or satellites at lower altitudes will be necessary.

Since lower altitude satellites would complicate the problems associated with drag, the satellites would probably have to be drag-free. Adequate surface gravity data to define the higher degree terms provides another approach. Improvements for some of the lower order coefficients could be expected from tracking data on satellites with lower inclinations since 28° is the lowest inclination currently available. The proposed PEOLE satellite ($i = 14°$) could provide data in the void region. There are inclination gaps of approximately 10° in existing sets of data and data from inclinations that would fill these gaps could lead to some improvements.

3. Summary

Geodetic Satellite Program data has proven a necessary and valuable supplementary source for Air Force geodetic satellite projects. The short arc work in South America and the long arc worldwide project would not be feasible without this source of observational information. Future needs for GSP data in the dynamic approach will depend on the availability of data for low altitude and low inclination satellites. The short arc method will be used to position selected sites and data will need to be augmented with observations from the Geodetic Satellite Data Service.

NATIONAL GEODETIC SATELLITE PROGRAM
(NGSP)
STATION SOLUTIONS

BY
A. MANCINI AND L. GAMBINO
Research Associates
Hawaii Institute of Geophysics

J. REECE AND J. RICHARDSON
Geonautics, Incorporated

Prepared for

National Aeronautics and Space Administration

under Contract No. NSR 12-001-055

INTRODUCTION

This paper contains the results of an NGSP geodetic, short-arc solution from optical observations of PAGEOS. The simultaneous, short-arc adjustment produced excellent results.

Observations used in this solution included all BC-4 camera data on the PAGEOS satellite available from the NASA Data Center. The observations were collected from the Phase I sites, Figure 1, and were final reduced by the Coast and Geodetic Survey according to procedures given in Reference 1. The satellite directions are given for each image of the traces in terms of apparent right ascension and declination uncorrected for satellite parallax, phase angle, and aberration. The observational time is given in UT-1 system with corrections applied to refer the time to the adopted longitude of NAD relative to the Naval Observatory. The PAGEOS field work has progressed appreciably beyond the Phase I stage but the data from these other phases have not been deposited at the Data Center.

METHOD OF REDUCTION

The short-arc solutions were obtained by using the NEO-EMBET (N-Epoch Orbital Error Model Best Estimate of Trajectory) approach which was developed by DBA Systems, Inc. [2]. Unlike those data reduction methods where the orbit model is Keplerian or where it is represented by polynomials, the NEO-EMBET technique is carried out in a rectangular, inertial coordinate

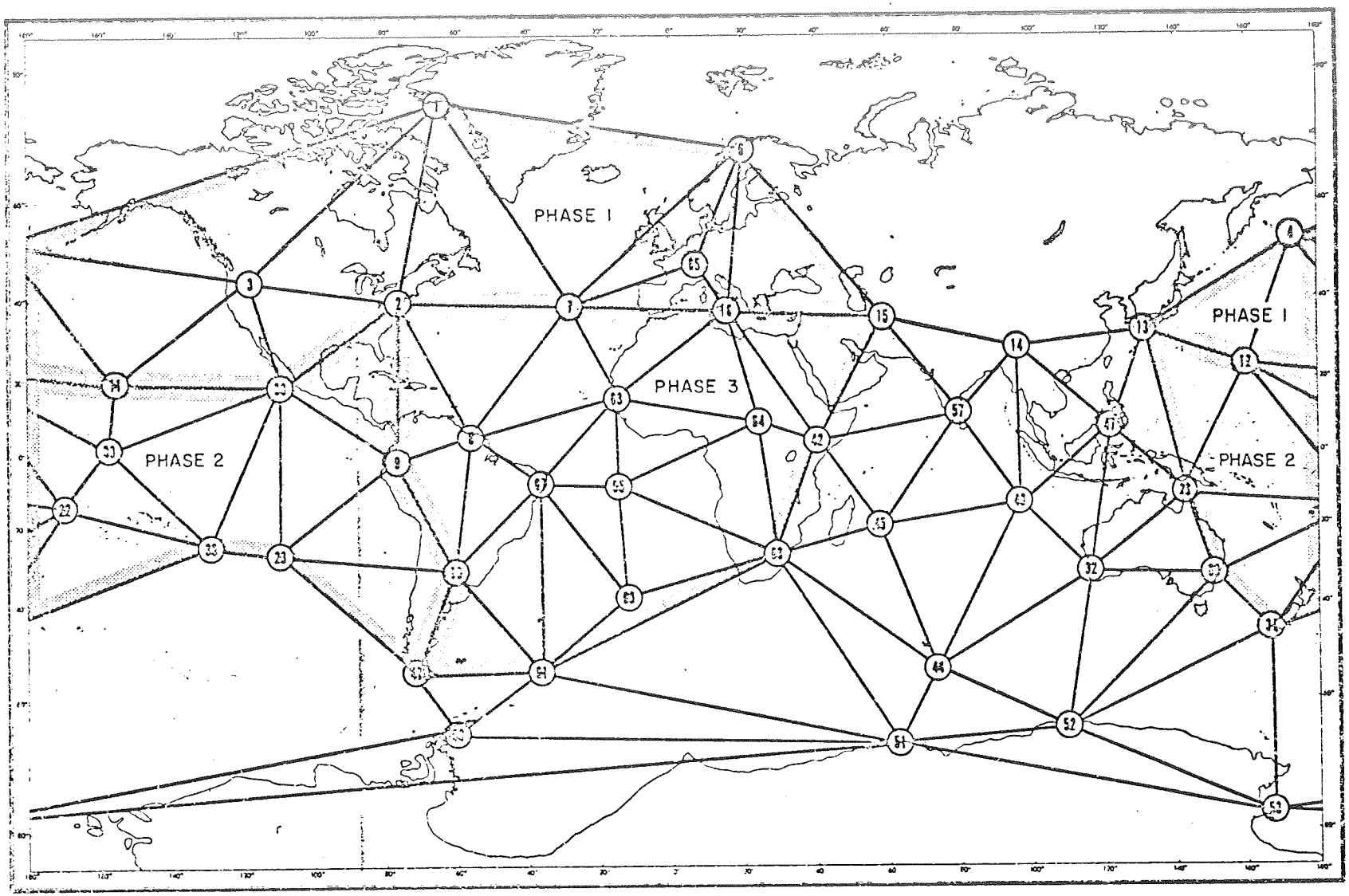

Figure 1

GEOMETRIC SATELLITE NETWORK (PAGEOS)

system resulting in three second order differential equations. The orbital integrator is that developed by Hartwell [3]. Hartwell developed the recursive analytic continuation technique wherein each coefficient of the power series is formed in terms of its predecessor. The series solution to the system of differential equations truncates the gravitational potential at n=7, excluding non-zonal terms. This technique of handling the orbital solution precludes singularities due to small orbital eccentricities and instability due to very short orbits.

NEO-EMBET uses two categories of parameters; namely, the inner loop parameters and the outer loop parameters. In general, the outer loop parameters are those which are common over all satellite passes, and the inner loop parameters are those which change from pass to pass. The coordinates of the observing sites are the most common set of outer loop parameters and the six orbital elements are typical inner loop parameters. A large scale, simultaneous adjustment of inner and outer loop parameters becomes practical by taking advantage of the highly patterned system of normal equations. The inner loop parameters in the normal equation system are 6 X 6 block diagonal matrices.

RESULTS

Starting Coordinates

In order to obtain approximate starting coordinates on an existing earth centered system, the local datum coordinates of the BC-4 net was transformed to the SAO-C7 Geocentric System [6]. The quantities used to

effect the datum shifts were the following:

SAO-C7 = NAD + [X = -26m, Y = 155m, Z = 185m] (1)

SAO-C7 = ED + [X = -92m, Y = -132m, Z = -143m] (2)

SAO-C7 = Old Haw. + [X = 59m, Y = 263m, Z = -203m] (3)

The stations receiving datum shift (1) were Beltsville (6002), Moses Lake (6003), and Shemya (6004); shift (2) was applied to stations Catania, Sicily (6016), Tromso, Norway (6006), and Mashhad, Iran (6015); and shift (3) was applied to station Maui, Hawaii (6011). Stations Thule, Greenland (6001), Gigedo Islands, Mexico (6038), Lajes AFB, Azores (6007), and Wake Island (6012) were either astronomic or map-scaled positions and received no shift to C7. The last station, Hohenpeissenberg, W. Germany, was defined on the Old Bavarian Geodetic Datum and it was shifted by X = 620m, Y = 4m, and Z = 418m, to place it on the SAO-C7 system. The local datum positions and the SAO-C7 starting positions for these stations are given in Tables 1 and 2. The C7 system was further enforced through the following SAO earth constants:

a_e = 6 378 142 m, ellipsoidal semi-major axis,

f^{-1} = 298.255, ellipsoidal flattening,

GM = 3.986009×10^{14} m^3 sec^{-2}, Constant of gravitation times the Earth's mass.

$J_2 = 1082.639 \times 10^{-6}$

$J_3 = -2.565 \times 10^{-6}$

$J_4 = -1.608 \times 10^{-6}$

$J_5 = -0.174 \times 10^{-6}$

$J_6 = 0.542 \times 10^{-6}$

$J_7 = -0.419 \times 10^{-6}$

Zonal coefficients of the Earth's gravitational field.

Initial Orbital Elements

The approximate position and velocity vectors for each orbit was obtained by selecting three simultaneous observations from two stations and geometrically intersecting these points to obtain the X, Y, Z space position of the satellite. One point was taken at the center of the satellite trace and the other two points were taken at the two ends of the shortest arc. The position of the mid-point was used as the position vector of the orbit and differences $\frac{\Delta X}{\Delta t}$, $\frac{\Delta Y}{\Delta t}$, $\frac{\Delta Z}{\Delta t}$, Δt = time increment, were used as average velocities. The station coordinates used for triangulating the orbit were the local datum positions, astros, or map-scaled locations as given in the NASA Station Directory and as shown in Table 1. The approximate orbital elements obtained in this manner were sufficiently well determined as not to require more than two or three iterations before converging to a final set.

TABLE 1

LOCAL COORDINATES OF THE BC-4 PAGEOS SITES

(PHASE 1 STATIONS)

Sta. No.	Sta. Name	Latitude (N)	Longitude	h*(m)	Datum
6001	Thule, Greenland	76° 30' 00".000	291° 27' 30.000E	215/	Astro
6002	Beltsville, Maryland	39 01' 39".003	283 10 26.942E	44/45	NAD-27
6003	Moses Lake, Wash.	47 11 07".132	240 39 48.118E	369/358	NAD-27
6004	Shemya, Alaska	52 42 54".894	174 07 37".870E	35/-9	NAD-27
6006	Tromso, Norway	69 39 44".336	18 56 31.920E	106/	ED
6007	Azores	38 45 36".725	27 05 38.936W	52/-32	Local, Internat
6011	Hawaii; Maui	20 42 38".561	203 44 28.529E	3048/	Old Hawaii
6012	Wake Is.	19 17 23".227	166 36 39.780E	2/	Local Astro, Int.
6015	Mashhad, Iran	36 14 29".527	59 37 42.729E	989/953	ED 1950, Int.
6016	Catania, Italy	37 26 42".628	15 02 47.308E	8/46	ED,Int.
6038	Socorro, Mex.	18 43 44".93	110 57 20.72E	21/-13	Astro.
6065	Peisen, W. Germany	47 48 07".139	11 01 29.507E	943/	Old Bavarian

* h (m): elevations in meters above mean sea level and above the ellipsoid, respectively.

TABLE 2

STARTING COORDINATES

Station	Latitude (N)	Longitude	Altitude (m)
6001 Thule, Greenland	76° 30' 00.00"	291° 27' 30.00"	215
6002* Beltsville, Md.	39 01 39.33	283 10 27.36	10.4
6003* Moses Lake, Wash.	47 11 06.43	240 39 43.43	347
6004* Shemya, Alaska	52 42 50.02	174 07 29.80	78.4
6006* Tromso, Norway	69 39 44.77	18 56 23.14	97.5
6007 Azores	38 45 36.72	332 54 21.06	103.3
6011* Maui, Hawaii	20 42 26.70	203 44 37.66	3059
6012 Wake Island	19 17 23.23	166 36 39.78	23
6015* Mashhad, Iran	36 14 26.00	59 37 43.45	996
6016* Catania, Sicily	37 26 38.54	15 02 43.10	17
6038 Gigedo, Mex.	18 43 44.93	249 02 39.28	-8
6065* Hohenpeissenberg W. Germany	47 48 03.76	11 01 24.01	954

* On the C7 System

Station Sigmas

The starting C7 coordinates of the BC-4 sites were constrained by modest amounts as compared to the actual estimates of station accuracy published by SAO. A priori sigmas of 300 meters in geodetic latitude and longitude and 100 meters in ellipsoidal height were applied to astronomic stations Thule, Azores, Wake Island and Gigedo; 80m in latitude, longitude and height were applied to stations Shemya, Tromso, Maui, Sicily, Mashhad, and Hohenpeissenberg; and 8 meters in the three position components was applied to Moses Lake. Station Beltsville (6002) served as the origin of the network and its coordinates were held fixed at the C7 values. The small sigmas of 8m for Moses Lake were chosen so that they would correspond to a scale of approximately one part in 400,000 between it and the Beltsville station. This scale is compatible with the scale of the orbit provided by GM - 398601 ± 1 km^3 sec^{-2}.

The results of the adjustment proved that the above positional constraints were realistic. Only in two cases did the station corrections exceed one half of the value of the constraint. The exceptions were the astro station Gigedo which moved 399 meters northward and Mashhad which changed by 88m and 83m in geodetic latitude and longitude, respectively.

The observational sigmas were taken as one second of arc.

Adjustment by Short Arcs

The short arc adjustment was generated with essentially no constraint on the orbital elements. The standard deviations of the position and velocity vector of the orbits were set at 10^8 meters in all six

components so that the orbit would adjust freely. Only every other data point of the satellite trace was used in the solution. The solution involved 423 unknowns; 390 orbital elements and 33 station parameters, using approximately 16,250 observations. Table 3 shows the orbits (events), participating stations, and the orbit residuals. Figure 2 shows the station network.

The station corrections relative to the starting C7 coordinates are shown in Table 4 in terms of geodetic latitude, longitude, and height. Aside from the initial astro stations, most of the station movements look fairly good in view of the amount of data available. The standard deviations are a bit smaller than expected but they certainly should not be larger than twice their listed values. One of the more surprising aspects of the results was the uniformity and the relative low sigma values in station height. It had been expected, based on previous geometric solutions and various simulation studies of geometric networks, that these sigmas would be 1.5 to 2 times higher than the sigmas in the latitude and longitude components. As it turned out, the magnitude of σ_h was the same as σ_ϕ and σ_λ - a fact probably attributable to the uniform scale provided by GM over the whole network.

From inspecting Table 4, one can make the following general remarks regarding the adjustment: 1) the movement of station Thule was to be expected in view of its initial map-scaled position, 2) Moses Lake, assigned a σ_ϕ, σ_λ, σ_h of 8 meters, changed consistent with the NAD positional accuracy relative to Beltsville, 3) Shemya's positon on NAD has

TABLE 3

ORBIT RESIDUAL

Orbit	Station	Residuals (RMS) Sec of Arc		Orbit	Station	Residuals (RMS) Sec of Arc	
		RA cos δ	Dec			RA cos δ	Dec
2472	6007	1.6	1.8	2891	6006	1.6	2.4
	6016	1.6	2.2		6016	1.9	2.2
2497	6002	0.9	0.8	2893	6001	1.1	1.8
	6003	1.1	1.2		6002	1.2	1.4
2505	6007	1.8	1.4	2894	6001	1.3	1.8
	6016	1.2	1.4		6011	3.0	2.4
2520	6007	2.0	2.4	2909	6002	1.6	1.6
	6016	1.4	1.8		6007	2.2	2.6
2523	6002	1.1	1.0	2958	6006	1.7	2.4
	6003	1.0	1.4		6016	2.2	2.2
2531	6002	1.6	1.2	3173	6001	1.7	1.8
	6007	1.8	1.8		6003	1.0	1.0
2542	6002	0.8	0.8	3185	6001	1.0	1.6
	6003	1.2	1.2		6003	2.0	1.2
2611	6015	1.6	1.4	3352	6016	1.5	1.6
	6016	1.6	1.8		6065	1.7	1.8
2626	6006	1.6	2.2	3409	6004	2.0	2.6
	6016	1.4	1.8		6012	1.4	1.8
2646	6006	1.3	1.8	3429	6006	1.6	2.4
	6015	2.7	1.8		6065	1.3	1.2
2661	6003	1.2	1.2	3436	6001	1.6	1.4
	6011	2.1	2.2		6006	2.9	2.8
	6012	1.4	1.6	3447	6016	1.4	2.2
2672	6003	1.0	1.2		6065	1.7	1.8
	6011	1.5	1.6	3448	6001	2.2	1.4
2675	6007	1.8	2.2		6006	1.6	2.0
	6016	1.4	1.8	3481	6001	4.2	1.4
2678	6003	1.0	1.8		6006	2.1	2.0
	6011	1.6	2.0	3483	6001	3.5	1.6
2679	6011	1.7	1.8		6004	1.9	2.2
	6012	1.6	1.8		6006	2.2	2.8
2694	6002	1.2	1.2	3488	6004	1.7	1.8
	6007	1.4	1.2		6011	1.9	1.8
2703	6011	2.1	2.2	3535	6001	1.2	1.4
	6012	2.8	3.2		6016	3.1	3.2
2736	6011	2.1	2.4	3538	6001	1.2	1.4
	6012	1.7	2.0		6002	1.2	1.4
2818	6006	1.2	1.4	3539	6002	1.0	0.8
	6016	3.0	2.8		6003	1.0	1.0
2866	6004	1.5	2.0	3545	6015	1.5	1.6
	6012	1.9	1.8		6016	1.8	1.6
2883	6006	1.4	1.8	3560	6001	1.2	1.6
	6007	2.5	2.2		6002	1.2	1.4

TABLE 3

ORBIT RESIDUAL (Continued)

Orbit	Station	Residuals (RMS) Sec of Arc		Orbit	Station	Residuals (RMS) Sec of Arc	
		RA cos δ	Dec			RA cos δ	Dec
3772	6001	1.5	1.6	4259	6002	1.4	1.4
	6065	1.2	1.0		6038	2.4	2.2
3775	6001	1.2	1.4	4267	6002	2.0	1.8
	6004	1.8	1.8		6003	1.0	1.6
3787	6001	1.8	1.6		6038	1.6	1.4
	6002	1.8	1.6	4276	6003	1.5	1.2
3795	6001	1.5	1.6		6038	3.2	2.8
	6003	2.1	1.2	4406	6011	1.4	1.8
3837	6001	1.3	1.6		6038	1.8	1.4
	6003	1.9	1.6				
3939	6006	1.5	1.8				
	6065	1.8	1.4		Average	= 1.7	= 1.8
3978	6003	1.8	1.6				
	6004	2.1	1.4				
4020	6006	1.7	2.0				
	6065	1.2	0.8				
4061	6001	1.7	2.0				
	6003	1.6	1.8				
4083	6006	1.4	1.8				
	6007	4.2	2.8				
4182	6002	1.9	1.2				
	6003	2.5	1.4				
	6038	1.5	2.6				
4196	6003	1.3	1.8				
	6038	2.1	2.2				
4210	6007	2.3	2.2				
	6065	1.3	1.2				
4212	6003	1.0	1.8				
	6011	1.3	2.0				
	6038	2.9	3.2				
4233	6015	1.7	2.0				
	6016	3.0	2.6				
	6065	1.1	0.8				
4236	6002	1.1	1.6				
	6003	1.2	2.6				
4244	6002	1.2	1.4				
	6038	2.4	2.0				
4245	6011	2.8	3.2				
	6038	2.4	2.2				
4251	6001	1.2	1.4				
	6002	1.0	1.2				
	6038	1.9	1.6				

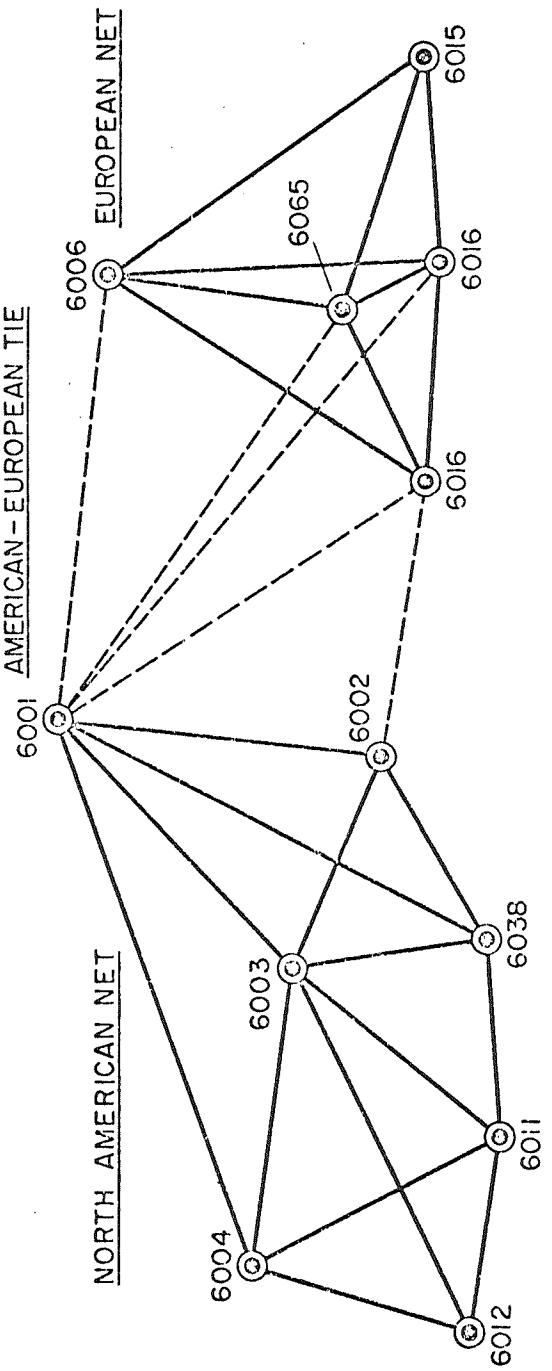

Figure 2

ADJUSTED NETWORK

TABLE 4

CORRECTIONS TO PROVISIONAL COORDINATES

Station No.	Name	Correction (m)	Sigmas (m)
6001	Thule, Greenland	$\Delta\phi$ (m) = 141.8 $\Delta\lambda$ (m) = 176.1 Δh (m) = -26.4	± 8 ± 2 ± 4
6003	Moses Lake, Wash.	$\Delta\phi$ (m) = 5.1 $\Delta\lambda$ (m) = -14.8 Δh (m) = -12.4	± 1 ± 7 ± 3
6004	Shemya, Alaska	$\Delta\phi$ (m) = -57.4 $\Delta\lambda$ (m) = -68.4 Δh (m) = -38.4	± 8 ± 10 ± 9
6006	Tromso, Norway	$\Delta\phi$ (m) = 16.2 $\Delta\lambda$ (m) = 26.7 Δh (m) = 19.5	± 5 ± 10 ± 7
6007	Azores	$\Delta\phi$ (m) = -37.8 $\Delta\lambda$ (m) = 58.8 Δh (m) = 16.3	± 4 ± 9 ± 5
6011	Hawaii	$\Delta\phi$ (m) = 1.1 $\Delta\lambda$ (m) = 0.5 Δh (m) = 24.0	± 7 ± 10 ± 9
6012	Wake Island	$\Delta\phi$ (m) = 152.6 $\Delta\lambda$ (m) = 1.2 Δh (m) = -4.6	± 10 ± 9 ± 15
6015	Mashhad	$\Delta\phi$ (m) = -83.3 $\Delta\lambda$ (m) = 88.1 Δh (m) = 5.0	± 12 ± 9 ± 15
6016	Catania, Sicily	$\Delta\phi$ (m) = -19.5 $\Delta\lambda$ (m) = 0.2 Δh (m) = 24.9	± 8 ± 10 ± 10
6038	Gigedo	$\Delta\phi$ (m) = 399.2 $\Delta\lambda$ (m) = 49.6 Δh (m) = 12.3	± 5 ± 5 ± 4
6065	Peisen, Germany	$\Delta\phi$ (m) = -26.0 $\Delta\lambda$ (m) = -8.1 Δh (m) = -4.3	± 7 ± 10 ± 8

never been considered more accurate than 50 meters in its horizontal position, consequently a shift Δ_ϕ = -57m, $\Delta\lambda$ = -68m, and Δh = -38 should be expected, 4) the shift to Tromso are essentially within the estimated accuracy of the SAO-C7 system, 5) Azores is an astro and its geodetic shift is difficult to estimate but the values listed are acceptable, 6) Hawaii is definitely within the C7 uncertainties, 7) Wake is an astro and its corrections look valid, 8) Mashhad's corrections appear large based on our present knowledge of the ED extension to that area, 9) station movements for Catania and Hohenpeissenberg are of the order expected, and 10) Gigedo is an astro and could well receive a shift of $\Delta\phi$ = 399m, $\Delta\lambda$ = 50m and Δh = 12m.

The final positions of the solution are listed in Table 5.

Orbit Residuals

Table 3 shows the root mean square (RMS), about the mean of the residuals for each orbit in the adjustment. The average RMS from all entries in this Table is 1.7 arc sec in right ascension and 1.8 arc sec in declinations. These values are almost identical to the results obtained from earlier work which involved the representation of the PAGEOS traces by orthogonal polynomials. The RMS of this work averaged 1.7" and 1.6" in right ascension and declination, respectively. The slight RMS difference in declination, (1.8" - 1.6" = 0.2"), between the orbit residuals and the polynomial fit is probably due to the larger number of orbits used in obtaining the mean RMS from the polynomial results.

TABLE 5

FINAL COORDINATES OF SHORT ARC ORBITAL ADJUSTMENT

(a_e = 6 378 142, f^{-1} = 298.255)

Station	φ (N) / X (m)	λ (E) / Y (m)	h (m) / Z (m)
6001	76° 30' 04.73" 546 554m	291° 27' 54.43" -1 389 990m	188.6 6 180 202m
6002*	39 01 39.33 1 130 773	283 10 27.36 -4 830 833	10.4 3 994 706
6003	47 11 06.60 -2 127 831	240 39 42.70 -3 785 842	334.6 4 656 029
6004	52 42 48.11 -3 851 788	174 07 26.04 396 420	40.0 5 051 319
6006	69 39 45.31 2 102 913	18 56 25.69 721 648	78.0 5 958 139
6007	38 45 35.46 4 433 660	332 54 23.57 -2 268 179	119.6 3 971 641
6011	20 42 26.71 -5 465 988	203 44 37.69 -2 404 386	3035.0 2 242 199
6012	19 17 28.32 -5 858 557	166 36 39.79 1 394 511	18.4 2 093 808
6015	36 14 23.22 2 604 337	59 37 47.09 4 444 269	1001.0 3 750 279
6016	37 26 37.89 4 896 430	15 02 43.10 1 316 145	41.9 3 856 647
6038	18 43 58.24 -2 160 983	249 02 41.02 -5 642 717	4.3 2 035 369
6065	47 48 02.89 4 213 588	11 01 24.01 820 820	949.7 4 702 735

* 6002 Beltsville, was held fixed on the SAO, C7 System; the shifts applied for North American Datum to C7 system were:

X (C7) = X (NAD) - 26m

Y (C7) = Y (NAD) + 155m

Z (C7) = Z (NAD) + 185m

Table 6 shows the residuals of Table 3 grouped according to observing stations and camera systems; the 300mm FL and 450mm FL camera. Notable in this table are the slightly larger mean RMS for the BC-4-300 system. The average RMS for each camera is:

BC-4-450: R.A. cos δ = 1.6", Dec = 1.6"

BC-4-300: R.A. cos δ - 2.0", Dec = 2.1"

These RMS' are within 0.1 arc seconds of the corresponding mean from the Orthogonal Polynomial fit.

Correlation

Statistics on each orbit resulting from the short arc solution are too voluminous to include in this paper; however, the overall results can be adequately illustrated by two orbits (Tables 7, 8, and 9).

Orbit 4236 in these tables shows appreciably larger sigmas and a higher degree of correlation than orbit 2472. If we also look at Table 10 we note that orbit 2472 represents a fairly strong geometric situation. Both satellite traces are fairly long, both traces are about the same length, and the excursion in elevation angle is also good from both observing stations.

It can also be seen from Table 10 that orbit 4236 has a less amount of observational overlap and shorter range in elevation angles. These conditions lead to higher correlation among certain orbital parameters than we had for orbit 2472. Orbit 4236 represents the extreme case of correlation rather than a representative case. The correlation matrices for most of the orbits are very similar to the results of orbit 2472, Table 8.

TABLE 6

ORBIT RESIDUALS GROUPED ACCORDING TO STATIONS

Total Orbits Observed	Station	(Sec.) RA x cos δ	(Sec.) Dec	Camera F.L.
18	6001	1.7	1.6	450
17	6002	1.3	1.3	450
19	6003	1.4	1.5	450
6	6004	1.8	2.0	450
14	6006	1.7	2.1	450
10	6007	2.2	2.1	300
11	6011	2.0	2.1	300
6	6012	1.8	2.0	300
4	6015	1.9	1.7	300
14	6016	1.9	2.1	300
10	6038	2.2	2.2	300
7	6065	1.4	1.3	450

TABLE 7
ORBITAL SIGMAS
(Meters and Meters/Sec.)

Orbit Elements / Orbit No.	X	Y	Z	$\dot{X}$	$\dot{Y}$	$\dot{Z}$	σ_x	σ_y	σ_z	$\sigma_{\dot{x}}$	$\sigma_{\dot{y}}$	$\sigma_{\dot{z}}$
2472	7049830	4385083	8392169	-4386	- 902	3783	2	1	4	.02	.01	.04
4236	305782	-9707089	4194090	- 213	-3065	-5310	20	113	8	.17	.94	.08

TABLE 8
CORRELATION MATRIX: ORBIT 2472
Stations 6007, 6016

	X	Y	Z	$\dot{X}$	$\dot{Y}$	$\dot{Z}$
X	1	.4	.6	-.3	-.2	-.1
Y		1	.3	-.2	-.4	-.1
Z			1	-.2	-.1	-.2
$\dot{X}$				1	.4	.5
$\dot{Y}$					1	.3
$\dot{Z}$						1

TABLE 9

CORRELATION MATRIX: ORBIT 4236

Stations 6002, 6003

	X	Y	Z	$\dot{X}$	$\dot{Y}$	$\dot{Z}$
X	1	-.96	-.72	.97	.94	-.41
Y		1	-.75	.90	.99	-.44
Z			1	-.68	-.74	-.80
$\dot{X}$				1	.87	-.38
$\dot{Y}$					1	-.46
$\dot{Z}$						1

TABLE 10

ORBITAL SPAN

Orbit	Station	Time (Sec.)			DECLINATION Angles (Deg.)		
		Start	End	Span	Start	End	Span
2472	6007	290	685	394	34	53	19
	6016	332	652	320	53	74	21
4236	6002	12875	13004	129	9	1	8
	6003	12842	12891	49	2	0	2

Comparison of Results

Since the final positions of the short-arc solution should represent geocentric coordinates, it is desirable to check its values with another set also derived by the dynamic method. The two stations to be compared below are two nearby stations of the TRANET and PAGEOS net; the TRANET station coordinates having been solved for by NWL, reference [4]. The local survey information tying the stations is available from the NASA Station Directory so that the position of the PAGEOS site can be reconstructed from the TRANET station.

The comparison for stations Hawaii (6011) and Shemya (6004), with respect to the NWL results, reference [4], are as follows:

6011, Hawaii, (NWL & BC-4 Comparison)

	Latitude (N)	Longitude (E)	Height (m)
NWL Position (7100), C7	21° 31' 15.49"	202° 00' 09.04	405
Local Survey	- 48 48.30	1 44 27.92	--
Position of 6011	20 42 27.19	203 44 36.96	--
Short Arc Solution	26.71	37.69	3035
Difference	0.48"	-0.73"	--
Difference (m)	12m	-20m	--

6004, Shemya, (NWL & BC-4 Comparison)

	Latitude (N)	Longitude (E)	Height (m)
NWL Position (7739), C7	52 42 55.37	174 06 38.46	46
Local Survey	-6.63	46.44	-4
Position of 6004	52 42 48.74	174 07 24.90	42
Short Arc Solution	48.11	26.04	40
Difference	0.63	-1.14"	2m
Difference (m)	18m	-17m	2m

The agreement with the NWL solution is quite good inasmuch as the NWL estimated accuracy for Hawaii and Shemya are 15m and 25m, respectively.

A more direct comparison can be made with respect to an OSU solution, reference [5], which also employed the short-arc method in the adjustment and also used BC-4 PAGEOS data. The OSU solution held the Beltsville station as the origin of its triangulation and solved for the coordinates of three other stations (6003, 6001, 6038) on the C5 system.

After converting the OSU C5 coordinates to the C7 a_e = 6378 142 and f (inverse) = 298.255, the agreement for station Gigedo (6038) is as follows:

OSU	18° 43' 58.43"	249° 02' 41.38"	19m
Short-Arc	18 43 58.24	249 02 41.02	4m
Difference	0.19	0.36	15m
Difference (m)	6m	10m	15m

In view of the fact that the scale of the OSU solution was provided by the chord distance between 6002 and 6003 as derived from their NAD coordinates, the agreement is as good as can be expected.

As an additional test for consistency, the twelve BC-4 station coordinates were also used in a least squares solution to compute the ellipsoidal semi-major axis, a_e, and the semi-minor axis, b_e. This was accomplished by computing the total geocentric radius for each station, subtracting the mean sea-level height from it, and fitting the resulting X,Y,Z coordinates at mean sea-level to the standard ellipsoidal expression. As expected, the results for both a_e and b_e were not very good, the flattening computing to 1/297.60 with a correlation between a_e and b_e of 0.7. However,

when the flattening was inforced to 1/298.255, the resulting semi-major axis was a_e = 6378 141 meters.

A value of a_e = 6378 141.5m was achieved when the Baker-Nunn stations on page 87 of reference [6], were added to the solution with the BC-4 positions.

SUMMARY

The coordinates of the BC-4 (phase I) sites from the short arc solution are determined to an average standard deviation of ±8 meters in each positional component based on the assumption that each satellite direction was good to 1 sec of arc and by using every other data point of each trace. If a mean observational sigma of 1.7 sec in both right ascension and declination had been used (as suggested by the RMS of the station residuals) the resulting sigma in position would have been about ±12 meters. The 12m also appears to be a more realistic value from comparisons with Doppler at stations Hawaii and Shemya which show an agreement of 14 meters in each coordinate, and the comparison with OSU for Gigedo is also within the 12 meter value. Based on these comparisons and for reasons given below, it is felt than an accuracy of ±15 meters is a valid estimate for the final coordinates. Future large-scale determinations incorporating more PAGEOS stations and more data should improve this accuracy by a factor of two.

The station corrections resulting from the short arcs (Table 4) are all realistic except for stations Shemya, 6004 and Mashhad, 6015. Since

the comparison of Shemya with the Doppler solution is in good agreement, the magnitude of the corrections must be due to a weak geodetic connection of that area relative to NAD and hence to C7. The large corrections for Mashhad, however, cannot be attributed to a similar cause. The fact that this station is at the edge of the triangulation network tends to suggest this as a possible cause but the results for other outlying stations do not confirm it.

The final coordinates of the BC-4 stations (Table 5), including those for Mashhad, were used to compute an equatorial radius by removing the mean sea level heights from each geocentric radii and enforcing a meridional flattening of 1/298.255. The results of that computation produced an earth radius of 6378 141m. A similar solution using the C7 coordinates of the Baker-Nunn sites with the BC-4 stations produced a radius of 637 142m. As expected, a computation of both axes, equatorial and polar, produced inferior results due to the small number and distribution of these stations.

REFERENCES

1. Butler, L.M. — Computer Program for Single Camera Orientation, B.R.L. Report No. 1268, December 1964.

2. Brown, D.C. — Advanced Techniques for the Reduction of Geodetic SECOR Observations, D. Brown Associates, Inc., July 29, 1966.

3. Hartwell, J.G. — A Power Series Solution for the Motion of an Artificial Satellite and its Concomitant Variational Equations, D. Brown Associates, Inc., April 16, 1968.

4. Anderle, R.J. and Smith, S.J. — NWL-8 Geodetic Parameters Based on Doppler Satellite Observations, NWL Report No. 2106, July, 1967.

5. Schwarz, C.R. — The Use of Short Arc Orbital Constraints in the Adjustment of Geodetic Satellite Data, OSU Department of Geodetic Sciences Report No. 118, 1969.

6. Gaposchkin, E.M. — Dynamical Determination of Station Locations Using GEOS-I Data published in Geodetic Satellite Results During 1967, SAO Special Report 264 Ed. by C.A. Lundquist, December 1967.

DATA ACQUISITION WITH THE PC-1000 CAMERA SYSTEM

N. R. Goff
1st Geodetic Survey Squadron
F. E. Warren AFB Wy. 82001

Prepared for
GEOS-2 Review Conference

June 22-24, 1970

DATA ACQUISITION WITH THE PC-1000 CAMERA SYSTEM

N.R. Goff

INTRODUCTION:

The development of optical satellite triangulation camera systems grew out of work with ballistic cameras which were used to study missile trajectories during the 1950's. With the coming of the satellite age in the late 50's, the basic theory had been developed to use satellites photographed against a star background, for geodetic positioning.

The first data were collected by photographing an active (flashing light) satellite against a star background. This required photographing stars before and after each satellite event to orient the camera direction precisely.

ANNA 1B was the first successful active optical satellite. The optical beacon consisted of two pairs of Xenom-filled stroboscopic lamps with reflectors. An emergency manual over-ride system (EMOS) was used to trigger the lamps throughout most of ANNA's life. Five flashes were produced about 5 seconds apart having a duration of 1.2 milliseconds, and a light output of 8800 candle seconds.

GEOS B, which was a follow-on active satellite, is still operable although two of its lights are dead. Even with this limitation, successful missions were being executed up until its shutdown, due to funds shortage, in early January of this year (1970).

The next generation of geodetic satellite was the passive (sun illuminated) variety of which ECHO I, ECHO II, and PAGEOS are examples. The camera shutter was opened and closed very rapidly to chop the satellite trail and provide point images of the satellite. This technique required basic changes in camera shutters and timing.

The first PC-1000 camera system, had the electronic camera control and timing equipment housed in a van and the camera installed some distance away. The electronics system, compared to today's standards, was extremely primitive. Shutter programming was done by a rotating aluminum disk, that could not be readily changed to alter the program sequence. Timing was done by electro-mechanical clocks with a drift rate of 4 to 5 milliseconds per hour. Timing accuracies and shutters in this system were not adequate to collect geodetic quality data from passive satellites.

The second generation system, called MOD II, was then developed. This system had several improvements over the MOD I. The timekeeping portion of the system was improved so that time could be kept to one part in 10^{10}. The system, however, still lacked the chopping shutter required to record geodetic data from passive satellites.

The next improvements, MOD III, were made to incorporate better time recording, better shuttering and lighter weight. The first MOD III systems were more portable, more automatic, more accurate and had the first passive satellite capability. Later an internal shopping shutter was incorporated to allow even more and faster data collection.

It is relevant to note that the only component of the system not changed was the camera itself.

The lens used is the F5 40 inch Baker lens developed by Dr. James Baker of Harvard University in the early 1940's. This lens was developed for high altitude reconnaissance use. It was developed to be distortionless. By the standard of that day it was the most nearly perfect lens, metrically, of its time. And, although numerous lens manufacturers have been contacted, a better lens has not been found.

CAMERA CALIBRATION:

The various lens distortion characteristics necessary for accurate data reduction are precisely computed from calibration plates shot for this purpose. Comparison studies of lens distortion values over long periods show that the PC-1000 is very stable. This stability, plus the narrow field of view of the camera, make daily calibrations unnecessary. When a camera is first moved to an operational location, zenith plates are taken for a camera calibration. To insure continuing accuracy of the derived lens distortion values, calibration is repeated on site once per month. It is also done each time the camera is moved to a new location or disassembled for maintenance. Shutter calibration of the internal shutter is necessary for data reduction. Photo diodes are placed behind each shutter to record the first light of opening and the full opening point. These times are recorded on a visicorder and used to determine the delays that are encountered relative to electronic indicated times. The tolerance for these calibrations presently is $\pm$50 microseconds.

SITE LAYOUT:

Prior to deployment of a stellar camera in the field, a reconnaissance team of staff officers visits the area to be occupied. This team selects the best available camera site location based on weather conditions, on criteria established in DOD "Guidelines for Geodetic Satellites Programs", and in the case of South Vietnam, on security.

PAD CONSTRUCTION:

Site layout is determined by the recon team and arrangements are made for pad construction, connection to power, and geodetic survey connection to local control.

CONEXES:

In Vietnam, protection of the electronic equipment was sometimes provided by a CONEX container and sand bags.

COMPLETED PAD:

A General Reconnaissance Information Report is prepared by the recon team immediately following the reconnaissance and forwarded to the Geodetic Satellite Records Center.

A camera team consists of three-man military personnel including a ground power specialist, an electronics specialist, and a precision photographic repair specialist. The team has the capability to operate, maintain and perform minor repair in the field. The team members have technical school training in their individual specialties prior to assignment to the 1st Geodetic Survey Squadron. Extensive training was given prior to deployment to familiarize the personnel with the camera and timing systems of the MOD III and to mold the team into a fast efficient unit capable of meeting the demands of an all-night, 7-day schedule. The personnel are given specific practice missions to execute. The procedures are repeated until they are able to perform efficiently with active and passive shots, and also with rapid swing shots. The teams are schooled in record keeping, communications, plate handling, equipment set up, and calibration plate execution.

TIMEKEEPING:

The components of the MOD III timekeeping system are:

The WWV receiver
The Loran C receiver
The VLF receiver (including a phase comparator chart recorder)
Frequency standard
Divider and display
Printer

These devices are used to monitor the drift of an on-site oscillator. Dividers in the system allow the frequency to be related to real time for mission timing.

The printer allows the printout of UTC time of shutter function during the mission. In addition to the above components, a portable cesium beam atomic clock is transported to each site on a four to six-week basis to insure correct time.

LOOK ANGLES:

Look angles are received at the 1st Geodetic Survey Squadron which Squadron selects specific look angles from these data to permit intervisible observations at two or more stations. In selecting these look angles, the following criteria are used: The image size must be large enough to be "seen"; the sun's elevation must be negative at least 15 degrees (i.e., 15° below the station's horizon). Elevation angles must be greater than 30°; the satellite must be between the two intervisible stations. In addition, the sun must be in proper position for passive satellite reflection and the moon must be out of the field of view of camera. Strict quality control effort is exerted to assure accuracy of look angle numbers used. Every number sent to a field team is repeated three times as a check. The selected look angle data is sent by message with voice radio and telephone communications used as a backup. Ordinarily, messages are sent once a week. There are times when the look angle runs are received late. To insure no break in observations when this occurs, updates of the previous week's look angles are made and sent to the teams, followed as soon as possible by the new data.

MISSION PLATE:

The actual observation program (pre-calibration - event - post-calibration) has been well standardized for each satellite to give optimum results on the plates. The selected program is preset in the camera control unit which, when activated, executes the entire program without further adjustments. For the

pre-calibration, the internal shutter is open for two sets of the following intervals: 4 seconds, 2 seconds, 1 second, .7 second, .3 second. The internal shutter is then left open for the event while the satellite flashes. The internal shutter is then used to perform two sets of post-calibration observations similar to the pre-calibrations.

A passive satellite observation is identical except that during the event time the internal shutter chops with 30 milliseconds open, 470 milliseconds closed, for approximately one minute.

MULTIPLE SHOTS:

The team is capable of performing multiple observations on a single satellite. That is, the teams are trained to swing the camera and photograph the same satellite up to five times on a single pass thereby multiplying the data collected. It is possible to swing the camera, reload, and shoot again with 1 1/2 minutes between the last post-calibration and the next pre-calibration, with only five or six minutes between actual events. This multiple shot capability greatly increases the amount of data collection possible with the PC-1000.

DATA PROCESSING:

The entire record of a stellar camera system consists of a 9-inch x 9-inch glass photographic negative with its associated timing record. The loss of either renders the data useless. The processing, therefore, must be done very carefully to preserve this record. After the plate has been exposed, it is sent to the 1st Geodetic Survey Squadron for processing and evaluation along with the corresponding time record. The photographic plate is processed and evaluated under strict laboratory conditions by a highly trained civilian photographic specialist at the 1st Geodetic Survey Squadron at F.E. Warren AFB, WY. In early stellar

camera operations, the teams processed their plates in the field. However, we have found that with central plate processing now used, improved quality of data can be obtained with no loss in operational efficiency and with considerable reduction in weight of the camera system. The development of the plate at the home station is rigidly controlled to get maximum data. Stars are identified, satellites are located, and detailed records are kept for later reference. If camera problems are identified in this process and satellite difficulties are detected (such as PAGEOS elongation and GEOS light problems), observation teams and data reducers in the field are, of course, immediately notified. In addition to plates, timing tapes are also processed at the 1st Geodetic Survey Squadron. The required corrections, such as shutter calibration, time drift rate, propagation delay, and polar motion are added to the raw times to adjust to Universal Time (UT-1). This time is corrected to mid-event time in UT-1 and this time and the corresponding plate are supplied to ACIC for use in data reduction. A quality control method which uses a triple check system insures that data is correct before being released. From this point on, ACIC reduces the data to obtain geodetic positions. Data reduction techniques along with final computational results will be covered by ACIC in their presentation which will follow.

GEOCEIVER AS A RANGING SYSTEM

By

Duane C. Brown
DBA Systems, Inc.
Melbourne, Florida

Presented at the GEOS-2 Review Conference held at
Goddard Space Flight Center, Greenbelt, Maryland,
June 22-24, 1970

Geoceiver as a Range Measuring System

ABSTRACT

As originally conceived, the Geoceiver was regarded as providing a measure of the change in slant range over preset readout intervals of nominally one minute. However, by virtue of the strict continuity of its cycle counting process, the Geoceiver may alternatively be viewed as providing a measure of the change in range from the original initiation of cycle counting to the time of readout of each cycle count. The conventional view leads to range-difference observational equations involving unknown parameters consisting of the coordinates of the tracking station and the frequency offset of each pass. The alternative view leads to ranging observational equations involving an additional unknown parameter for each pass consisting of the range of the satellite at the initiation of cycle counting. The ranging approach must also taken into account as constrained parameters such effects as: drifts in satellite and Geoceiver frequencies, the bias in the adopted value of the satellite frequency, and residual tropospheric refraction (these effects can be neglected over the short intervals involved in the range-difference approach). Despite the greater complexity of its error model, the ranging approach is of such geometrical superiority that it can recover coordinates of tracking stations to a much greater accuracy than can the range-difference approach. In fact, if $2n+1$ denotes the typical number of readouts per pass, the ranging approach can potentially generate coordinates having standard deviations only about $3/n^2$ as large as those resulting from the range-difference approach. Reduction of a set of 14 passes of a U.S. Navy navigational satellite observed by a prototype Geoceiver not only establishes the technical soundness of treating Geoceiver as a ranging system but also demonstrates that the standard deviation of Geoceiver ranging observations is on the order of 0.10 meter. Numerical simulations employing this figure indicate that when the ranging approach is adopted, a strong short arc net of Geoceivers operating over a period of only two days can be expected to recover coordinates of participating stations to within a few tenths of a meter over regions of continental extent.

GEOCEIVER AS A RANGING SYSTEM [1]

By

Duane C. Brown

1. Introduction

In 1965 the development of a new doppler tracking system specifically optimized for geodetic applications was formally proposed to the US Navy by APL. The proposed system, the Geoceiver, was designed to be fully as accurate as the TRANET system, but physically was to be far more compact. Instead of requiring a sizable van and diesel generator, the Geoceiver was to be hand-portable (capable of being carried on a commercial airliner as ordinary luggage) and was to consume only about 80 watts of electricity. Stansell, et. al. (1965) describes the physical characteristics of the Geoceiver in considerable detail (the artist's concept of the Geoceiver shown in Figure 1 below is taken from this reference).

In December 1968, a breadboard unit and a prototype unit of the Geoceiver were successfully tested at APL over a two week period during which scores of passes of Navy Navigational Satellites were tracked. A co-located TRANET system and an AN/SRN-9 Doppler Receiver also participated in the test. Results from the reduction of the test are reported by Smith (1969). Smith concluded that "the Geoceivers were shown to be able to consistently produce position solutions of a quality comparable to the TRANET doppler Stations." It is noteworthy that this conclusion was reached despite the fact that the data rate of the Geoceiver (one readout per minute) was only one fifteenth that of the TRANET system (one readout per four seconds).

As a consequence of the successful testing of the Geoceiver, the Department of Defense placed an order with Magnavox Corporation to manufacture a total of 33 Geoceivers with delivery to begin by early 1971. Of these, most are to be assigned to the Navy, and the remainder to the Air Force and to the Army.

Intrigued by the potential of the Geoceiver and anticipating its successful development, we at DBA Systems submitted in early 1966 an unsolicited proposal to AFCRL to develop a

---

(1) This work was supported by Air Force Cambridge Research Laboratories under Contract F19628-69-C-0264, Mr. George Hadgigeorge, contract monitor.

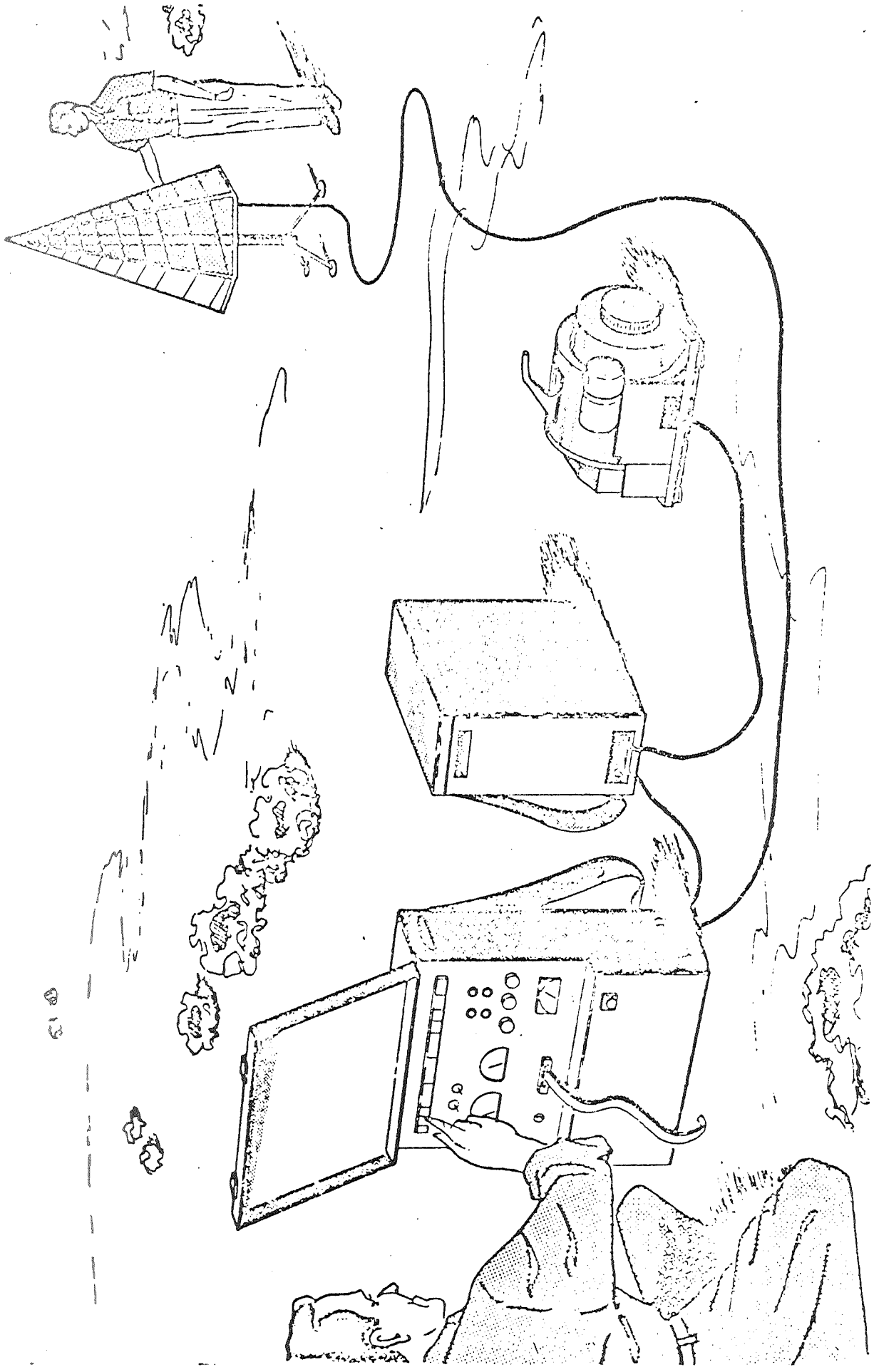

FIGURE 1. Conceptual drawing of Geoceiver station (from Stansell, et. al., 1965).

computer program optimized for short arc geodetic reductions with especial emphasis being placed on the processing of the then-yet-to-be-developed Geoceiver. This proposal resulted in a contract award in September 1967, and the computer program SAGA (Short Arc Geodetic Adjustment) was delivered in February 1969 (Brown, Trotter, 1969). It was not until late 1969, however, that actual Geoceiver observations from the December 1968 test, referred to above, were made available to DBA by NWL (through AFCRL) for experimental processing through SAGA.

In this paper we shall review the results of the SAGA reductions and shall consider their implications to space geodesy — implications that may well be profound.

2. Geoceiver Observational Equations

The measurements made by Geoceiver are best explained with the aid of Figure 2 which is taken from Brown, Trotter (1969). Plotted in the figure are cycles of beat frequency

$$(1) \qquad \Delta f = f_o' - f$$

which are generated when the frequency f received from the satellite is subtracted from the frequency f_o' generated locally by the Geoceiver oscillator. The output of the Geoceiver consists of cycle counts of beat frequency defined thusly:

$$(2) \qquad \Delta N_j = \int_{\tau_{j-1}}^{\tau_j} \Delta f \, dt$$

in which τ_{j-1} and τ_j represent the times of the first positive cycle crossings following successive triggering marks T_{j-1} and T_j as shown in Figure 2. The triggering marks may either be internally generated by the digital clock of the Geoceiver or else they may be recovered from the timing words impressed on the satellite signal. The latter mode makes possible the determination of the absolute timing offset of the local Geoceiver clock with respect to the master satellite clock to an accuracy of about 50 microseconds (one sigma). In the prototype Geoceiver triggering marks occur at one minute intervals (an option for a 30 second interval will be provided in the production models).

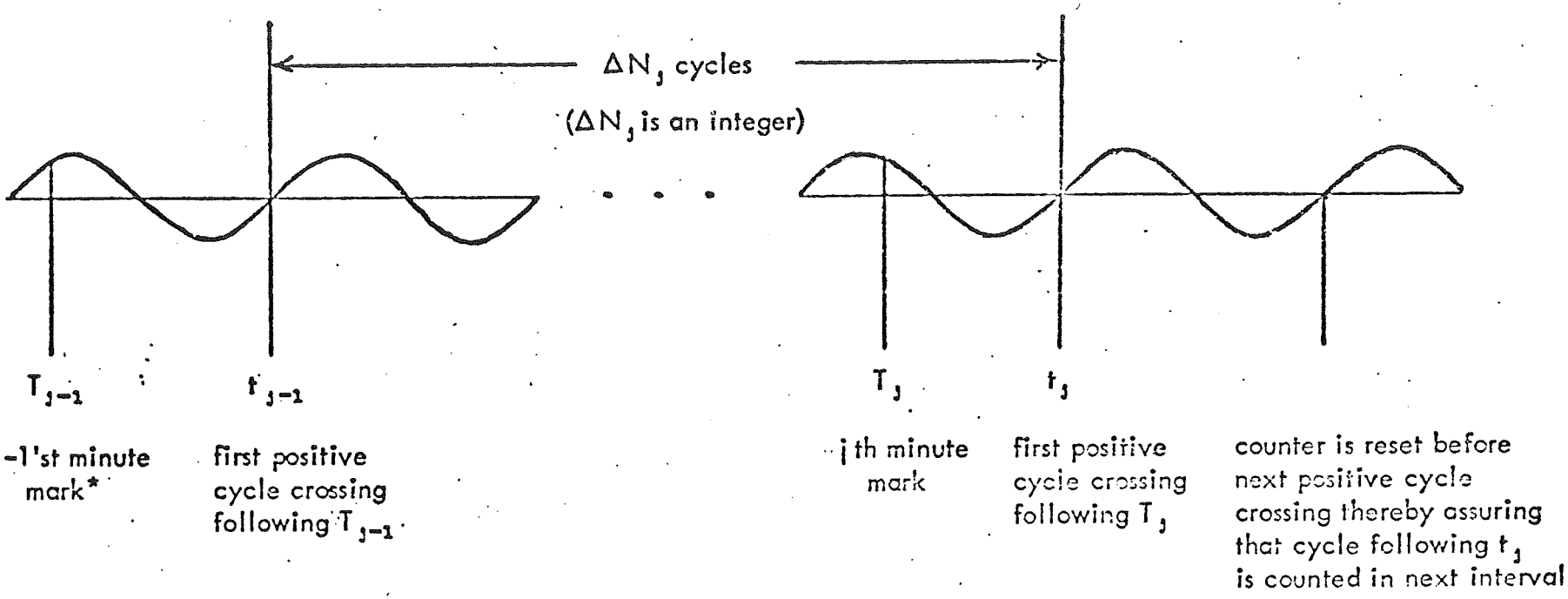

*NOTE: When Transit satellites are tracked, one minute marks for triggering readout are generated by interpolation within the standard two minute synchronization words impressed on the received signal; otherwise, one minute marks are generated internally.

FIGURE 2. Illustrating method used by Geoceiver to obtain continuous count of cycles of beat frequency.

An important point made clear in Figure 2 is that strict continuity of cycle count is maintained by the Geoceiver, for, following readout, the counter is reset to zero before the first positive cycle crossing of the next interval can occur. Accordingly, each and every cycle of beat frequency is counted and the cycle count ΔN_j, being an integer, may be viewed as flawless when the Geoceiver is functioning properly. The quantities actually subject to error are the times τ_{j-1}, τ_j defining the beginning and end of each counting interval.

By virtue of the continuity of cycle count, it becomes admissible to write:

$$(3) \quad N_j = \int_0^{\tau_j} \Delta f \, dt = \int_0^{\tau_1} \Delta f \, dt + \int_{\tau_1}^{\tau_2} \Delta f \, dt + \ldots + \int_{\tau_{j-1}}^{\tau_j} \Delta f \, dt$$

$$= \Delta N_1 + \Delta N_2 + \ldots + \Delta N_j = N_{j-1} + \Delta N_j .$$

That is, the total cycle count from the original initiation of counting ($\tau=0$) to the end of the j th counting interval ($\tau=\tau_j$) can be recovered simply by the addition of all cycle counts up to and including the j th count. One might expect from (3) that errors in successive N_j would be highly correlated by virtue of being formed from common ΔN's. This is not the case, however, when Geoceiver is functioning properly (i.e., no actual cycles are dropped from each count nor are any spurious cycles added to each count), for the ΔN_j, being whole numbers, are free of error. So too, then, are the cumulative cycle counts N_j. As we have already indicated, the quantity actually in error is the time τ_j associated with the cumulative count N_j. There is no reason to expect that errors in successive readouts τ_j, τ_{j-1} will be correlated to any significant degree.

If we ignore relativistic considerations, we may relate the measurements N_j, τ_j made by Geoceiver to physical properties of the satellite trajectory by means of the simple form of the doppler equation,

$$(4) \quad \dot{r} = c \, \frac{f_o - f}{f_o}$$

in which

$\dot{r}$ = $dr/d\tau$ = rate of change of range between satellite and tracking station at time τ,

f_0 = frequency transmitted from satellite,

f = frequency received at station at time τ,

c = velocity of light in vacuo.

Let us further define:

f_0' = reference frequency generated by Geoceiver,

λ = c/f_0 = wave length of frequency transmitted from satellite,

Δf = $f_0' - f$ = beat frequency between received frequency and local reference frequency.

Then the doppler equation can be expressed in the form:

(5) $\dot{r} = \lambda[(f_0' - f) + (f_0 - f_0')] = \lambda[\Delta f + (f_0 - f_0')]$.

Let us momentarily assume that f_0 and f_0' are constant over the tracking interval. Then we can integrate both sides of (5) between the start of cycle counting $\tau = 0$ and the end of the jth counting interval τ_j to obtain:

(6) $r_j - r_0 = \lambda N_j + \lambda (f_0' - f_0)\tau_j$

in which N_j is as defined in equation (3) and

r_j = range at time $\tau = \tau_j$,

r_0 = range at time $\tau = 0$.

Equation (6) may be viewed as a simplified form of the observational equation relating Geoceiver observations to changes in the range between tracking station and satellite. In practice one must give consideration to the fact that the frequencies f_0 and f_0' are neither perfectly known, nor are they perfectly stable. This can be accounted for by expressing f_0

and f'_0 as:

$$f_0 = f_\infty + \delta f_0 + \dot{f}_0 \tau$$

(7)

$$f'_0 = f'_\infty + \delta f'_0 + \dot{f}'_0 \tau$$

in which

f_∞, f'_∞ = adopted values of satellite and Geoceiver frequencies,

δf_0, $\delta f'_0$ = biases in f_∞ and f'_∞ at $\tau = 0$ (initiation of cycle counting),

$\dot{f}_0$, $\dot{f}'_0$ = drift rates of f_0 and f'_0.

When these expressions are substituted into equation (5), both sides are integrated over the interval $(0, \tau_j)$, and other sources of error are taken into account, the basic observational equation for Geoceiver assumes the form derived in Brown, Trotter (1969):

$$(8) \quad r_j = \lambda_0 (N_j - \Delta f_\infty \tau_j) + a_0 + a_1 \left(1 + \frac{\dot{r}_j}{c}\right) \tau_j + a_2 \tau_j^2$$

$$+ a_3 (r_j - \dot{r}_j \tau_j) + a_4 \dot{r}_j + a_5 f(E) + \Delta r_j$$

in which

$\lambda_0 = c/f_\infty$ = wavelength of adopted frequency of satellite oscillator,

$\Delta f_\infty = f_\infty - f'_\infty$ = adopted offset frequency,

and the error coefficients a_1 through a_5 are of the form

$a_0 = \left(1 + \frac{\delta f_0}{f_\infty}\right) r_0$ = range at initiation of cycle count rescaled according to proportional error in adopted wavelength (Note: $\delta f_0 / f_\infty = \delta \lambda_0 / \lambda_0$),

$a_1 = \lambda_0 (\delta f_0 - \delta f'_0)$ = λ_0 x error in adopted frequency offset,

$a_2 = \frac{1}{2}\lambda_0(\dot{f}_0 - \dot{f}'_0) = \frac{1}{2}\lambda_0 \times$ relative drift rates,

$a_3 = -(\delta f_0/f_{00})$ = proportional frequency bias (satellite oscillator),

$a_4 = \delta\tau_0$ = bias in Geoceiver clock (relative to master clock) at initiation of cycle count,

a_5 = error in coefficient used for correction of tropospheric refraction (Note: $f(E) = 1/[\sin E + (\sin^2 E + k)^{\frac{1}{2}}]$ where E denotes elevation angle and k is a constant).

The term Δr_1 in (8) accounts for a specific set of preprocessing corrections consisting of:

(a) two frequency correction for ionospheric refraction;

(b) nominal correction for tropospheric refraction;

(c) correction for propagation delay;

(d) correction for special relativistic effect (time dilation);

(e) correction for general relativistic effect (gravitation).

Explicit expressions for each of these corrections are given in Brown, Trotter (1969).

3. Range vs Range Difference Approaches to Geoceiver Reduction

Equation (8) provides the observational equation adopted in SAGA for the reduction of Geoceiver observations. It is clear from (8) that if the error coefficients a_1 through a_5 were somehow all accurately known, Geoceiver could be viewed as being the equivalent of a range measuring system. The same consequence would hold if the error coefficients, though initially unknown, could be recovered within the reduction itself to a sufficient degree of accuracy. 'Sufficient', in geodetic applications would mean that recovered coordinates of tracking stations are not significantly compromised in accuracy because of errors in the recovered values of the error coefficients.

From numerical simulations we have found that if equation (8) does indeed provide a valid model, a sharp and effective self-calibration of the error coefficients can be effected, even though a fresh set of coefficients must be recovered for each observed pass. Some of these simulations will be discussed in detail later. Simulations, however, are at best a guide. While they do demonstrate that, in theory, a short arc Geoceiver network is

asymptotically equivalent to a ranging network, the question remains as to whether Geoceiver observations can, in reality, be successfully treated in this manner. The validity of the model can, of course, be established only through the reduction of actual observations. Prior to any undertaking with actual observations, it is well that we consider just what should be expected from a successful treatment of Geoceiver in accordance with the ranging model. A good indication is provided by the Geoceiver error budget presented by Stansell, et. al. (1965). This budget, which is reproduced in Table 1, indicates that for the ranging approach to be successful, the rms error of the ranging residuals obtained from an adjustment based on equation (8) should amount to only about 0.2 meters. An rms error in ranging residuals of 0.2 meters is clearly a formidable requirement, being fivefold smaller than has been experienced thus far with lasers and tenfold smaller than has been experienced with Geodetic Secor. Yet, if we accept the error budget, an rms error significantly greater than 0.2 meters would be indicative of unresolved systematic error and the ranging approach could not be sustained.

TABLE 1. Geoceiver internal error budget.

Error Source	150-400 MC (cycles RMS)	162-324 MC (cycles RMS)
Reference oscillator stability	.192	.156
Clock readout resolution	.052	.042
Receiver phase shifts (doppler)	.136	.136
Refraction count roundoff	.045	.045
Receiver phase shifts (refraction)	.059	.091
Combined errors, cycles RMS	.252	.234
meters RMS	.19	.21

It should be made clear that equation (8) does not constitute the observational equation that was originally envisioned by the developers of the Geoceiver and has subsequently been adopted by APL and NWL. Instead, a range-difference equation of the form:

$$(9) \qquad r_j - r_{j-1} = \lambda \Delta N_j + \lambda (f_0 - f_0')(\tau_j - \tau_{j-1}) + \text{neglected higher order terms},$$

forms the basic observational equation used by these organizations (Stansell, et. al.,1965). This result can immediately be derived by first evaluating equation (6) for times τ_j and τ_{j-1} and then subtracting the second resulting expression from the first. If the time interval $\tau_j - \tau_{j-1}$ is not too great, the higher order terms (differential frequency drift, differential tropospheric refraction, etc.) will not assume significance and thus can be ignored. The frequency offset $f_0 - f_0'$, on the other hand, remains significant and is treated in APL/NWL reductions as an unknown to be recovered for each pass observed from each station.

An objection that can be raised to the use of the range-difference approach based on equation (9) is that it does not really exploit the continuity of the cycle count achieved by the Geoceiver. Clearly equation (9) would remain valid if cycle counting were to proceed only intermittently as in the TRANET system. With TRANET, a cycle count is initiated at preset intervals (typically every four seconds) and counting continues until a preset number of cycles has been accumulated, whereupon the time interval of the count is read out and counting ceases until the start of the next interval. If τ_{a_j}, τ_{b_j} were to denote the beginning and end of the jth counting interval, equation (9) could equally well be expressed as:

$$(10) \quad \Delta r_j = r_{b_j} - r_{a_j} = \lambda \Delta N_j + \lambda (f_0 - f_0')(\tau_{b_j} - \tau_{a_j})$$

where, for intermittent counting, $\tau_{b_j} \neq \tau_{a\,j+1}$. When counting is truly intermittent, as with TRANET, errors in successive range differences Δr_{j-1}, Δr_j are uncorrelated. However, when counting is truly continuous ($\tau_{b_j} = \tau_{a\,j-1}$), as with Geoceiver, errors in successive range differences are negatively correlated, the coefficient of correlation being precisely -0.5. Unless this correlation is taken explicitly into account in the reduction, any special benefits to be gained from continuity of cycle count will be lost.

What, then, are the benefits to be gained from full exploitation of continuity of cycle counting? And why, indeed, should equation (8) with its greater complexity be preferred over equation (9)? Although results to be presented in due course will clarify this matter, a heuristic consideration of these questions is illuminating.

In Figure 3a we have indicated the character of the geometry pertinent to intermittent,

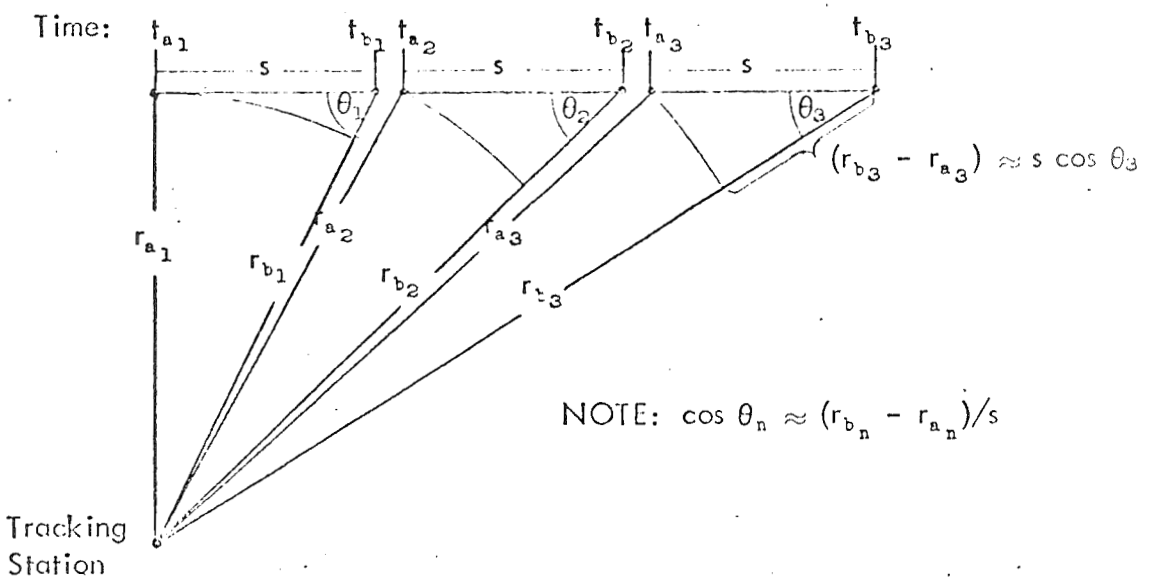

Figure 3a. Illustrating essential geometry of hypothetical tracking of straight line trajectory by system generating intermittent counts of beat frequency.

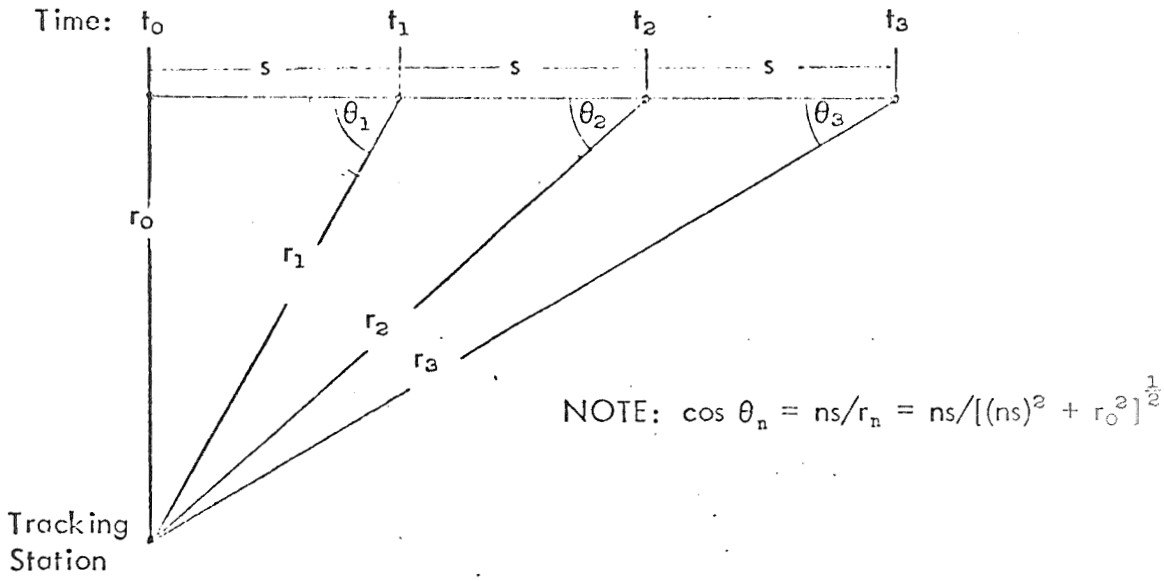

Figure 3b. Illustrating essential geometry of hypothetical tracking of straight line by system generating continuous counts of beat frequency.

range-difference tracking of a straight line trajectory of constant velocity sampled at equal time intervals. Because the trajectory is assumed to be known, each observed segment of length 's' becomes tantamount to a known baseline, and the range difference system becomes geometrically equivalent to a sequence of radio interferometers. Accordingly, each range difference defines the direction cosine of the tracking station relative to the baseline defined by the tracking interval. As indicated in the figure, the n th tracking interval (counted from a midarc origin taken as the point of closest approach) generates the observation:

$$(11) \qquad \hat{\ell}_n = \cos\theta_n = (r_{b_n} - r_{a_n})/s .$$

If var $(r_{b_n} - r_{a_n}) = \sigma^2$, it follows that the standard deviation of $\hat{\ell}_n$ is:

$$(12) \qquad \sigma_{\hat{\ell}_n} = \sigma/s .$$

Figure 3b shows the corresponding situation for a range measuring system. Here, the value $\cos\theta_n$ is defined by:

$$(13) \qquad \ell_n = \cos\theta_n = ns/r_n$$

and if var $(r_n) = \sigma^2$ (the same value as adopted for var $(r_{b_n} - r_{a_n})$), the standard deviation of ℓ_n becomes

$$(14) \qquad \sigma_{\ell_n} = ns\sigma/r_n^2 .$$

Inasmuch as $r_n^2 = r_o^2 + (ns)^2$, equations (13) and (14) yield the relation:

$$(15) \qquad \sigma_{\ell_n}/\sigma_{\hat{\ell}_n} = 1/\left(n + \frac{K^2}{n}\right) \leqq 1/n$$

where $K = r_o/s$. From this result it follows that a total of n^2 independent repetitions of range-difference determinations of $\cos\theta_n$ must be averaged in order to yield a mean result as accurate as a single ranging determination of $\cos\theta_n$. More generally, it follows that to yield an end result (e.g., survey) equivalent to that to be expected from a set of $N = 2n+1$ successive

ranges, one would require a set of approximately:

$$2(1^2 + 2^2 + 3^2 + \ldots + n^2) = 2n(n+1)(2n+1)/6 \approx 2n^3/3$$

range differences, a ratio on the average of about $n^2/3$ range-difference observations for each ranging observation.

Because of the necessity for recovering the zero set (r_0) in range (along with other error coefficients), the foregoing heuristic discussion holds only in an asymptotic sense for Geoceiver (the stronger the tracking network, the more closely Geoceiver approaches being equivalent to a true ranging system).

Even so, from related geometrical considerations one may conclude that a ranging system can be expected to produce geodetic results of far higher accuracy than can a range difference system having a comparable sampling rate and level of random error. This, then, provides ample motivation for our attempt to treat Geoceiver as a ranging system by virtue equation (8) the validity of which stems from the strict continuity of the Geoceiver cycle count.

3. Experimental Procedure

A set of fourteen of the passes observed by the prototype Geoceiver during the December 1968 test of the system was subjected to experimental processing by DBA. Because observations were available from only a single Geoceiver station, it was not possible to perform a multi-station short arc reduction to establish internal consistencies of Geoceiver observations. Accordingly, we adopted the same general procedure as was used by NWL (Smith, 1969), namely, to enforce long arc orbits generated by NWL from reductions of observations made by the global TRANET network. With orbital state vectors thus considered to be known for each pass, we subjected the Geoceiver observations to two different reductions:

(a) independent reduction of each pass with height h of the station held fixed but with latitude φ and longitude λ free to adjust for each pass (along with coefficients of the error model);

(b) simultaneous reduction of all fourteen passes with a common φ, λ, h recovered for all passes and a fresh set of error coefficients recovered for each pass.

Because the NWL long arc orbits were locked down in the reductions, the results (and especially the recovered coordinates of the Geoceiver) will be compromised to some degree by the errors in the enforced orbits. As we shall presently see, indications from the results are that actual accuracies of the reference orbits are probably on the order of ±5 to ±10 meters for passes over North America.

A plot of the ground tracks of the fourteen reduced passes is given in Figure 4. Taken as a whole, the passes are fairly well balanced in their geometrical distribution about the tracking station. A cutoff of 5° in elevation angle was adopted in the selection of observations to be reduced for each pass.

4. Results of Single Pass Reductions

All of the coefficients of the error model were assigned a priori values of zero. The zero set coefficient a_0, which represents essentially the slant range to the satellite at the initiation of cycle counting, was assigned a one sigma constraint of 10^7 meters. The a priori constraints for the remaining coefficients are listed in Table 2. In all cases, the constraints were taken to be conservative. The adjustments resulting from the single pass reductions are also given in Table 2 for all error coefficients except a_0.

The corrections to a_1 are referred to an adopted frequency offset of 31,955.9 Hz which was provided by NWL. The adjusted values of a_1 for the first seven passes are fairly constant. This may be attributed to the fact that during the period spanned by these passes the quartz oscillator of the Geoceiver was bypassed, and the APL Cesium frequency standard was employed in its place to generate the local reference frequency. For the final seven passes, on the other hand, the Geoceiver's own oscillator was exercised. As we see from Table 2, the variation in a_1 is considerably more pronounced for these passes. A plot of the values of a_1 for passes 8 through 14 is given in Figure 5. The points lie almost perfectly on a straight line, indicating the validity of the assumption of linear drift of frequency. The slope of the fitted line corresponds to change in frequency of only about 0.08 Hz per day. In view of the nominal magnitude of the offset frequency (32k Hz), this corresponds to a long term

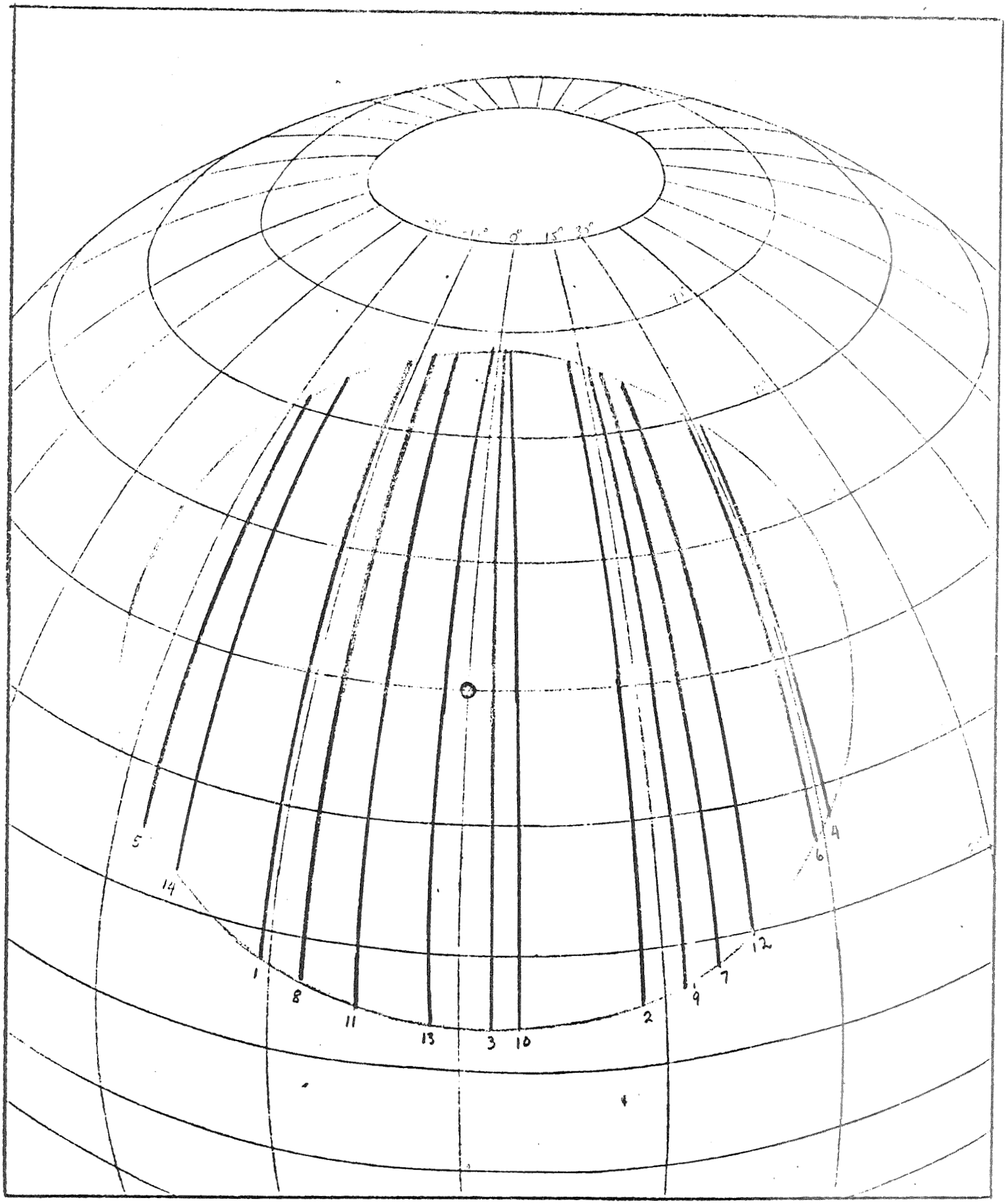

FIGURE 4. Geometry of ground tracks of 14 passes of Navy Navigational Satellite observed by Geoceiver and processed through SAGA (shown relative to 5° cutoff horizon of tracking station).

TABLE 2. Adjustments to error coefficients resulting from single pass reductions.

		ERROR COEFFICIENT				
		a_1 (freq. offset)	a_2 (freq. drift)	a_3 (freq. bias)	a_4 (time bias)	a_5 (refraction)
A priori One Sigma Constraint		10 (M/Sec)	2×10^{-4} (M/Sec^2)	5×10^{-7}	$.1 \times 10^{-3}$ (Sec)	0.20 (Meters)
ADJUSTMENTS TO APRIORI COEFF.	Pass No.					
	1	-.033	*$-.17 \times 10^{-4}$	0.3×10^{-7}	$.00 \times 10^{-3}$	.006
	2	-.039	-.22	-0.1	.00	.010
	3	-.047	-.12	0.0	.00	.006
	4	-.041	-.20	0.0	.00	-.009
	5	-.058	.10	0.2	.00	-.014
	6	-.043	.13	0.0	.00	.008
	7	-.033	-.13	0.2	.00	-.018
	8	-.355	-.07	-0.0	.00	.004
	9	-.363	-.08	0.0	.00	-.004
	10	-.407	-.52	0.5	.00	-.017
	11	-.428	-.11	0.1	.00	-.003
	12	-.456	-.36	0.1	.00	-.043
	13	-.525	-.11	-0.5	.00	.008
	14	-.527	-.26	-0.0	.00	-.005

*All entries in a column should be multiplied by the same power of 10 as the first entry.

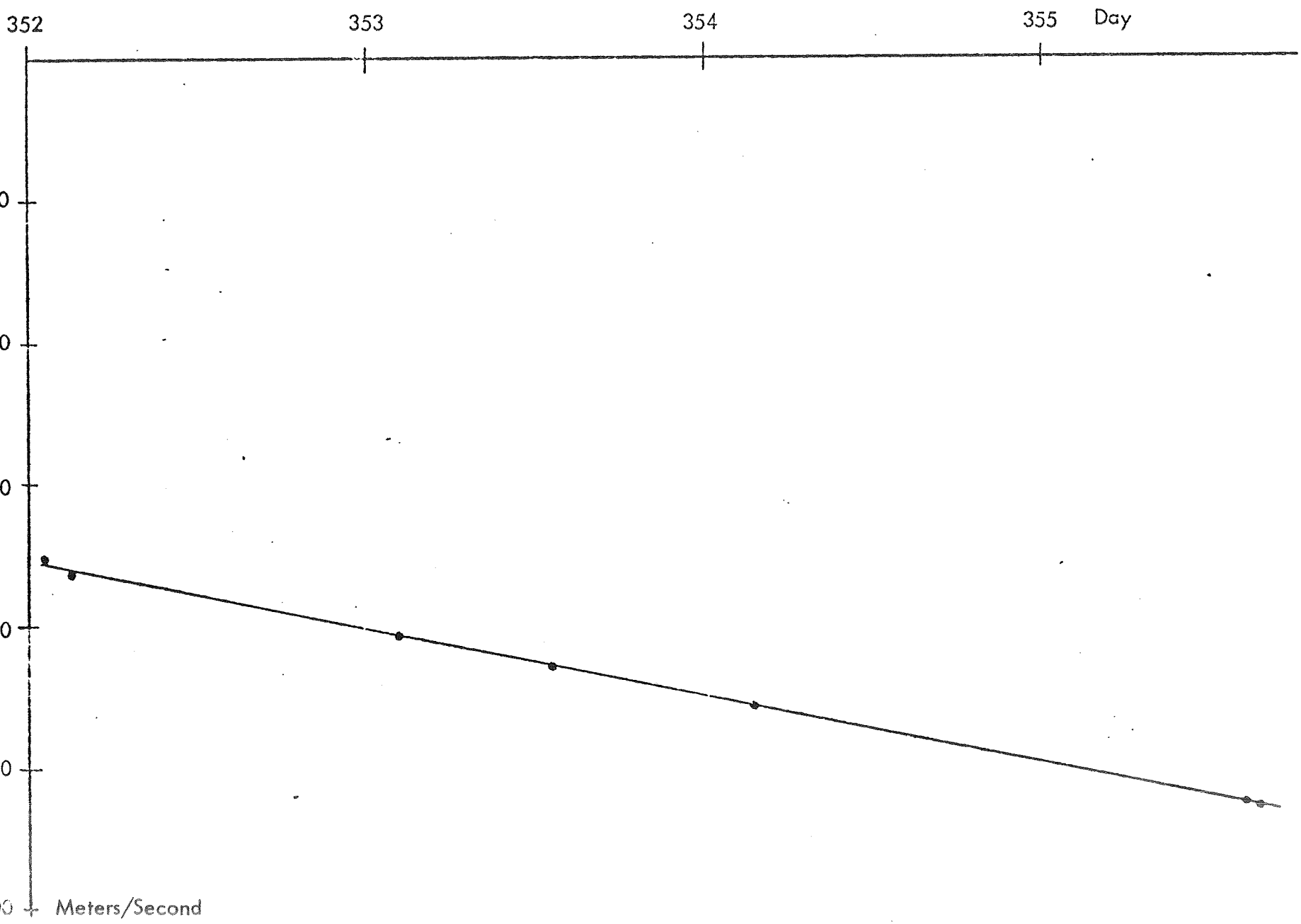

FIGURE 5. Plot of corrections to frequency offset term versus time from single pass reductions of passes 8 through 14 (divide by λ_o = .75m to convert to cycles per second).

differential stability in frequency between satellite and Geoceiver oscillators of only 3 parts in 10^{11} per day.

The largest value found for a_2 (frequency drift), namely $-.52 \times 10^{-4}$ m/sec^2 for pass 10, corresponds to an error of only 0.19m in range over an interval of one minute (i.e., $(-.52 \times 10^{-4})(60)^2$). However, by the end of the pass (τ = 14 minutes = 840 sec) the contribution of this value of a_2 to range grows to $(0.19) \times (14)^2$ or 37.3m.

Adjustments to a_3 (proportional frequency bias) turn out to be insignificantly small being equivalent to a range correction of only 0.2m in the worst case.

Although the coefficient accounting for timing bias a_4 was constrained to 100 microseconds (one sigma), the adjustments to the a priori values turned out to be essentially zero in every case. This may be attributed to the fact that the effect of timing bias can be almost perfectly offset in a single pass adjustment by the horizontal adjustment of the station.

The fact that the adjustments to the refraction coefficients a_5 are so small, likewise, suggests that compensation for residual refraction is largely being effected by other adjustable parameters. The largest value of a_5 (-.043 from pass 12) corresponds to a range correction of about -0.2m at the adopted cutoff angle of 5°. The a priori constraint of 0.2m adopted for a_2 is consistent with an assumption that the nominal correction for tropospheric refraction is accurate to about 5 percent.

The residuals produced by the single pass reductions are given for each pass in Table 3. The typical rms value of the residuals is under 0.10 meters, an amount less than half as great as that to be expected from the APL error budget reviewed earlier! Part of the discrepancy can be accounted for by the fact that the major contributor to the error budget, namely reference oscillator stability, does not apply to the reduction used in SAGA. This is because frequency drift is explicitly modeled and recovered in the reduction. When allowance is made for this consideration, one obtains better agreement between the error budget and the residuals. Even then, the residuals are smaller than the design budget would allow, a tribute to the integrity of the APL design and to the conservativeness of Geoceiver specifications.

TABLE 3. Geoceiver ranging residuals produced by SAGA from single pass reductions.

Point	Pass 1	2	3	4	5	6	7	8	9	10	11	12	13	14
1	-.05m	.06m	.01m	-.03m	-.05m	.04m	.02m	.14m	-.01m	-.14m	-.12m	-.01m	.06m	.00m
2	.16	-.14	.04	.09	.15	-.10	.03	-.16	.06	.17	.14	.01	-.09	.05
3	-.02	.05	-.01	-.05	-.07	.07	-.05	-.06	-.08	.06	.10	.04	-.02	-.08
4	-.17	.12	-.08	.04	-.07	-.03	-.11	-.01	-.01	-.02	-.04	-.05	.01	-.04
5	-.02	.00	-.09	-.03	-.07	.05	.10	.09	.08	-.06	-.11	.05	.13	.07
6	.12	-.14	.24	.03	.15	-.04	.01	.04	-.04	-.11	-.06	-.04	-.08	.06
7	.09	.03	-.11	.03	.09	.02	.04	.03	.01	.10	.01	.00	-.08	-.03
8	-.09	.13	.05	-.03	-.11	-.05	-.02	-.02	.01	-.01	.10	.04	.14	-.11
9	-.06	-.13	.03	-.01	-.09	.06	-.02	-.11	-.06	.03	.07	-.01	-.02	-.05
10	-.03	.05	-.12	.05	.01	-.05	-.05	.02	.03	.02	-.06	.00	-.05	.17
11	.09	.05	.08		.10	.07	-.08	-.05	.04	-.03	-.07		-.01	.05
12	.11		.08		.00	.03	.11	.16	-.03	-.05	.05		.02	-.09
13	-.10		.02		-.03	-.07	.12	.03		-.02	-.04		.00	
14	.04		.02				-.11	-.09		.05	.03			
15	-.06		-.09											
RMS	.09	.10	.09	.04	.09	.06	.07	.09	.05	.08	.08	.03	.07	.08

The smallness of the Geoceiver residuals produced by SAGA goes far towards establishing the validity of treating Geoceiver as a ranging system. Further evidence is provided in Table 4 which lists the adjustments produced by SAGA to the horizontal coordinates of the Geoceiver station. These are compared with the corresponding adjustments produced by NWL using the range difference approach (Smith, 1969). Of particular interest, are the relative standard deviations (σ_N, σ_E) of the SAGA and NWL adjustments. These reflect the marked geometrical superiority of the ranging approach over the range difference approach. The values of σ_N and σ_E, of course, have only a provisional validity for they are based (in both adjustments) on the assumption that the enforced reference orbit and station height are flawless.

Bull's eye plots of the horizontal positions listed in Table 4 are provided in Figure 6. Although the scatter of the SAGA positions is somewhat smaller than the NWL positions, both are dominated by errors inherited from the orbit. In view of the small sigmas of the SAGA positions (typically less than 2 meters), we may infer from the scatter of the individual solutions that the long arc ephemeris is probably good to about ±7 meters, one sigma.

5. Results of Combined Reduction

In the single pass reductions the horizontal coordinates of the station were free to adjust, thereby providing partial internal compensation for orbital and other errors. A more severe test of the Geoceiver is one in which all passes are reduced simultaneously with only a single, three dimensional adjustment of survey being admitted. Such an adjustment was performed and the resulting solutions for error coefficients are provided in Table 5.

In comparing Tables 2 and 5 we find that results for the coefficients a_1 and a_2 are generally in good agreement. On the other hand, both frequency bias and time bias (a_3 and a_4) in Table 5 showned a much greater tendency to adjust than in Table 2. This is clearly a consequence of the loss in the combined adjustment of the compensative capability (afforded in the single pass reductions) of the pass-by-pass horizontal adjustment of the station. Accordingly, a_3 and a_4 adjust to compensate as well as possible for errors in the enforced orbit.

As in the single pass reductions, the refraction coefficients a_5 from the combined

TABLE 4. Comparative adjustments of station position produced by single pass solutions.

PASS/ MAX. EL. ANGLE	DAY	SAGA ADJUSTMENTS				NWL ADJUSTMENTS			
		ΔN (North)	ΔE (East)	σ_N	σ_E	ΔN (North)	ΔE (East)	σ_N	σ_E
1 (33°)	345[d] 02[h]	0.3m	3.6m	0.9	3.2	- 7.8m	5.2m	6.9m	7.5m
2 (37°)	345 03	- 4.4	8.4	2.2	2.7	- 1.1	4.3	5.7	6.7
3 (80°)	345 15	- 7.6	9.2	1.2	3.2	- 2.2	-12.1	3.9	26.8
4 (11°)	345 16	- 6.0	10.8	1.0	2.0	-13.4	17.3	42.9	32.2
5 (14°)	346 01	- 1.3	4.7	0.6	1.1	--*	--	--	--
6 (11°)	346 04	- 7.6	9.7	0.5	0.6	-13.4	8.6	48.1	26.5
7 (27°)	346 16	- 4.7	1.8	0.4	0.6	-12.2	15.5	9.4	9.8
8 (40°)	352 01	- 6.9	10.3	0.6	0.8	- 4.5	5.2	5.5	7.0
9 (31°)	352 03	- 8.0	6.2	0.3	0.6	- 8.9	11.2	8.1	7.6
10 (39°)	353 02	- 5.3	2.8	0.5	1.2	- 3.3	3.5	3.3	9.8
11 (57°)	353 13	2.5	16.3	0.4	0.8	- 1.1	19.0	3.8	7.4
12 (22°)	354 03	-12.1	14.7	0.2	0.4	- 6.7	10.4	12.1	9.9
13 (78°)	355 14	- 0.3	15.3	0.6	1.9	- 3.3	21.6	4.0	20.8
14 (16°)	355 15	- 2.0	10.0	1.3	3.1	- 6.7	6.0	10.8	7.3

*NWL solution failed to converge on Pass 5.

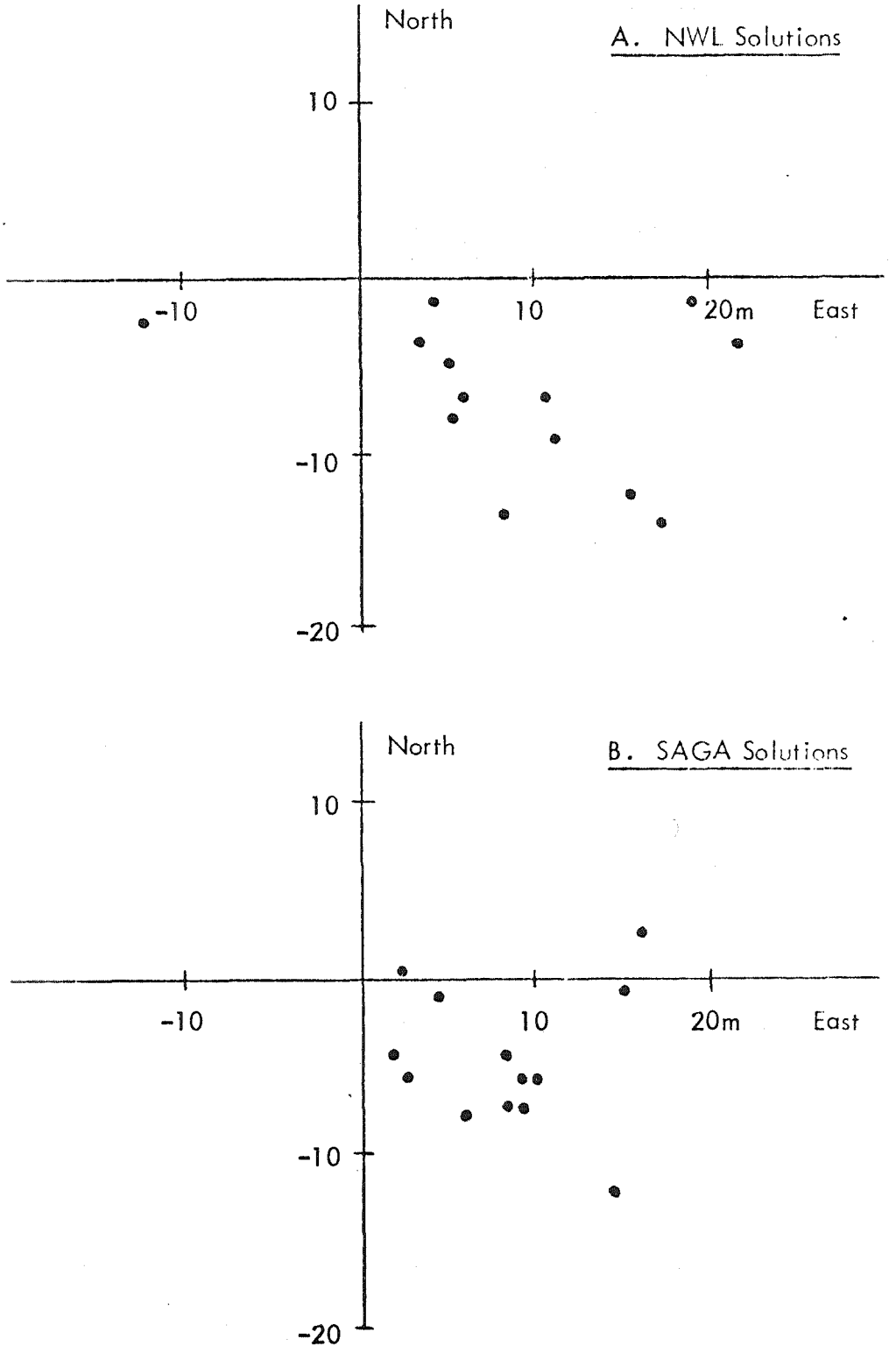

FIGURE 6. Bull's eye plot of single pass solutions for Geoceiver location: A. NWL Solutions, B. SAGA Solutions.

TABLE 5. Adjustments to error coefficients resulting from combined reduction of all passes.

		ERROR COEFFICIENT				
		a_1 (freq. offset)	a_2 (freq. drift)	a_3 (freq. bias)	a_4 (time bias)	a_5 (refraction)
Apriori One Sigma Constraint		10 (M/Sec)	2×10^{-4} (M/Sec^2)	5×10^{-7}	$.1 \times 10^{-3}$ (Sec)	0.20 (Meters)
ADJUSTMENTS TO APRIORI COEFF.	Pass No.					
	1	-.035	*$-.20 \times 10^{-4}$	4.4×10^{-7}	$-.61 \times 10^{-3}$	-.008
	2	-.038	-.06	0.2	.02	.008
	3	-.048	-.29	7.2	-.44	-.024
	4	-.038	-.14	0.1	.02	-.014
	5	-.060	.08	-2.2	-.20	.025
	6	-.045	.17	2.2	-.35	-.008
	7	-.033	-.12	-5.8	-.13	.041
	8	-.356	-.07	3.0	-.32	-.018
	9	-.367	-.10	0.7	-.42	.011
	10	-.407	-.51	1.3	-.09	-.017
	11	-.433	-.10	-1.3	-.85	.024
	12	-.464	-.12	1.8	-.31	-.012
	13	-.527	-.05	-1.1	-.33	.009
	14	-.532	-.22	0.2	-.06	-.001

* All entries in a column should be multiplied by the same power of 10 as the first entry.

reduction show only a slight tendency to adjust.

From Table 6 we see that the residuals from the combined solution, though still quite small, are in some cases appreciably greater than their counterparts from the single pass reductions. This, too, we may attribute to the influence of errors in the reference orbits. We consider the residuals from the single pass reductions to be more representative of what can be expected when Geoceivers are employed in short arc configurations. This is because the orbit is free to adjust in a short arc adjustment and the residuals, therefore, are not contaminated by an erroneous reference orbit.

In order to ascertain more clearly the effects of orbital errors, we repeated the multi-pass adjustment allowing a slight relaxation in the state vector for each pass. A priori sigmas of 5 meters were assigned to the X, Y, Z components of the state vector and sigmas of .005 m/sec were assigned to the $\dot{X}, \dot{Y}, \dot{Z}$ components. The residuals from the resulting adjustment turned out to be so similar to those obtained from the single pass adjustments (Table 3) that there is no need to reproduce them separately. The same can be said of the adjusted values of the error coefficients. The largest adjustment to the positional components of the state vector was a value of -5.8 meters in Z for Pass 11 and the next largest was -4.0 meters in Y for Pass 1. The rms values of the adjustments to the X, Y, Z components amounted to 0.9, 1.6 and 2.5 meters, respectively. The components of velocity showed very little tendency to adjust, with only a few corrections reaching as much as .001 m/sec and an rms adjustment amounting to less than .0005 m/sec in all components.

The coordinates of the Geoceiver station resulting from the two versions of the multi-pass reduction are given in Table 7 and are compared with the corrections obtained from NWL's combined solution. The agreement between SAGA Solution A (orbits held) and the NWL solution (orbits also held) is especially good, discrepancies of 0.4, 0.2 and -0.5 meters being obtained in North, East and Up respectively. Discrepancies between SAGA Solution B (orbits slightly relaxed) and the NWL solution are somewhat greater, on the average, amounting to 0.9, 1.3 and -0.1 meters in the three coordinates.

The excellence of the agreement between SAGA and NWL solutions provides final

TABLE 6. Geoceiver ranging residuals produced by SAGA from combined reduction.

Point	Pass 1	2	3	4	5	6	7	8	9	10	11	12	13	14
1	-.15m	.05m	-.07m	.00m	-.08m	-.11m	.07m	.04m	-.16m	-.05m	-.21m	-.09m	-.08m	-.03m
2	.12	-.13	.00	.08	.12	-.09	.01	-.17	.04	-.14	-.14	.04	-.04	.06
3	.01	.06	.02	-.08	-.08	.18	-.12	.00	.01	.00	.19	.11	.11	-.05
4	-.08	.11	.01	.00	-.05	.10	-.17	.07	.13	.11	.24	.01	.08	-.02
5	.09	-.02	.02	-.06	-.01	.14	.08	.17	.22	-.16	.18	.06	-.05	.08
6	.20	-.16	.31	.02	.23	-.03	.08	.07	.03	.10	.09	-.08	-.02	.04
7	.09	-.03	-.15	.05	.15	-.05	.16	.01	-.03	.19	-.03	-.07	.15	-.06
8	-.18	.15	-.08	.00	-.11	-.15	.08	-.09	-.12	-.08	-.08	-.01	.05	-.12
9	-.15	-.11	-.13	.06	-.16	-.02	-.01	-.18	-.22	-.13	-.15	-.02	-.17	-.05
10	-.08	.08	-.13	-.06	-.10	-.08	-.13	-.02	-.08	-.15	-.22	.06	-.14	.18
11	.07	.01	.11		.01	.08	-.19	-.07	.04	-.13	-.12		-.03	.06
12	.11		.11		-.01	-.03	.03	.17	.15	-.07	.09		.06	-.09
13	-.09		.03		.09	.07	-.01	.03		.04	.05		.07	
14	-.05		-.09				-.11	-.05		.17	.12			
15	.09		.04											
RMS	.11	.10	.12	.05	.11	.10	.11	.10	.12	.12	.15	.06	.09	.08

TABLE 7. Coordinates obtained from combined reductions.

	Original Coordinates			Values Obtained from SAGA (degrees and minutes omitted)			Corrections in North, East, Up		
				Solution A	Solution B		Solution A*	Solution B*	NWL**
φ	39°	09'	48".506	48".366	48".349	ΔN	-4.5m	-5.0m	-4.1m
λ	283°	06'	11".592	12".329	12".282	ΔE	8.0m	6.9m	8.2m
h			102.8m	105.4	105.0	ΔU	2.6m	2.2m	2.1m

* From combined reduction of 14 passes of satellite No. 59.
** From combined reduction of 37 passes of satellite No. 59.

verification of the validity of the ranging approach to Geoceiver observations.

When a ranging sigma of 0.1 meters is propagated through the SAGA reductions, the following sigmas for geocentric position are obtained:

Solution A (orbits fixed)	Solution B (orbits relaxed)
$\sigma_x = 0.45$m	$\sigma_x = 2.50$m
$\sigma_y = 0.25$m	$\sigma_y = 1.84$m
$\sigma_z = 0.21$m	$\sigma_z = 1.66$m.

As we shall presently see, the sigmas corresponding to Solution A are indicative of what can actually be expected from the Geoceiver system when it is employed in strong short arc configurations and is reduced as a ranging system.

6. Special Data Editing for Cycle Count Errors

The measurements made by Geoceiver consist of two quantities ΔN_j and τ_j, that is, the number of whole cycles of beat frequency cumulated over an interval and the time of the zero crossing of the last cycle. As we have already noted, ΔN_j being an integer should be error free, provided each positive cycle crossing is indeed counted and no spurious crossings are counted. Thus, in principle, all of the error in Geoceiver observations can be attributed to the error in the times accompanying the cycle counts. Unfortunately, in practice this situation does not appear to hold, at least with the breadboard and prototype Geoceivers. Smith (1969) reports that when both of these Geoceivers were operating from the same antenna, the integrated doppler count was found to differ in a number of instances by 10 to 20 cycles. Indeed, this was the case in 27 of the 137 observed passes. Although passes where counts differed by 10 or more cycles were rejected in the reductions performed by NWL, the surviving passes could be affected by discrepancies of up to 9 counts. Recognizing this, NWL employed digital filtering of range-difference residuals in an attempt to detect and correct such cycle count errors. Apparently, this filtering process was not totally successful. An inspection of a sample of NWL results vs our results indicates that while most of the errors of 3 or more counts were generally

detected and corrected, many of the smaller cycle count errors eluded detection.

The pertinence of foregoing considerations is illustrated in Figure 7 in which we have plotted three sets of residuals from Pass 3:

(a) residuals from a SAGA reduction in which no cycle count editing was performed;

(b) residuals from a SAGA reduction following cycle count editing on residuals from (a) (see Table 6 for listing);

(c) residuals from the NWL range difference reduction.

The residuals listed earlier in Table 3 indicate that a value of 0.10m may be taken as a nominal estimate of the standard deviation of Geoceiver ranges. On the other hand, a single cycle count error corresponds to an error in range of 0.75 meters (i.e., one wavelength at 400m Hz). The rather sizable ratio of 7.5 to 1 between the two effects is what makes practical the detection and removal of cycle count errors from an analysis of preliminary residuals. As can be seen in Figure 7, when a suitable filtering algorithm is applied to the residuals from (a), the rms of the residuals improves from 0.36m to 0.11m, and the wide systematic excursions of the residuals in curve (a) are eliminated.

The final NWL range-difference residuals (curve (c)) have an rms value about tenfold greater than the final SAGA residuals. This is attributable, in part, to unresolved cycle count errors remaining in the NWL reduction. We suspect, however, that some of the higher order effects neglected in the range-difference equation (frequency drift, in particular) may significantly contribute to the magnitude of the residuals. This, in turn, would tend to lessen the effectiveness of editing for cycle count errors. The coefficient of correlation of -0.5 between successive range difference errors (refer back to Section 2), no doubt, is a contributing factor as well (this accounts also for the sawtooth runs of residuals that have been found to be characteristic of range-difference reductions).

In view of the above, we may conclude that not only is the ranging approach geometrically superior to the range-difference approach, but it also has the advantage of generating residuals which permit a finer degree of editing than is possible with range-difference residuals. While cycle count errors are a nuisance, they can almost unfailingly be detected and removed

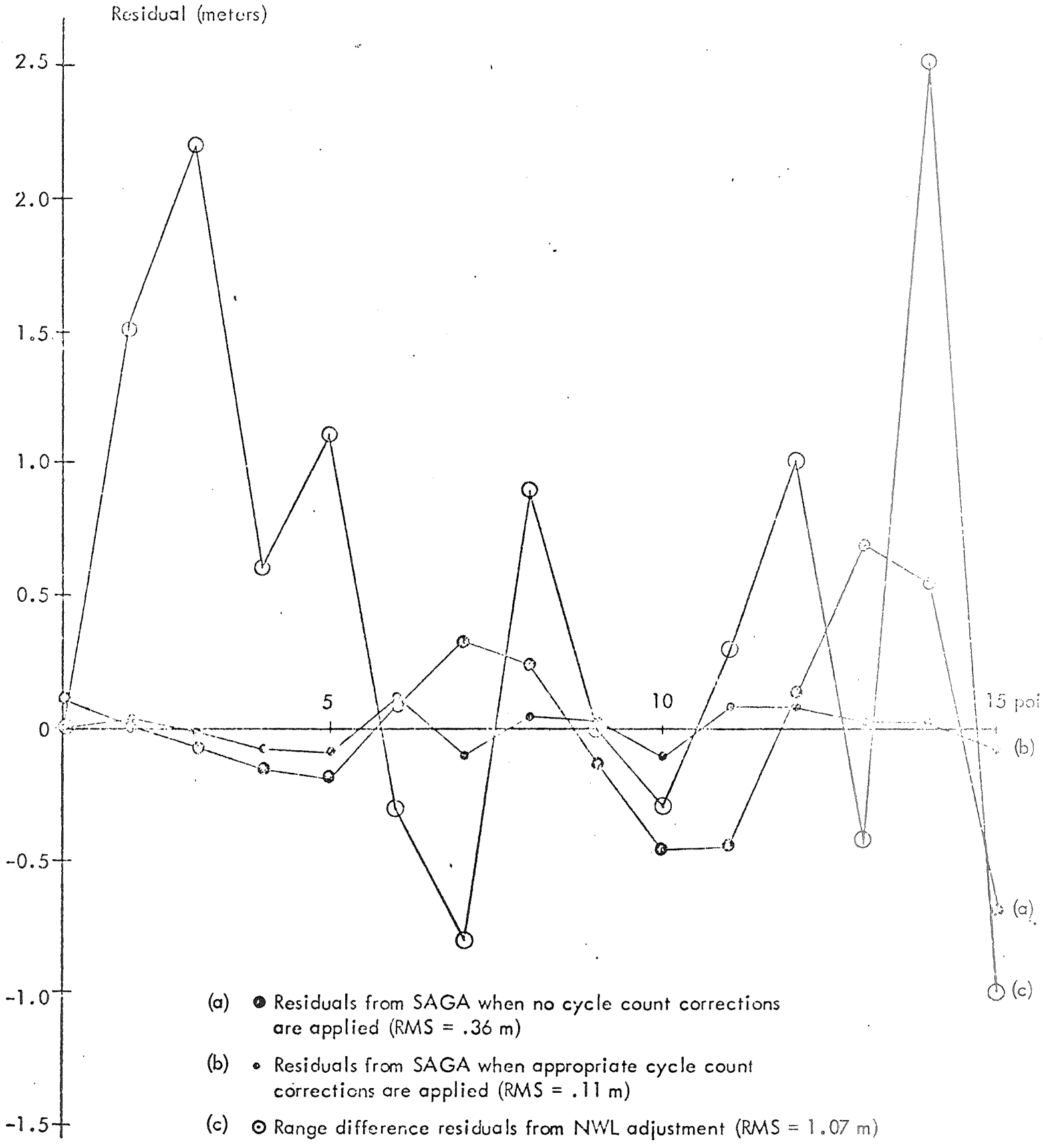

FIGURE 7. Residuals from various reductions of Pass 3.

in the SAGA reduction and so in the end, do not compromise the accuracy of the system.

The cycle count errors deduced from preliminary SAGA reductions and applied in subsequent reductions are listed in Table 8 for each of the 14 passes carried in our test. Each count is equivalent to a range error of 0.75m. The counts listed under 'a' in the table represent the errors in the original counting intervals; those listed under 'b' represent their cumulative effect on range. Of the 14 passes, only 3 were free of cycle count errors. Overall, about one counting interval in five is affected by an error of one or more counts. It is perhaps significant that the seven passes (8-14) occurring near the end of the testing period have a much lower error rate (about 1 in 9) than do the seven passes (1-7) occurring near the beginning of the testing period (about 1 in 3). Hopefully, the production models of the Geoceiver will overcome the shortcomings of the breadboard and prototype units by reducing the error rate in counting to very low level.

7. Numerical Simulations of Short Arc Geoceiver Networks

We have demonstrated with real data that the ranging approach to Geoceiver reduction adopted in SAGA is indeed sound and that a value of 0.10m can safely be adopted as the nominal standard deviation of the observations. The precise significance of these key facts to satellite geodesy remains to be investigated. Real data from strong multi-station networks will not become available until production models of the Geoceivers have been delivered in quantity. Lacking such data, we can nonetheless ascertain the accuracies to be expected from hypothetical networks by means of numerical simulation. In the next sections we shall review the results of three fairly large-scale simulations designed to shed light on the capabilities of the Geoceiver and to reveal the most effective deployment of the system. The three simulations may be described as:

I. 25 station continental network employing 11 interlocking subnets of 7 Geoceivers, each observing 11 passes (for a total of 121 passes);

II. 25 station continental network with all stations simultaneously occupied and tracking a common set of 39 passes;

III. 18 station intercontinental network consisting of 6 stations in North America, 6 in South America, and 6 in Northern Africa/Southern Europe (designed for continental drift experiment).

TABLE 8. Geoceiver cycle count errors (a. errors in one minute counts; b. errors in cumulative counts).

Pass	Point														
	1	2	3	4	5	6	7	8	9	10	11	12	13	14	15
1a	0	0	0	0	0	0	1	-1	0	0	0	1	1	0	0
b	0	0	0	0	0	0	1	0	0	0	0	1	2	2	2
2a	0	1	0	0	-1	0	0	0	0	0	-1	-	-	-	-
b	0	1	1	1	0	0	0	0	0	0	-1	-	-	-	-
3a	0	0	0	0	0	0	1	0	0	0	-1	2	1	0	-2
b	0	0	0	0	0	0	1	1	1	1	0	2	3	3	1
4a	0	1	0	0	0	0	0	0	-1	0	-	-	-	-	-
b	0	1	1	1	1	1	1	1	0	0	-	-	-	-	-
5a	-3	-2	-1	0	0	0	1	0	1	1	1	0	-1	-	-
b	-3	-1	0	0	0	0	1	1	2	3	4	4	3	-	-
6a	0	-4	2	1	1	0	0	0	0	0	0	0	-1	-	-
b	0	-4	-2	-1	0	0	0	0	0	0	0	0	-1	-	-
7a	0	0	0	0	0	0	0	0	0	0	0	0	0	0	-
b	0	0	0	0	0	0	0	0	0	0	0	0	0	0	-
8a	0	1	0	-1	0	0	0	0	0	0	0	0	0	0	-
b	0	1	1	0	0	0	0	0	0	0	0	0	0	0	-
9a	0	0	0	0	0	0	0	0	0	0	0	0	-	-	-
b	0	0	0	0	0	0	0	0	0	0	0	0	-	-	-
10a	0	0	0	0	0	0	0	0	0	0	0	-1	1	0	-
b	0	0	0	0	0	0	0	0	0	0	0	-1	0	0	-
11a	-1	1	0	0	0	0	0	0	0	0	0	0	0	0	-
b	-1	0	0	0	0	0	0	0	0	0	0	0	0	0	-
12a	-1	1	0	0	0	0	0	0	0	0	-	-	-	-	-
b	-1	0	0	0	0	0	0	0	0	0	-	-	-	-	-
13a	-1	1	0	0	0	0	0	0	0	0	0	0	0	0	-
b	-1	0	0	0	0	0	0	0	0	0	0	0	0	0	-
14a	0	0	0	0	0	0	0	0	0	0	0	0	0	0	-
b	0	0	0	0	0	0	0	0	0	0	0	0	0	0	-

The simulations were executed by means of a special version of SAGA designed expressly for studies of error propagation. In all cases, the state vector for each orbital pass was considered to be unknown, and the effects of errors in the determination of the state vector as well as errors in the recovered error coefficients were propagated into the recovered coordinates of the tracking stations. Thus, the error propagations are comprehensive and fully rigorous.

8. Results of Simulation I

The tracking network adopted for the first simulation is pictured in Figure 8. Most of the stations correspond to sites that have been or are currently being used for space geodesy and include STADAN, SPEOPS, BC-4, PC-1000 and Baker-Nunn stations. The network embraces all but the northernmost reaches of North America. The guiding premise of the first simulation is that only 7 Geoceivers are considered to be available for the execution of the survey of the entire 25 station net. This means that the observations must be gathered by a suitable combination of interlocking subnets. We adopted a scheme in which the basic observational configurations consist of subnets of seven stations, six of which form a hexagon in which the seventh station is approximately centered. The overall network is comprised of a total of eleven such subnets formed according to the schedule indicated in Table 9. From the table, it can be seen that stations in the interior of the net participate in as many as seven different subnets, whereas those on the periphery participate in only two or three. Each subnet is considered to track a set of eleven passes of Navy Navigation Satellites, a cutoff elevation angle of 5° being adopted for all participating stations. The passes are chosen to be well distributed about each subnet as is typified in Figure 9 which shows the ground tracks of the set of passes observed by subnet no. 1.

The key remaining assumptions underlying the simulation can be summarized as follows:

(1) sigma of Geoceiver ranges is 0.10m;

(2) station no. 1 is adopted origin of network and is held fixed;

(3) orientation of the network is defined by locking both components of the direction of the baseline joining stations 9 and 15 and one component of the direction of the baseline joining stations 4 and 6;

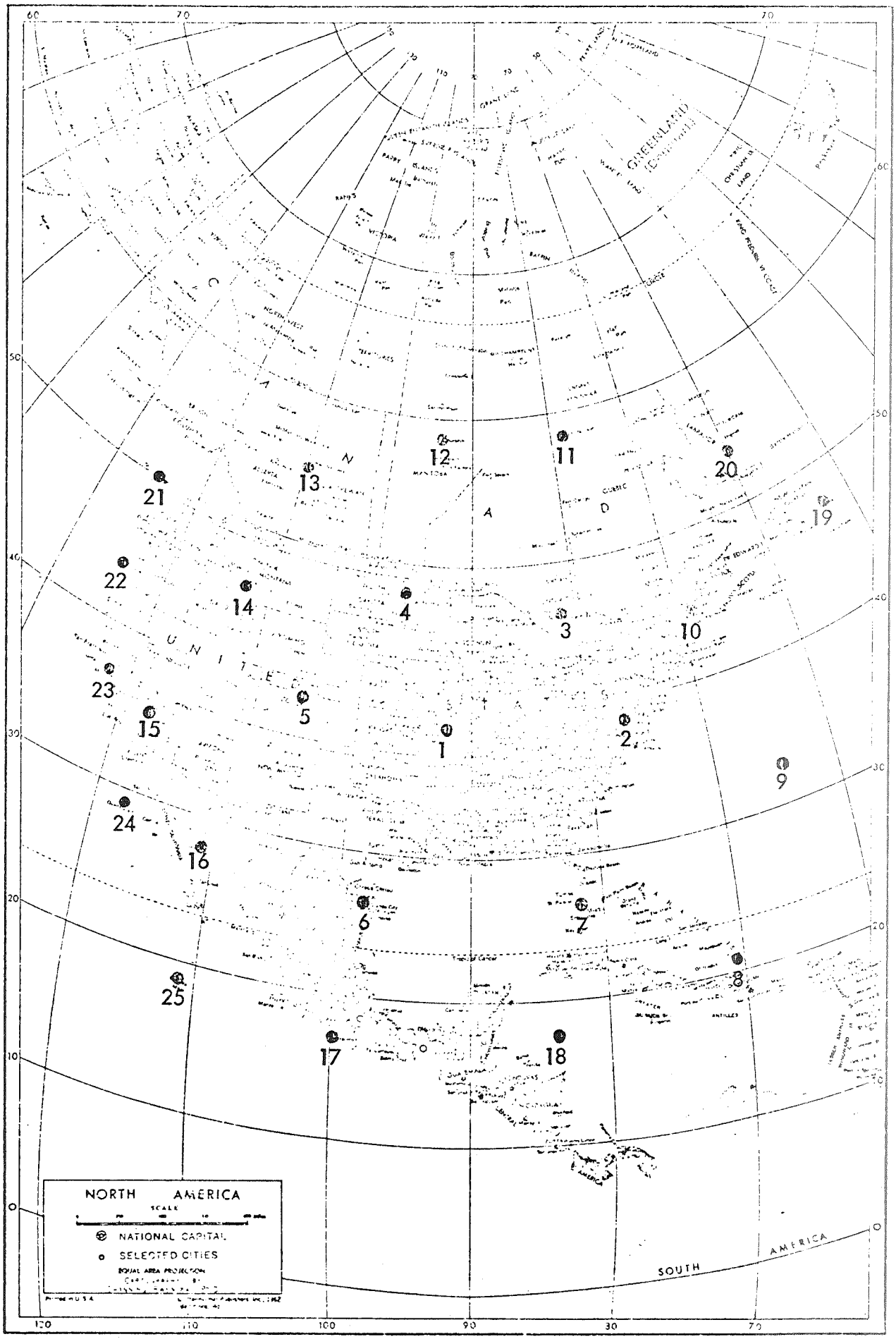

FIGURE 8. Illustrating 25 station net employed in Simulations I and II.

TABLE 9. Observational Schedule employed in Simulation I.

Station	φ	λ	Stations Participating in Observation of Passes: 1-11	12-22	23-33	34-44	45-55	56-66	67-77	78-88	89-99	100-110	111-121
1. Columbia	39°.0	92°.3	X	X	X	X	X	X	X				
2. Goddard	39.0	76.8	X	X	X				X	X			
3. Sudbury	46.4	81.3	X	X	X	X				X			
4. E.Grand Forks	48.0	97.0	X	X	X	X	X	X			X		
5. Denver	39.8	105.0	X			X	X	X			X	X	X
6. Edinberg	26.0	98.5	X				X	X	X				X
7. Ft. Myers	26.5	81.9	X						X				
8. Grand Turk Is.	21.2	71.1		X					X				
9. Bermuda	32.4	64.7		X					X	X			
10. Bangor	44.7	68.8		X	X					X			
11. Port Harrison	58.3	79.0			X					X			
12. Churchill	58.7	92.0			X	X							
13. Cold Lake	54.5	110.3				X					X		
14. Butte	46.4	112.5				X	X				X	X	
15. Mohave	35.3	116.9					X				X	X	X
16. Guaymas	27.8	111.2					X	X				X	X
17. Acapulco	16.3	100.0						X					X
18. Swan Is.	17.3	84.1						X	X				
19. St. Johns	47.7	52.7								X			
20. Goose Bay	53.3	60.0								X			
21. Vancouver	49.0	124.0									X		
22. Coos Bay	43.0	124.3										X	
23. Monteray	36.5	123.0										X	
24. Guadalupe	29.0	118.3										X	X
25. Socotto Is.	18.8	110.9									X		X

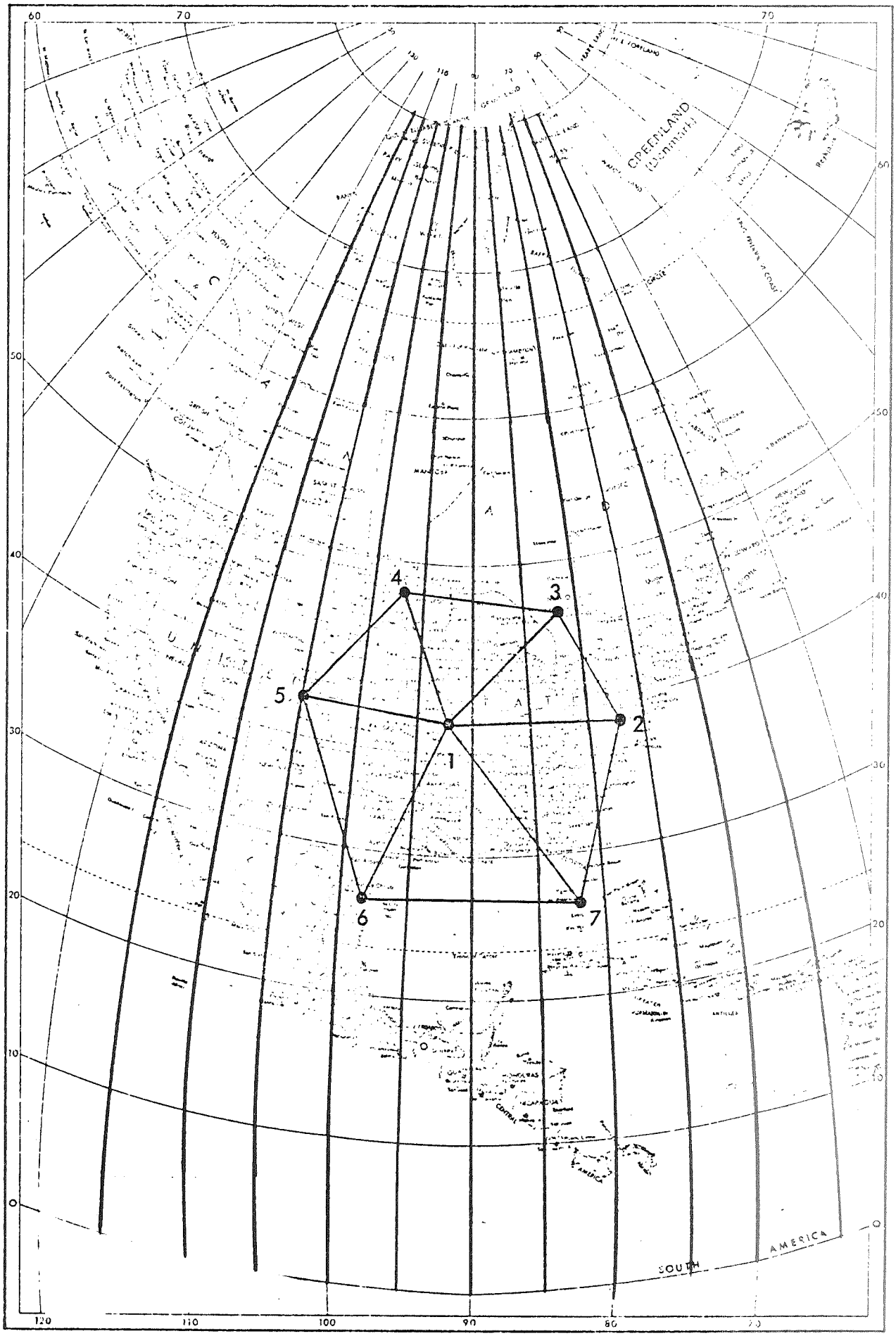

FIGURE 9. Geometry of 11 passes observed by Subnet 1 in Simulation I.

(4) orbital state vectors are completely unknown;

(5) a priori one sigma constraints on error coefficients are:

(a) a_0 (zero set), 10^7 m,

(b) a_1 (freq. offset), $\lambda_0 \times 10$ Hz,

(c) a_2 (freq. drift), $\frac{1}{2} \lambda_0 \times 10^{-3}$ Hz/sec,

(d) a_3 (satellite proportional freq. bias): 10^{-9} ,

(e) a_4 (timing bias), zero for central station in each subnet,
.000050 sec. for all others,

(f) a_5 (refraction, 0.2m),

(6) data rate is two points per minute (consistent with capabilities of future Geoceivers).

A few comments are in order regarding these assumptions. Regarding 3, we would note that since a ranging network is geodetically indeterminant in angular orientation, any information that serves to orient the network uniquely can be rigidly enforced without causing internal contradiction. While orbital constraints can serve orient a ranging network dynamically, the precision is so low in short arc reductions that no great accuracy in enforced directions of baselines is needed to avoid internal contradiction.

It will be noted that the a priori constraint on the error coefficient a_3 is taken as 10^{-9} , which is tantamount to zero. This was done as a consequence of other simulations which showed that since an error in a_3 effectively constitutes an error in scale, it can set a limit to geodetic accuracies that no degree of tracking precision or redundancy can overcome. Fortunately, there is a simple way around this difficulty. It requires that at least one station participating in the tracking of each pass employ a local oscillator whose absolute frequency is known to a high order of accuracy. This can be accomplished either by employing a primary frequency standard at the station (e.g., a portable cesium beam standard) or by receiving VLF frequency transmissions to monitor the error in the local oscillator (this latter

approach can provide proportional accuracies in frequency of a few parts in 10^{10}). For the particular station having a near absolute, local frequency standard, the observation equation assumes a somewhat altered form. The term $\delta f_0'$ in the coefficient a_2 becomes highly constrained (see eq. (8)), and the term δf_0 can accordingly be separated out and absorbed into the coefficient a_3 which then becomes multiplied by the expression $(c\tau_j - r_j)$ in place of its former factor, namely $(-r_j)$. As a consequence of this change, the proportional frequency bias becomes sharply deterministic and can readily be recovered to within a few parts in 10^{10}. Since this bias refers to the satellite frequency, it is common to all stations participating on the same pass. Accordingly, when the local frequency at one station in a subnet is known with great accuracy, one is justified in numerical simulations in suppressing the coefficient a_3 for all stations in the subnet. This is precisely what we have done in all of the simulations to be presented here.

Now that the ground rules for the simulation have been explained, let us consider the results obtained. The solution of the normal equations for the adjustment of the hypothetical network involved the simultaneous recovery of 5883 parameters consisting of:

$3 \times 25 = 75$ unknown coordinates of tracking stations,
$6 \times 121 = 726$ unknown elements of orbital state vectors,
$7 \times 6 \times 121 = 5082$ unknown error coefficients.

The solution of such a large system of normal equations is practical only by virtue of the algorithm for second order partitioned regression incorporated into SAGA. The formation and inversion of the normal equations required 64 minutes on DBA's Xerox Sigma 5 computer. The results of major interest, the accuracies to be expected for the recovery of the coordinates of the tracking stations, are listed in Table 10.

From the table in conjunction with Figure 9, we see that stations in the interior of the net are determined to an accuracy ranging, for the most part, between 0.2 and 0.4 meters (one sigma), whereas those on the periphery are determined to about 0.7 to 1.5 meters. Such accuracies are on the order of five times better than has been experienced from optical networks of comparable scope (e.g., see Brown, 1968).

TABLE 10. Expected accuracies of station recovery resulting from Simulation I.

Station	Sigmas (meters)		
	X	Y	Z
1*	.00	.00	.00
2	.45	.37	.31
3	.39	.29	.25
4	.28	.17	.15
5	.37	.33	.27
6	.39	.20	.18
7	.59	.41	.31
8	.68	.64	.44
9	.80	.69	.54
10	.69	.55	.51
11	.63	.43	.42
12	.49	.32	.29
13	.67	.44	.45
14	.63	.49	.48
15	.75	.69	.59
16	.52	.56	.43
17	.56	.39	.30
18	.62	.51	.33
19	2.25	1.12	1.76
20	1.42	.79	1.12
21	1.43	.89	1.02
22	1.45	.90	1.03
23	1.33	.96	.89
24	.88	.82	.63
25	.72	.70	.47

* Adopted origin of survey.

Over a 24 hour period one would have no difficulty in observing a set of passes of Navy Navigational Satellites that approximates the geometry of the set of eleven passes adopted in the simulation for each subnet. Accordingly, most of the time and effort required for the data gathering phase of the hypothetical operation would be spent in the travel and logistics required to shift Geoceivers from one subnet to the next. If a total of ten days is budgeted for the travel, logistics, and data gathering for each subnet, the overall field operation could be completed in about four months. This is comparable with the period that would be required for an equivalent network of 25 optical tracking stations to observe from 100 to 150 good passes of a flashing light satellite (this assumes that all 25 optical stations are occupied throughout the entire period). It follows, then, that in a four month operation 7 Geoceivers can survey a 25 station, intracontinental network to an accuracy about five times greater than can 25 cameras operating for the same length of time. Thus, the geodetic potential of the Geoceiver is impressive indeed.

The capability of the Geoceiver for short arc orbital determination is also a matter of considerable interest. As a by-product by the error propagation for survey, we obtain from SAGA a partial error propagation for the recovery of elements of the orbital state vector. By partial, we mean that errors remaining in the survey are not taken into account (i.e., it is as if the survey were flawless). However, all other errors are rigorously taken into account, including those remaining in the recovered error coefficients of the trackers. A very good idea of the tracking capabilities of a seven station Geoceiver net can be had from Table II, which lists the sigmas obtained for the state vectors of the eleven passes pictured in Figure 9. Accuracies in position at epoch (taken at midarc) are seen to range from as little as 0.5 meters, or better, for the more central passes to as much as 3 to 7 meters for extra-peripheral passes. The only tracking system we know of that can rival such accuracies for central passes is the GLOTRAC system of the Air Force Eastern Test Range. This system, however, is no longer operational.

The surpassing capability of a strong Geoceiver network for short arc tracking may well generate far more applications for the system than was ever envisioned by its originators. For the near term, a natural application of the system would be in conjunction with the GEOS C

TABLE 11. Accuracies to be expected for recovery of orbital state vectors of passes observed by Subnet 1 in Simulation I.

Pass No.	Sigmas of Components of Orbital State Vectors*					
	Position (meters)			Velocity (meters/sec)		
	X	Y	Z	X	Y	Z
1	5.1	10.4	5.9	.005	.009	.006
2	2.3	2.7	1.5	.003	.004	.003
3	1.3	.9	.5	.002	.002	.001
4	.9	.4	.3	.001	.001	.001
5	.7	.3	.3	.001	.001	.001
6	.5	.3	.4	.001	.001	.001
7	.7	.3	..3	.001	.001	.001
8	.8	.3	.3	.001	.001	.001
9	1.0	.6	.4	.002	.002	.001
10	1.6	1.5	1.0	.002	.003	.002
11	3.4	5.4	3.3	.004	.006	.004

* Epoch at midarc.

radar altimeter experiment. For evaluating the accuracy of the altimeter, a six or seven station Geoceiver net, well distributed about the Carribean, could generate short arc ephemerides to accuracies of better than one meter over a considerable area.

9. Results of Simulation II

In viewing the results of Simulation I, we became curious about what could be expected if all 25 stations in our hypothetical net were to be occupied simultaneously by Geoceivers. We were particularly stimulated by consideration of Figure 10, which is a plot of actual ground tracks (relative to a tracking horizon of 5°) of Navy Navigational Satellites observable from a typical station at midlatitudes during a 48 hour period when four satellites are in operation. Accordingly, we undertook a simulation employing the same general assumptions as before except for the following:

(1) a total of 25 Geoceivers are committed to the operation (hence all stations are simultaneously occupied);

(2) the operation is consistent with what could be expected from a 48 hour period and involves observation of the set of 37 passes pictured in Figure 11;

(3) each of the 25 stations tracks every pass reaching a maximum elevation angle of at least 10° above a cutoff horizon of 5°.

In view of the production run of 33 Geoceivers, assumption (1) can potentially be realized. This possibility is enhanced by the short period of commitment demanded by assumption (2).

As a result of assumption (3), 27 of the 37 passes are tracked by at least 15 stations and all are tracked by at least 9. The observing schedule for the simulation is provided by Table 12.

An assumption tacitly made in Simulation I is that the location of the Earth's center of mass is known flawlessly relative to the adopted origin. In Simulation II we drop this assumption and exercise an option in SAGA for carrying the coordinates of center of mass as constrained parameters. By so doing, we avoid introducing any dynamical inconsistency that would otherwise result when one elects in a short arc reduction to hold fixed an adopted set of coordinates for the particular station selected to be the origin of the network. Although

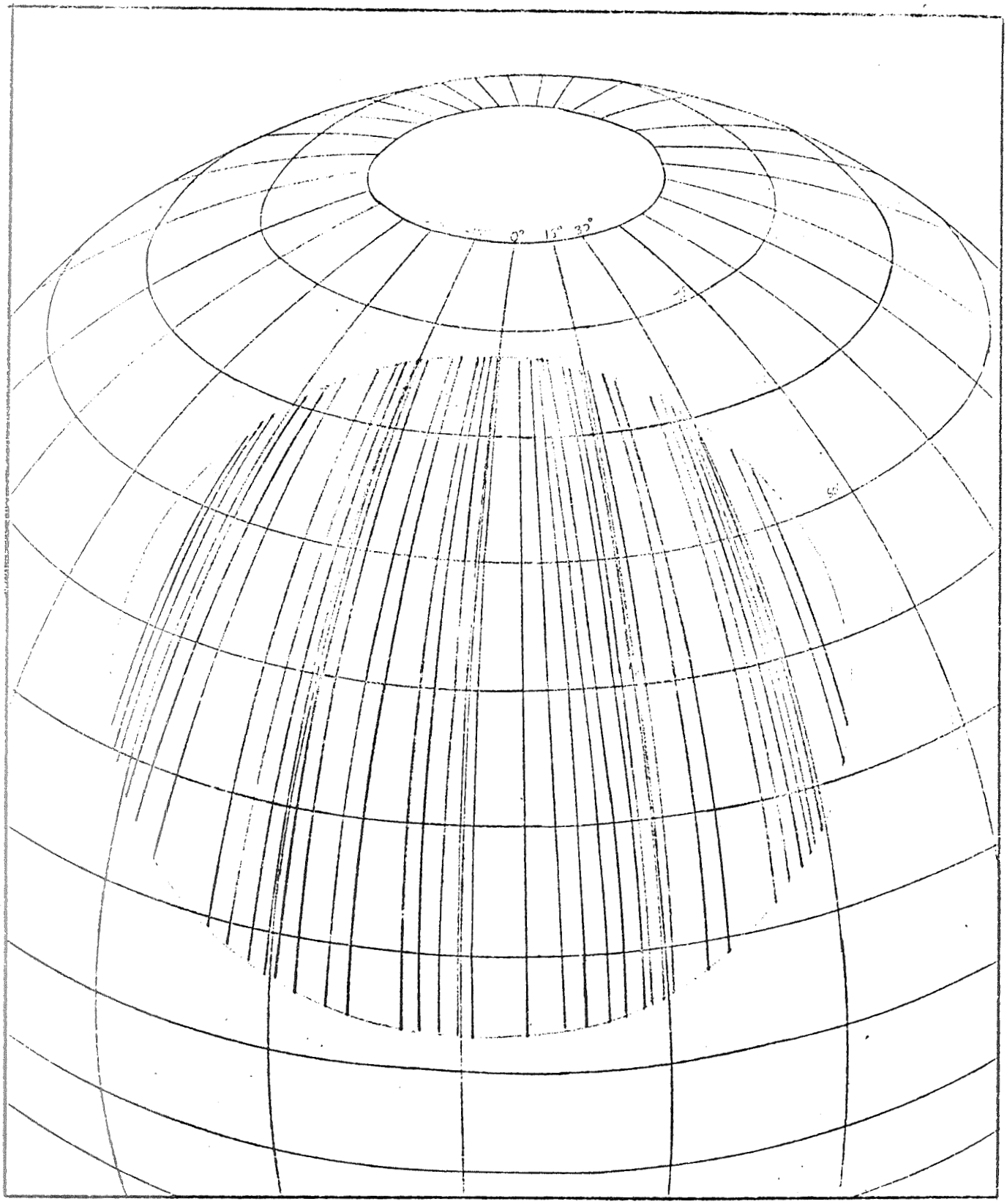

FIGURE 10. Illustrating an actual set of ground tracks of 39 passes of Navy Navigational Satellites as seen by station at 40° latitude during a 48-hour period (cutoff elevation angle, 5°).

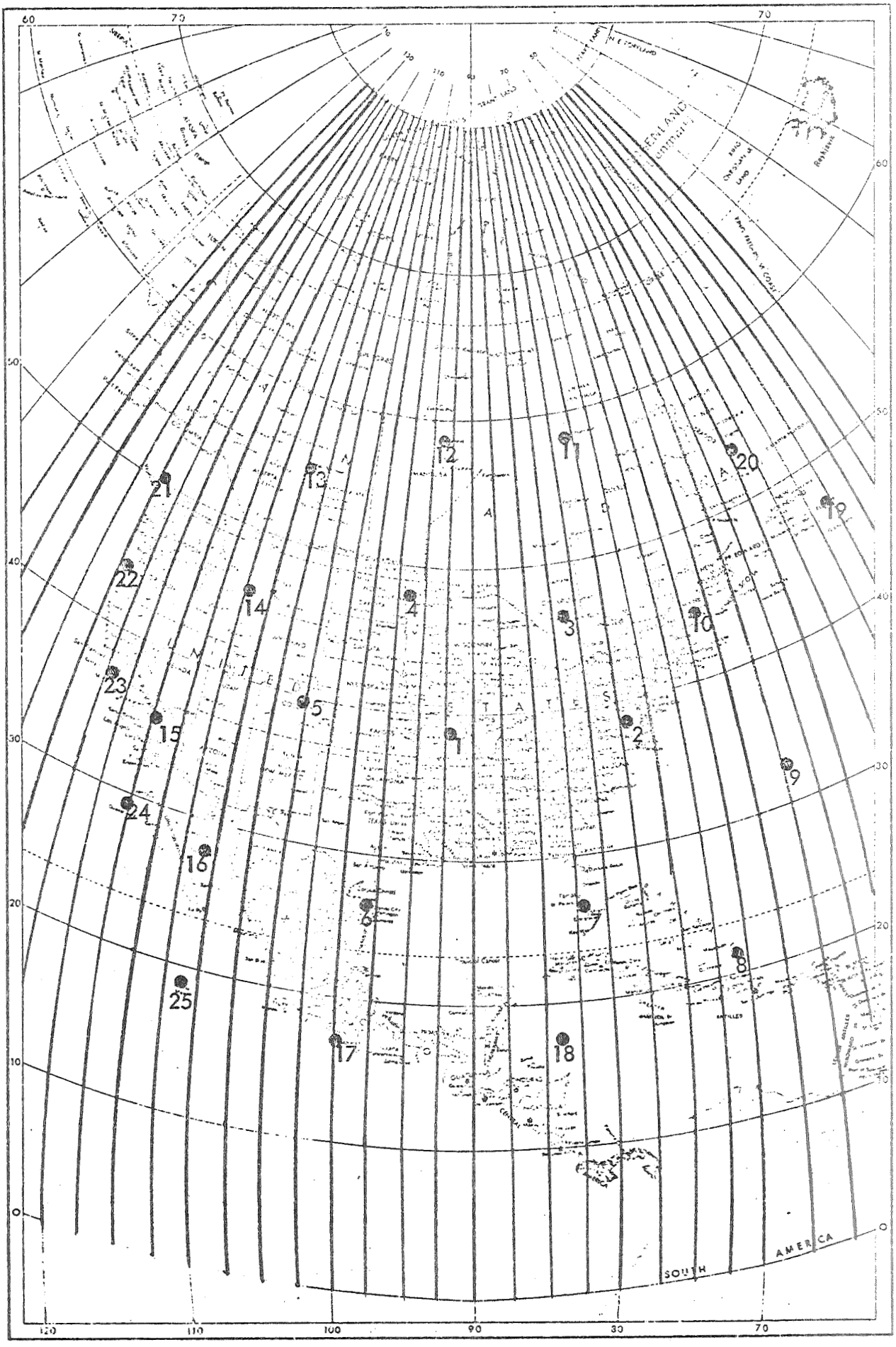

FIGURE 11. Geometry of 37 passes relative to tracking net employed in Simulation II.

TABLE 12. Observational schedule employed in Simulation II.

Station No.	Pass No. 1	2	3	4	5	6	7	8	9	10	11	12	13	14	15	16	17	18	19	20	21	22	23	24	25	26	27	28	29	30	31	32	33	34	35	36	37	Total Passes/ Station
1							X	X	X	X	X	X	X	X	X	X	X	X	X	X	X	X	X	X	X	X	X	X	X	X	X	X						27
2	X	X	X	X	X	X	X	X	X	X	X	X	X	X	X	X	X	X	X	X	X	X	X	X	X	X												26
3	X	X	X	X	X	X	X	X	X	X	X	X	X	X	X	X	X	X	X	X	X	X	X	X	X	X	X	X	X	X								30
4					X	X	X	X	X	X	X	X	X	X	X	X	X	X	X	X	X	X	X	X	X	X	X	X	X	X	X	X	X	X	X	X	X	X	32
5												X	X	X	X	X	X	X	X	X	X	X	X	X	X	X	X	X	X	X	X	X	X	X	X	X	X	26
6											X	X	X	X	X	X	X	X	X	X	X	X	X	X	X	X	X	X	X	X	X	X	X	X				24
7					X	X	X	X	X	X	X	X	X	X	X	X	X	X	X	X	X	X	X	X	X	X													22
8	X	X	X	X	X	X	X	X	X	X	X	X	X	X	X	X	X	X	X	X	X	X																22
9	X	X	X	X	X	X	X	X	X	X	X	X	X	X	X	X	X	X	X	X	X																	21
10	X	X	X	X	X	X	X	X	X	X	X	X	X	X	X	X	X	X	X	X	X	X	X	X														24
11	X	X	X	X	X	X	X	X	X	X	X	X	X	X	X	X	X	X	X	X	X	X	X	X	X	X	X	X	X	X	X	X	X	X	X	X	X	37
12	X	X	X	X	X	X	X	X	X	X	X	X	X	X	X	X	X	X	X	X	X	X	X	X	X	X	X	X	X	X	X	X	X	X	X	X	X	37
13								X	X	X	X	X	X	X	X	X	X	X	X	X	X	X	X	X	X	X	X	X	X	X	X	X	X	X	X	X	X	30
14													X	X	X	X	X	X	X	X	X	X	X	X	X	X	X	X	X	X	X	X	X	X	X	X	X	25
15																X	X	X	X	X	X	X	X	X	X	X	X	X	X	X	X	X	X	X	X	X	X	22
16																X	X	X	X	X	X	X	X	X	X	X	X	X	X	X	X	X	X	X	X	X	X	22
17													X	X	X	X	X	X	X	X	X	X	X	X	X	X	X	X	X	X	X	X	X	X				22
18							X	X	X	X	X	X	X	X	X	X	X	X	X	X	X	X	X	X	X	X													20
19	X	X	X	X	X	X	X	X	X	X	X	X	X	X	X	X	X	X	X																			19
20	X	X	X	X	X	X	X	X	X	X	X	X	X	X	X	X	X	X	X	X	X	X	X	X														24
21																		X	X	X	X	X	X	X	X	X	X	X	X	X	X	X	X	X	X	X	X	20
22																		X	X	X	X	X	X	X	X	X	X	X	X	X	X	X	X	X	X	X	X	20
23																				X	X	X	X	X	X	X	X	X	X	X	X	X	X	X	X	X	X	18
24																			X	X	X	X	X	X	X	X	X	X	X	X	X	X	X	X	X	X	X	19
25																	X	X	X	X	X	X	X	X	X	X	X	X	X	X	X	X	X	X	X	X	X	20
Total Stations/ Pass	9	9	9	9	10	11	13	14	14	14	15	16	18	18	18	20	21	23	24	24	24	23	22	22	20	20	17	17	17	17	16	16	16	15	13	13	13	

we inadvertently failed to exercise this option in Simulation 1, we know from other simulations that theoretical accuracies for recovery of survey of strong ranging nets remain virtually unaltered when coordinates of center of mass are allowed to adjust. Thus our results for Simulation 1 are valid, and the main consequence of our oversight is that we lack figures for the accuracy to be expected from the experiment for the location of the center of mass with respect to the adopted origin.

The standard deviations to be expected for the recovered coordinates are listed in Table 13. Results in this case are given both in terms of X,Y,Z components (to facilitate comparison with Table 10) and in terms of North, East and Up (N,E,U) components. We see that accuracies obtained from Simulation II are appreciably better than those obtained from Simulation I. For the most part, the sigmas from Simulation II are only about one half as great as those from Simulation I.

Especially noteworthy from Table 13 is the sharp recovery to be expected for the coordinates of center of mass; sigmas in Y and Z are less than one meter and the sigma in X is only about 1.5 meters. Thus we may conclude that not only can a strong Geoceiver network recover relative positions of stations throughout a continental net to within accuracies of a few tenths of a meter, but it can also generate mass-centered coordinates to within accuracies of a meter or two.

We find, then, that one can expect to obtain significantly better accuracies, overall, from a 25 station Geoceiver network observing a total of 37 passes than one can from 7 Geoceivers observing a total of 121 passes from interlocking subnets forming an equivalent 25 station net. This result is perhaps not too startling; what is indeed startling is that in the former situation, only a two-day observing period is needed, whereas in the latter situation something like four months is needed, a ratio of 60 to 1 in favor of the former. Clearly, then, if it could possibly be arranged, an actual experiment along the lines of Simulation II would be a most worthy undertaking, constituting (if successful) an event of epochal significance in satellite geodesy. We suggest that should such an experiment be undertaken, an intensive observational schedule over a period of at least ten days should be planned. This would allow

TABLE 13. Accuracies to be expected for station coordinates recovered from Simulation II.

Station	Sigmas (meters)					
	X	Y	Z	N	E	U
1*	.00	.00	.00	.00	.00	.00
2	.29	.23	.15	.22	.24	.23
3	.26	.19	.15	.24	.18	.18
4	.23	.13	.12	.18	.14	.18
5	.27	.21	.15	.18	.22	.24
6	.28	.16	.15	.19	.17	.25
7	.31	.25	.19	.22	.25	.29
8	.42	.42	.31	.33	.42	.40
9	.46	.43	.28	.40	.42	.37
10	.38	.34	.24	.38	.34	.24
11	.38	.27	.30	.43	.25	.23
12	.35	.21	.22	.33	.22	.24
13	.41	.29	.28	.30	.29	.40
14	.36	.31	.24	.24	.31	.37
15	.42	.41	.28	.25	.38	.47
16	.36	.35	.25	.25	.34	.36
17	.36	.26	.24	.26	.27	.34
18	.36	.33	.26	.27	.32	.35
19	1.01	.66	.83	1.29	.59	.34
20	.67	.49	.58	.86	.43	.30
21	.72	.53	.50	.32	.47	.86
22	.73	.55	.51	.32	.48	.88
23	.64	.57	.44	.29	.47	.79
24	.47	.49	.34	.28	.44	.56
25	.41	.40	.32	.31	.39	.43
C.M.**	1.51	.96	.95	-	-	-

*Adopted origin of net.
**Center of Mass.

five or more independent, two-day solutions to be executed, thereby providing a solid check of internal consistency. Should results conform to theoretical expectations, all passes could be merged into a single simultaneous reduction that would (for a ten-day experiment) produce coordinates having standard deviations about half as large as those in Table 13. One could also perform appropriate ancillary reductions, such as comparing results from processing of selected nighttime passes (low ionospheric refraction) with those from processing of selected daytime passes (high ionospheric refraction). In this way, one could ascertain whether or not higher order ionospheric refraction has any significant effect.

Even if the experiment just suggested were fully successful, one would not be completely assured that the accuracies indicated by the reduction were, in fact, actually achieved. Conceivably, systematic errors in the survey could be several times larger than the theoretical standard deviations. It does, after all, boggle the mind to contemplate attainment of geodetic accuracies of a few tenths of a meter from satellite observations made over a period of only a few days. Fortunately, there is a way to erase any doubts (pro or con) concerning the ultimate capabilities of the Geoceiver. This is by conducting an aircraft test that approximately simulates, on a small scale, the geometry of the satellite test as is later discussed in Section 11.

10. Results of Simulation III

The results of the previous simulations suggest that relative position accurate to a few tenths meter can be recovered for interior stations in strong Geoceiver nets of continental extent. This naturally engenders speculation concerning the potential capabilities of the system in establishing intercontinental ties. Could accuracies theoretically be achieved that would be worthwhile in investigations of continental drift or other geophysical phenomena. To gain some insight into this matter, we designed a simulation based on the geometry indicated in Figure 12. Here we have postulated the existence of an 18 station tracking net consisting of 6 stations in North America, 6 stations in South America and 6 stations in Northern Africa/ Southern Europe. In view of the results of our earlier simulations, we assume that the stations in each of these three subnets were previously embedded in much more extensive continental

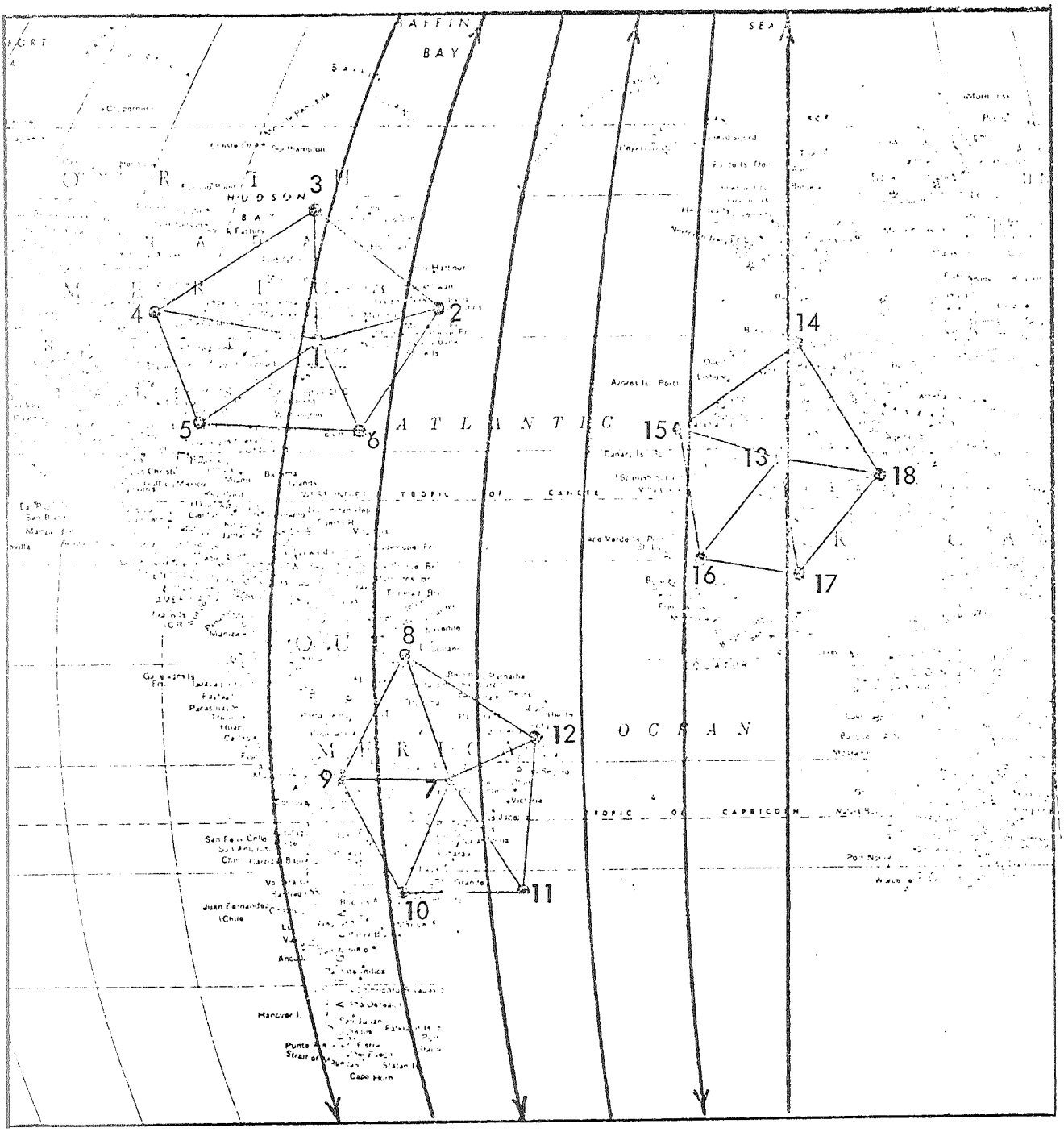

FIGURE 12. Geometry of 6 passes relative to tracking net employed in Simulation III.

nets in which a large number of passes of Navy Navigational satellites were observed. Accordingly, we may assume that the relative positions of the stations within each subnet have been pre-established to within a few tenths of a meter. The locations and orientations of the subnets with respect to one another are, however, assumed to be unknown. To interrelate the subnets, we assume that they participate in the tracking of a high altitude satellite (h = 6400km) in a circular polar orbit. A total of 6 passes spaced at 15° intervals across the equator (Figure 12) is assumed to be observed. Assumptions concerning ranging sigmas, data rates, cutoff angles, and error models are the same as in the other simulations. As in Simulation II, we assume that the location of the Earth's center of mass with respect to the adopted origin is unknown.

An assumption in Simulation III that has no counterparts in the other simulations is that the 15 baselines within each of the three subnets are constrained in distance to 0.2 meters (one sigma). This artifice serves to establish relative positions within each subnet to accuracies of a few tenths of a meter and yet leaves the subnets unconstrained in absolute location and orientation. The North American subnet is given preference in that Station 1 is locked down, as also are two components of the direction of baseline $\overline{2,4}$ and one component of the direction of baseline $\overline{3,6}$. Thus the North American subnet incorporates the adopted origin and is absolutely oriented. The question then becomes one of determining how well the locations of the stations of the other two subnets can be established relative to the preferred North American net. The answer is given in Table 14.

We see that for the South American subnet expected accuracies relative to the adopted North American origin average about 0.4m, 0.7m and 0.5m in North, East and Up; for the Euro-African subnet they are similar, averaging about 0.6m, 0.6m, and 0.5m in North, East and Up. Recovery of center of mass is quite good, amounting to 1.5m, 1.1m and 3.1m in X,Y,Z.

The results of Simulation III do indeed indicate that the Geoceiver system is potentially capable of establishing intercontinental ties to accuracies sufficiently great to be of value in geophysical investigations of continental drift (especially so, when it is considered that the simulation employed only six passes of a satellite). The experiment simulated may well be far

TABLE 14. Accuracies to be expected for station coordinates recovered from Simulation III.

Station	Location		Sigmas (meters)					
	φ	λ	X	Y	Z	N	E	U
1*	45°	73°	.00	.00	.00	.00	.00	.00
2	47	52	.12	.20	.20	.20	.19	.14
3	59	77	.17	.20	.21	.18	.19	.21
4	48	97	.13	.26	.20	.12	.26	.20
5	33	88	.18	.22	.20	.17	.22	.20
6	32	65	.17	.26	.22	.21	.26	.18
7	-11	49	.61	.69	.32	.35	.73	.54
8	2	51	.48	.55	.31	.31	.56	.47
9	-11	65	.59	.66	.29	.31	.69	.54
10	-23	58	.72	.80	.31	.41	.85	.60
11	-22	41	.75	.81	.36	.48	.88	.59
12	- 7	36	.61	.67	.37	.39	.72	.54
13	29	1	.61	.52	.59	.65	.61	.44
14	44	- 1	.57	.49	.58	.64	.57	.40
15	33	16	.42	.48	.45	.52	.46	.37
16	15	13	.55	.58	.51	.53	.61	.49
17	13	- 2	.77	.61	.63	.66	.76	.59
18	27	-14	.88	.52	.75	.81	.82	.53
C.M.**	-	-	1.50	1.11	3.05	-	-	-

* Adopted origin of net.
** Center of Mass.

from optimum for this purpose. Accordingly, a more extensive study of the matter would seem to be warranted, especially so in view of the promising character of our present results.

11. Aircraft Test of Geoceiver Accuracies

Our simulations serve only to indicate what can be expected from a tracking configuration under a given framework of assumptions. They do not prove anything. However, in view of the enormous promise indicated by the results, we feel that a definitive test should be undertaken to establish whether or not the indicated potential of the system can, in fact, be realized. This would be a simple matter if one knew the coordinates of a moderate number of widely separated stations to sufficient accuracy (namely, to within one to two tenths of a meter). As it is, nothing available even remotely approaches this requirement. Accordingly, an alternative to a full-scale direct test must be sought.

A consideration of pivotal importance with regard to the practicability of designing such a test is that nothing prevents Geoceiver observations from being subjected to a strictly geometric reduction. Orbital constraints are by no means essential to a Geoceiver reduction, although they do add significantly to the strength of the result when only a relatively small number (say less than 5 or 6) of stations participate on each pass. However, when the number of participating stations rises to about 10 or 12 with good distribution, the exercise of orbital constraints leads to only minor improvement over what can be obtained from a purely geometric reduction. The mathematics of the geometric reduction are fully developed in the EMBET (Error Model Best Estimate of Trajectory) reduction derived in Brown, Bush, Sibol (1964) and elaborated on in Brown (1966). Only a few minor changes in the ranging error model of these references are necessary for the application to Geoceiver. Recently (Gyer, 1970), we have extended the scope and efficiency of the geometric reduction by exploiting the algorithm for second order partitioned regression developed in Brown, Trotter (1969).

One other consideration is important to the practical evaluation of the absolute accuracies obtainable from Geoceivers. This concerns the fact that with a true ranging system, wherein σ_r is independent of r, the accuracy to be expected for recovery of survey does not depend on the scale of the tracking geometry. This means that if surveys can be recovered to, say 0.2m, from a configuration having baselines averaging, say 20km, they can also be recovered to

this very same accuracy in a scaled-up configuration with baselines averaging, say, 2000km. This statement would apply without qualification to the Geoceiver, were it not for the presence of terms in r and $\dot{r}$ in the Geoceiver error model. As a practical matter, the term in r (satellite frequency bias) causes no especial difficulty for, as we have already noted, it can be suppressed when at least one participating Geoceiver employs a primary frequency standard (or its practical equivalent). Accordingly, only the term in $\dot{r}$ (timing bias) would have a different effect in an aircraft test (max $\dot{r} < 200$ m/sec) than in a satellite test (max $\dot{r} < 8000$ m/sec.). If due allowance is made for this consideration in interpreting the results, findings from a suitably designed aircraft test can be extrapolated with confidence to apply to a geometrically similar satellite test.

The ideal place to conduct the suggested aircraft test is over the USCGS geodimeter/triangulation survey of east-central Florida (Figure 13). The accuracy of this survey is better than 1 part in 10^6, which is equivalent to about 0.02 meters for the relative positions of adjacent stations. Moreover, the net contains 64, fairly uniformly distributed stations from which a selection can be made approximating the relative geometry of a continental network. To approximate the tracking geometry of Simulation II, one would employ an aircraft flying at an altitude of about 10km and proceeding at 300 knots along 37 parallel flight lines of 100 to 200km length spaced at intervals of about 2km. The aircraft would, of course, carry a transmitter equivalent to those used on Navy Navigational Satellites.

If the survey recovered from the suggested aircraft test should agree with the USCGS survey to within a few tenths of a meter, one would have a solid basis for proceeding with the analogous satellite experiment. If not, one would at least have ample observational material for an investigation into the reasons why theoretical expectations were not being achieved.

Because of the problem of instrumenting an aircraft, the suggested aircraft test would actually be more troublesome and costly to arrange than would the continental test of Simulation II. After all, the satellites required for the continental test are continuously operational and cost nothing to use. For this reason, it would probably be best to perform the continental test first to determine whether or not the system can pass a full-scale test of internal consistency. A partial evaluation of absolute accuracy, applicable to stations of

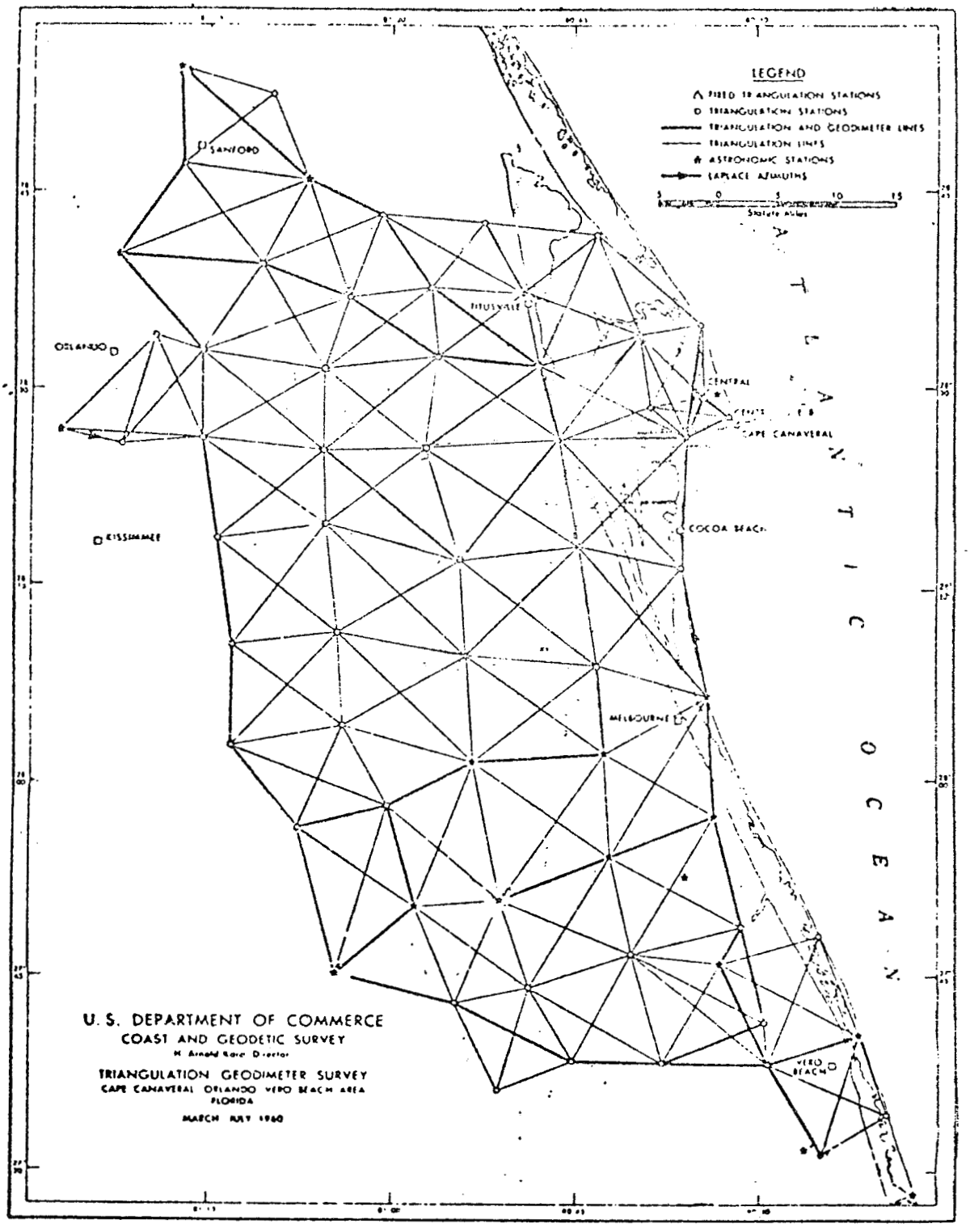

FIGURE 13. Layout of USCGS geodimeter/triangulation survey of East-Central Florida.

limited separation, could be incorporated into such a test. This would entail enlarging the net to include at least three Geoceivers operating from stations on the Florida net of Figure 13. In this way, one would be able to ascertain the precise degree to which relative positions could be recovered for stations separated by a few tens of kilometers. A favorable outcome in this regard could not, however, be validly extrapolated to widely separated stations. This is mainly because systematic errors in recovered orbits would have similar effects on closely spaced stations and so would not seriously compromise the recovery of their relative positions. On the other hand, because of their geometrical diversity, widely separated stations would not enjoy such immunity to systematic error with respect to the recovery of their relative positions. Accordingly, an aircraft test appears, at this time, to provide the most practicable means for the evaluation of the ultimate capabilities of the Geoceiver in establishing relative positions throughout a geometrically diversified net.

12. Conclusions

By virtue of the approach adopted in SAGA of treating the Geoceiver as a ranging system, rather than a range-difference system, an order-of-magnitude improvement in the capability of the system for geodetic positioning, particularly in the short arc mode, emerges as a new factor in satellite geodesy. Accuracies in station recovery of a few tenths of a meter from observations taken over a few days appears now to be feasible. Should it live up to its theoretical expectations, the Geoceiver could have a truly revolutionary impact on satellite tracking and satellite geodesy. In particular, it would establish beyond any reasonable doubt the technical feasibility of SURSAT, the 'Satellite Surveying Utility' proposed in Brown (1968) for use in a wide range of general and commercial surveying applications. SURSAT receivers would be simple in the extreme (costing under $10K or about one tenth as much as a Geoceiver), yet would produce coordinates accurate to 0.1 to 0.2 meters from observations taken over a period of only two to three hours.

REFERENCES

Brown, D.C., 1966. Advanced Techniques for the Reduction of Geodetic SECOR Observations. Final Report prepared for GIMRADA under U.S. Army Contract No. DA-44-009-AMC-937(X).

Brown, D.C., 1968a. Short Arc Optical Survey of the GEOS North American Tracking Network, GSFC Report X-550-68-439, Goddard Space Flight Center, Greenbelt, Maryland.

Brown, D.C., 1968b. Feasibility of a Satellite Surveying Utility, presented at the 49th Annual Meeting of the American Geophysical Union, April 8-11, 1968, Washington, D.C.

Brown, Bush, Sibol, 1964. Investigation of the Feasibility of Self-Calibration of Tracking Systems. AF Cambridge Research Labs. Report No. 64-441.

Brown, Trotter, 1969. SAGA, A Computer Program for Short Arc Geodetic Adjustment of Satellite Observations, AF Cambridge Research Labs. Report No. 69-0080.

Gyer, M., 1970. An Investigation of the Long Range Position Determining System (LRPDS) by Digital Simulation Methods, Final Report prepared for U.S. Army Engineer Topographic Laboratories (ETL) under Contract No.: DAAK02-70-C-0200.

Smith, S.L., 1969. Analysis of Data From the Geoceiver Collocation Test, NWL Technical Report TR-2338.

Stansell, Bourguignon, Karl, Marth, 1965. Geoceiver: An Integrated Doppler Geodetic Receiver, TG-710 (John Hopkins Applied Physics Lab), revised 1968.

SECTION II

GEOS-C

GEOS-C PLANS

Robert M. Rados

GEOS-C Project Manager (Acting)
Goddard Space Flight Center
Greenbelt, Maryland

Presented at GEOS-2 Program Review
Meeting, Goddard Space Flight Center,
22-24 June 1970

GEOS-C PLANS

Robert M. Rados

This afternoon's session is entitled "GEOS-C Plans". However, the session really can be divided into two parts: The first papers deal primarily with the Earth Physics and Geodesy Program as a whole. It is from these programs that the objectives for GEOS-C were derived. The second section of this session is concerned with a few of the proposed instrument systems for GEOS-C.

The management for GEOS-C was assigned to Goddard Space Flight Center last February. Since that time, there has been a concentrated effort to study and define the complete GEOS-C mission.

First, the geodesy Working Group under Dr. Vonbun provided the GEOS Project study group a list of objectives and potential instrument systems. From the objectives, a requirement for a low inclination orbit is deduced. There were two basic constraints applied to the design of GEOS-C, (1) Delta Launch and (2) Budget. This second constraint is the one which determines how many and which of the objectives will be pursued.

During the first part of the study all objectives and all instrumentation systems were considered, irrespective of cost. As you might expect, none of the instrumentation and, therefore, the complexity, were deleted because they lacked support for an objective or because they were technologically infeasible. Therefore, it became necessary to reanalyze our goals in terms of meeting objectives which are within our budgetary constraints. Figure 1 is a summary of the constraints and the proposed instrumentation for GEOS-C.

The Radar Altimeter is the prime system and the major change to GEOS I & II. The specific approach and detail specifications have not been finalized. Later Mr. Bryan of GSFC will relate some of the factors which will be influencing the decision on Radar Altimeter specifications.

The so called "bare bones" spacecraft will contain, in addition to the altimeter, two flashing lights, laser reflector panels, two C-band transmitters, Tranet, as in GEOS II and a Unified S-Band transponder which, like the Radar Altimeter, will be new to GEOS.

The spacecraft will have two axis stabilization as in GEOS II, PCM for telemetry, a new command format, an updated power system to provide increased capability, and an attitude determination system to provide data for evaluation of the Radar Altimeter.

The orbit, as defined now will be: Eccentricity .014 to .020, inclination 22°, and altitude between 750 and 1500 KM.

We are continuing to investigate the other systems (Items 7-12 of Figure 1) especially toward defining more specifically the complexities and costs of inclusion in GEOS. One of the more desirable systems being studied is the GRARR/ATS relay. This system would require a comparatively major change in the structure of GEOS.

Where do we stand? What is the Schedule? Before answering these questions, I would like to say that the study is a combined effort of many interested parties, however, the final plan must be a compromise based on the resources available. We hope that the final draft of a Project Plan will be complete in two weeks. Upon approval by GSFC top management and subsequently NASA Headquarters, the GEOS-C fabrication will get underway. We believe that the Radar Altimeter is the pacing item and together with procurement lead times, etc. it is probable that the launch will occur no earlier then 2nd Quarter Calendar Year 1973. Before I introduce the next speaker, I would like to acknowledge the efforts of many who are contributing to the study and the planning, many of whom are present here today.

G E O S - C

INSTRUMENT SYSTEMS

1. RADAR ALTIMETER
2. UNIFIED S-BAND
3. LASER RETROREFLECTOR ARRAY
4. C-BAND (NON-COHERENT) (2)
5. FLASHING LIGHTS (2)
6. TRANET
7. GRARR/ATS RELAY
8. MISTRAM
9. C-BAND COHERENT
10. VAN ATTA ARRAY
11. LASER INFRARED RETROREFLECTOR
12. LASER DETECTOR

CONSTRAINTS

1. DELTA LAUNCH
2. BUDGET
3. ORBIT

INCLINATION	22°
ECCENTRICITY	0.014 - 0.020
ALTITUDE	750 - 1500 KM

SPACECRAFT SYSTEMS

2 AXIS STABILIZATION

IMPROVED POWER SYSTEM

NEW COMMAND FORMAT

PCM FOR TELEMETRY

ATTITUDE DETERMINATION SYSTEM

PLANS BY SAO FOR THE USE OF GEOS C IN GEODETIC AND EARTH-PHYSICS INVESTIGATIONS

Charles A. Lundquist and George C. Weiffenbach

Presented at the Geos 2 Review Meeting
Goddard Space Flight Center, Greenbelt, Maryland

June 1970

Smithsonian Institution
Astrophysical Observatory
Cambridge, Massachusetts 02138

006-68A

PLANS BY SAO FOR THE USE OF GEOS C IN GEODETIC AND EARTH-PHYSICS INVESTIGATIONS

Charles A. Lundquist and George C. Weiffenbach

At the Smithsonian Astrophysical Observatory (SAO), investigations based on satellite tracking stress topics of a comprehensive, global character. The 1969 Smithsonian Standard Earth (II) is a typical example of the research to which SAO scientists have devoted their principal efforts (Gaposchkin and Lambeck, 1970; Gaposchkin and Kaula, 1970). Such research has distinctive features that are pertinent to plans to utilize data from Geos C.

SAO analyses depend on the combination of a variety of data, both optical and radio, from a substantial variety of independent orbits, involving many satellites--for example, 12 in the determination of zonal-harmonic coefficients (Kozai, 1969) and 21 in the determination of tesseral-harmonic coefficients of the geopotential (Gaposchkin and Lambeck, 1970). The 1969 Standard Earth also incorporates geometric solutions using simultaneous observations of satellites, surface-gravity compilations, and results from radio tracking of deep-space missions.

Hence, future plans must recognize that Geos C is an additional satellite with particular characteristics that will provide an increment of data to an already existing and continuously growing collection of data from many other sources. This same situation was emphasized in SAO plans before Geos 2 (Lundquist, 1968), and subsequent results confirm the validity of this viewpoint.

This work was supported in part by grant NGR 09-015-002 from the National Aeronautics and Space Administration.

The new and distinctive characteristics of Geos C that are of particular interest to SAO are its orbit and altimeter. Our geodetic objectives will encompass dynamic analyses for the determination of both zonal and non-zonal harmonics, both dynamic and geometric solutions for station positions, and a direct determination of the geoid (more precisely, mean sea level) from the altimeter data. SAO will concentrate on the acquisition of laser range measurements because of their high accuracy, although we believe Baker-Nunn camera observations will still be useful and will photograph Geos C in both active (flashing-light beacon) and passive (reflected sunlight) modes.

Inherent in all of these studies will be the continuing evaluation and intercomparison of the various satellite measuring techniques, with emphasis on the altimeter--both for direct geoid mapping and as an additional source of tracking data for dynamic orbit analysis. This intercomparison will be greatly facilitated by having the instruments on a common vehicle.

The most important single characteristic of the Geos C orbit will be its inclination. There are at this time no geodetic data of high accuracy archived for any orbital inclination below 40 degrees. The successful launch of Peole at i = 14 degrees will change this situation, and the Geos C inclination should be modified accordingly, preferably to i $\sim$ 28 degrees. These lower inclination orbits are peculiarly well suited to the determination of zonal and near-zonal harmonics, the latter harmonics being the least accurately determined in current geopotential models. For example, an orbit with i = 20 degrees is almost completely insensitive to tesserals of order $m > 7$, but is strongly perturbed by zonal ($m = o$) and near-zonal ($o < m < 4$) harmonics. This discrimination is unique to low-inclination orbits, so such an orbit would satisfy the criterion of being distinct from, or independent of, the set of higher inclination orbits that has provided the data base for previous analyses.

It is necessary to select a large enough orbital eccentricity that a precise measure of perigee motion can be gotten. The primary effect of the zonal harmonics is to produce secular precessions of the node and line of apsides. We have previously determined zonal harmonics mainly by measuring nodal precession rates. A conspicuous flaw in the present values of zonal coefficients is their inability to correctly predict perigee rates. The best approach is to deduce the zonals from observations of both nodal and perigee (apsidal) motions. For the expected accuracy of the Geos C tracking data, a minimum difference of 200 km between apogee and perigee altitudes would be desirable to get adequate definition of perigee position.

The lower the orbital altitude, the larger are the physical perturbations on the satellite trajectory produced by the gravity field. This is a selective process, in that the higher degree terms are more strongly attenuated by an increase in altitude, the effect being proportional to r^{-n}, where n is the degree of the harmonic. To maximize the geodetic information contained in a satellite trajectory, the orbital altitude should be as low as possible. The lower limit is set by station coverage and atmospheric drag. These criteria suggest a perigee altitude in the range 700 to 800 km.

The criteria for obtaining adequate data coverage for dynamic geodesy derive from the need to observe the periodic perturbations generated by non-zonal harmonics, and the secular perturbations generated by the zonals. The periodic terms of greatest importance have periods that lie close to the orbital period and its second harmonic, and periods of 24 hours/m, where m is the order of the harmonic. Thus, we will need observations that are well distributed in phase over perturbations with periods of 50 minutes to 24 hours.

Obtaining appropriate data coverage for measuring secular perturbations will require observations over at least a full revolution of the line of apsides or of the node, whichever is longer. For Geos C, this minimum interval will be of the order of 60-75 days.

In addition, the low inclination of Geos C will be of particular value for eliciting seasonal variations in the zonal coefficients (as discussed below), so observations at some lower level of data density should be taken for a much more extensive period of time--perhaps 2 years or longer.

Thus, the observations of Geos C should include several intervals of 2-3 weeks duration with maximum concentration incorporated into a 6-month campaign of moderate intensity of observations, plus a lower level of observing activity over the full life of the satellite. To obtain the required data and to ensure the widest possible geographic coverage, two things will be necessary: altimeter data must be obtained for all ocean areas overflown by Geos C; and second, the satellite should be tracked by as many observers as possible.

Precedent would suggest that a cooperative international tracking effort will be scheduled following the launch of Geos C and that it will involve most of the other satellites in orbit with retroreflectors for laser tracking. The campaigns organized by SAO in 1967 and 1968 and the CNES-managed ISAGEX campaign scheduled for 1970-71 (CNES, 1970) are examples of the tracking activity that should be anticipated in association with the Geos C project. The large number of stations that can be brought into an international campaign would provide excellent coverage even at lower orbital altitudes.

After the observations have been reduced and assembled, SAO would expect to combine the data from the earlier campaigns--particularly from ISAGEX--with those for several satellites from the campaign associated with Geos C. The combination solution would again incorporate simultaneous satellite observations, updated surface-gravity information, and perhaps results from the tracking of interplanetary spacecraft.

It should be noted that if the launch of the French satellite Peole is successful, the Geos C inclination should be about 28 degrees rather than 20 degrees, to increase the differentiation from the planned Peole inclination of 14 degrees. All the comments above are essentially unchanged for this modest adjustment.

Another characteristic of past and anticipated Smithsonian Standard Earth solutions is the use of data from a variety of systems tracking the same satellite. For example, the 1969 solution used significant numbers of both photographic and laser observations. In this vein, the instrumentation planned for Geos C offers an opportunity to diversify further the tracking techniques providing data for orbital analyses. This is of particular importance for the altimeter, but only if synoptic data are available from this instrument.

SAO would prepare to determine Geos C orbits of several weeks duration, using measurements from all the precision systems supported by the satellite. In particular, these calculations would embrace laser ranges, satellite-to-satellite tracking, and satellite-to-ocean altitudes. For this multisystem calculation, the data from these new systems would be processed in accordance with the findings of the several groups that will carry out calibration experiments of various kinds.

Satellite-to-satellite tracking of Geos C will require that accurate orbits be concurrently determined for ATS-F, the other satellite in the system (Felsentreger, Grenchik, and Schmid, 1970). Presumably, laser and long-baseline interferometry tracking data can be acquired for the ATS satellite. A combined solution for the orbits of both satellites is possible with techniques similar to those used in other solutions combining orbits of several satellites.

The satellite-to-ocean altitudes can be used as tracking data for orbit determination, but they also carry information about the ocean geoid and hence about the geopotential (Lundquist and Giacaglia, 1969).

Both satellite-to-satellite tracking and satellite-to-ocean altimetry can, in principle, provide information for more detailed geopotential representations than are possible from analysis of orbital perturbations alone (Kaula, 1970a). One way to evaluate and exploit this capability is to experiment with geopotential refinements based on a combination of the orbital-perturbation method and the alternative methods that should be possible with these new data forms. SAO anticipates performing such experiments. Presumably, the strongest geopotential solution following Geos C must result from such a combination, because the information content of the Geos C data alone is severely limited by the orbital inclination and hardware constraints.

Thus, SAO would adopt a comprehensive geopotential refinement as one of its principal objectives for the Geos C project. This solution would combine orbital data for many satellites, the most recent surface-gravity tabulations, the altitude measurements from Geos C, tracking data between ATS-F and Geos C, and such deep-space tracking or other available information as may seem valuable. (Cf. Gaposchkin, 1970.)

The resulting geopotential should have important implications for earth physics. The remarkable interpretations of the 1969 Smithsonian geopotential (Kaula, 1970b; Gaposchkin and Kaula, 1970) are but an indication of the still greater insights into earth processes to be expected from a more accurate and detailed representation of the potential.

As the static geopotential becomes better defined, separation of time dependency in the potential becomes easier and more accurate. Kozai (1968) and Newton (1968) have independently studied earth tides and elastic properties of the earth through the effect of the associated mass displacements on the geopotential and hence on the orbits of satellites. Kozai (1970a, b) has

also identified an annual term in satellite orbits that seems to be due to an annual variation of J_2. Such studies will benefit not only from the refined static potential but also from improved tracking accuracy and from further tracking of satellites such as Geos 1. Thus, activities in connection with Geos C can be expected to advance research on those physical phenomena that produce mass displacements in the earth.

A related topic concerns the determination of values for the coefficients C_{21} and S_{21} in the spherical-harmonic description of the potential. If the Z axis of the adopted terrestrial coordinate system coincided with the principal axis of inertia of the earth, then these coefficients would be rigorously zero. Owing to polar motion, the elasticity of the earth, and perhaps other physical processes, the principal axis of inertia probably moves with respect to the terrestrial coordinate system conventionally adopted (Gaposchkin, 1968). This would result in nonzero, time-dependent values for C_{21} and S_{21}. These values, or refinements of them, should be sought in the course of geopotential studies associated with the Geos C program. Although several satellites will be involved in these analyses, the low inclination of Geos C may make it more valuable than other individual satellites.

The position and motions of the rotation axis of the earth must be known in order to support many of the planned analyses. Also, these polar motions themselves have significance to the physics of the earth (Smylie and Mansinha, 1968). Anderle and Beuglass (1970) have shown that the pole position can be extracted by appropriate treatment of satellite-tracking data. It seems likely that a similar calculation to determine the geometrical position of the pole should be included in plans for the tracking data generated by the Geos C project. This determination of the pole motion must be compared with determinations by other techniques and correlated with various geophysical phenomena that may influence pole position.

The position angle of the earth about its rotational axis — i.e., UT1 — must also be known precisely to facilitate all the anticipated analyses of the tracking data. But variations of the rotation rate are again of geophysical

significance in themselves. They are intimately related to mass displacements in the earth and to momentum exchanges between parts of the earth. If no alternative of greater accuracy is available, a determination of UT1 is, in principle, possible from the satellite-tracking data themselves.

In summary, using data related to the Geos C project, SAO hopes to investigate a comprehensive range of geodetic and earth-physics topics: details of the geopotential, the ocean geoid, time dependence of the geopotential, polar motion, the rotation of the earth, etc. All these phenomena are interrelated in complex ways not completely understood. Thus, a comprehensive, integrated examination of these topics is a desirable ingredient of plans for the Geos C project.

REFERENCES

ANDERLE, R. J., and BEUGLASS, L. K.

1970. Polar motion for 1967 and 1968 derived from doppler satellite observations. Trans. Am. Geophys. Union, vol. 51, p. 266.

CENTRE NATIONAL d'ÉTUDES SPATIALES

1970. International satellite geodesy experiment. Preliminary Experiment Plan, May 20.

FELSENTREGER, T. L., GRENCHIK, T. J., and SCHMID, P. E.

1970. Geodetic Earth Orbiting Satellite (Geos-C) — Applications Technology Satellite (ATS-F) tracking experiment. Goddard Space Flight Center preprint X-552-70-96, March.

GAPOSCHKIN, E. M.

1968. The motion of the pole and the earth's elasticity as studied from the gravity field of the earth by means of artificial earth satellites. In Proceedings of the Symposium on Modern Questions of Celestial Mechanics, Centro Internazionale Mathematico Estiva.

1970. Future uses of laser tracking. This conference.

GAPOSCHKIN, E. M., and KAULA, W. M.

1970. 1969 Smithsonian Standard Earth (II) and global tectonics. This conference.

GAPOSCHKIN, E. M., and LAMBECK, K.

1970. 1969 Smithsonian Standard Earth (II). Smithsonian Astrophys. Obs. Spec. Rep. No. 315, 93 pp.

KAULA, W. M., Chairman

1970a. The terrestrial environment: Solid-earth and ocean physics. NASA Contractor Report NASA CR-1579, April.

1970b. Earth's gravity field: Relation to global tectonics. Submitted to Science.

KOZAI, Y.

1968. Love's number of the earth derived from satellite observations. Publ. Astron. Soc. Japan, vol. 20, pp. 24-26.

KOZAI, Y.

1969. Revised values for coefficients of zonal spherical harmonics in the geopotential. Smithsonian Astrophys. Obs. Spec. Rep. No. 295, 17 pp.

1970a. Seasonal variations of the geopotential inferred from satellite observations. Smithsonian Astrophys. Obs. Spec. Rep. No. 312, 6 pp.

1970b. Temporal variations of the geopotential derived from satellite observations. Presented at the COSPAR Meeting, Leningrad, May.

LUNDQUIST, C. A.

1968. Anticipated contributions of GEOS-B to investigations at the Smithsonian Astrophysical Observatory. In Proceedings of the GEOS Program Review Meeting 12-14 December 1967, ed. by C&S, Inc., vol. 1, pp. 177-183.

LUNDQUIST, C. A., and GIACAGLIA, G. E. O.

1969. Possible geopotential improvement from satellite altimetry. In Smithsonian Astrophys. Obs. Spec. Rep. No. 294, pp. 1-44.

NEWTON, R. R.

1968. A satellite determination of tidal parameters and earth deceleration. Geophys. Journ. Roy. Astron. Soc., vol. 14, pp. 505-539.

SMYLIE, D. E., and MANSINHA, L.

1968. Earthquakes and the observed motion of the rotation pole. Journ. Geophys. Res., vol. 73, pp. 7661-7673.

SOME RESULTS OF A SHORT-ARC, ORBIT-DETERMINATION STUDY RELATED TO THE GEOS-C ALTIMETER EXPERIMENT

(Presented to the GEOS II Review Meeting
GSFC on June 24, 1970)

by

Robert M. L. Baker, Jr., Dirk Ourston, and
Norman H. Schroeder

1.0 INTRODUCTION

Studies have been accomplished that have dealt with short-arc orbit determination (supported, in part, under contract NASW-1918). Our definition of a "short arc" is two-fold. First, we require that the satellite traverses less than one radian on its orbit. Second, we require that the satellite is visible from three or more designated radar sensors over the entire arc. Both of these requirements are satisfied in the Caribbean area for the nominal GEOS-C orbit and for arcs of 5,000 km or less. The original purpose of these short-arc studies was to confirm the results of other researchers that indicated that force-model, observational, and station-location errors would not completely render satellite altimeter data useless, that is, that these errors would not mask the results of an altimeter test over a 1000 km or so ocean subsatellite track. We were able to corroborate these other conclusions and, thereby, lend more support to the feasibility and utility of the GEOS-C altimeter experiment.

Unexpectedly we obtained an ancillary benefit from our study. We discovered, while exercising our analytical procedures, that conventional orbit determination (e.g., minimum-variance or conventional weighted least-squares differential correction) is ill suited to the GEOS-C altimeter experiment over short arcs. Furthermore, we conceived of a novel approach to short-arc orbit determination that would be far superior to the conventional one and involves what we have termed "mini-arc" orbit determination.

The justification for the use of mini-arc orbit determination and its unique value to the GEOS-C altimeter program will be the subject of my brief talk this morning.

2.0 THE IMPORTANCE OF SYSTEMATIC VS. RANDOM ERRORS

The key feature of the problem, as previously noted by Dr. Fritz von Bun, is that in calibrating the altimeter and in sensing local depressions in sea level (e.g., the Puerto Rican Trench) the absolute location of the GEOS-C satellite short-arc track is not nearly as important as is the determination of the relative or biased location of the track.

During the course of the basic study the effects of systematic station location and range errors were evaluated using an analytical solution, thereby greatly reducing the number of computations required. The efficiency of the calculations permitted evaluation of station location and range error "volumes," and the resulting satellite position error "volume" was determined.

The effects of radar random error and timing biases were evaluated using an orbit simulation/determination program specialized for this study. The program was developed using an analytical single-conic solution for the orbit. This was done since it minimized the required computations and accurately portrayed the error effects to first order.

An important feature of the problem is that systematic errors due to station location, timing bias, refraction, and force-model are time constant and relatively quite large when compared with the random (time-variable) observational errors in range. Thus if we look at each possible combination of systematic error (e.g., station-location error relative to the geocenter) we find that we have a set of "error fibers." The shape of a particular fiber will be determined by a particular set of systematic errors (i.e., the systematic deviation from the true trajectory), while the width of each fiber will be due to the random range errors of the sensors. The manifold of all of these fibers represents the overall (random plus systematic) error. As already noted, all that we are concerned about in the altimeter experiment is that we are following a well-defined fiber--and if all of the fibers are nearly parallel, then it makes no difference which fiber the GEOS-C satellite is following as far as the altimeter test is concerned.

The difficulty here is that conventional orbit determination (e.g., minimum-variance or weighted-least-squares differential correction) does not define the cross section of these fibers, but rather yields the mean "path" down the much wider manifold of fibers or error tube (including a secular increase in residuals). Thus a conventional orbit determination simulation of the GEOS-C arc would probably give rise to the erroneous results that large satellite-location errors would mask, say, local depressions in sea level, and perhaps make the calibration of the altimeter very uncertain. Another way to look at the situation is to recognize that conventional orbit determination attempts a grand reconcilement of all errors including force-model, station-location, sensor, etc. Thus in trying to bring observations (usually taken over several revolutions) into agreement with both systematic and random errors, conventional orbit determination degrades or "smooths" through the short-arc prediction process as applied to a relative arc. Such an approach is perfectly satisfactory for conventional orbit determination when absolute orbital tracks over many orbits are desired, but not for the short-arc orbit determination problem. In this latter case it is irrelevant how well the estimated orbit fits observations outside of the GEOS-C altimeter experiment areas.

As an illustrative example of the situation, let us hypothesize that all three of the sensors are systematically located 10 meters further from the geocenter than expected. Conventional differential correction would accept the range data and attempt to fit an orbit through these observations (assumed to be complete positional fixes obtained by three simultaneous range measures). Because of the dynamics that are inherent in the orbit determination process, the geometrical best-fit track would apparently be 10 meters closer to the geocenter than it actually was. Thus the dynamics would indicate that the satellite should be moving more rapidly than the timed sequence of data points would indicate. The conventional differential correction would attempt to reconcile these two effects and would exhibit a trending of the residuals to larger values on each end of the observational arc. In this particular situation it would have been better either to define the orbit purely on the basis of a "floating" datum or to obtain a set of very-short-arc-determined ("mini-arc") osculating orbits.

The following subsections present our analysis methods used in the study and some of the numerical results that we obtained to support our recommendation for the use of mini-arc orbit determination.

2.1 ANALYSIS METHODS

The approach taken in the study was to develop and investigate new or specialized methods of error analysis which would take into account the unique characteristics and requirements of the GEOS-C radar altimetry experiment. Initially, it was recognized that for altimeter calibration and ocean mapping purposes, it is more important to determine the position of the satellite as accurately as possible over a relatively small portion of its orbit than to determine the entire orbit accurately. In addition, for ocean mapping purposes (i.e., measuring the Puerto Rican Trench), it was determined that knowing the absolute satellite location was not nearly as important as knowing the shape of the curve which it was following. This is because for certain applications we are more interested in determining the "shape" of the ocean's surface than its actual distance from the Earth's center of mass. The satellite altimeter provides a direct method of connecting the "shape" of the ocean's surface (see Figure 2.1-1).

As a result of these considerations, the study evaluated specialized methods for determining the shape of the satellite trajectory, and investigated means of accurately calibrating and using the satellite altimeter, without undue emphasis on classical orbit determination/error analysis. Extensive use was made of the properties of the satellite/tracking net combination.

In order to make a meaningful test of the techniques obtained, and also to utilize realistic data, the following tracking net was chosen from data obtained from Dr. Fritz von Bun:

Antigua: $\phi_g = 17.^{\circ}02$, $\lambda_E = -61.^{\circ}7$, H = 28 meters

Canal Zone: $\phi_g = 9.^{\circ}0$, $\lambda_E = -80.^{\circ}0$, H = 10 meters

Key West: $\phi_g = 23.^{\circ}5$, $\lambda_E = -82.^{\circ}0$, H = 10 meters.

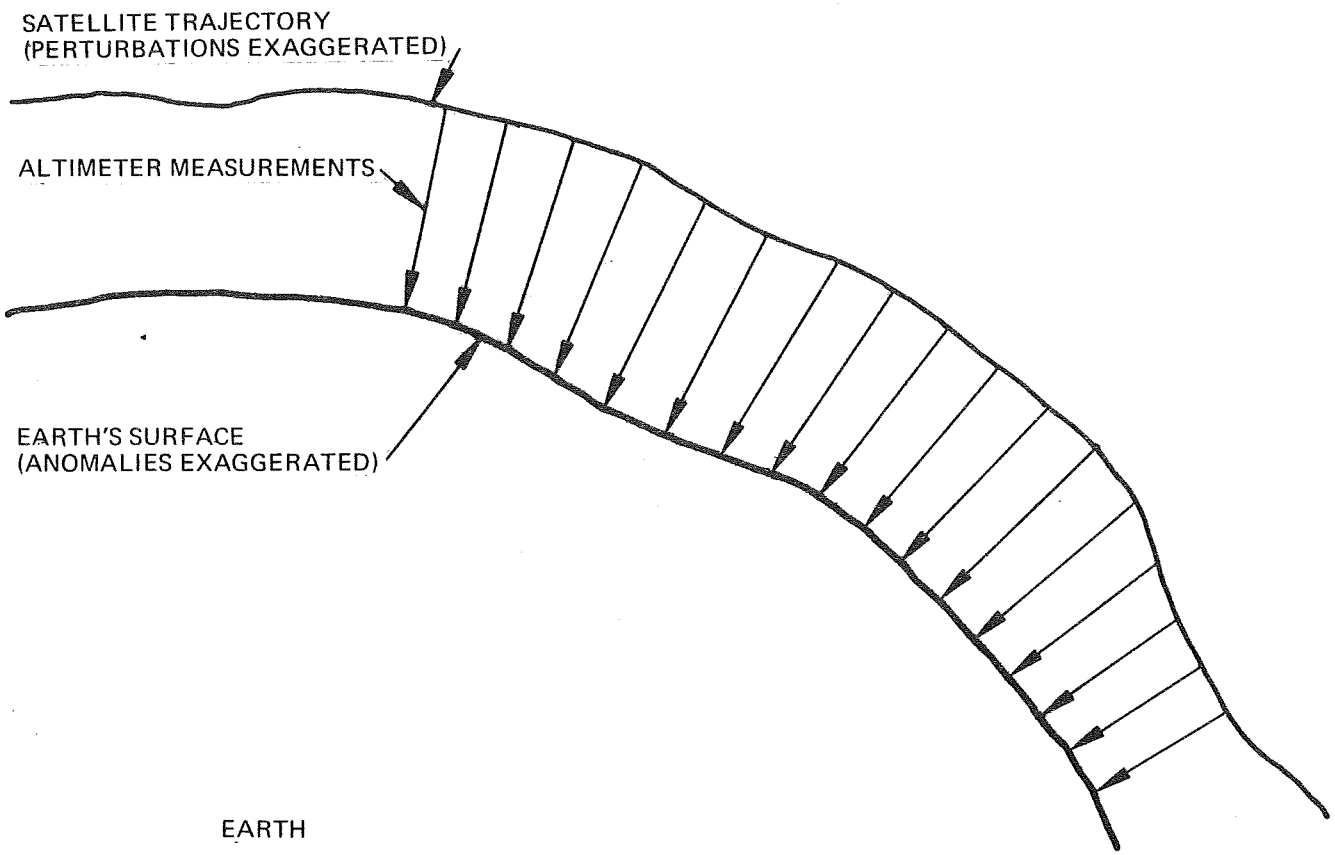
SATELLITE TRAJECTORY
(PERTURBATIONS EXAGGERATED)
ALTIMETER MEASUREMENTS
EARTH'S SURFACE
(ANOMALIES EXAGGERATED)
EARTH

Figure 2. 1-1

Radar random range error (all errors are one sigma) was assumed to be two meters, systematic range bias was five meters, and timing bias was 0.001 seconds. Station location errors were assumed to be 10 meters relative to the Earth's center of mass (geocenter) plus 5 meters relative to each other. Radar azimuth and elevation errors were neglected as previous studies had shown these to have a relatively small effect on orbital errors if high-accuracy range data from three or more stations was utilized.

The first investigation performed was merely to determine suitable trajectories which passed over the "mutual visibility" region of the tracking net (that region where the satellite was simultaneously visible to all three stations). This was done by varying the longitude of the ascending node of the satellite orbit, and determining the portion of the satellite track where it was mutually visible to all stations. For our study, the longitude of the ascending node was referenced to Greenwich since we were not interested in a particular time frame. The results of mapping out the mutual visibility region are shown in Figure 2.1-2.

The resulting longitudes of the ascending node (as well as the remaining orbital elements) were used as inputs to a specialized short-arc orbital simulation/determination program. The program uses the three ground based stations as sensors and a solution to determine the orbit. A conic (two-body) solution was deemed sufficient for this application, as we are attempting to determine the effects of random radar error, rather than force model error. The program calculates a nominal two-body orbit, calculates the slant range from the given station, and "noises up" the resulting slant range data. The data is "noised up" using a random number generator with a normal distribution corresponding to a given mean and standard deviation (in our case 0 and 2 meters, respectively). It then attempts to "fit" the simulated data using a least squares differential correction procedure. The resulting epoch error volume is calculated (in our study, epoch was taken as the first point of the observation interval), and propagated using the standard state transition matrix formulation. One of the principal advantages of using the single conic formulation was the savings in computation time, without any significant sacrifice of accuracy, for this application. The results of this study are presented in Section 2.2.

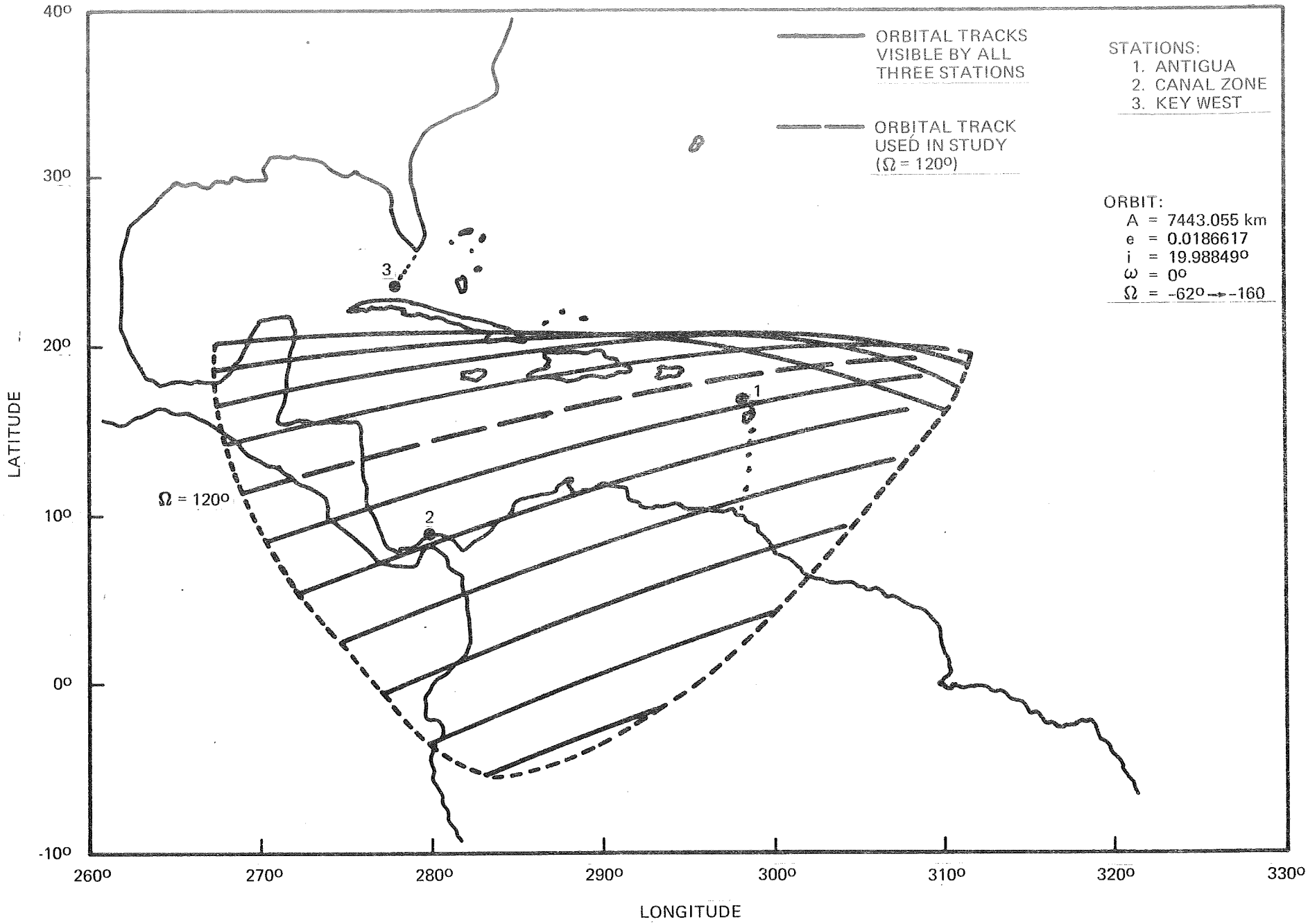

Figure 2.1-2. Caribbean Tracking Net

The effects of radar timing errors were also investigated, using the Keplerian solution. In the worst case, all radars would have their maximum timing bias error. In the absence of all other errors, this would result in a determined orbit for which the caluclated position for each observation would be correct, but for which the computed ephemeris time would be incorrect by exactly the amount of timing bias. Hence, the worst case error due to timing bias corresponds to the amount that the satellite would move during the period of the timing bias. This solution was obtained and is presented in Section 2.2.

Systematic station location and slant range errors were also investigated using an analytical solution. The analytical solution used was the standard three range solution, which determines a satellite position uniquely using slant ranges from three observing stations. The justification for using this method is as follows:

Assume systematic errors were present in the observational data and that this data was processed using a standard orbit determination program. In the absence of all other errors, the program would attempt to fit the observation data as closely as possible and in the ideal case, exactly. The observation data under consideration is radar slant range data. Therefore, in the presence of systematic error in either station location or slant range, a traditional orbit determination program would construct an orbit which yielded a satellite position which would have the observed slant range from each station. Assuming simultaneous observations, this is exactly what the three range solution does, working from the opposite direction. That is, given slant ranges from three stations, it calculates a satellite position which fits these ranges exactly.

Since the three range solution requires very little computer time, the effects of a wide variety of systematic station location errors were able to be examined (essentially, a station location "error volume"), and the resultant "error volume" in satellite position was then determinable. The same procedure was followed for systematic slant range error, and the resultant satellite position error volume was determined. Such extensive analysis would not normally be practicable with an

orbit simulation/determination program due to the prohibitive computer run time required. In addition, the three range solution allows exact determination of the path which would be followed by the satellite for a given set of station location errors (the so-called error fiber). The results of this study are presented in Section 2.3.

2.2 RESULTS OF ANALYSIS OF RADAR RANDOM ERRORS AND TIMING BIASES

From previous studies, it has been determined that by far the largest contribution to radar random error is manifested in the slant range. Therefore, the study simulated radar error by adding an appropriate random error to the radar slant range measurement. The random error was simulated using a normal distribution with a standard deviation of 2 meters. Refraction errors were not included as they were considered outside the scope of the study.

A number of different cases representing parametric variations in satellite flight path, radar observation rate, and orbital orientation, were simulated. The non-varying elements of the GEOS-C orbit were taken as:

$$a = 7,442.732,1 \text{ km}$$
$$e = 0.018,598,605$$
$$i = 19.988,49^{\circ} .$$

Nominally, perigee was assumed to occur at the midpoint of the observation interval.

Table 2.2-1 identifies the range of parameters investigated during the study. Cases 1-14 were used to map out the region shown in Figure 2.1-2 and evaluate geometrical effects on the epoch error volume. Cases 15-18 determined the variation in error volume when apogee occurred over the visibility region. Cases 19-26 were designed to determine the effects of varying the observation rates.

The epoch error volume variances (eigenvalues of the epoch covariance matrix) corresponding to each case are shown in Table 2.2-2. Since the epoch state vector consisted of position and velocity, σ_1 to σ_3 are the position variances,

TABLE 2.2-1

PARAMETER VALUES USED IN STUDY

CASE	Ω(deg)*	Obs. Rate (obs/sec)
1	-62	.1
2	-65	.1
3	-70	.1
4	-80	.1
5	-90	.1
6	-100	.1
7	-110	.1
8	-120	.1
9	-130	.1
10	-140	.1
11	-150	.1
12	-160	.1
13	-170	.1
14	-180	.1
15+	-62	.1
16+	-80	.1
17+	-120	.1
18+	-160	.1
19	-62	1
20	-80	1
21	-120	1
22	-160	1
23	-62	2
24	-80	2
25	-120	2
26	-160	2

* Ω is the longitude of the ascending node referenced to Greenwich.

a (orbital semi-major axis) = 7,442.732,1 km

e (orbital eccentricity) = 0.018,598,605

i (orbital incluination) = 19.988,49°

\+ Designed so that apogee, rather than perigee occured at midpoint of interval

TABLE 2.2-2

EPOCH ERROR VOLUME VARIANCES

CASE	$\sigma_1^2(m^2)$ *	$\sigma_2^2(m^2)$ *	$\sigma_3^2(m^2)$	$\sigma_4^2(m^2/sec^2)$ *	$\sigma_5^2(m^2/sec^2)$ *	$\sigma_6^2(m^2/sec^2)$ *
1	125.210	3.031	3.969	4.995-3	1:163-4	1.902-5
2	5.045+1	1.479	2.162-1	3.627-4	1.042-5	2.092-6
3	2.184+1	8.393-1	1.608-1	7.649-5	2.907-6	7.064-7
4	6.759	4.75-1	1.373-1	1.745-5	1.202-6	3.233-7
5	2.561	3.518-1	1.429-1	7.783-6	1.006-6	2.812-7
6	1.107	3.469-1	1.307-1	2.882-6	6.426-7	1.791-7
7	6.232-1	3.889-1	1.242-1	1.797-6	6.033-7	1.593-7
8	4.464-1	4.232-1	1.407-1	1.837-6	7.450-7	1.889-7
9	4.547-1	3.708-1	1.451-1	1.946-6	7.675-7	1.875-7
10	4.403-1	3.395-1	1.594-1	2.382-6	8.550-7	1.817-1
11	4.615-1	3.403-1	1.496-1	2.306-6	7.580-7	1.515-7
12	4.538-1	3.156-7	1.459-1	2.338-6	7.512-7	1.317-7
13	4.558-1	3.056-1	1.399-1	2.313-6	7.929-7	1.307-7
14	4.336-1	3.074-1	1.488-1	2.086-6	8.343-7	1.249-7
15	99.938	5.520	4.307-1	8.225-4	1.246-4	1.554-5
16	4.890	4.729-1	1.284-1	1.101-5	1.071-6	2.518-7
17	5.167-01	3.738-1	1.316-1	1.655-6	5.754-7	1.343-7

* σ_1 to σ_3 are the position variances, σ_4 to σ_6 are the velocity variances.

TABLE 2.2-2 (continued)

CASE	$\sigma_1^2(m^2)$	$\sigma_2^2(m^2)$	$\sigma_3^2(m^2)$	$\sigma_4^2(m^2/sec^2)$	$\sigma_5^2(m^2/sec^2)$	$\sigma_6^2(m^2/sec^2)$
18	7.408-1	2.081-1	1.873-1	3.663-6	1.334-6	8.615-8
19	13.894	2.970-1	4.488-2	4.816-4	1.118-5	1.838-6
20	6.884-1	4.535-2	1.425-2	1.730-6	1.189-7	3.186-8
21	4.492-2	4.238-2	1.492-2	1.769-7	7.230-8	1.716-8
22	4.557-2	3.242-2	1.428-2	2.267-7	7.278-8	1.220-8
23	7.061	1.661-1	2.299-2	2.394-4	5.606-6	9.144-7
24	3.455-1	2.315-2	7.173-3	8.657-7	5.957-8	1.595-8
25	2.237-2	2.082-2	7.120-3	8.850-8	3.615-8	8.593-9
26	2.288-2	1.626-2	7.243-3	1.134-7	3.645-8	6.106-9

and σ_4 to σ_6 are the velocity variances.

The variation in the epoch error volume due to geometrical effects is shown in Figure 2.2-1. Note that the error volume dimensions increase rapidly as the longitude of the ascending node varies from -80° to -60°. This is due to a combination of bad geometry and decreasing track length for these longitudes. In no case is the greatest upper bound error volume dimension greater than four meters, and over a wide region it is less than 0.5 meters.

The variation in error volume size with tracking rate is shown in Figure 2.2-2. Assuming statistical independence of all measurements, one would expect the error volume dimensions to decrease as $1/\sqrt{n}$, where n is the number of measurements. This fact is evidenced in the figure. Correspondingly, the reduction in error volume size in going from 0.1 obs/sec to 1 obs/sec is much more dramatic than in going from 1 obs/sec to 2 obs/sec.

The effects of radar timing bias errors are shown in Figure 2.2-3. A worst case situation was assumed where all radars had the same bias of +0.001 sec. As can be seen from the plot, timing bias error does not contribute significantly to the over-all orbital error. This effect was found to be true in all cases, with the over-all error due to timing bias found to be less than 1.4 meters during any portion of the orbit. A more detailed look at the error volume variation over the region of interest is given in Figures 2.2-4 to 2.2-19. These figures represent a detailed look at error volumes corresponding to Ω's of -52°, -80°, -120° and -160°, parametrically varying the other elements. The epoch error volumes were propogated using the standard state transition matrix formulation.

Figure 2.2-4 to 2.2-7 correspond to an observation rate of 0.1/sec (1 observation every 10 seconds). The minimum error dimension appears to remain roughly constant for all cases (reaching a minimum of about 0.2 meters), while the maximum error dimension decreases by an order of magnitude in going $\Omega = -62^{\circ}$ to $\Omega = -160$ (going from a minimum of 6.4 meters to a minimum of 0.4 meters). This indicates the error volume is changing from a cylindrical shape ($\Omega = -60^{\circ}$), to a more nearly spheroidal shape ($\Omega = -160^{\circ}$). The maximum error dimension

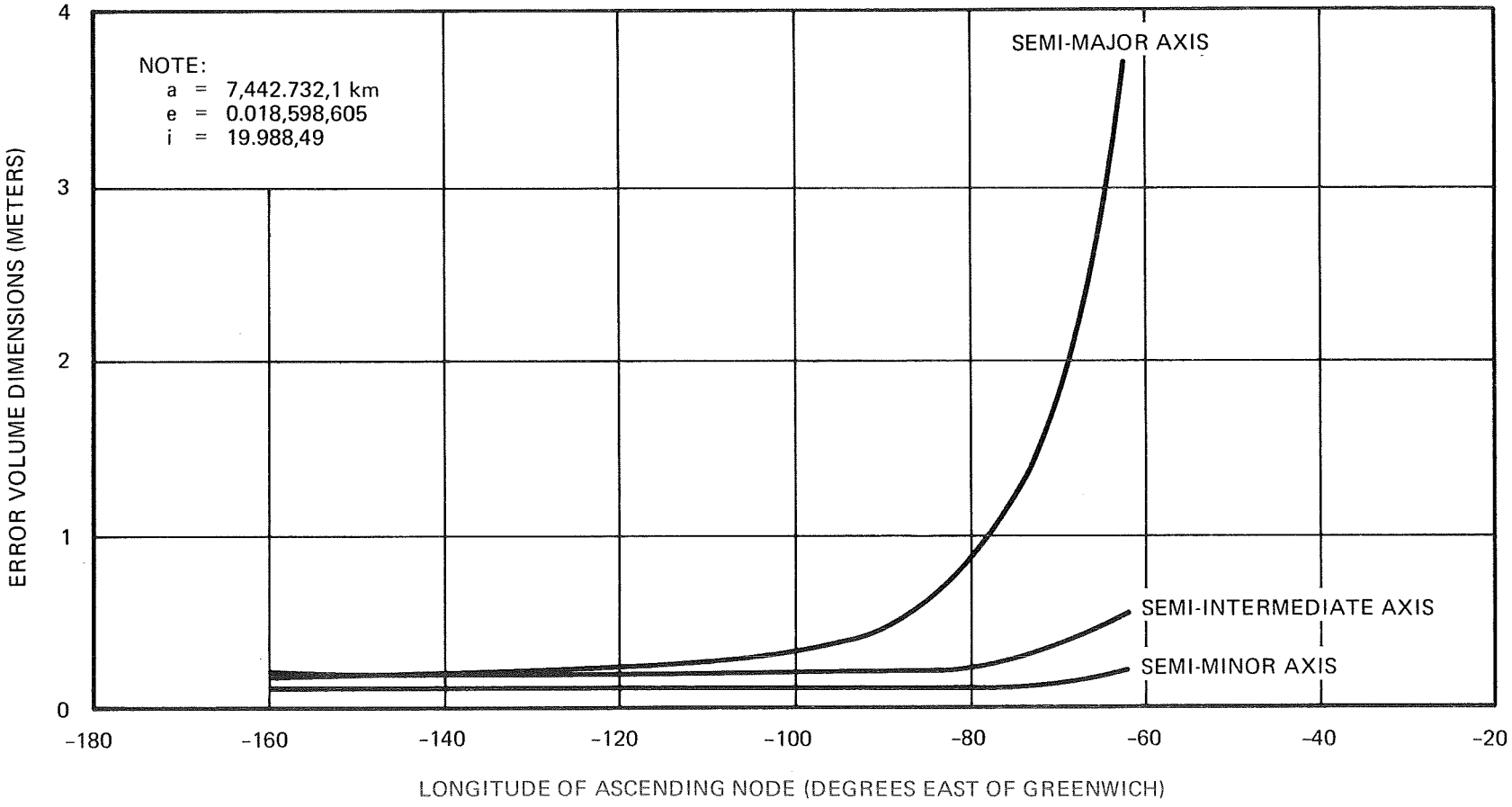

Figure 2.2-1. Variation in Epoch Error Volume with Longitude of the Ascending Node (1 Observation/Sec)

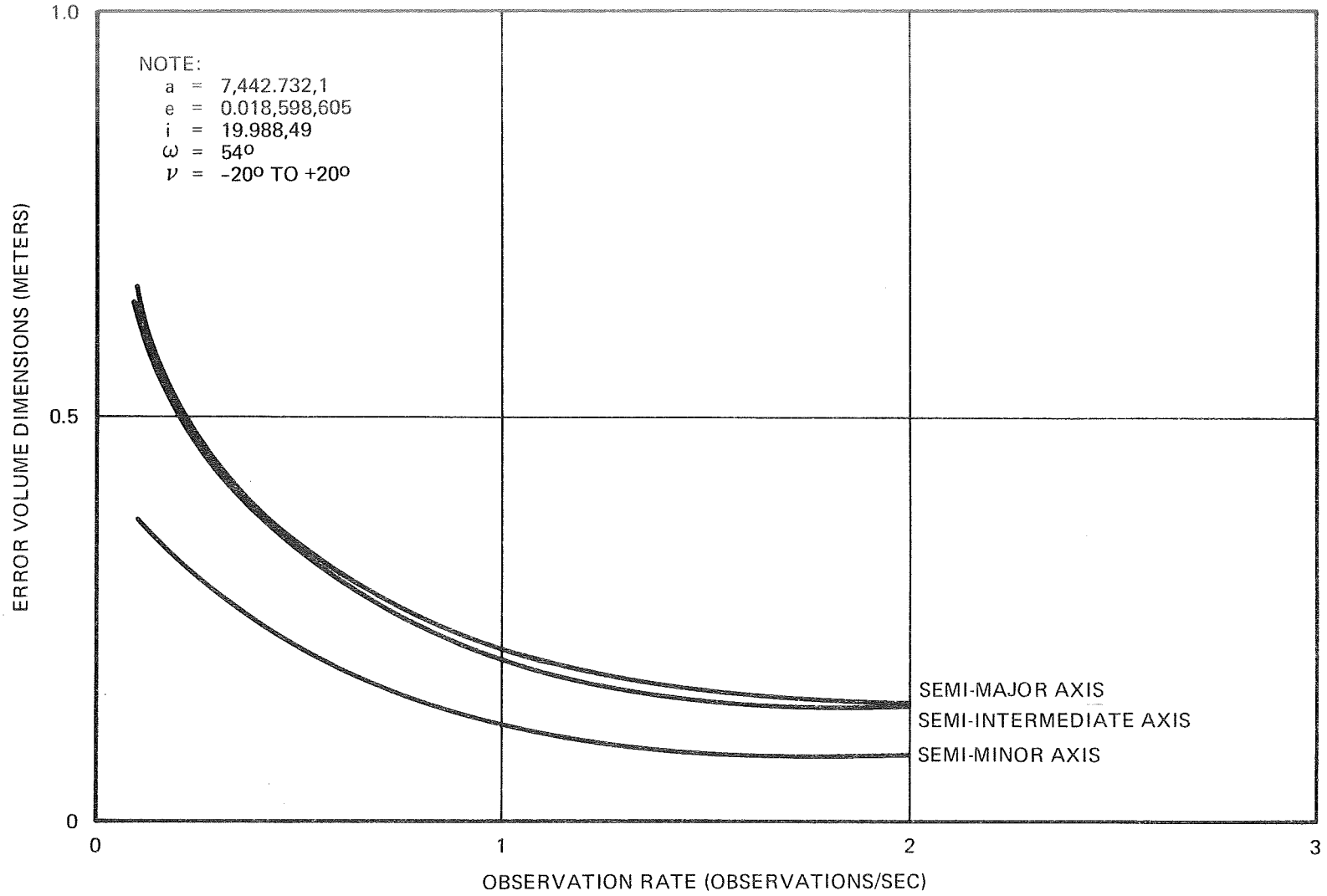

Figure 2.2-2. Variation of Epoch Error Volume with Observation Rate (Ω -120°)

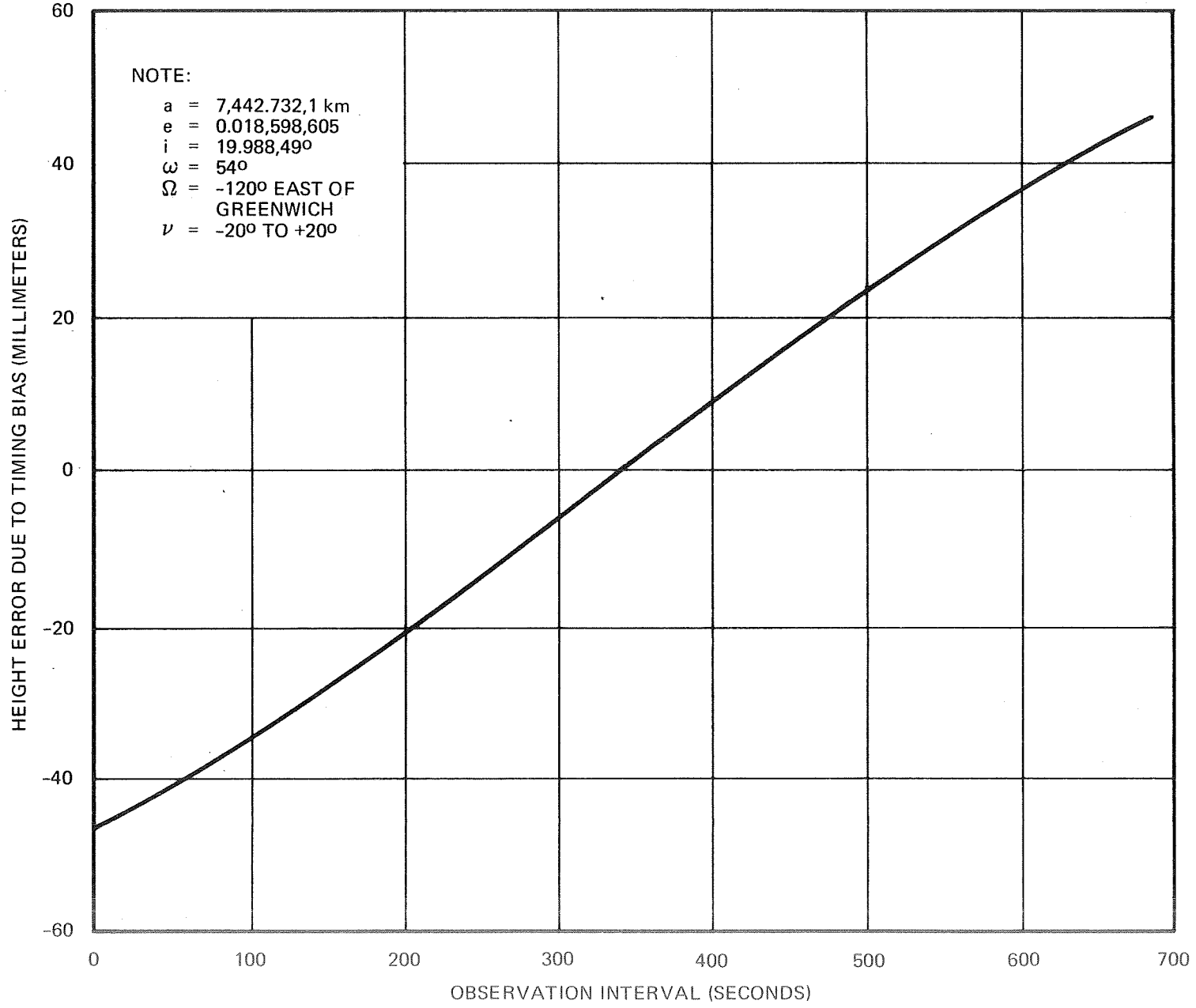

Figure 2.2-3. Height Error Due to Timing Bias - Case 21

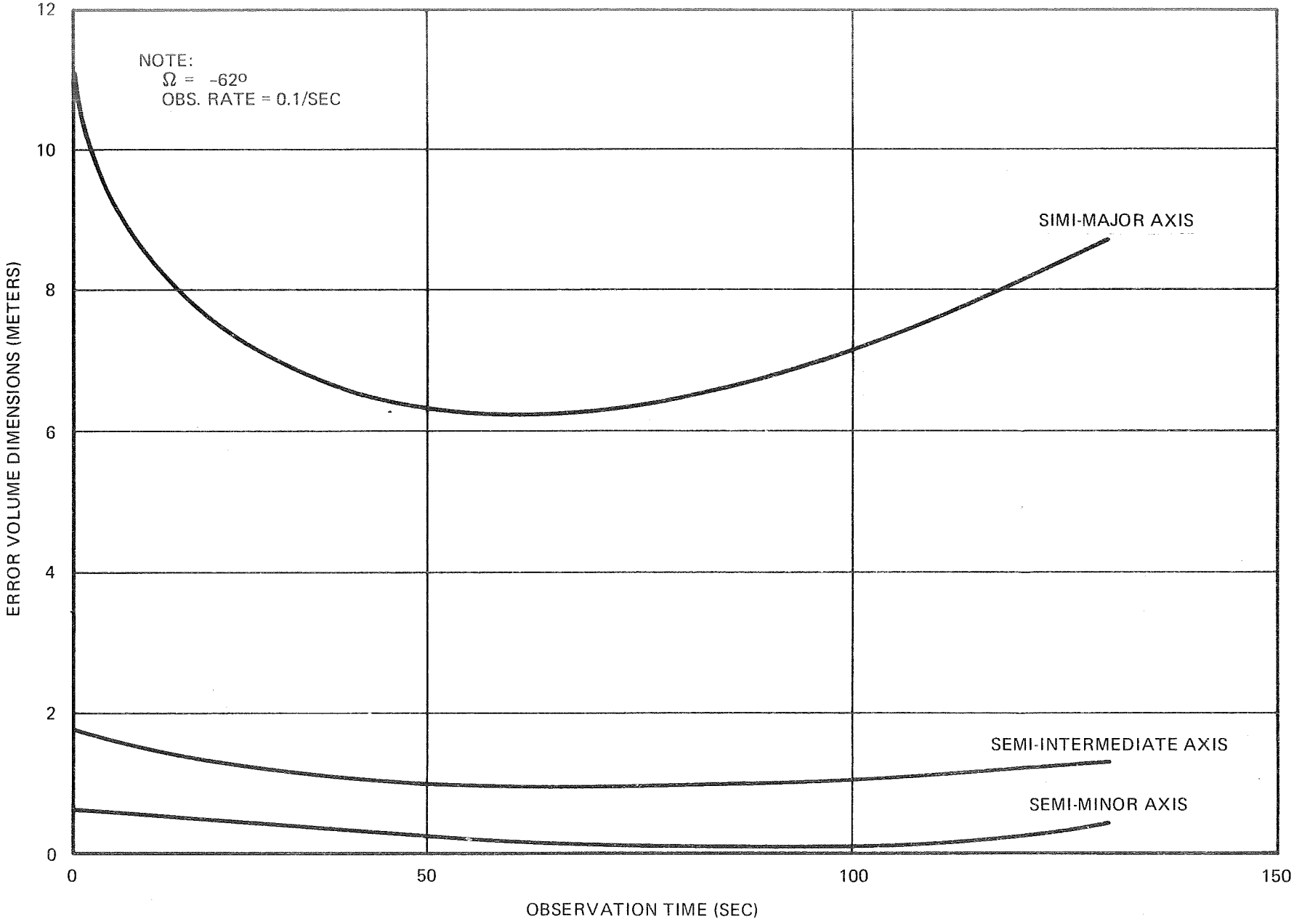

Figure 2.2-4. Error Volume Dimensions - Case 1

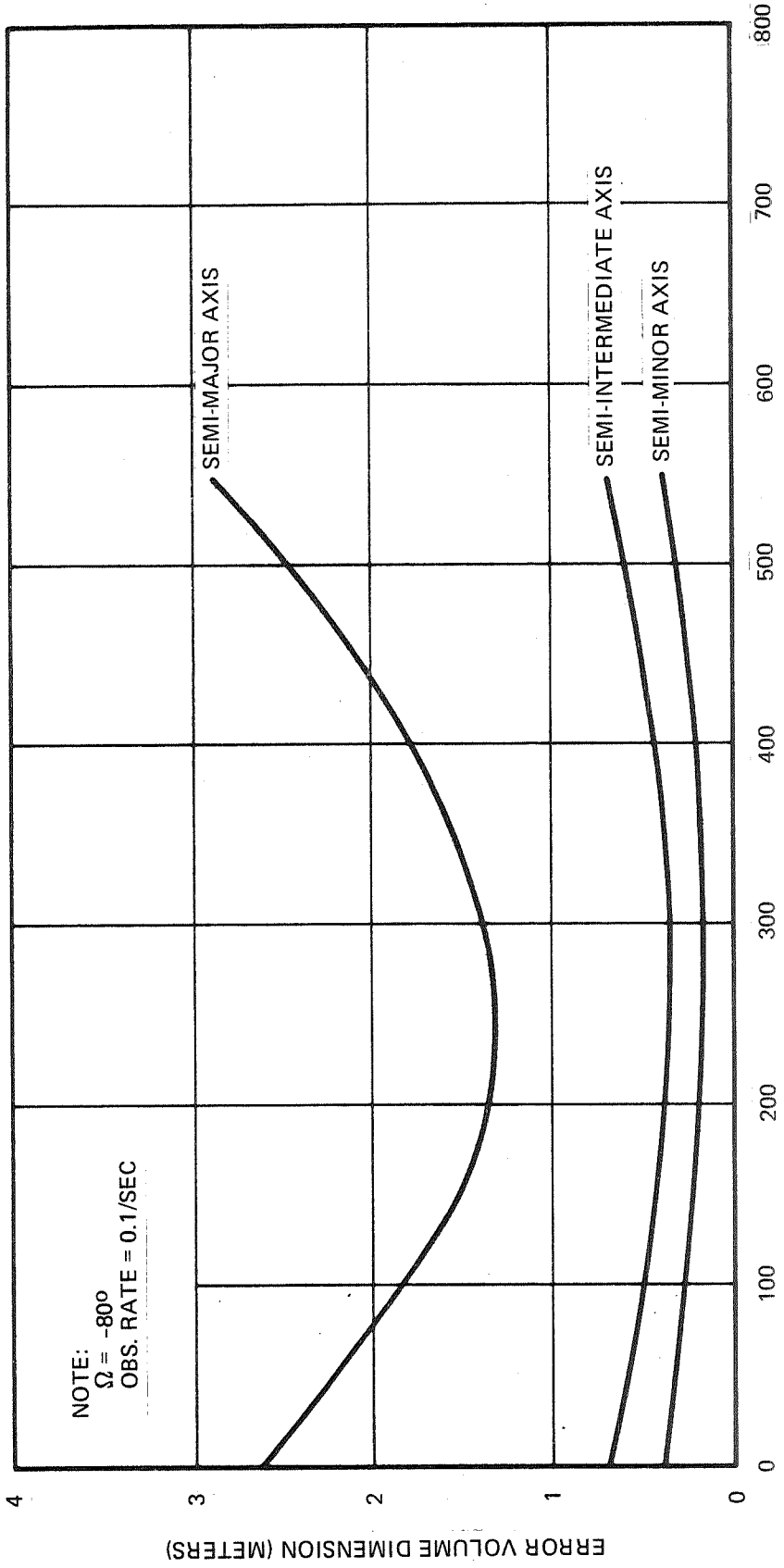

Figure 2.2-5. Error Volume Dimensions - Case 4

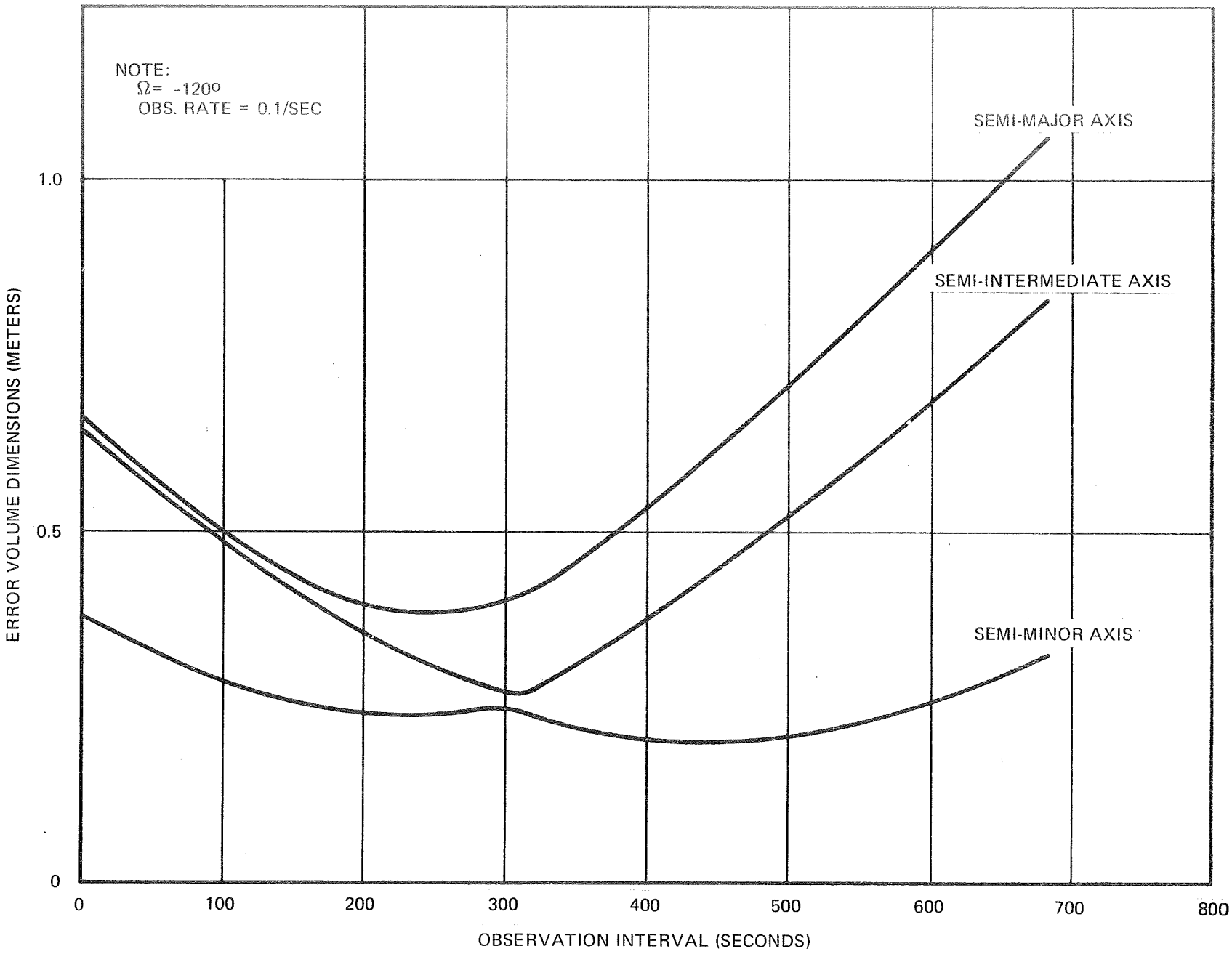

Figure 2.2-6. Error Volume Dimensions - Case 8

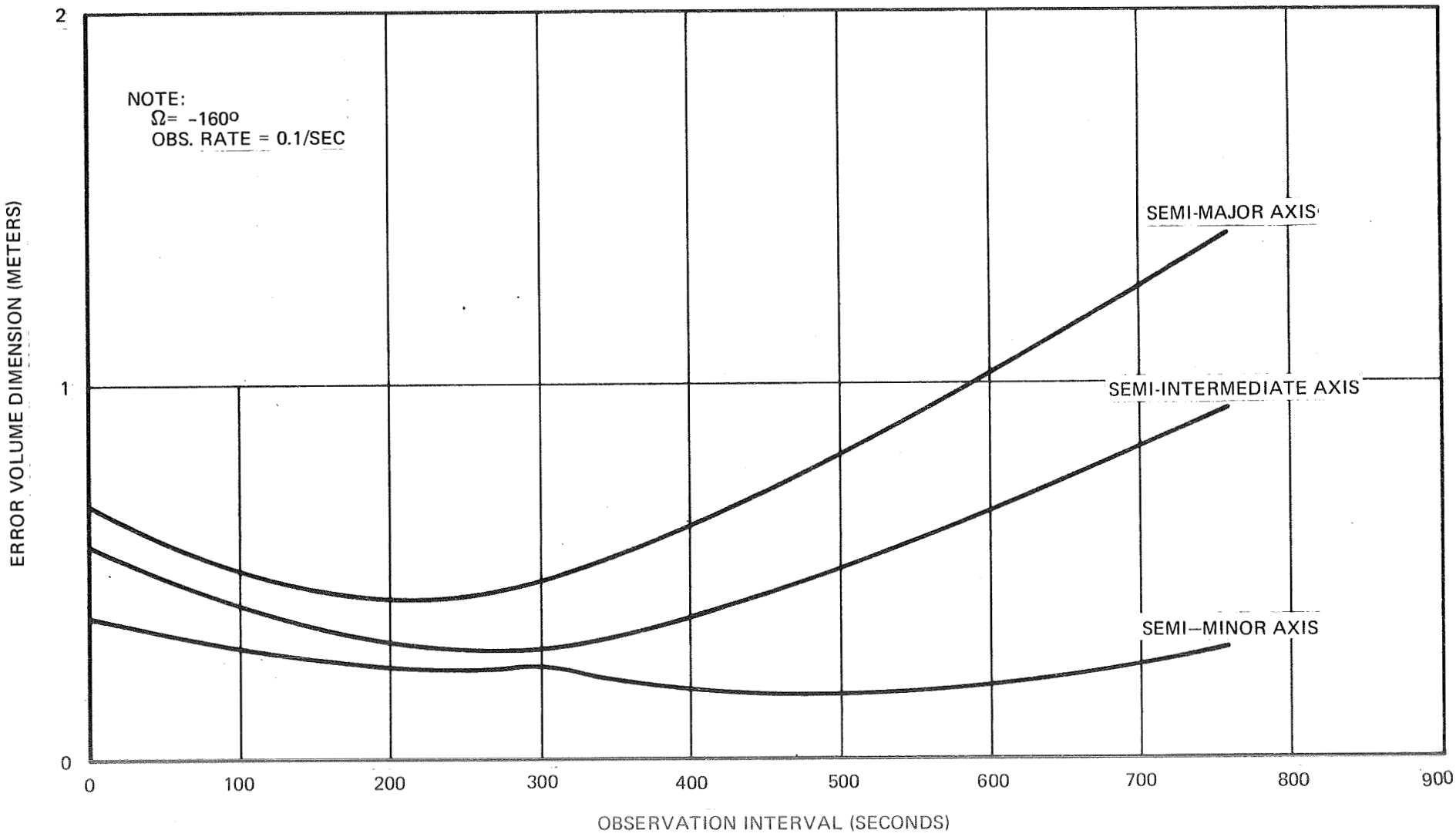

Figure 2.2-7. Error Volume Dimensions - Case 12

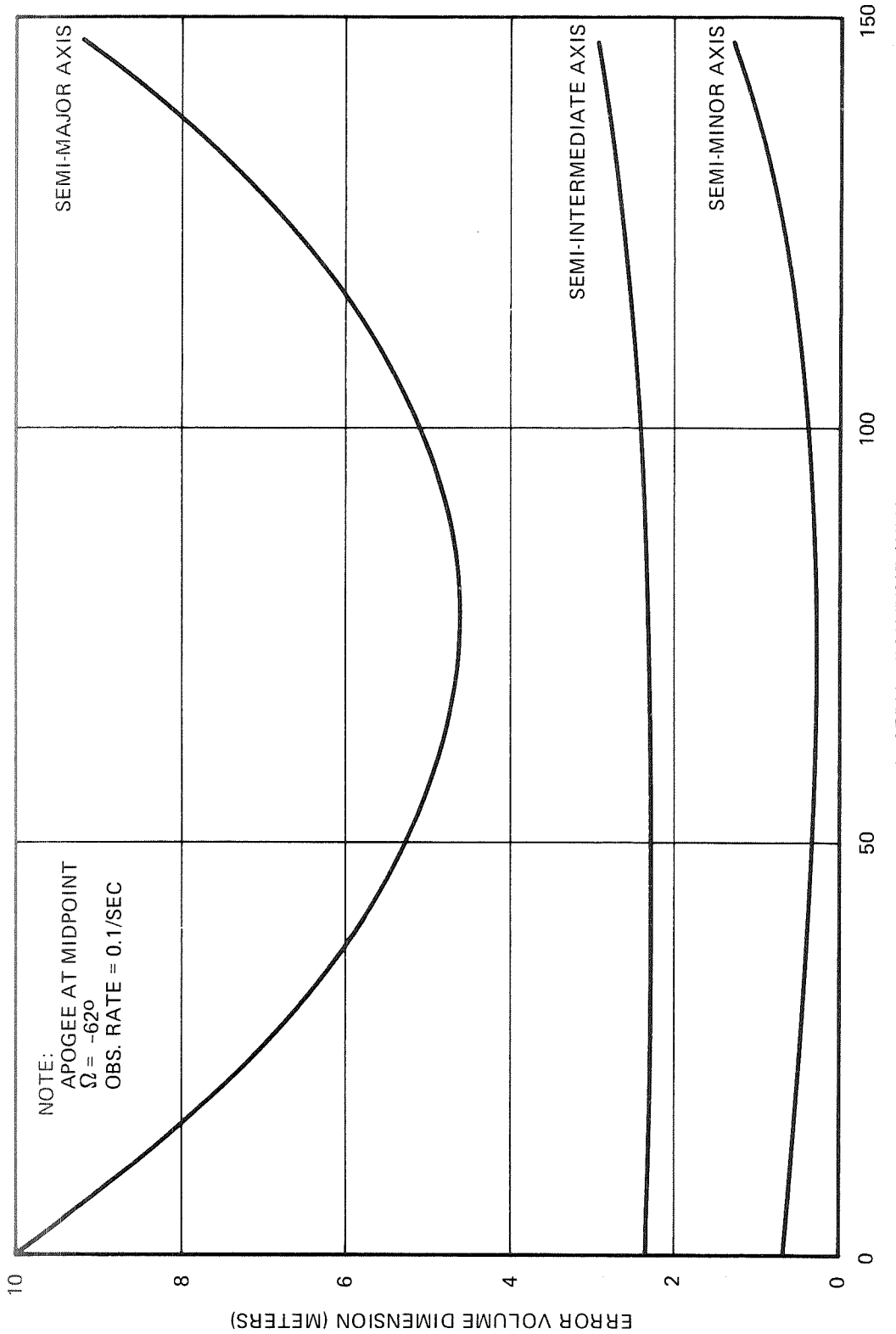

Figure 2.2-8. Error Volume Dimensions - Case 15

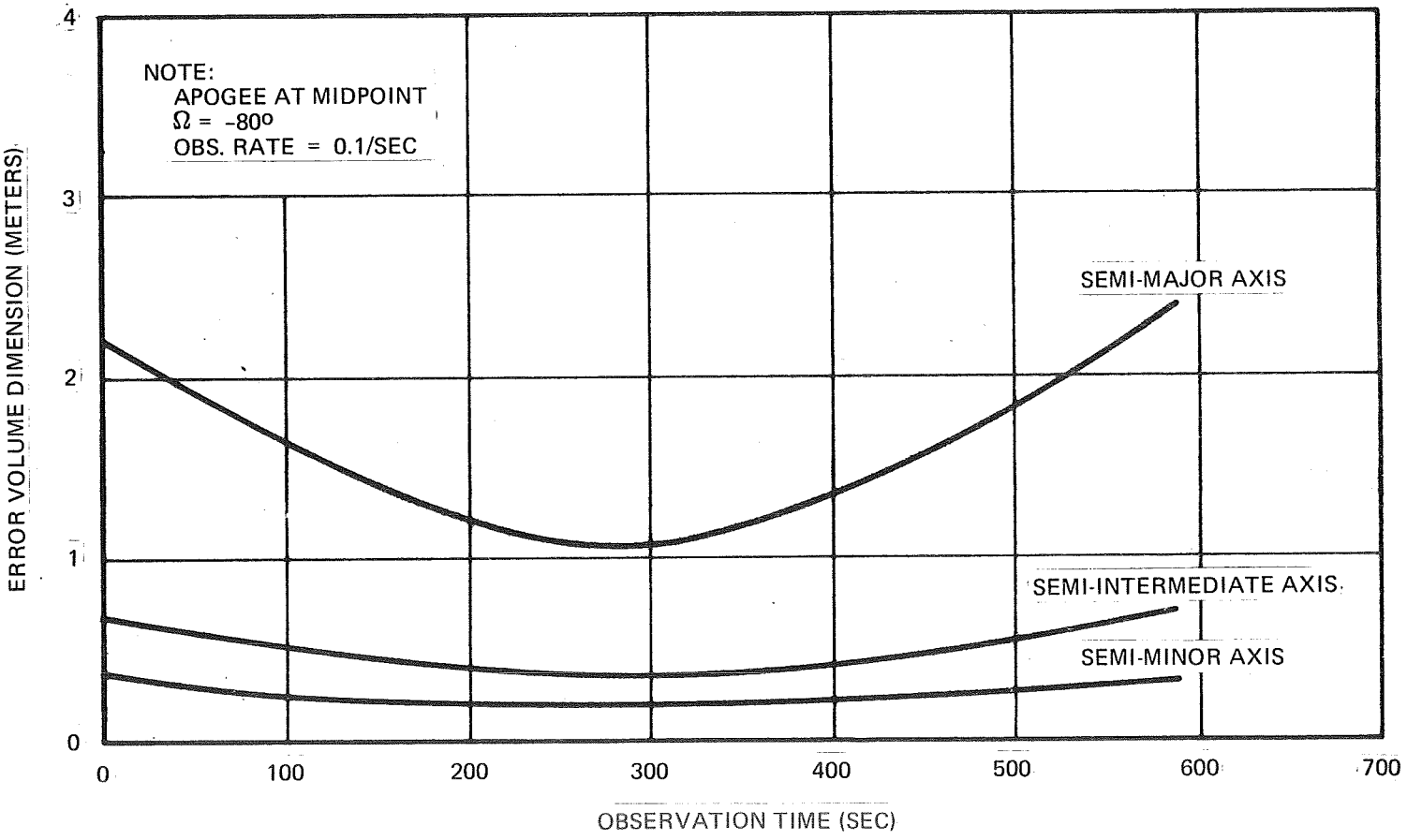

Figure 2.2-9. Error Volume Dimensions - Case 16

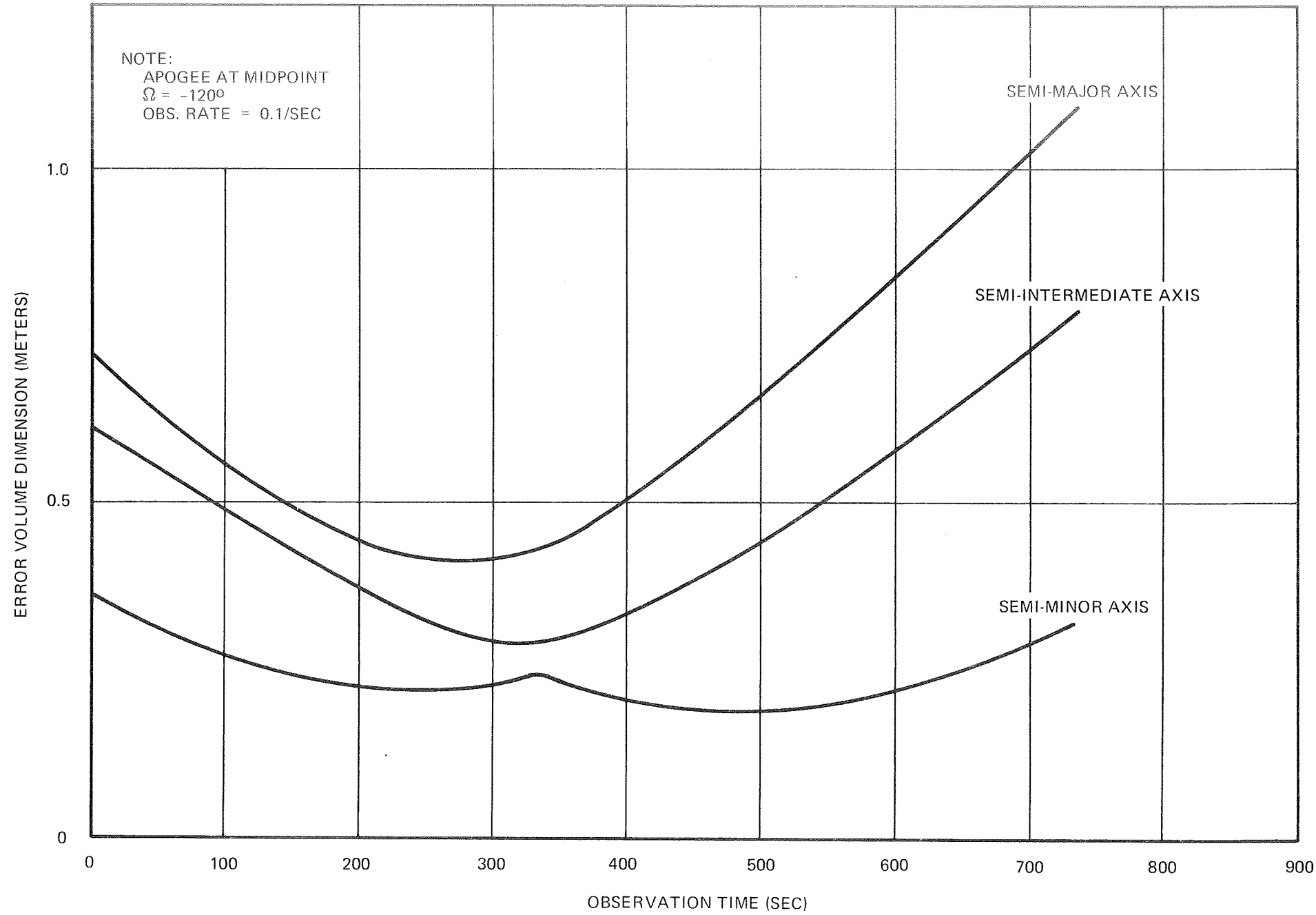

Figure 2.2-10. Error Volume Dimensions - Case 17

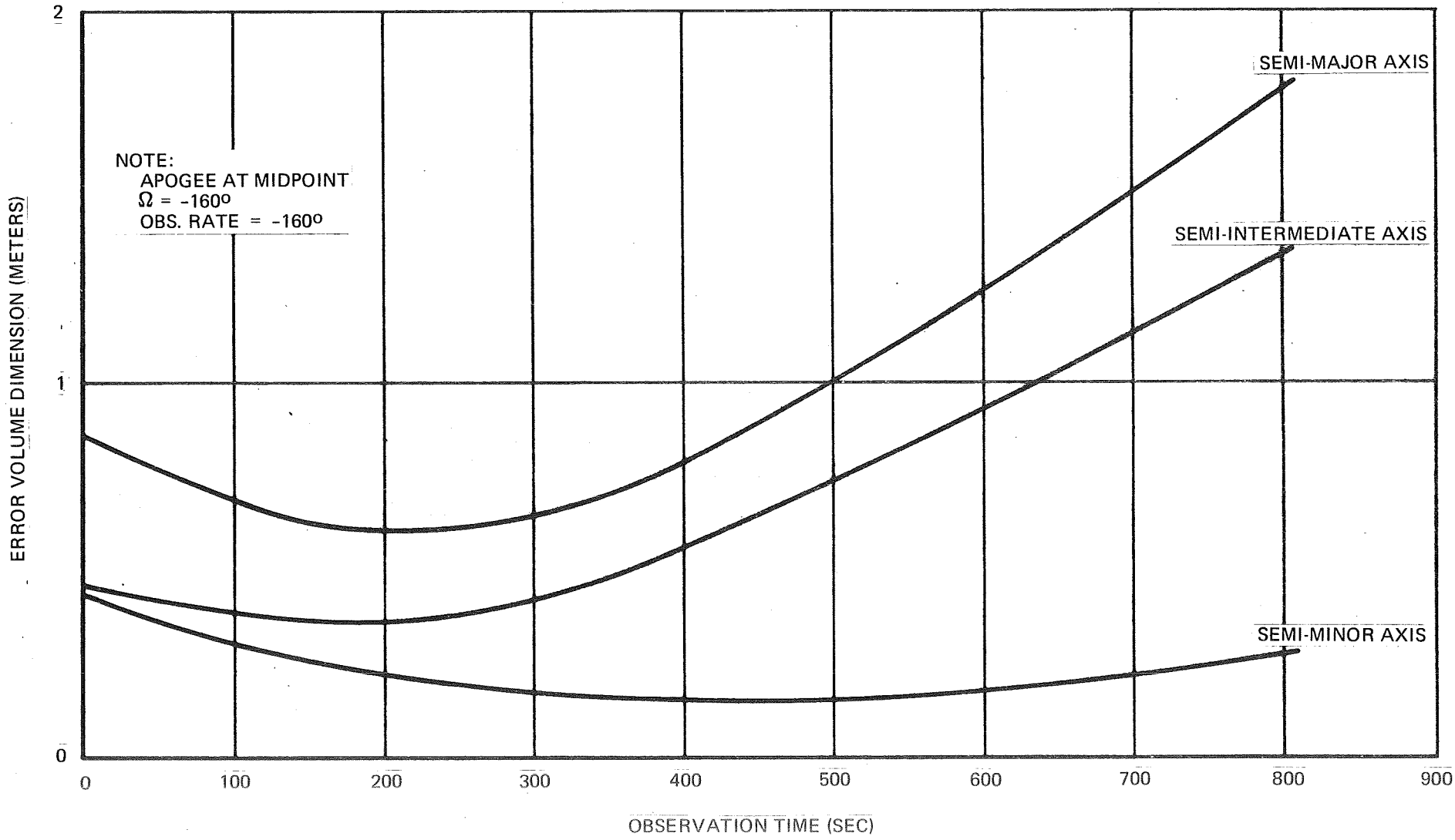

Figure 2.2-11. Error Volume Dimensions - Case 18

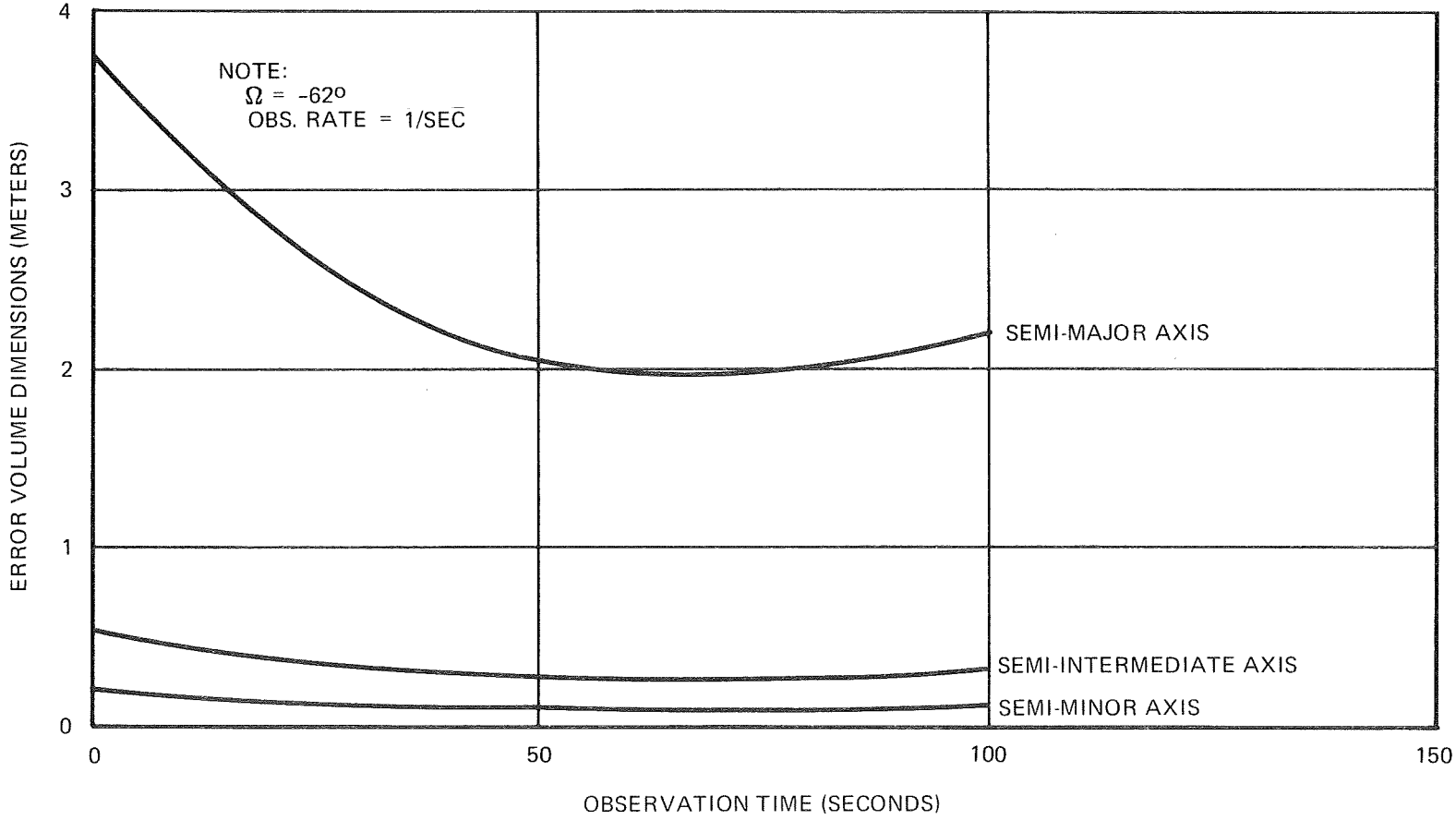

Figure 2.2-12. Error Volume Dimensions - Case 19

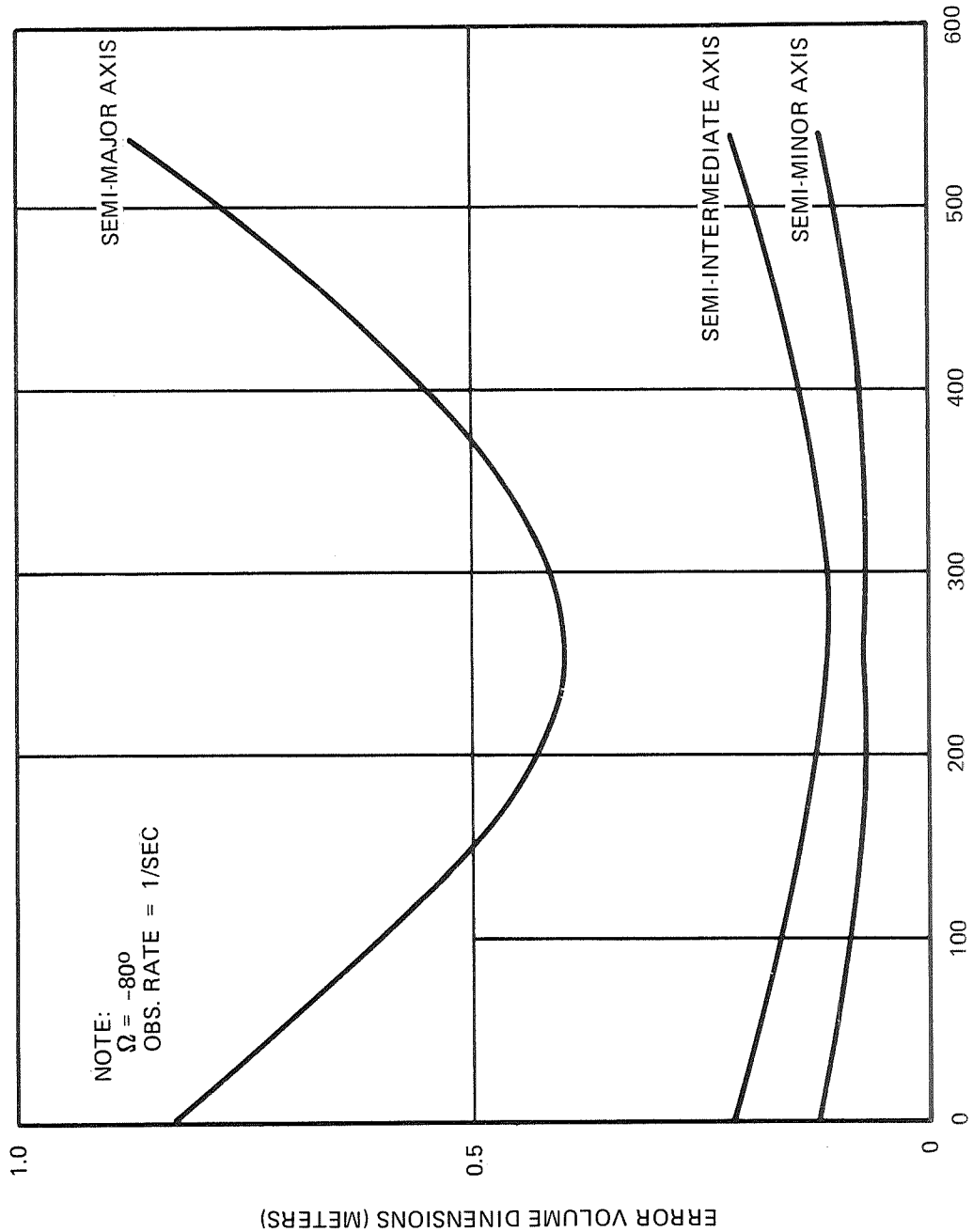

Figure 2.2-13. Error Volume Dimensions - Case 20

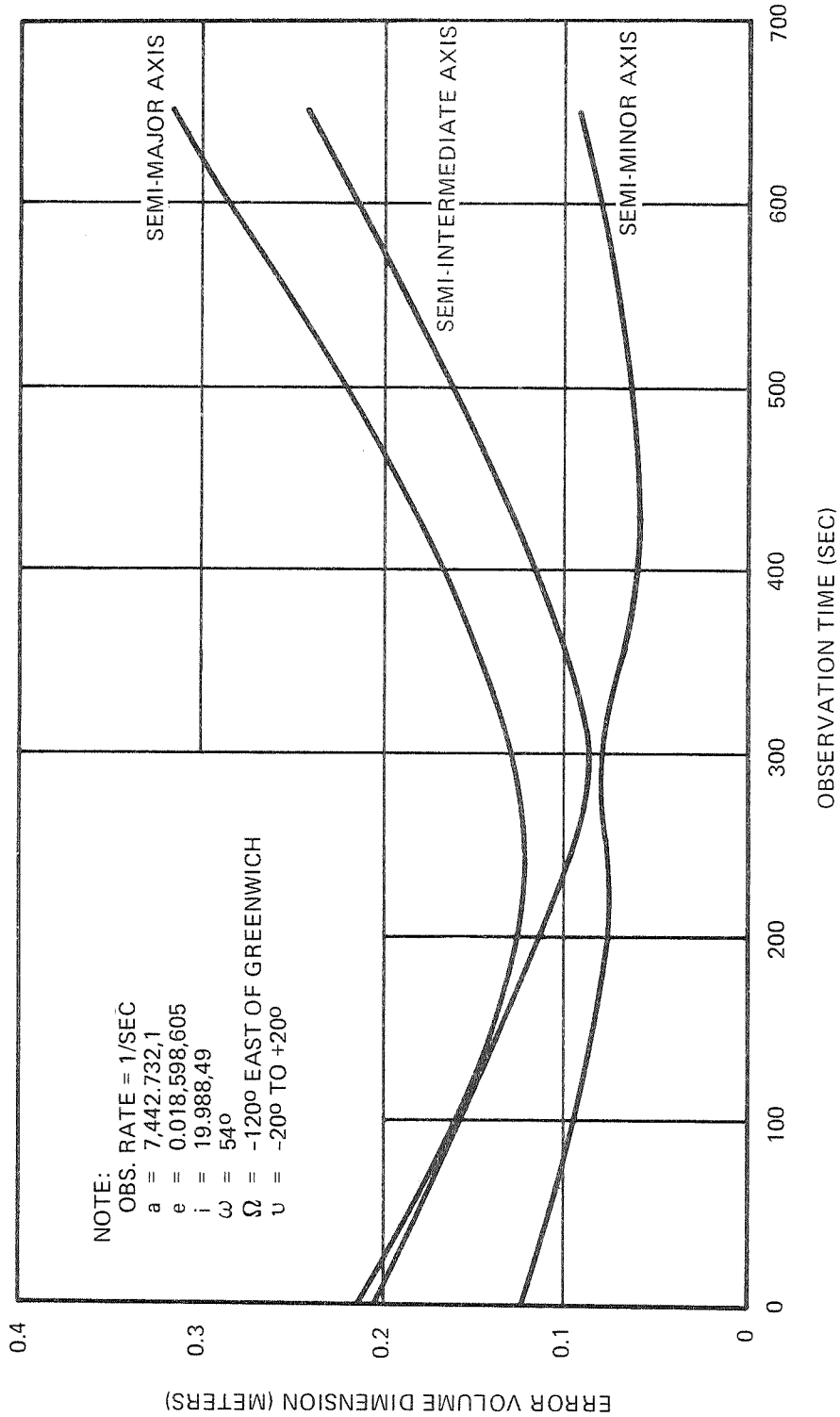

Figure 2.2-14. Error Volume - Case 21

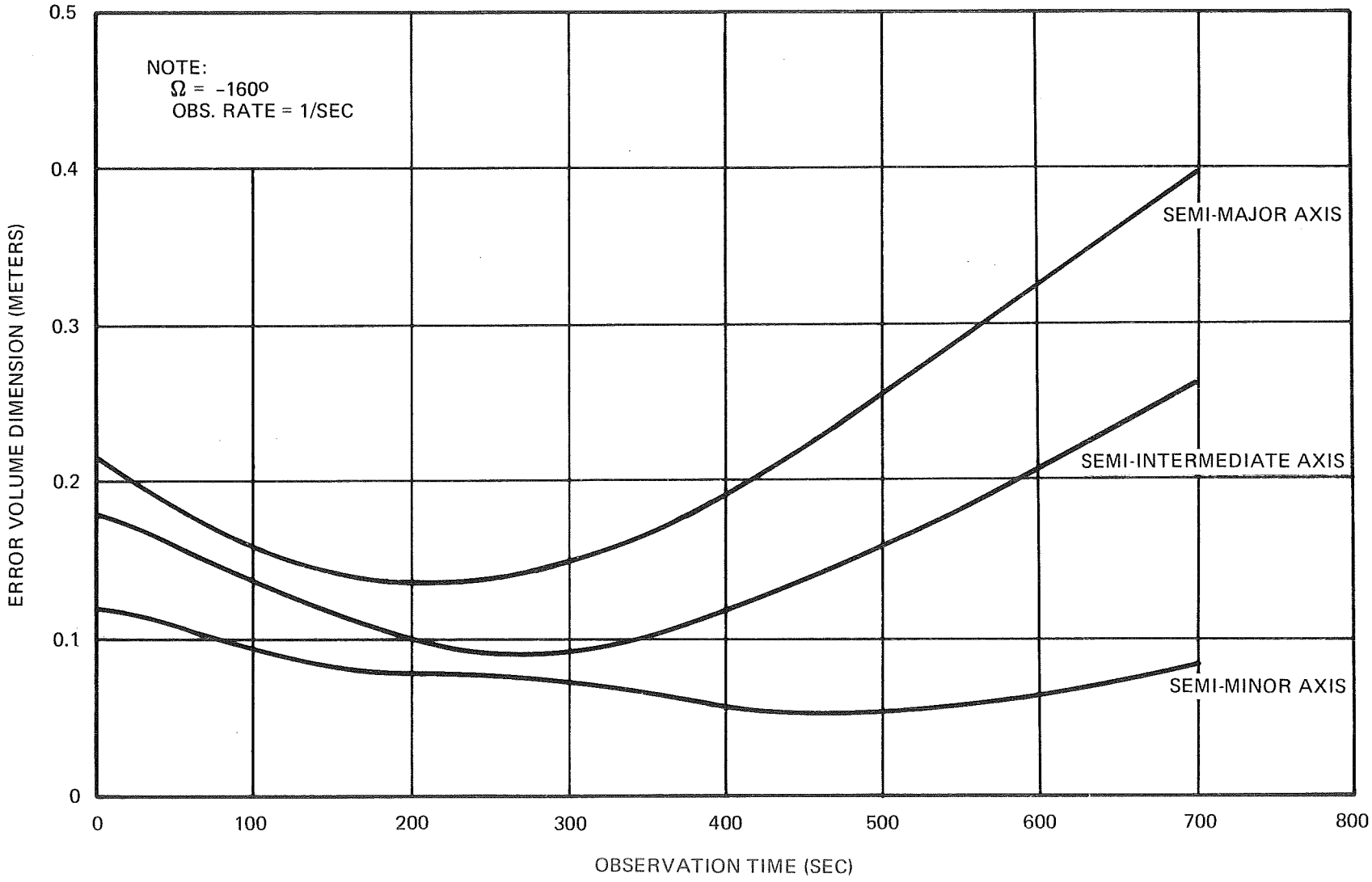

Figure 2.2-15. Error Volume - Case 22

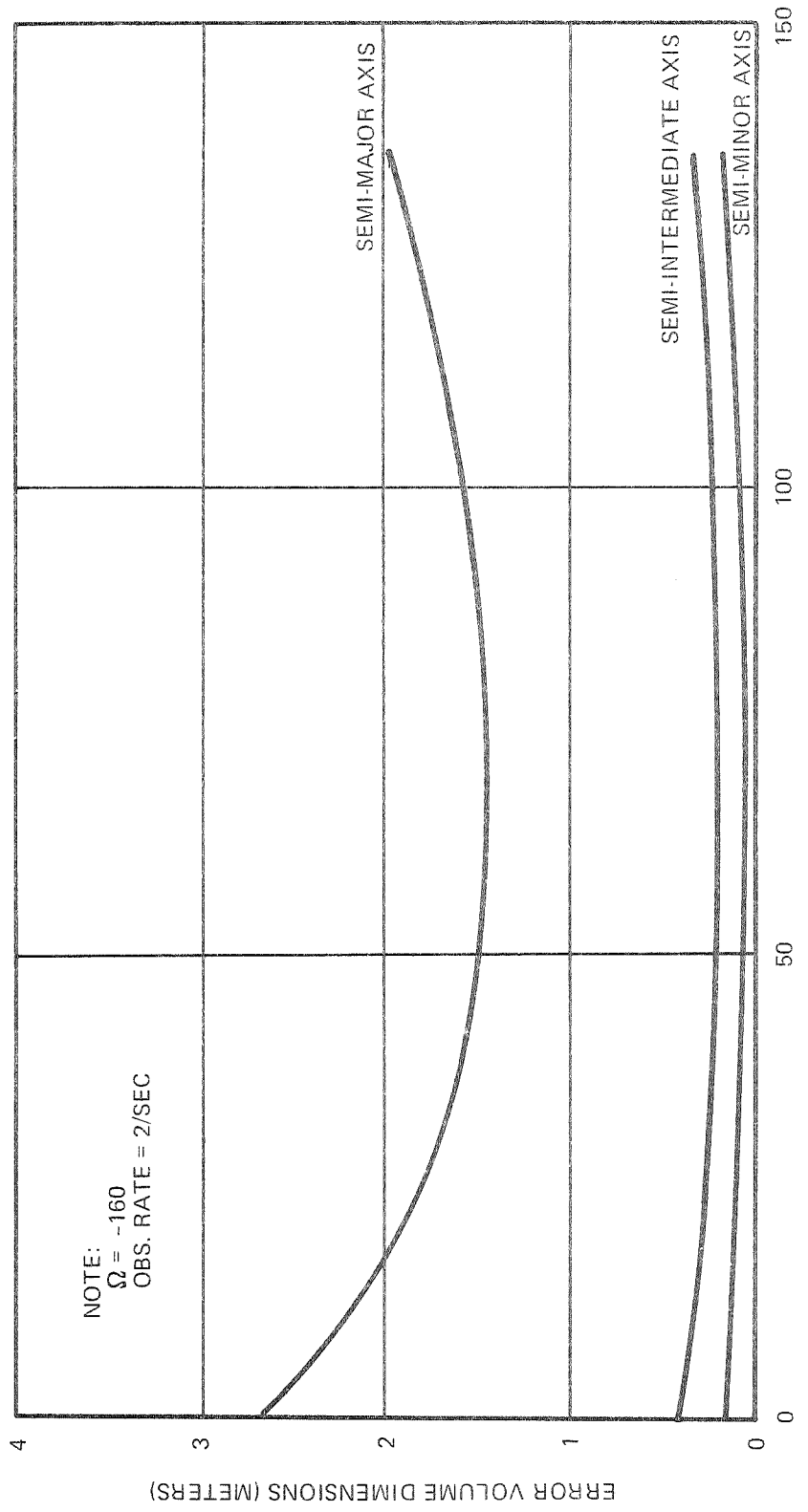

Figure 2.2-16. Error Volume Dimensions - Case 23

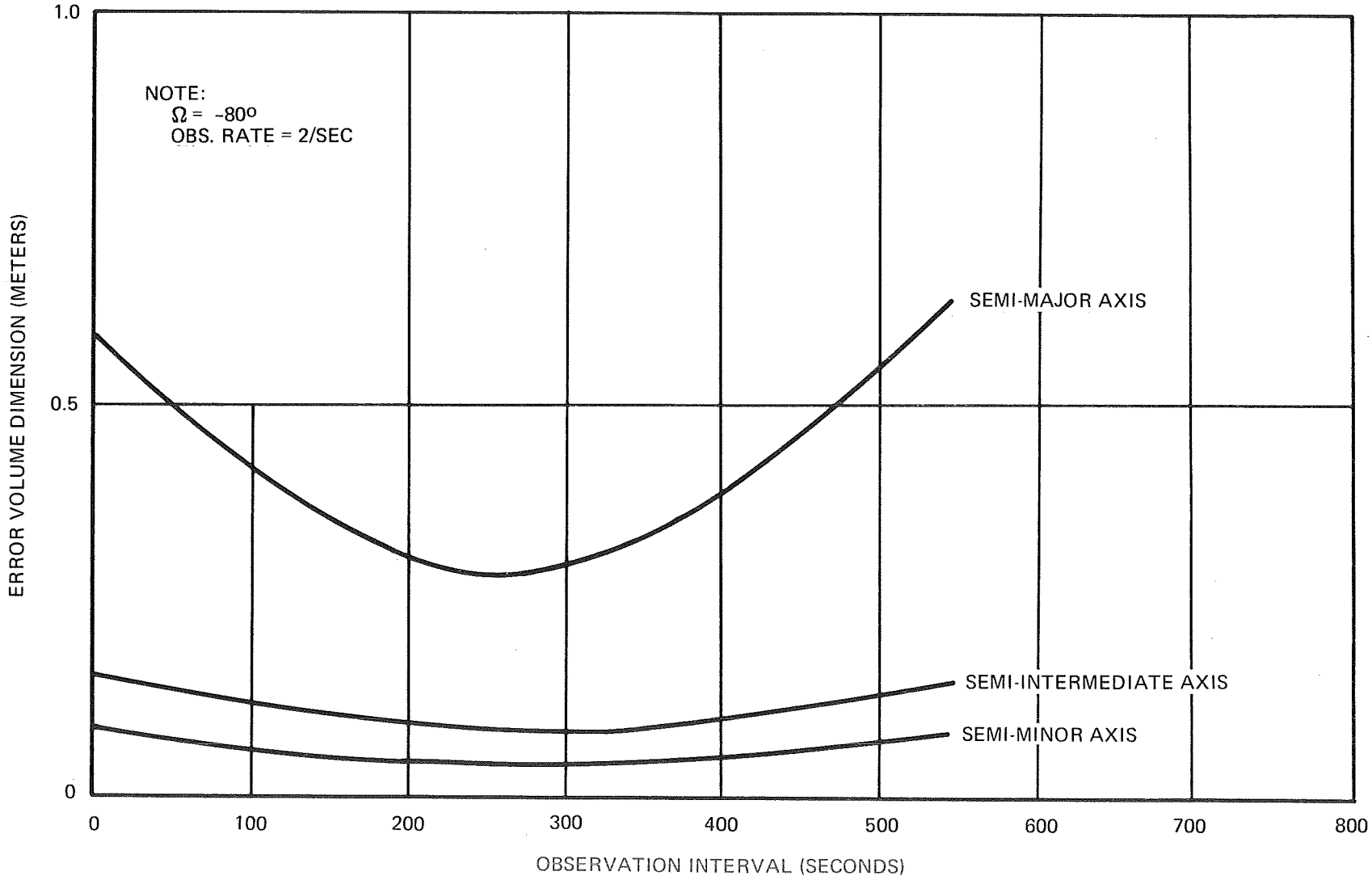

Figure 2.2-17. Error Volume Dimensions - Case 24

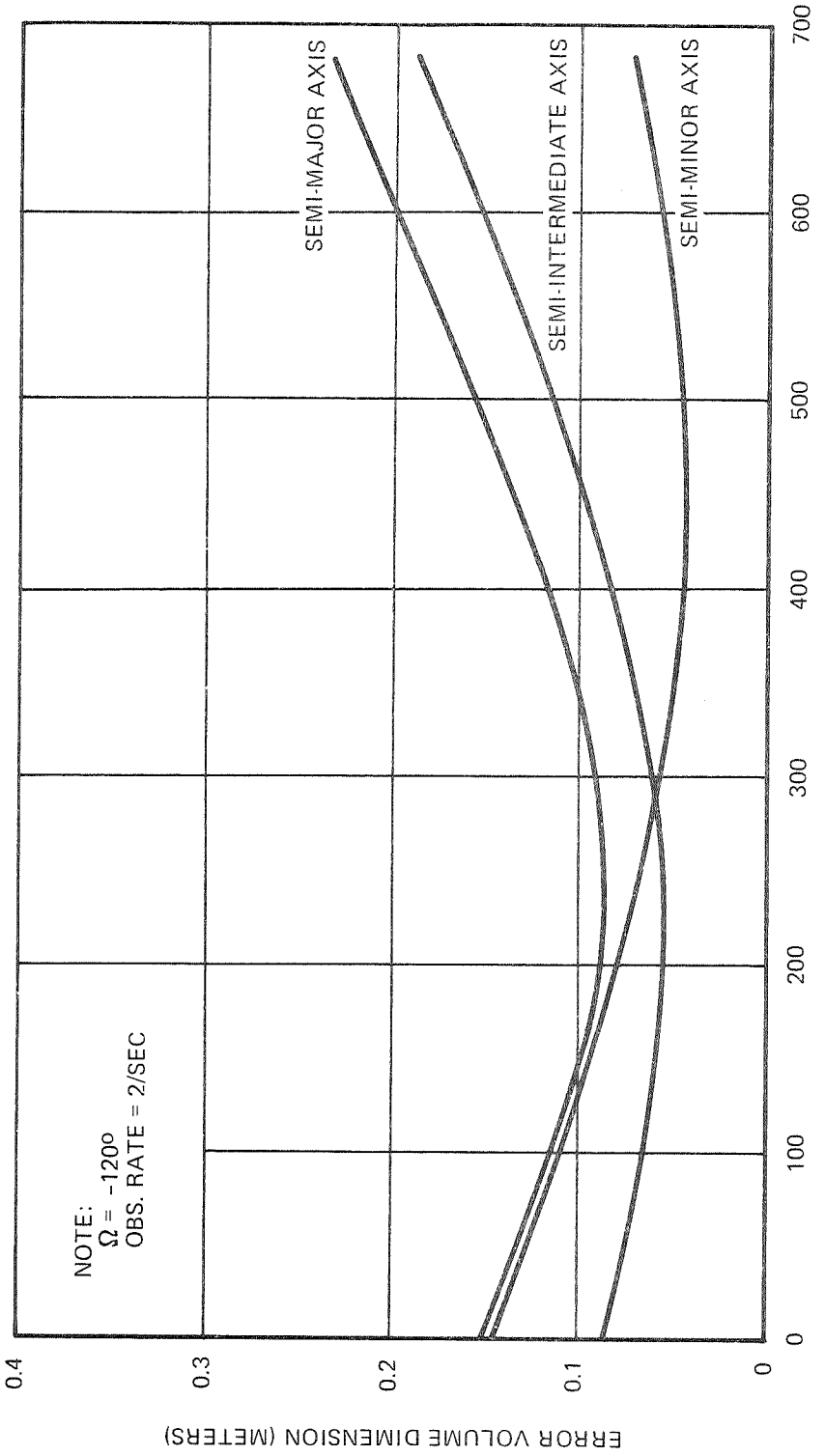

Figure 2.2-18. Error Volume Dimensions - Case 25

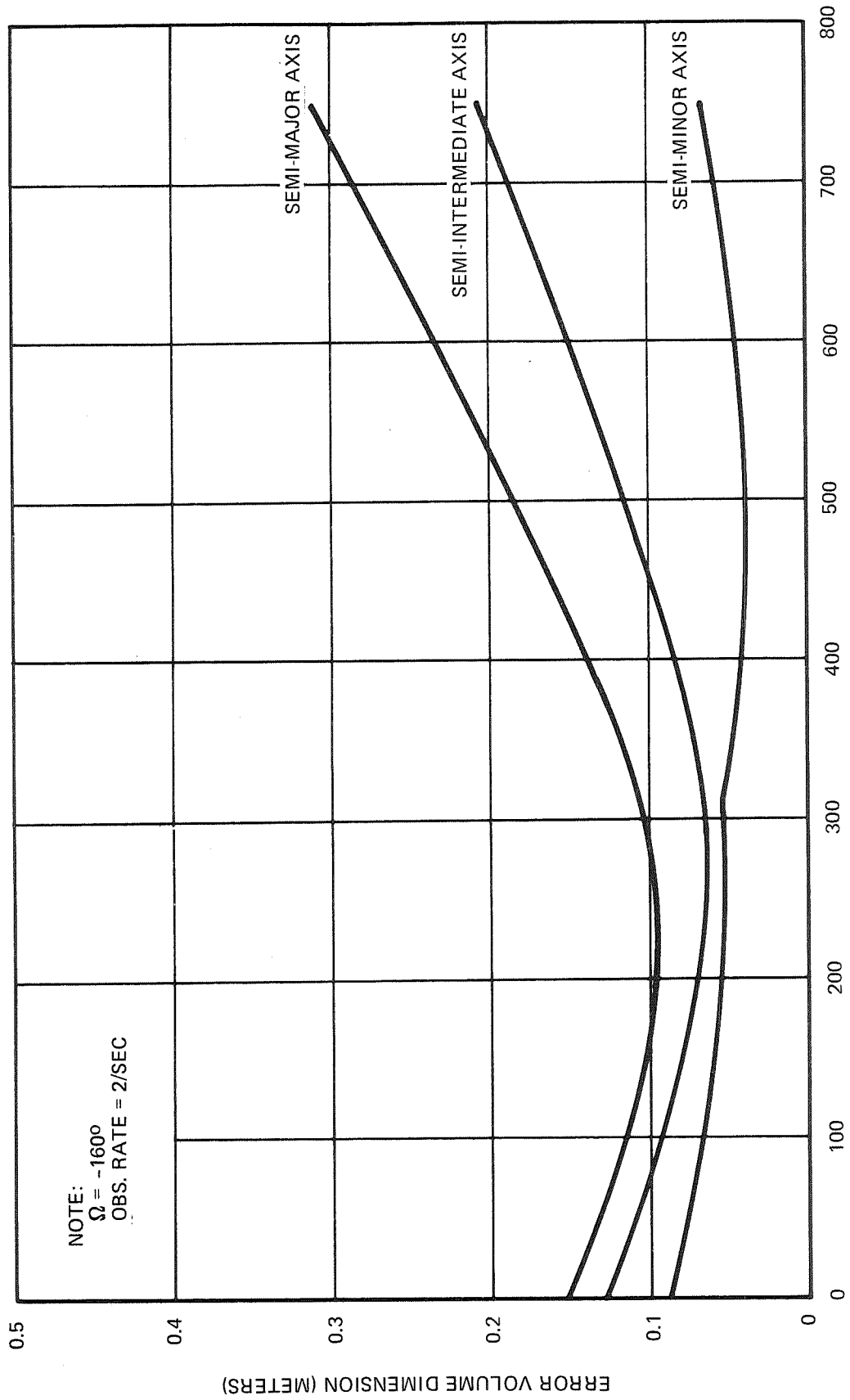

Figure 2.2-19. Error Volume Dimensions - Case 26

for all cases corresponds to $\Omega = -62^{\circ}$ and is 11.4 meters.

Figures 2.2-8 to 2.2-11 illustrate the effect of placing apogee over the midpoint of the observation interval. Comparing these figures to Figure 2.2-4 to 2.2-7 (where perigee was over the midpoint of the observation interval), indicates that the minimum value for each error volume dimension appears to be slightly lower when apogee occurs over the interval. This is probably a result of the improved geometry for this orientation during the period close to apogee.

Figures 2.2-12 to 2.2-19 illustrate the effect of varying the observation rate. Figures 2.2-13 to 2.2-15 correspond to a 1 observation/sec rate, while Figures 2.2-16 to 2.2-19 correspond to an observation rate of 2 observations/sec. As was mentioned above, the error volume dimensions appear to vary as $1/\sqrt{n}$, where n is the number of observations.

2.3 ANALYSIS OF SYSTEMATIC STATION LOCATION AND RANGE BIAS ERROR VOLUME

A typical GEOS-C orbital segment was selected such that the satellite would be visible to all three stations over the segment (see Figure 2.1-2). Using the nominal locations of the observing stations, ranges from the stations to the satellite were determined at selected points on the orbital segment. For a given change in station location or slant range, the position of the satellite at each selected point on the orbital segment could then be recomputed (using a three range position determination), and the resulting difference in satellite positions would be entirely due to the change in station location or slant range. Thus, by this procedure, the effect of station locations and slant range errors on the position determination of the satellite would be completely isolated from other systematic, random, and force model errors.

In the calculation of the difference between the nominal satellite position and the new satellite position due to change in station location or slant range, the difference was computed in intrack, crosstrack, and radial orthogonal components. Because the altimeter measures only in the radial direction, the intrack and crosstrack position differences were discarded for the purposes of this study.

The station location errors were taken to be $\pm$ 15 meters relative to the geocenter. Since all three sensors are quite close together and part of the same datum, a substantial part of this error could be expected to be identical for all three sensors, while the remainder of the error would be relative error between the sensors themselves. Thus, the station location error was divided into two parts, $\pm$ 10 meters error for the entire three sensor group and $\pm$ 5 meters relative error between the three sensors.

For the cases where the sensor group has a common error $\pm$ 10 meters, the radial component of the difference in satellite position (nominal minus error-perturbed position) has been plotted in Figure 2.3-1 for 21 points equidistant in time along the orbit segment. The eight traces on the figure represent all possible cases when the height, latitude, and longitude of the station group are all simultaneously offset by $\pm$ $10/\sqrt{3}$ meters. Thus, the magnitude of the error vector of the station group is 10 meters, while the direction of the error vector systematically trisects each of the eights octants surrounding the nominal group station location. As one might expect, the minimum error exists when the satellite is in the middle of the orbital segment, since at that time the subsatellite point lies inside the triangle formed by the three observing stations.

For the cases where the sensors have a relative error of $\pm$ 5 meters, the radial component of the difference in satellite position has been plotted in Figure 2.3-2 for 21 points equidistant in time along the orbital segment. The 26 traces on the figure represent about 5% of the 512 possible cases when the height, latitude, and longitude of each station are systematically and simultaneously offset by $\pm$ $5/\sqrt{3}$ meters. (For each station, the height, latitude, and longitude may each be offset in either the + or - direction, giving $2 \cdot 2 \cdot 2 = 8$ combinations of station position offset from the nominal. For all three stations, $8 \cdot 8 \cdot 8 = 512$ possible combinations.) The envelope of all 512 cases is also plotted. Again, it is noted that minimum error occurs in the middle section of the orbital segment.

The envelope of all the cases should be considered to be more than a 1σ limit to the altitude error. The station location error of $\pm$ 5 meters is a 1σ error, therefore, 32% of the time, the magnitude of the error in individual relative station

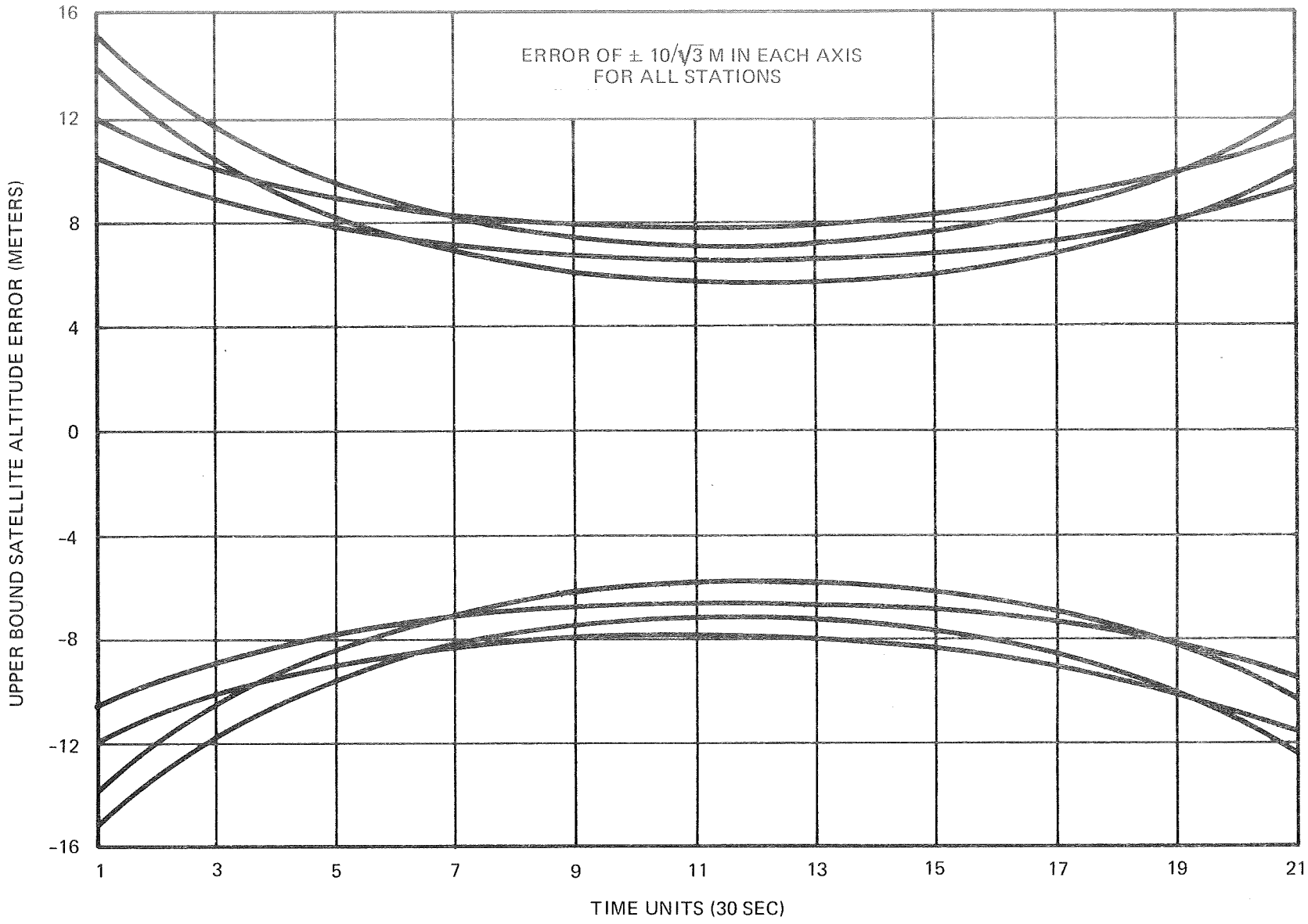

Figure 2.3-1. Satellite Altitude Error vs Time for Observing Station Location Group Errors

locations will be larger than this value. However, the likelihood of the error being greater than 5 meters and occuring in any one of the octants surrounding each station position is 32%/8 = 4%. In order for some part of any one of the error traces in Figure 2.3-2 to fall on the envelope, each station location must be offset in a particular octant such that the combination of the three station location offsets results in the indicated altitude error. The possibility of this occuring is $(0.04)^3 = 0.000064$ (about 4σ) for all three stations to be displaced in such a way. Obviously, the 2σ error limit would be substantially within the indicated error envelope.

Figure 2.3-3 indicates the altitude errors for the cases where there is a sensor systematic range bias of $\pm$ 5 meters. Again, assuming that the bias is either +5 or -5 meters, there are $2 \cdot 2 \cdot 2 = 8$ possible traces that combine these bias errors for three observing stations. It is noted that on these traces, the "envelope" between time units 7 and 17 is caused by the cases where the range biases for the three stations are all either +5 meters or -5 meters. For each radar, there is a 32% possibility that the bias will be 5 meters or greater, thus, for all three radars to have a bias of this magnitude and to be all either too long or too short, the probability is $(.32)^3 = 0.033$, or less than 2σ.

Perhaps the most striking aspect of the three figures is the very short orbital segment over which systematic station location and range biases produce minimal error. Figures 2.3-2 and 2.3-3 indicate this minimal error span to be from time units 7 to 17, or a total orbital time of 5 minutes. At either end of the orbital segment, station location and range biases produce increasingly larger altitude errors. Figure 2.3-1 is less clear in defining an exact time span of minimal error, but the traces do have a minimum altitude error, a minimum between time units 10 and 13.

The very short nature of the minimum error orbit segment leads to the conclusion that proper selection of orbital segments of concurrent observational data can provide great benefit in alleviating systematic observational errors due to station location and range biases.

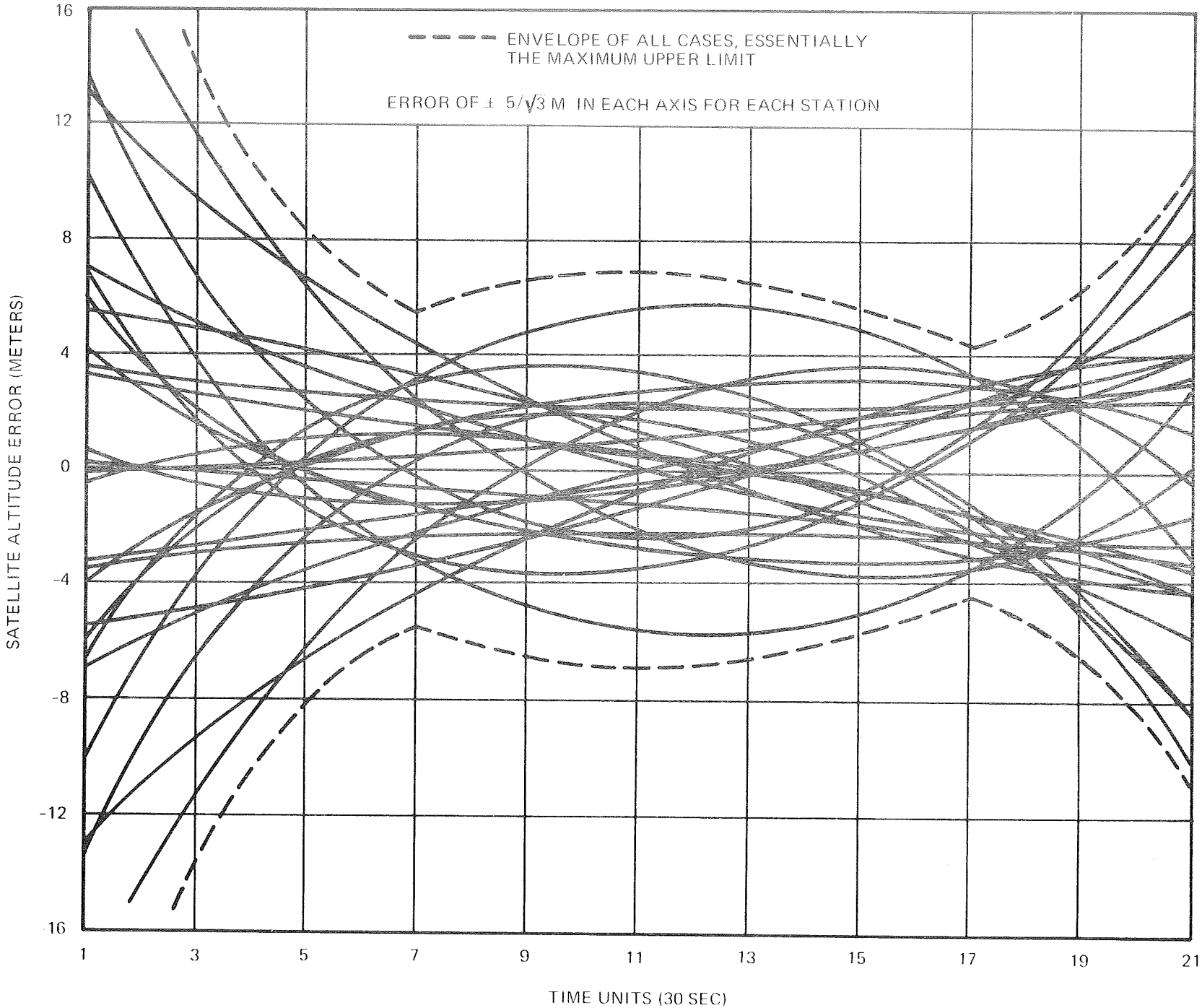

Figure 2.3-2. Satellite Altitude Errors vs Time for Observing Station Location Errors (5% of Possible Cases)

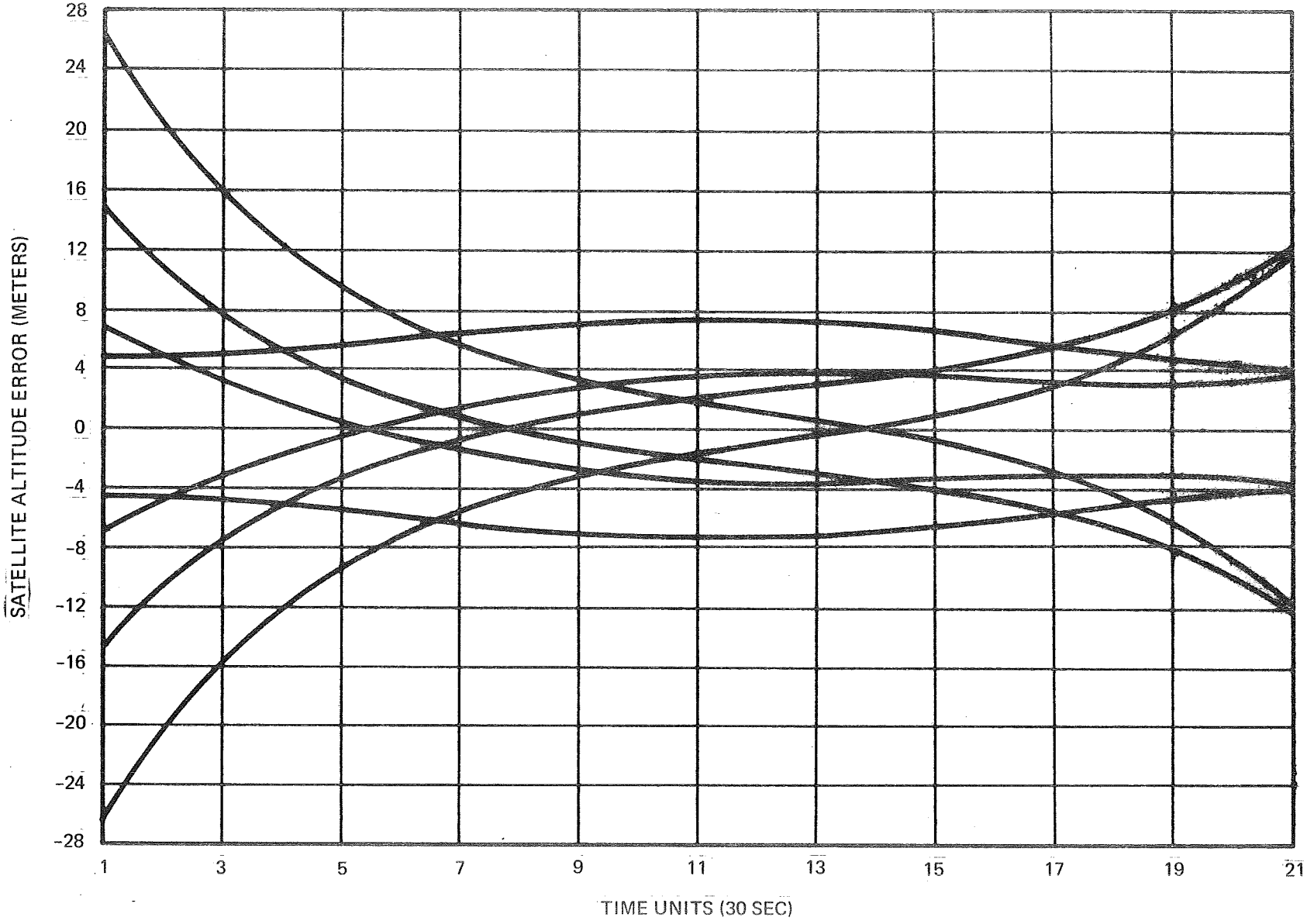

Figure 2.3-3. Satellite Altitude Error vs Time for Observing Station Range Errors (Radar)

When the satellite is in a position where it can be tracked by more than three sensors, the effect of additional tracking data may improve the satellite positions by reducing the effect of the positional error of any one sensor. The amount and extent of the improvement (if any) is open to question, however, since the satellite position error is highly dependent on the satellite orbital position, the relative locations of the observing stations, and the actual magnitude of the station location errors. Further investigation of this situation is needed to provide a quantitative solution.

3.0 SIGNIFICANCE OF GRAVITY-MODEL ERRORS

3.1 INTRODUCTION

Time-constant systematic errors in station-location, which were discussed in the last section, would not mask any "fine-structure" (e.g., the Puerto Rican dip) aspects of the altimeter data. If one had confidence that there existed no unpredictable "wiggles" in the GEOS-C satellite orbit, then one could utilize the altimeter data alone to define local sea-level variations (fine structure) even if one had a systematically off-set orbital path. Thus for relative profiling of the sea-level it is important to study the errors that one might expect to find in the orbital path due to uncertainties in the Earth's gravity model.

As a first-cut at the problem let us suppose that there exists an error in any one of the harmonic coefficients of the gravitational field that is between $\pm$ 0.02 and $\pm$ 2 x 10^{-6} in characteristic units. For example, Cook reported in 1965 that the zonal harmonic J_8 had an error of $\pm$ 0.2 x 10^{-6} and Kaula in 1968 (private communication) suggested that the error in the normalized values of the tesseral harmonics would be on the order of $\pm$ 0.08 x 10^{-6}. Since these are given in characteristic units we can make a gross estimate of the effect of anyone such error over one unit of tau (characteristic) time--about 13 minutes, i.e.,

$$\Delta s \cong \frac{1}{2}(\text{coefficient error})\,\tau^2 .$$

For the stated errors one would expect an orbital "wiggle" having an amplitude of from 6 meters to 6 centimeters. The combination of all of the coefficient errors would probably be larger and would be correlated with any local gravitational anomalies such as the one that causes the Puerto Rican dip. Figure 3-11 illustrates this effect and the over-three-meter orbital dip does indeed occur when the nominal GEOS-C orbit passes over the Java deep. Thus the uncertainty in the Earth's gravitational field might partially mask any local sea-level variations unless the orbit was carefully "followed" over a short arc.

3.2 ANALYSIS APPROACH

For a determination of the influence of the gravitational potential upon GEOS-C, a decision was made to use analytical partial derivatives that incorporate the effects of any harmonic. Since the primary interest is in the errors associated with height determination, the particular error component that most concerns us is the radial error. The analytical formulation, although somewhat difficult to derive, does allow one to easily separate out the radial errors due to errors in the determination of various harmonics. The derivation of the radial partials are outlined below.

The gravitational potential at a point, P, is defined by

$$\Phi = \frac{k_e^2}{r} \sum_n \sum_m \left(\frac{a_e}{r}\right)^n \left\{ C_{nm} \cos m\lambda + S_{nm} \sin m\lambda \right\} P_{nm}(\sin \varphi') \qquad (3\text{-}1)$$

where

k_e^2 = A function of the gravitational constant and the mass of the Earth.

r = The geocentric radial distance of point P being disturbed.

λ = The longitude of P.

φ' = The geocentric latitude of P.

a_e = The mean equatorial radius of the Earth.

C_{nm}&S_{nm} = Constants of spherical harmonics of degree n and order m.

$P_{nm}(\sin \varphi')$ = The associated Legendre function defined by:

$$(1 - \sin^2 \varphi')^{\frac{m}{2}} \frac{d^m P_n(\sin \varphi')}{d(\sin \varphi')^m} .$$

The perturbative effect of Φ on a satellite's orbit results in the added acceleration, $\dot{\underline{r}}$. The perturbation may be expressed in terms of its radial, transverse, and orthogonal components with respect to the orbit-plane, $\dot{r}$, $r\dot{v}$, and $r\dot{b}$, respectively:

$$\dot{\underline{r}} = \dot{r}\,\underline{U} + r\dot{v}\,\underline{V} + r\dot{b}\,\underline{W} \tag{3-2}$$

where the unit vectors $\underline{U}$, $\underline{V}$, $\underline{W}$, are usually referred to an inertial cartesian coordinate system. The components are then obtained from the potential function:

$$\begin{aligned} k_e^2 \dot{r} &= \frac{\partial \Phi}{\partial r} \\ k_e^2 r\dot{v} &= \frac{1}{r}\frac{\partial \Phi}{\partial v} \\ k_e^2 r\dot{b} &= \frac{1}{r}\frac{\partial \Phi}{\partial b} \end{aligned} \tag{3-3}$$

The first time derivatives of any set of elements may also be written in terms of $\dot{r}$, $r\dot{v}$, $r\dot{b}$. For instance, we have selected the a_{xn} set of elements which are

a_{xn} = e cos ω

a_{yn} = e sin ω

n = The mean motion

U = The mean argument of latitude

i = Orbital inclination

Ω = The longitude of the ascending node.

This set was selected because it eliminated certain indeterminacies for low orbital eccentricities. To the zeroth order in eccentricity, the time derivative of a_{xn} can be written as

$$\frac{da_{xn}}{dt} = \frac{a^{5/2}}{\sqrt{\mu r^2}} (\sin u \dot{r}\hat{} + 2 \cos u r\dot{v}\hat{}) + O[e] \quad , \tag{3-4}$$

or, it can be taken with respect to u, the true argument of latitude in the form

$$\frac{da_{xn}}{du} = \frac{a^2}{\mu} (\sin u \dot{r}\hat{} + 2 \cos u r\dot{v}\hat{}) + O[e] \quad . \tag{3-5}$$

The use of u as the independent variable eliminates the need for the G_{nmpq} eccentricity function associated with the mean anomaly. The partials for the radial component in this report are complete to the first order in eccentricity although they may be derived to any order. Equation (3-3) can be substituted into Eq. (3-5) so that the derivative of a_{xn} with respect to u is in terms of the accelerations due to the gravitational potential. If these expressions are integrated with respect to u, one obtains the analytical partials a_{xn}, a_{yn}, $\delta n/n$, δU, δi, and $\delta\Omega$ due to gravitational perturbations. δr can be expressed in the form that includes δa_{xn}, δa_{yn} and $\delta n/n$:

$$\delta r = -a\left[\frac{2}{3}\frac{\delta n}{n} + \cos u\, \delta a_{xn} + \sin u\, \delta a_{yn}\right] \quad . \tag{3-6}$$

Substituting the appropriate expressions into Eq. (3-6) one obtains the complete expression for δ_r Eq. (3-7):

$$\delta_r = \frac{1}{2} a \left(\frac{a}{e}\right)^n \sum_{p=o}^{n} F_{nmp} \left\{ C_{nm} \left[4 \frac{(n-2p)}{(n-2p)+\epsilon_1} \begin{matrix}\cos \\ \text{or} \\ \sin\end{matrix} [(n-2p)u + m(\Omega-\theta)] \right.\right.$$

$$+ \frac{(n-1)-2(n-2p-1)}{(n-2p-1)+\epsilon_1} \left(\begin{matrix}\cos \\ \text{or} \\ \sin\end{matrix} [(n-2p-1)u + m(\Omega-\theta)] \cos u \right.$$

$$\left. - \begin{matrix}\sin \\ \text{or} \\ \cos\end{matrix} [(n-2p-1)u + m(\Omega-\theta)] \sin u \right)$$

$$- \frac{(n-1)+2(n-2p+1)}{(n-2p+1)+\epsilon_1} \left(\begin{matrix}\cos \\ \text{or} \\ \sin\end{matrix} [(n-2p+1)u + m(\Omega-\theta)] \cos u \right.$$

$$\left. \left. + \begin{matrix}\sin \\ \text{or} \\ -\cos\end{matrix} [(n-2p+1)u + m(\Omega-\theta)] \sin u \right) \right]$$

$$+ S_{nm} \left[4 \frac{(n-2p)}{(n-2p)+\epsilon_1} \begin{matrix}\sin \\ \text{or} \\ -\cos\end{matrix} [(n-2p)u + m(\Omega-\theta)] \right.$$

$$+ \frac{(n-1)-2(n-2p-1)}{(n-2p-1)+\epsilon_1} \left(\begin{matrix}\sin \\ \text{or} \\ -\cos\end{matrix} [(n-2p-1)u + m(\Omega-\theta)] \cos u \right.$$

$$\left. + \begin{matrix}\cos \\ \text{or} \\ \sin\end{matrix} [(n-2p-1)u + m(\Omega-\theta)] \sin u \right)$$

$$- \frac{(n-1)+2(n-2p+1)}{(n-2p+1)+\epsilon_1} \left(\begin{matrix}\sin \\ \text{or} \\ -\cos\end{matrix} [(n-2p+1)u + m(\Omega-\theta)] \cos u \right.$$

$$\left. \left. \left. - \begin{matrix}\cos \\ \text{or} \\ \sin\end{matrix} [(n-2p+1)u + m(\Omega-\theta)] \sin u \right) \right] \right\} \qquad (3\text{-}7)$$

where:

$$\epsilon_1 = m\left(\frac{d\Omega}{du} - \frac{d\theta}{du}\right)$$

The form of Eq. (3-7) is general and can include the effects of any tesseral and sectorial or even zonal harmonic. The equation does become indeterminant for odd zonal harmonics and they have not, as yet, been considered in this study. The harmonic effects include short period, long period, secular, diurnal, and resonance terms. Equation (3-7) is used in program /GRAV/ to compute the radial departure due to any harmonic from a nominal orbit at a point in time. These effects are not integrated with or applied to the nominal orbit. The nominal orbit is considered to be an unperturbed, two-body one except for the fact that the line of nodes is allowed to regress.

For this study, the radial departures due to the various harmonics were determined for the GEOS class of orbits. The nominal orbit was taken to be similar to GEOS-B whose elements were considered to be:

h_1 = 600 n.mi. (apogee)

h_2 = 850 n.mi. (perigee)

M_0 = 0° (mean anomaly at epoch)

i = 20° (inclination)

ω = 30° (argument of perigee)

Ω_0 = 30° (longitude of ascending node)

θ_{go} = 0° (sidereal time of Greenwich meridian at epoch).

Ω_0, ω, and θ_0 were selected arbitrarily. The values of the harmonics used in this Appendix are listed below in Table 3-1 and 3-2. Table 3-1 lists the values of the even zonal harmonics due to Kozai and Table 3-2 lists the tesseral harmonics determined by Kohnlein (Lundquist, 1968).

Table 3-1. Even Zonal Harmonics Due to Kozai x 10^{-6}

$J_2 = 1082.639 \pm .007$	$J_8 = -0.128 \pm .064$
$J_4 = -1.608 \pm .021$	$J_{10} = -0.338 \pm .054$
$J_6 = 0.542 \pm .041$	

Table 3-2. Normalized Tesseral and Sectorial Harmonics

n	m	$\bar{C}_{nm} \times 10^6$	$\bar{S}_{nm}$	n	m	$\bar{C}_{nm} \times 10^6$	$\bar{S}_{nm}$
2	2	2.38	-1.35	8	1	-0.01	-0.01
3	1	1.71	0.23	8	2	0.04	0.04
3	2	0.84	-0.51	8	3	-0.03	0.00
3	3	0.66	1.43	8	4	-0.17	-0.02
4	1	-0.47	-0.39	8	5	-0.09	-0.09
4	2	0.35	0.48	8	6	-0.01	0.30
4	3	0.92	-0.24	8	7	0.02	0.04
4	4	0.04	0.30	8	8	-0.18	0.03
5	1	-0.06	-0.05	9	1	0.11	0.00
5	2	0.53	-0.21	9	2	0.03	0.05
5	3	-0.40	0.07	9	3	-0.03	-0.01
5	4	-0.20	0.02	9	4	0.07	0.02
5	5	0.18	-0.56	9	5	-0.04	0.04
6	1	-0.08	0.01	9	6	0.04	0.01
6	2	0.01	-0.27	9	7	0.04	-0.02
6	3	-0.04	0.03	9	8	0.13	0.00
6	4	-0.08	-0.48	9	9	0.08	0.04
6	5	-0.26	-0.46	10	1	0.10	-0.07
6	6	-0.02	-0.16	10	2	-0.08	-0.06
7	1	0.17	0.11	10	3	-0.08	-0.05
7	2	0.32	0.16	10	4	-0.06	-0.08
7	3	0.18	0.00	10	5	0.02	-0.02
7	4	-0.16	-0.04	10	6	-0.04	-0.01
7	5	0.07	-0.01	10	7	0.04	-0.05
7	6	-0.23	0.10	10	8	0.04	-0.05
7	7	0.07	0.06	10	9	0.05	-0.04
				10	10	0.03	-0.02

The effect of errors in the harmonics upon the radial vector of GEOS-C were computed by differencing the radial effect due to a given harmonic and the radial effect plus one sigma. The results are shown in Figures 3-1 to 3-7. A minus one sigma error would simply reverse the error curves. The one sigma error in the tesseral harmonics was considered to be $\pm 0.08 \times 10^{-6}$ on all normalized values of C and S (Kaula, 1968). By looking at Figures 3-1, 3-2, and 3-3, it is evident that the even zonal harmonics are well determined with the maximum one sigma error of all even zonals slightly greater than ten millimeters. Actually, of all even zonals, J_4 is one of the largest sources of error in the radial direction. The plus one sigma error of J_4 is in the opposite direction of the J_2 error and so they effectively cancel each other out. If plus one sigma is added to J_4 and a minus one sigma added to J_2, the zonal error would be about ten times larger or about 0.1 meter. This is still in the noise level so that errors in the even zonals may be neglected.

The tesseral harmonics do present a greater problem with a maximum radial error of over three meters. This error is primarily due to J_{31}, J_{32}, and J_{33} contributing 1.5 meters, J_{22} contributing about 0.5 meter and the fourth order harmonics contributing another 0.5 meter. The dip in the Figure on page 3-11 occurs at the Java Deep. Again it must be mentioned that the amplitudes of these errors are in proportion to the radial displacement. Over a ten-minute short-arc orbit determination the errors would reduce to about 1 or 2 meters. It is again to be emphasized that these are instantaneous errors at a point in the orbit, and do not represent accumulation of the error over many orbits. Thus we find the requirement for following the orbit via mini-arc techniques.

FIGURE 3-1

The Effect of a 1σ Error in All Even Zonals Through J_{10} upon the Radial Distance

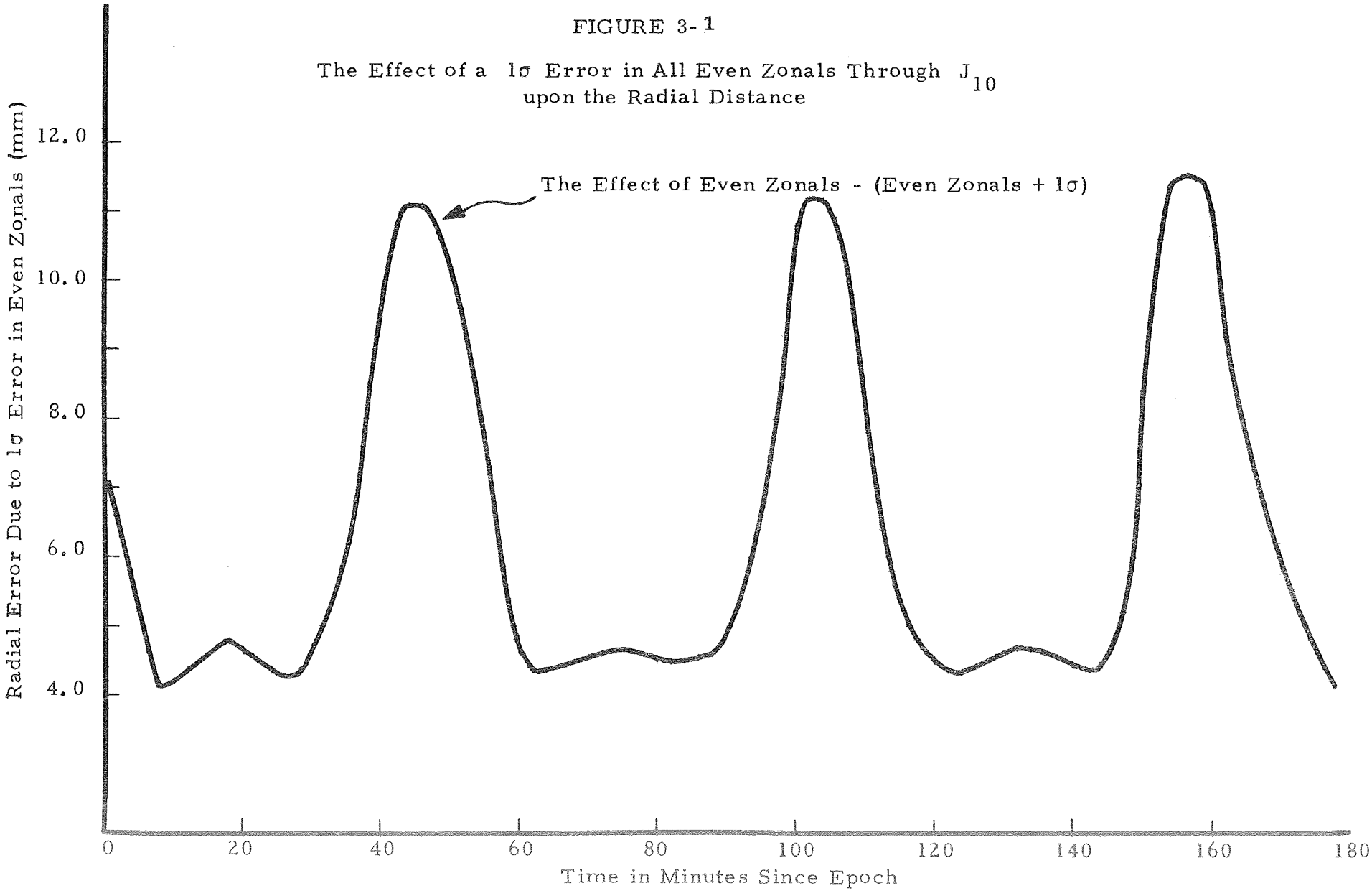

FIGURE 3-2

The Effect of an Error in J_2 upon the Radial Distance

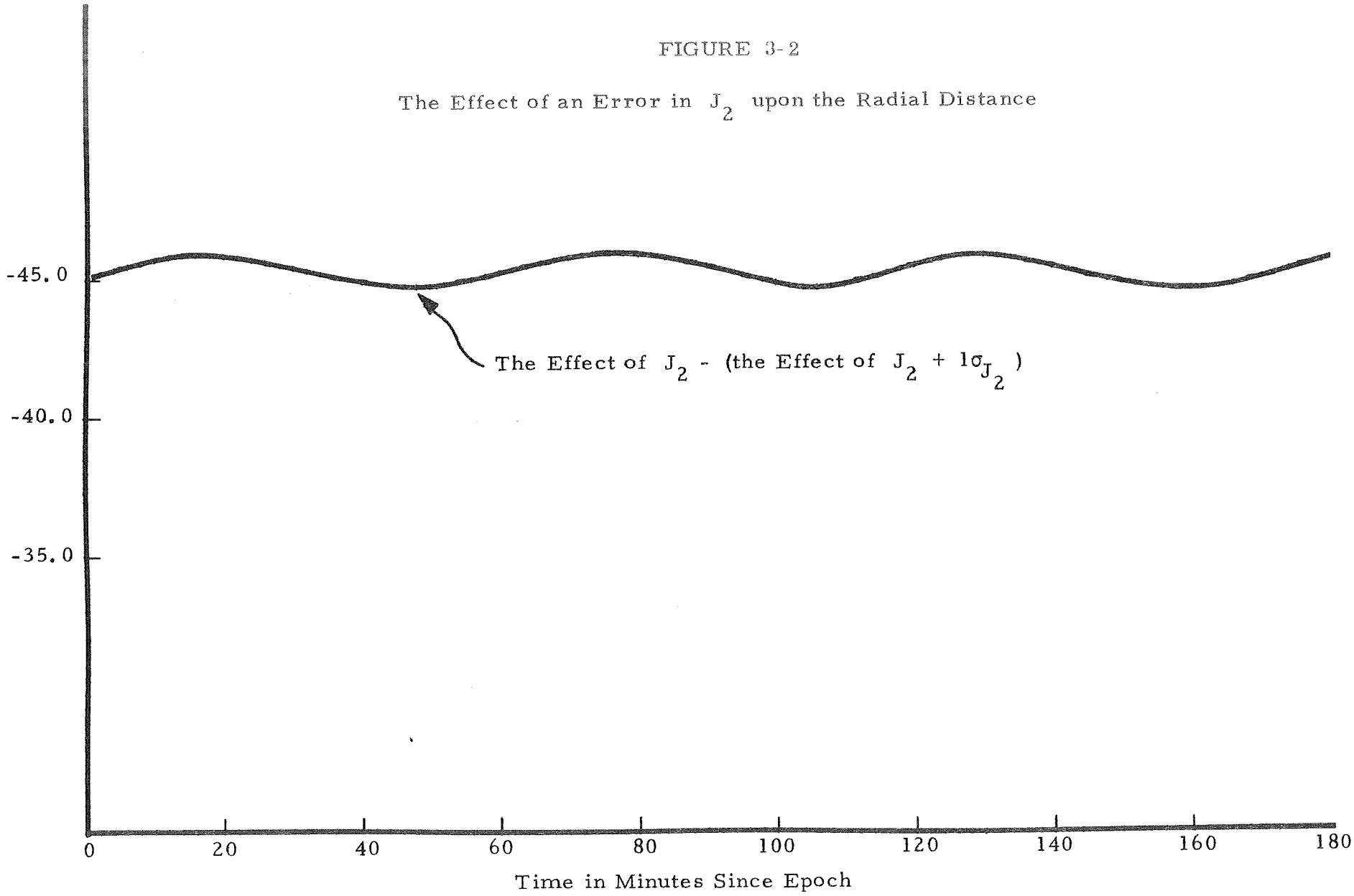

FIGURE 3-3

The Effect of an Error in J_4 upon the Radial Distance

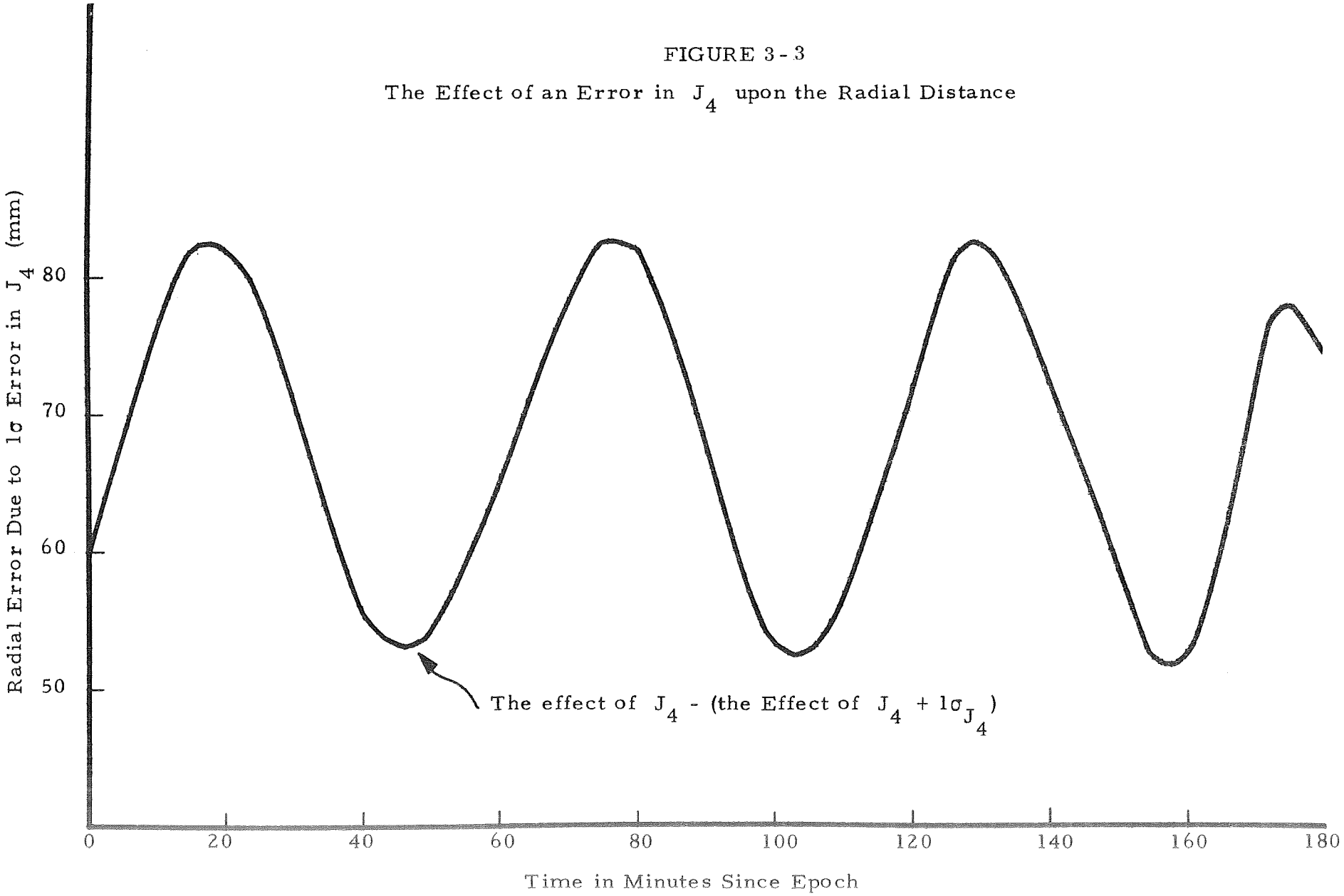

FIGURE 3-4
The Effect of a 1σ Error in All Tesseral Harmonics Through $J_{10,10}$
upon the Radial Distance

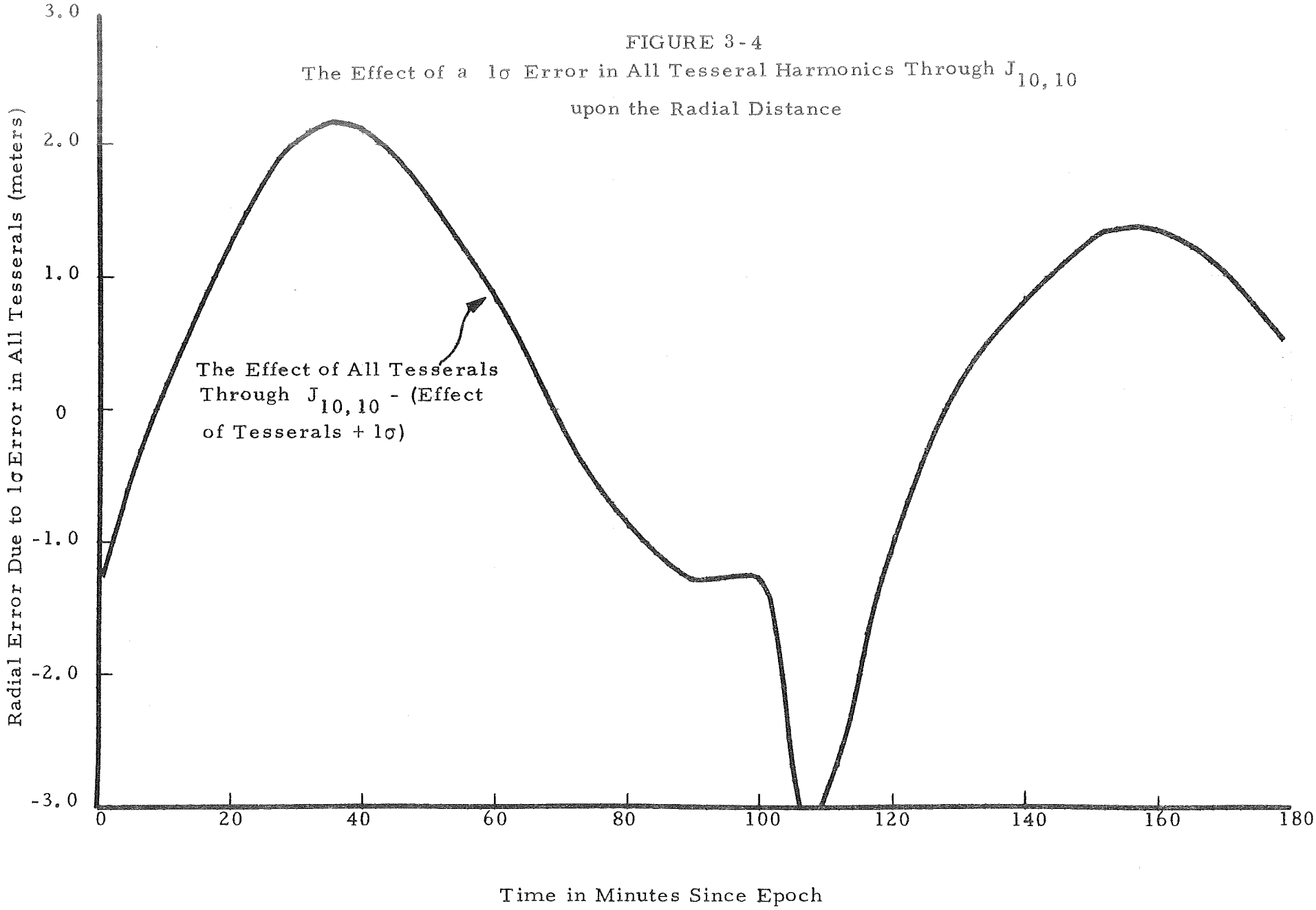

FIGURE 3 - 5

The Effect of an Error in C_{22} and S_{22} upon the Radial Distance

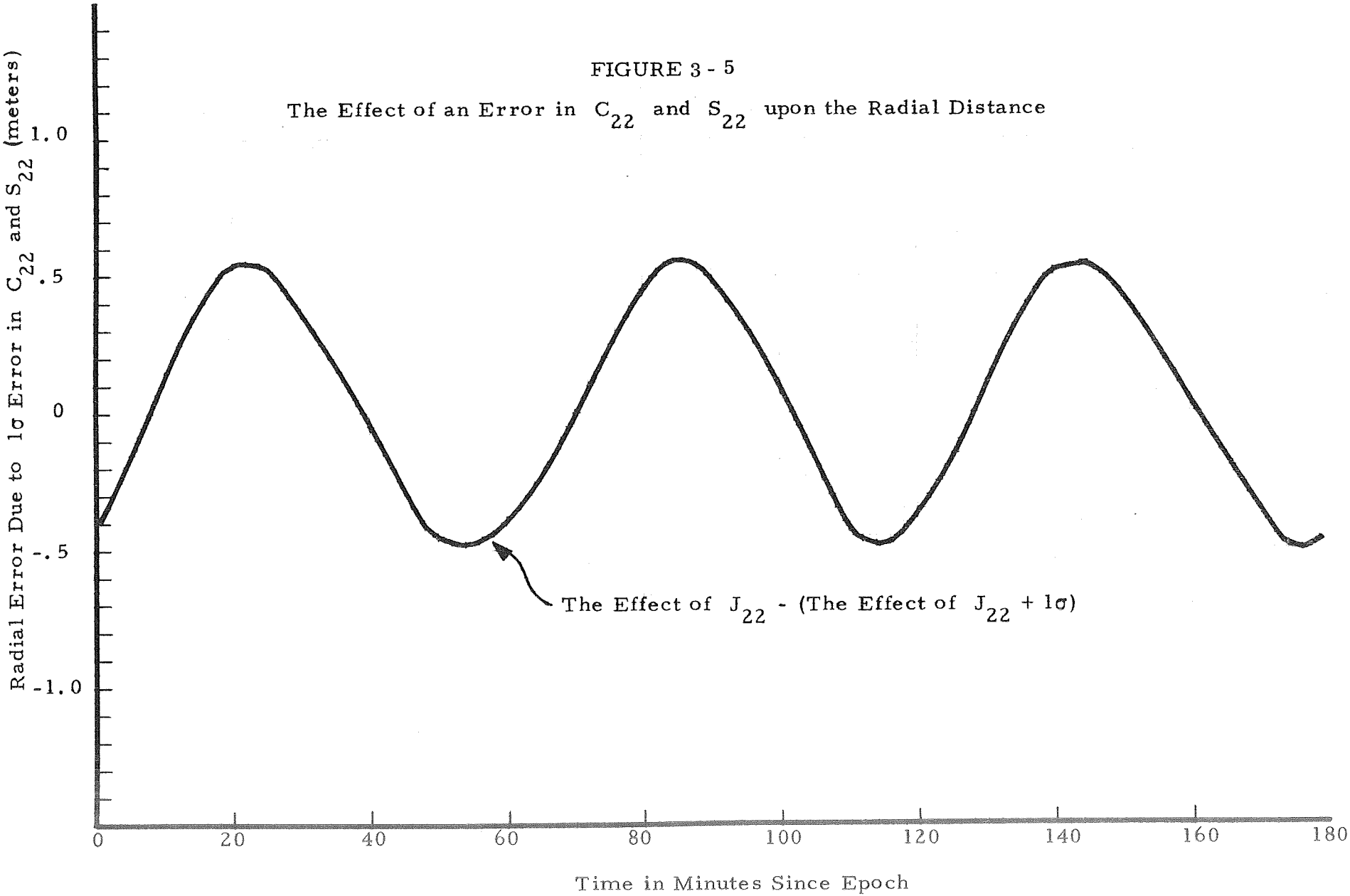

FIGURE 3-6

The Effect of a 1σ Error in J_{31}, J_{32}, J_{33} upon the Radial Distance

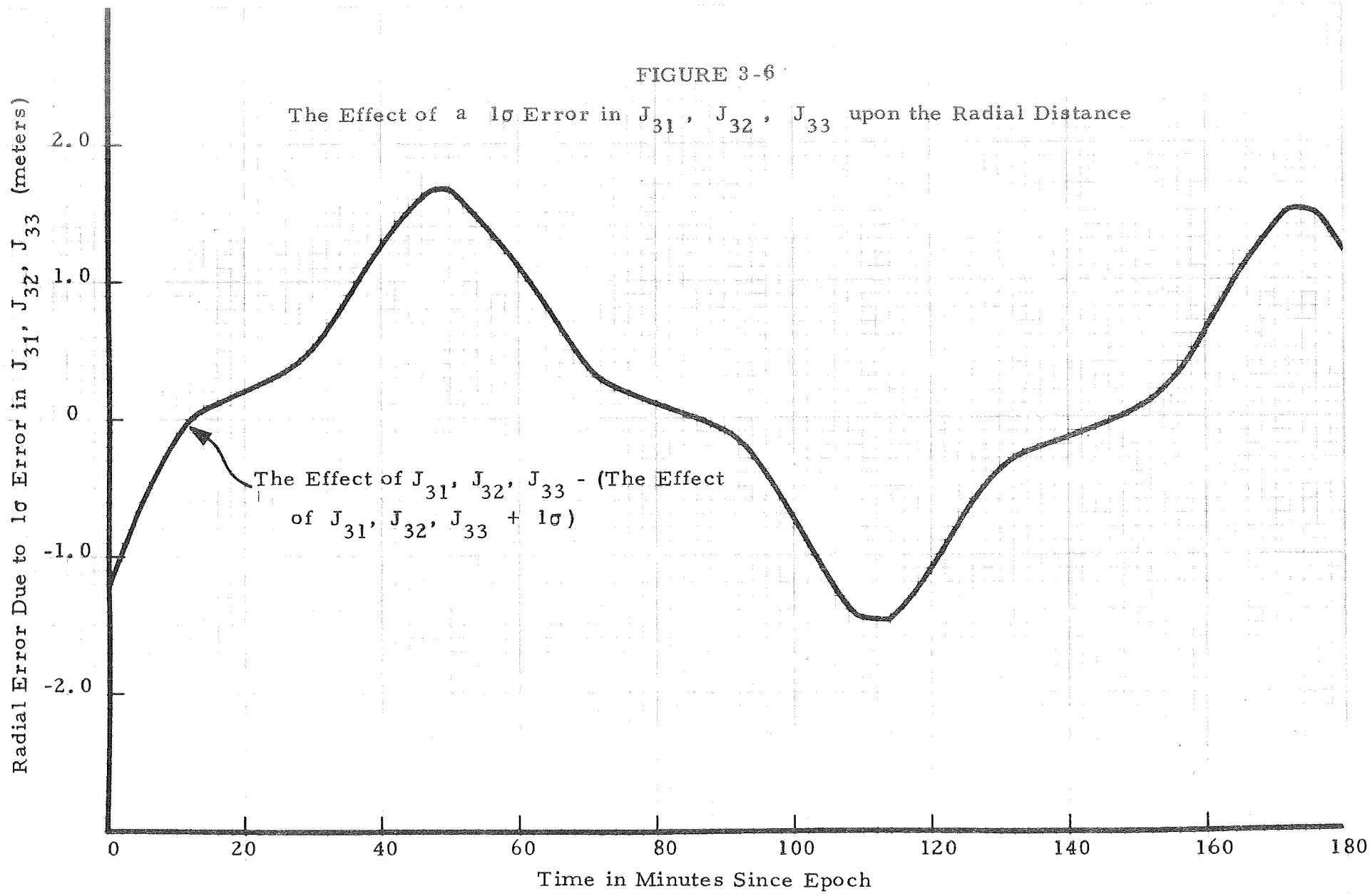

FIGURE 3-7

The Effect of a 1σ Error in J_{41}, J_{42}, J_{43} and J_{44} upon the Radial Distance

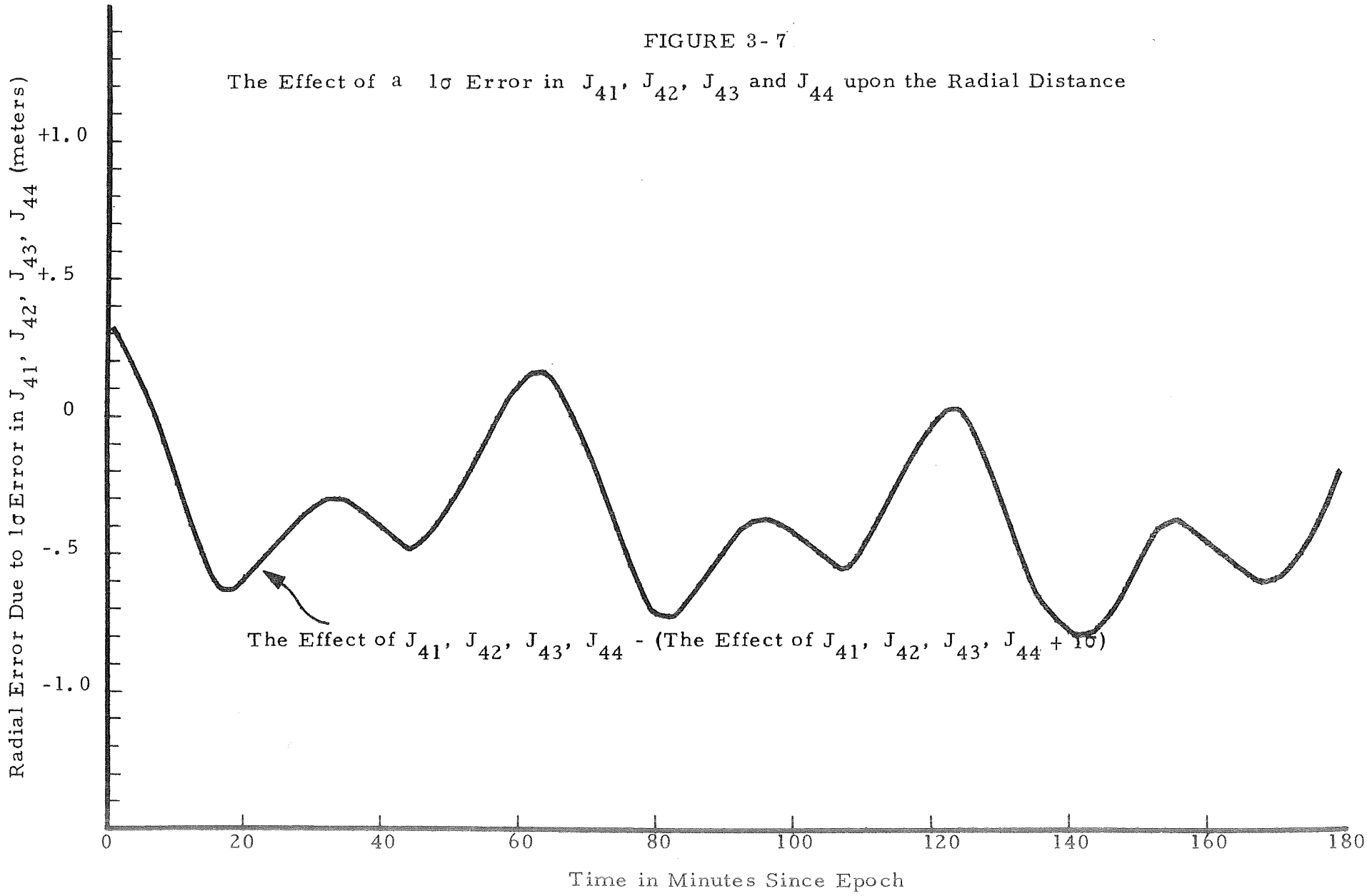

4.0 CONCLUSIONS AND RECOMMENDATIONS

Probably the most significant error source in the GEOS-C satellite orbit determination problem is the station location error. Initial results indicated possible radial errors of 30 meters and more. However, two factors tend to alleviate this problem:

1. Errors due to station location are extremely geometry dependent and are much larger at either end of the tracking interval than they are in the middle. Therefore, reducing the size of the tracking interval should minimize these errors.

2. The tracking stations investigated are all part of the same datum. Therefore, relative errors between the stations are expected to be smaller than their absolute error, and the absolute errors tend to be in the same direction. This means the shape of the satellite track will tend to be preserved, even though its absolute error may be large. This should allow more accurate mapping of the shape of the ocean's surface than the absolute error would suggest.

Systematic slant range error also contributes significantly to the overall orbital error. However, these errors, too, are extremely geometry dependent and can be greatly reduced by taking data from the middle of the tracking interval.

The remaining error sources have been shown to yield much smaller contributions to the orbital error. In particular, timing bias was shown to yield an error of about 50 millimeters, and random error contributes 0.2 meters nominally over short arcs. As demonstrated, however, in Section 3 there do exist uncertainties in the Earth's gravitational field that might cause orbital path undulations or local "wiggles" or "humps" that could at least partially mask the relative sea-level profile features measured by the altimeter. All of these aforementioned factors suggest the use of very-short-arc (mini-arc) orbit determination techniques.

The specific recommendations are as follows:

1. To develop a very-short-arc (mini arc) orbit determination technique. One possibility would be the use of a modified f and g series, perhaps restricted to the definition of radial distance (of prime importance to the GEOS-C altimeter experiment) and the determination of its coefficients (2 to 5 of them). One possible set might be the magnitude of the radial distance at epoch, r_o, the magnitude of the rate of chance of radial distance at epoch, $\dot{r}_o$ and 1/a. Another possibility in addition to the f and g series method, might be the method of multiple preliminary orbits. Limited dynamics would be included in the procedure since a purely geometrical curve fit is undesirable. A dynamical path restriction would preclude the use of a high-order series representation that could lead to the fictitous result that all observations would be "perfectly" fitted and the residuals identically zero.

2. To determine the criteria governing the length of such mini-arcs (roughly 10 to 100 seconds) based upon the following considerations: unforeseen orbital-path "humps" due to gravitational constant and gravitational anomaly uncertainty (such humps may build up an amplitude of from a fraction to a meter or two over about a thousand kilometers or less of orbital track and interfere with the interpretation of altimeter data), data rate of the sensor(s), anticipated data accuracy, amount of intervisibility, visibility geometry and number of orbital constants required for solution. One possible criterion would be the sum of the squares of the residuals given simulated observational data and a hypothesized gravitational field uncertainty.

3. To study the connections among mini-arc-determined orbital segments separated by non-data arcs, in order to obtain the best overall orbital track for the purposes of satellite altimetry. The results of this research should be especially applicable to the determination of sea level over regions of the ocean during which the GEOS-C is not visible to appropriate sensors. A modified weighted least squares procedure would be one possible approach to this study in which the mini-arc would be treated as "normal places."

4. To investigate the incorporation of satellite height data directly into orbit determination. The study would concentrate on new approaches and will not

simply treat the altimeter data as just another data type and introduce it directly into a conventional differential correction scheme. For example, methods of best utilizing the data obtained during a sensor overflight should be examined. In addition, the study should investigate the capability of identifying specific characteristics of the gravitational field based on the fine structure of the mini-arcs, without filtering the data through a conventional differential correction scheme.

5. To further investigate single station tracking, in particular, where the satellite passes directly (or very nearly so) over the sensor. Single station tracking, by fixed observation stations or tracking ships, appears to be the most ideal and accurate method that is possible for altimeter calibration. Further investigation is needed to define the accuracy of the method, to discover the limitations of the method, and to quantify the accuracy of the calibration procedure for systematic and random errors of range and station location.

ALTIMETER BIAS RECOVERY FROM RANGE AND ANGLE OBSERVATIONS

Prepared for the GEOS-2

REVIEW CONFERENCE

June 22 - 24, 1970

By

J. Berbert
F. Loveless

ALTIMETER BIAS RECOVERY FROM RANGE AND ANGLE OBSERVATIONS

J. Berbert
F. Loveless

The overall system accuracy sought for the GEOS-C altimeter system has been established at 5 meters. This figure includes the error contributions from several sources. The known system error sources and estimates of their nominal magnitudes are the following:

Altimeter System Measurement Error Sources	Error (meters)
• Altimeter instrumentation	2.0
• Refraction	0.2
• Reflection from Waves	0.5
• Spacecraft Attitude (non-nadir reflection)	2.0
Root Sum Square (RSS)	2.9

The root sum square (RSS) of the altimeter system errors is 2.9 meters, leaving only 4.1 meters for the RSS of the calibration system errors, if the 5.0 meter RSS system evaluation goal is to be met. This means the calibration system must determine reference heights of the spacecraft above mean sea level (MSL) to an accuracy of 4.1 meters.

Several studies have investigated alternate methods of determining GEOS-C heights for altimeter calibration purposes. The techniques already studied include; a) geometric trilateration of GEOS-C from 3 ranging stations (reference 1), b) GEOS-C height determination with satellite to satellite tracking data from the ATS-F link (Reference 2), and, c) GEOS-C height determination with C-band radar data (Reference 3). The purpose of this paper is to investigate GEOS-C height determination from various combinations of range (laser, C-band) and angle (camera, laser, C-band) data.

A single trajectory (Figure 1), based on a nominal 20° inclination GEOS-C orbit, was tracked by simulated data fron n ranging stations, $n = 1 \ldots 4$, at different sites in the Caribbean. For the n ranging sites, there were k collocated angle tracking sites, $k = 0, 1 \ldots n$, (no more than one per site) so that the number of angle sites was always less than or equal to the number of ranging sites. The sites selected for this study were Antigua, Grand Turk, Curacao, and Trinidad. These were ordered respectively one through four as indicated below.

Range Sites \ Angle Sites	0	Ant 1	Gtk Ant 2	Cur Gtk Ant 3	Trin Cur Gtk Ant 4
Ant, 1	X	X			
Gtk, Ant, 2	X	X	X		
Cur, Gtk, Ant, 3	X	X	X	X	
Trin, Cur, Gtk, Ant, 4	X	X	X	X	X

In Figure 2, the elevation angles at the four tracking sites are given as a function of time for the selected pass.

Simulated data were generated by the NAP-2 program for the range and angle systems and for the altimeter, using the selected orbit and estimates of system noise. The range, laser angle, and altimeter data were generated at 40 second intervals throughout the pass for elevation angles above 20^{o}. The camera angle data were generated at 4 second intervals over a 24 second span, equivalent to one GEOS plate per camera, observed at the middle of the laser data span.

The estimates of system measurement noise and error model parameters used in generating the simulated data were:

Measurement	RMS Noise
Laser or C-band range	2 meters
Laser or C-band Az-El angles	100 arc sec
Camera R.A.-Dec angles	1 arc sec
Altimeter height	10 meters

Later, using the simulated data, the short arc orbital elements, station surveys, range biases, and altimeter bias were allowed to simultaneously adjust and were recovered along with their uncertainties by the NAP-2 program. In the adjustment each measurement type was weighted inversely proportional to the square of the RMS noise above. The a priori uncertainties attached to the recovered parameters were:

- Orbital Elements
  - Position (X, Y, Z) = $\pm$(1, 1, 1) kilometers
  - Velocity ($\dot{X}$, $\dot{Y}$, $\dot{Z}$) = $\pm$(1, 1, 1) kilometers/sec
- Station Surveys (E, N, V) = $\pm$(30, 30, 1) meters
- System Bias
  - Laser or well calibrated C-band range = $\pm$2 meters
  - Altimeter height = $\pm$100 meters

Results

The altimeter bias recovery uncertainties for all the various measurement combinations are given in Figure 3. Here it is shown that, with the assumptions used in this study, the most economical combination of range and angle trackers which meets the 4.1 meter requirement is probably a single range station of laser quality collocated with a single angle station of camera quality. This combination achieves an altimeter bias uncertainty of $\pm$3.6 meters. When no cameras and only one or two lasers are used, it helps considerably to use the laser angles. For example, the one laser, no camera (1L0C) result is decreased from 38.7 to 4.7 meters, and the 2L0C result from 5.1 to 4.4 meters. But this still is not enough to satisfy the 4.1 meter requirement.

A more cost effective combination of trackers is the 2L2C case, considering the limited lifetime of the altimeter and the requirement for clear skies for the lasers and both clear and dark skies for the cameras. This combination is also equivalent to two 1L1C cases. The probability of clear and dark skies over at least one of the 1L1C sites is of course increased. When both sites are clear and dark the 2L2C case applies and the calibration is more accurate. In this study, the 2L2C combination achieves 3.2 meters, which is slightly better than the 3.4 meters from the 4L1C combination.

The results of this study depend on the a priori assumptions. Interpretation of the results should include consideration of the following:

- Actual range measurement data rates are usually higher than those chosen here (except for the SAO laser).
- The angle systems are also subject to some bias.
- The horizontal survey (E, N) a priori errors need not be as large as 30 meters. The large values were chosen to demonstrate that with a relatively closely spaced network of sites the horizontal error is less important. Decreasing these errors should improve the multi-station results. The ORAN error propagation program was used to demonstrate this. It showed that a 2L0C configuration determines height near the center of a pass between the two stations as well as a 1L1C configuration determines height overhead, provided the assumed a priori horizontal survey uncertainties are reduced to $\pm$6 meters at one site and fixed at the other.
- The vertical survey a priori error of 1 meter with respect to MSL is reasonable near the site, but not hundreds of kilometers away. The uncertainty of MSL relative to the height of a site in the Caribbean has been estimated to vary from about 0.5 meter near the site to about 5.0 meters at distances of 1000 to 2000 kilometers. The 1 meter estimate probably holds only out to about 150 kilometers (zenith angle of 9°). On the other hand, the laser bias is highly correlated with station height error for high elevation angle data and these parameters may be traded off to some extent. For example, the results with the laser bias uncertainty

of ±2.0 meters and the station height uncertainty of ±1.0 meter used here should not be significantly affected by reducing the laser bias uncertainty by 1.5 meters to 0.5 meter (probably a more realistic value with recent hardware improvements), and increasing the MSL with respect to station height uncertainty by 1.5 meters to 2.5 meters (also a more realistic value when more than several hundred kilometers from the site).

- These results implicitly assume the altimeter bias is constant throughout the pass. Consequently the bias uncertainties quoted may be valid only for short durations during the most accurate part of the reference trajectory.

Since the altimeter bias may not be constant throughout the pass, it is desirable to determine height to 4.1 meters for as much of the pass as possible. A point by point error propagation study was made for the pass over Antigua, assuming the same ranging data errors as above and angle data errors varying from camera quality (±1 arc sec) to laser angle quality (±100 arc sec). The propagation of these errors into altitude errors is given in Figure 4 as a function of elevation angle. This shows that altitude is determined to within ±4.1 meters using laser ranges supplemented by laser angles, only within a 2^{o} zenith angle. However, if the laser ranges are supplemented by camera angles, the useable zenith angle is extended to 30^{o}.

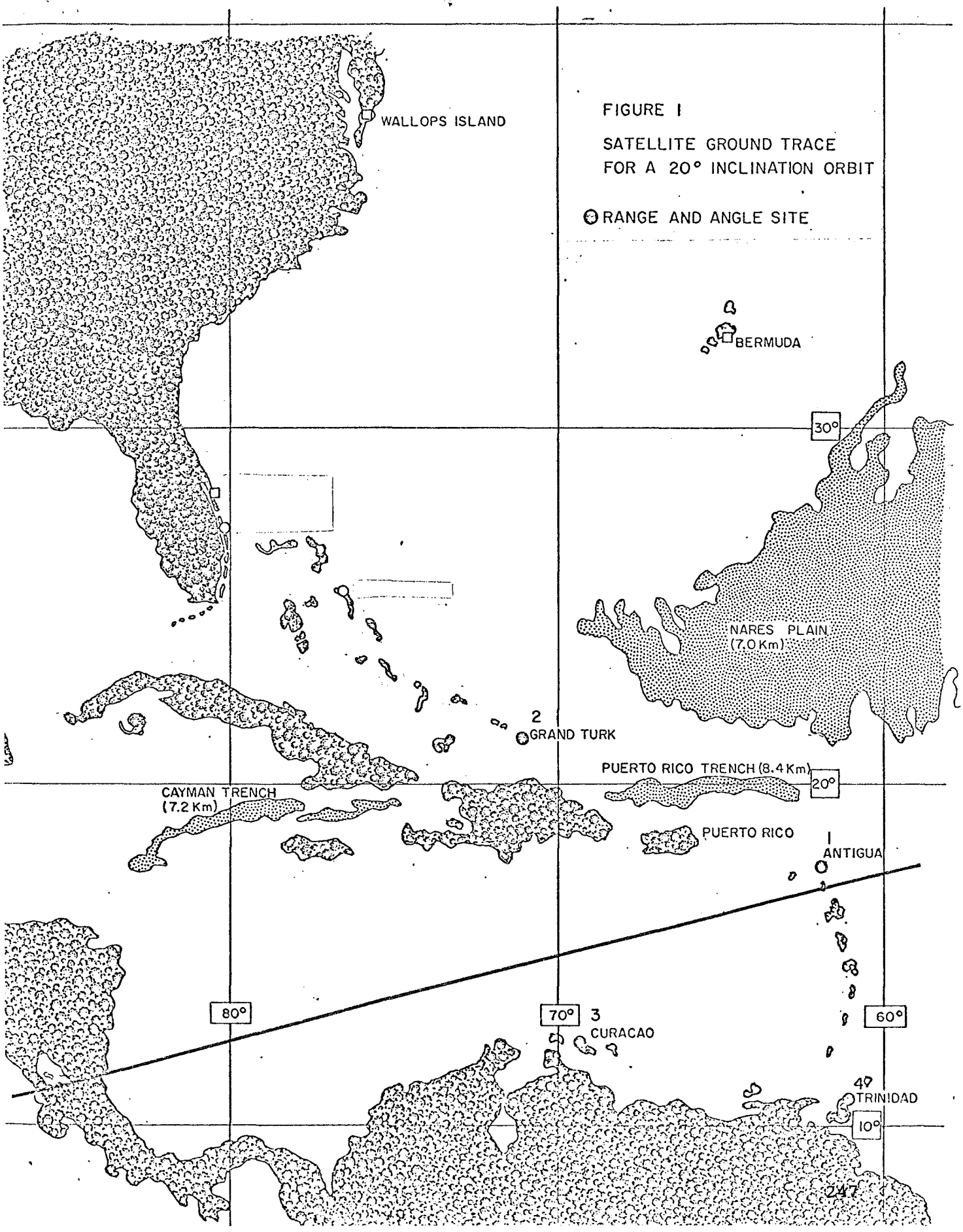

FIGURE 1

SATELLITE GROUND TRACE
FOR A 20° INCLINATION ORBIT

⊙ RANGE AND ANGLE SITE

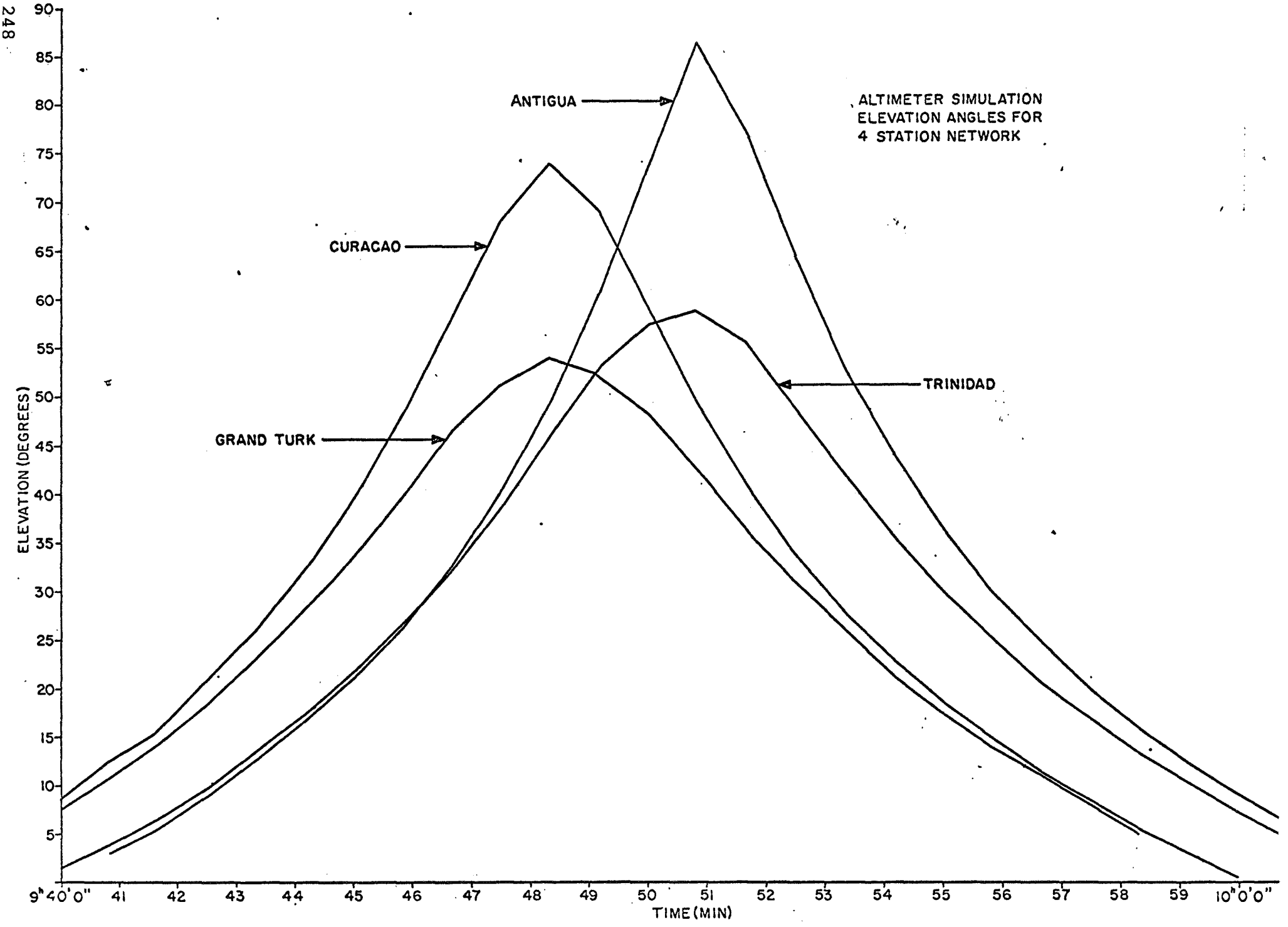
ALTIMETER SIMULATION
ELEVATION ANGLES FOR
4 STATION NETWORK
ANTIGUA
CURACAO
GRAND TURK
TRINIDAD
ELEVATION (DEGREES)
TIME (MIN)
90
85
80
75
70
65
60
55
50
45
40
35
30
25
20
15
10
5
9h40'0"
41
42
43
44
45
46
47
48
49
50
51
52
53
54
55
56
57
58
59
10h0'0"

FIGURE 2

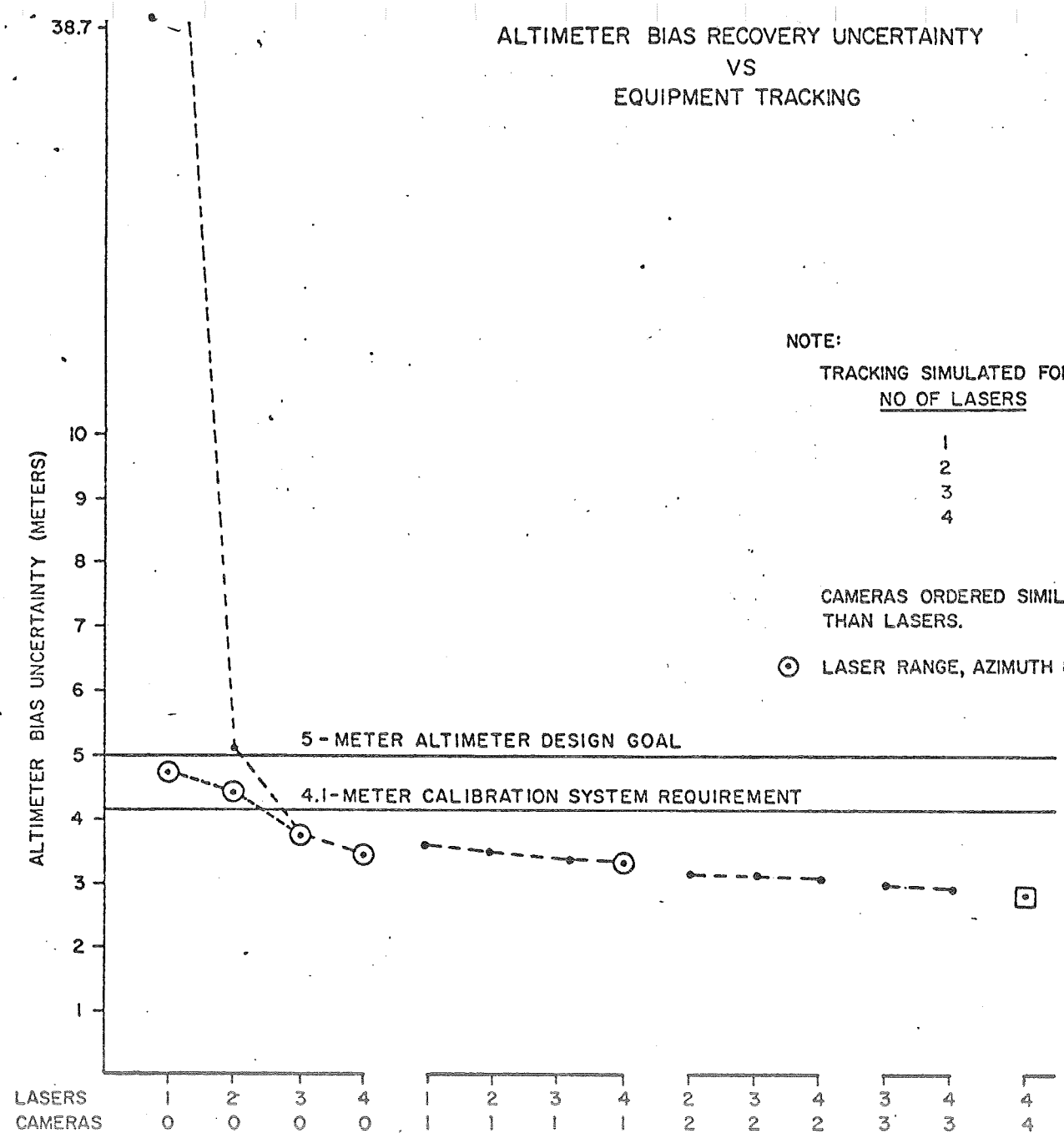

NOTE:

TRACKING SIMULATED FOR LASERS WAS ORDERED BY STATION.

NO OF LASERS	STATIONS
1	ANTIGUA
2	ANTIGUA, GRAND TRUK
3	ANTIGUA, GRAND TRUK, CURACAO
4	ANTIGUA, GRAND TRUK, CURACAO, TRINIDAD.

CAMERAS ORDERED SIMILIARLY. THERE WERE NEVER MORE CAMERAS THAN LASERS.

⊙ LASER RANGE, AZIMUTH & ELEVATION ANGLE DATA USED

FIGURE 3

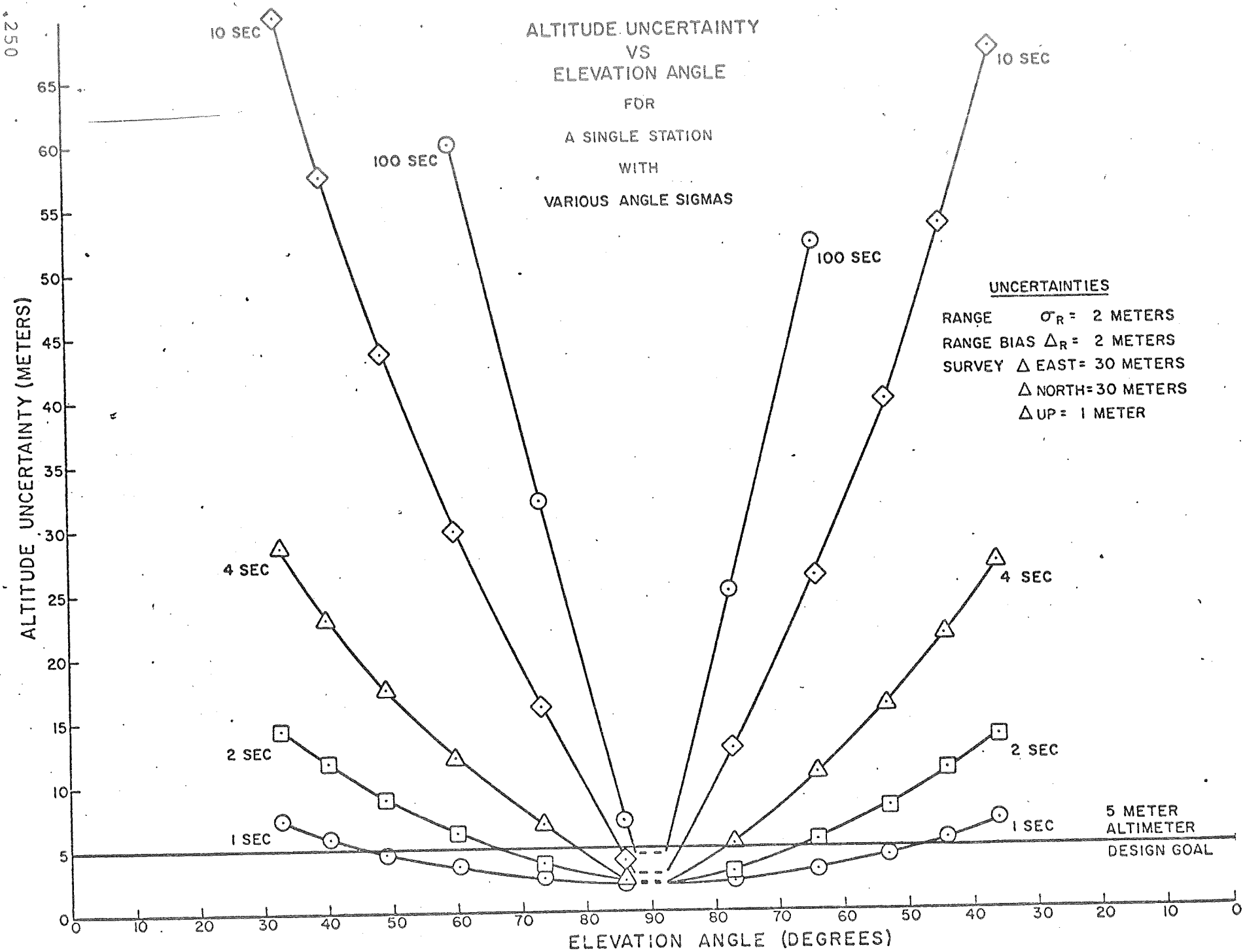
ALTITUDE UNCERTAINTY
VS
ELEVATION ANGLE
FOR
A SINGLE STATION
WITH
VARIOUS ANGLE SIGMAS
10 SEC
100 SEC
10 SEC
100 SEC
4 SEC
4 SEC
2 SEC
2 SEC
1 SEC
1 SEC
UNCERTAINTIES
RANGE σ_R = 2 METERS
RANGE BIAS Δ_R = 2 METERS
SURVEY Δ EAST = 30 METERS
Δ NORTH = 30 METERS
Δ UP = 1 METER
5 METER
ALTIMETER
DESIGN GOAL
ALTITUDE UNCERTAINTY (METERS)
0
5
10
15
20
25
30
35
40
45
50
55
60
65
0 10 20 30 40 50 60 70 80 90 80 70 60 50 40 30 20 10 0
ELEVATION ANGLE (DEGREES)

FIGURE 1

References

1. Vonbun, F. O., Memorandum, "Calibration of the Radar Altimeter for GEOS-C", February 4, 1970.

2. Vonbun, F. O., "Geodetic Satellite Mission and Spacecraft (GEOS-C)", XIIIth Plenary Meeting, COSPAR, Leningrad, 1970.

3. GEOS-B C-Band System Project Group and Wolf Research and Development Corporation, "Single Arc Tracking Errors Associated with Altimeter Measurements", February, 1970.

MSFN UNIFIED S-BAND METRIC TRACKING CAPABILITIES

Irving Salzberg

Goddard Space Flight Center
Greenbelt, Maryland

Presented at GEOS-2 Program Review
Meeting, Goddard Space Flight Center,
22-24 June 1970

MSFN UNIFIED S-BAND METRIC TRACKING CAPABILITIES

DEB / MFPAD
CODE 832
JUNE 1970

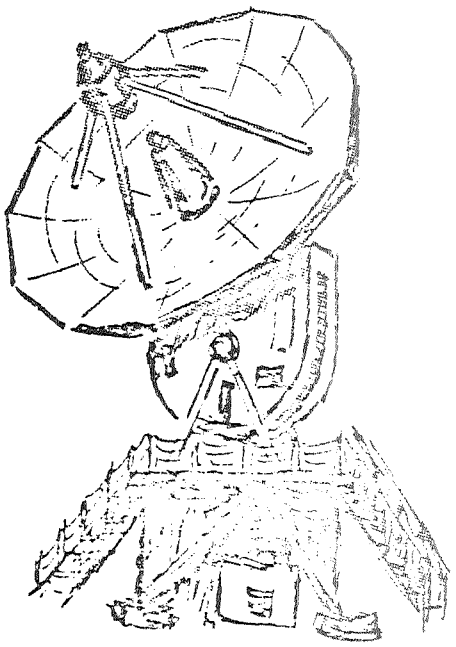

USB

ANGLES

RANGE

RANGE RATE

TRACKER ERROR SOURCES

GEODETICS

TIME

FREQUENCY

USB ANGLE PERFORMANCE [1]
(30' & 85')

	DESIGN SPECIFI-CATIONS	APOLLO 11 [3]	APOLLO 12 [3]	APOLLO 13 [3]	FUTURE
BIAS (DEGREES) [2]	.011	.035 (.015)	.025 (.010)	.030 (.015)	.015 (.005)
NOISE (DEGREES) [2]	.008	.030 (.020)	.025 (.015)	.055 (.025) [4]	.015 (.010)

NOTES -

(1) PERFORMANCE IMPROVEMENTS DUE TO BETTER EQUIPMENT OPERATION

(2) ANGLE RESOLUTION: .000686645 DEGREES/BIT

(3) APPROXIMATE MAXIMUM VALUES (TYPICAL VALUES ARE IN PARENTHESES)

(4) INCREASED NOISE POSSIBLE DUE TO LOWER SIGNAL/NOISE RATIO AFTER CSM MALFUNCTION

USB SITE ANGLE PERFORMANCE

SITE	X ANGLE BIAS (DEG.)			Y ANGLE BIAS (DEG.)		
	AS-506	AS-507	AS-508	AS-506	AS-507	AS-508
ACN	.034(1)	.005	.021	.035(1)	.019	-.003
ANG	.015(1)	-.001	(4)	-.003	-.004	(4)
BDA	-.001	.014	.011	.007	.008	-.001
CRO	.002	.004	.030	.018	.016	.000
CYI	-.004	.000	(3)	.003	.004	(3)
GWM	-.007	.004	.023	-.007	-.001	.003
GYM	(2)	(2)	.004	.021	(2)	.013
HAW	-.013	-.006	(3)	.003	.002	(3)
MIL	-.022	-.014	-.023	.006	.004	.001
TEX	-.014	-.020	(3)	-.002	-.001	(3)
GDS	-.009	-.016	-.005	.015	.017	.014
HSK	.001	-.003	(3)	.005	-.001	(3)
MAD	.010	.010	.006	-.012	-.019	-.015

NOTES -

(1) ADJUSTMENTS MADE AFTER MISSION

(2) INCONSISTENT BIAS

(3) INSUFFICIENT INFORMATION - BIAS APPEARS TO BE UNDER .01°

(4) NO FAR-EARTH ANGLE DATA

USB RANGE PERFORMANCE (1,2)

	DESIGN SPECIFI-CATIONS (1 δ)	APOLLO 11	APOLLO 12	APOLLO 13	FUTURE
BIAS (METERS)	15	30	30	30	10 (3)
NOISE (METERS)	10	10	10	10	5

NOTES -

(1) RANGE RESOLUTION: 1 RU $\approx$ 1.049 METERS

(2) LIMITATIONS DUE TO GROUND STATION DELAY, SPACECRAFT DELAY, AND GEODETICS.

(3) NEW CALIBRATION HARDWARE WILL IMPROVE GROUND STATION DELAY MEASUREMENT.

USB RANGE RATE PERFORMANCE

	DESIGN SPECIFICATIONS	APOLLO 11	APOLLO 12	APOLLO 13	FUTURE
BIAS (MM/SEC)[1]					
HI-SPEED NOISE (MM/SEC)	330/20[2]	330	330	17	10
1/6 SEC NOISE (MM/SEC)	5.5	5.5	5.5	5.5	.5[3]

NOTES -

(1) DIRECTLY RELATED TO:
- QUALITY OF BET
- STABILITY OF FREQUENCY STANDARD
- MODE OF OPERATION (2-WAY; 3-WAY)
- GEODETIC POSITION ERROR

(2) HI-SPEED (10/SEC) RANGE RATE RESOLUTION WAS IMPROVED BETWEEN APOLLO 12 AND APOLLO 13

(3) LOW SPEED RANGE RATE TTY DATA (1/6 SEC OR 1/10 SEC WILL HAVE REDUCED QUANTIZATION EFFECT FOR APOLLO 14.

EFFECTS OF GEODETIC ERROR ON RANGE RATE

MAXIMUM GEODETIC ERRORS: 3 ARCSECONDS
50 METERS HEIGHT

UNITS	EARTH ORBIT	TRANSLUNAR	LUNAR ORBIT
$\frac{\delta \dot{R}}{\delta R_S}$ METERS/SECOND / METER	.010 X 50 = .5	.00006 X 50 = .0030	.00003 X 50 = .0015
$\frac{\delta \dot{R}}{\delta \phi}$ METERS/SECOND / ARCSECOND	.325 X 3 = .975	.0008 X 3 = .0024	.0008 X 3 = .0024
$\frac{\delta \dot{R}}{\delta \lambda}$ METERS/SECOND / ARCSECOND	.875 X 3 = 2.625	.0021 X 3 = .0063	.0016 X 3 = .0048
RSS (METERS/SEC)	1.96	.007	.006
RMS (METERS/SEC)	1.13	.004	.003

LEGEND: R = RANGE, R_S = HEIGHT ABOVE ELLIPSOID, ϕ = LATITUDE, λ = LONGITUDE

ERROR SOURCES & THEIR MAGNITUDES

ERROR	*PRESENT*	*FUTURE*
GEODETIC	± 3 ARC SECONDS	± 0.5 ARC SECOND
	± 50 METERS HEIGHT	± 10 METERS
TIMING	± 200 MICROSECONDS	± 50 MICROSECONDS
FREQUENCY	± 5 PARTS IN 10^{12}	± 5 PARTS IN 10^{13}

EFFECTS OF GEODETIC ERROR ON RANGE

MAXIMUM GEODETIC ERRORS — 3 ARCSECONDS
50 METERS HEIGHT

UNITS	EARTH ORBIT	TRANSLUNAR	LUNAR ORBIT
$\frac{\delta R}{\delta R_S}$ $\frac{\text{METERS}}{\text{METER}}$	.75 X 50 = 37.50	.89 X 50 = 44.50	.62 X 50 = 31.00
$\frac{\delta R}{\delta \phi}$ $\frac{\text{METERS}}{\text{ARC SECOND}}$	19.2 X 3 = 57.60	16.0 X 3 = 48.00	23.0 X 3 = 69.00
$\frac{\delta R}{\delta \lambda}$ $\frac{\text{METERS}}{\text{ARC SECOND}}$	24 X 3 = 72.00	26 X 3 = 78.00	12 X 3 = 36.00
RSS (METERS)	99.53	101.82	83.77
RMS (METERS)	57.47	58.79	48.37

NOTES —
RANGE NOISE: 10 METERS
RANGE RESOLUTION: 1 METER

LEGEND
R - RANGE
RS - HEIGHT ABOVE ELLIPSOID
ϕ - LATITUDE
λ - LONGITUDE

EFFECTS OF TIMING BIAS ON RANGE

MAXIMUM TIMING BIAS: 200 MICRO SECONDS

	EARTH ORBIT	TRANSLUNAR	LUNAR ORBIT
$\frac{\delta R}{\delta t}$ · $\frac{\text{METERS}}{\text{MILLISECOND}}$	7.5 X.2 = 1.5 METERS	2.2 X.2 = 0.4 METERS	2.0 X .2 = 0.4 METERS

EFFECTS OF FREQUENCY BIAS ON RANGE RATE

2-WAY MODE OF OPERATION:

FREQUENCY BIAS HAS NO SIGNIFICANT EFFECT

3-WAY MODE OF OPERATION:

$\Delta R_{F3} = 1.38 \times \Delta F$ (MAXIMUM SINGLE STATION FREQUENCY OFFSET = 5 PARTS IN 10^{-1}

$= 1.38 \times 1$

$= 1.38$ MILLIMETERS/SECOND

WHERE: ΔR_{F3} = THREE WAY MODE RANGE RATE BIAS DUE TO FREQUENCY OFFSET IN MM/SECOND

ΔF = FREQUENCY OFFSET IN PARTS IN 10^{11} BETWEEN STATIONS

EFFECTS OF TIMING BIAS ON RANGE RATE

MAXIMUM TIMING BIAS: 200 MICRO.SECONDS

	EARTH ORBIT (1/6 SEC)	TRANSLUNAR (1/MIN)	LUNAR ORBIT (1/MIN)
$\frac{\delta \dot{R}}{\delta t}$ METERS/SEC / MILLISECOND	.240 X 0.2 = 0.05 METERS/SEC	.000021 X 0.2 = .004 MM/SEC	.0014 X 0.2 = 0.3 MM SEC
PRESENT QUANTIZING NOISE	.005	.0005	.0005

MSFN STATION LOCATIONS (APOLLO 13)

Call Letters	Station	Site	Geodetic Coordinates			Geocentric Rectangular Coordinates				
			Latitude	Longitude	Height above ellipsoid (m	Latitude	Radius (meters)	U (meters)	V (meters)	W (meters)
CKYF	Cape Kennedy	FPS-16	28°28'54.36"±1.0"	279°25'24.03"±1.2"	-14±40	28°19'14.77"	6 373 320	918 589±32	-5 534 758±38	3 023 550±34
MLAT	Merritt Island	TPQ-18	28°25'29.5"±1.0"	279°20'7.62"±1.2"	-16±40	28°15'50.66"	6 373 335	910 585±32	-5 539 123±38	3 018 004±34
MIL 3		USBS 30' MSFN(Dual)	28°30'29.78"±1.0	279°18'23.18"1.2"	-18±40	28°20'49.84"	6 373 307	907 067±32	-5 535 234±38	3 026 129±34
PATQ	Patrick Air Force Base	FPQ-6	28°13'35.59"±1.0"	279°24'2.03"±1.2"	15±40	28°03'59.40"	6 373 429	918 587±32	-5 548 400±38	2 998 672±35
GBIT	Grand Bahama Island	TPQ-18	26°38'10.86"±1.0"	281°43'55.75"±1.2"	12±41	26°28'56.84"	6 373 909	1 160 056±32	-5 585 914±39	2 842 277±34
GBM 3		USBS 30' MSFN	26°37'58.29±1.0"	281°45'43.89"(2)	18(2)	26°28'44.32"	6 373 916	1 163 021 (2)	-5 585 480 (2)	2 841 933 (2)
GTKT	Grand Turk Island	TPQ-18	21°27'46.40"±1.0"	288°52'3.87"±1.2"	28±42	21°19'55.84"	6 375 352	1 920 438±33	-5 619 464±40	2 319 189±34
ANTQ	Antigua Island	FPQ-6	17°08'38.34"±1.1"	298°12'25.30"±1.2'	42±42	17°02'09.22"	6 376 364	2 881 601±35	-5 372 581±40	1 868 088±34
ANG 3		USBS 30' MSFN	17°01'00.71"±1.1"	298°14'49.34"±1.2'	34±42	16°54'34.14"	6 376 383	2 887 304±35	-5 374 201±40	1 854 637±34
BDAF	Bermuda	FPS-16	32°20'53.04"±1.2"	295°20'46.09±1.4"	- 5±43	32°10'27.76"	6 372 075	2 308 890±39	-4 874 333±41	3 393 116±39
BDAQ		FPQ-6	32°20'52.54"±1.2"	295°20'46.30±1.4"	- 4±43	32°10'27.26"	6 372 076	2 308 899±39	-4 874 339±41	3 393 103±39
BDA 3		USBS 30' MSFN	32°21'04.50"±1.2"	295°20'30.32±1.4"	- 2±43	32°10'39.19"	6 372 077	2 308 438±34	-4 874 341±41	3 393 416±39
CYI 3	Grand Canary Island(G)	USBS 30' MSFN	27°45'52.33"±4.6"	344°21'69.05±1.3"	173±51	27°36'22.41"	6 373 728	5 439 146±40	-1 522 076±40	2 953 537±40
ASCT	Ascension Island (G)	TPQ-18	-07°58'21.00"±3.4"	345°35'55.77"±2.3'	103±73	-07°55'11.34"	6 377 860	6 118 533±43	-1 571 106±103	-878 787±105
ASCF		FPS-16	-07°57'04.51" (2)	345°35'16.49"±2.3'	70 (2)	-07°53'55.34"	6 377 829	6 118 518 (2)	-1 572 344 (2)	-876 455 (2)
ACN 3		USBS 30' MSFN(Dual)	-07°57'17.26"±3.4"	345°40'22.58"±2.3'	522±73	-07°54'08.02"	6 378 280	6 121 225±43	-1 563 360±103	-876 903±105
PRE 5	Pretoria, South Africa	MPS-25	-25°56'37.44±1.4"	28°21'29.83"±1.5'	1626±43	-25°47'33.74"	6 375 727	5 051 943±43	2 726 662±43	-2 774 183±43
CROQ	Carnarvon, Australia (G)	FPQ-6	-24°53'47.00"±2.3"	113°43'4.37"±1.0"	-11±83	-24°44'59.17"	6 374 390	-2 329 477±70	5 299 925±70	-2 668 677±70
CRO 3		USBS 30 MSFN(Dual)	-24°54'23.68"±2.3"	113°43'33.78"±1.0'	-15±83	-24°45'35.69"	6 374 383	-2 329 040±70	5 291 155±70	-2 669 699±70
WOMF	Woomera, Australia	FPS-16	-30°49'11.02"±2.3"	136°50'12.43"±2.5'	151±30	-30°39'02.50"	6 372 739	-3 898 914±70	3 750 402±70	-3 248 840±70
GWM 3	Guam (G)	USBS 30' MSFN(Dual)	13°18'38.07"(2)	144°44'11.74"±1.7'	143±55	13°13'28.64"	6 377 183	-5 068 925 (2)	3 584 141 (2)	1 458 903 (2)
HAWF	Hawaii (G)	FPS-16	22°07'24.61"±2.3"	200°20'4.79"±1.2"	1125±43	21°59'22.57"	6 376 279	-5 543 948±70	-2 054 582±70	2 387 523±70
HAW 3		USBS 30' MSFN(Dual)	22°07'34.71"±2.3"	200°20'6.21"±1.2"	1135±43	21°59'32.62"	6 376 288	-5 543 832±70	-2 054 583±70	2 387 815±70
CALF	Pt. Arguello, Calif.	FPS-16	34°34'58.45"±1.0"	239°26'19.34"±1.2'	646±40	34°24'11.95"	6 371 963	-2 673 168±33	-4 527 057±36	3 600 252±34
GYM 3	Guaymas, Mexico	USBS 30'	27°57'47.54"±1.0"	249°16'44.42"±1.2'	-22±41	27°48'14.90"	6 373 472	-1 994 695±33	-5 272 964±36	2 972 909±33
WHSF	White Sands, N.M.	FPS-16	32°21'29.60"±1.0"	253°37'49.05"±1.2'	1232±40	32°11'04.33"	6 373 310	1 520 204±31	-5 175 311±37	3 394 729±33
TEX 3	Corpus Christi, Tex.	USBS 30' MSFN(Dual)	27°39'13.50"±1.0"	262°37'16.99"±1.1'	-20±40	27°29'45.09"	6 373 565	-726 071±36	-5 606 820±38	2 942 578±32
EGLF	Eglin Air Force Base	FPS-16	30°25'18.36"±1.0"	273°12'6.27"±1.2"	28±40	30°15'14.48"	6 372 746	307 451±31	-5 496 185±38	3 210 809±33
MAD 8	Madrid, Spain (J) (ROBLEDO) (J)	USBS 85' MSFN	40°27'17.97"(2)	355°49'54.49"(2)	778(2)	40°15'54.48"	6 369 986	4 847 835 (2)	-353 297 (2)	4 117 684 (2)
MADW		USBS 85' DSN(Dual)	40°25'41.85"(2)	355°45'4.55"(2)	770(2)	40°14'18.46"	6 369 987	4 849 245 (2)	-360 253 (2)	4 114 822 (2)
HSK 8	Canberra, Australia (J)	USBS 85' MSFN(Dual)	-35°35'00.58"±2.3"	148°58'41.10"±2.5"	1145±30	-35°24'05.85"	6 372 110	-4 451 085±70	2 676 800±70	-3 691 391±70
HSKW	Tidbinbilla, Australia (J)	USBS 85' DSN(Dual)	-35°21'03.56"±2.3"	148°58'53.61"±2.5"	670±30	-35°13'10.23"	6 371 699	-4 460 993±70	2 682 389±70	-3 674 626±70
GDS 8	Goldstone, Calif. (J) (Mojave)	USBS 85' MSFN(Dual)	35°20'29.74"±1.1"	243°7'35.90"±1.2"	907±40	35°09'36.91"	6 371 958	-2 354 733±34	-4 646 789±37	3 669 389±35
GDSW	(Pioneer)(J)	USBS 85' DSN(Dual)	35°23'22.45"±1.1"	243°9'3.19"±1.2"	971±40	35°12'29.25"	6 372 005	-2 351 400±34	-4 645 082±37	3 673 767±35
TANF	Tananarive	FPS-16	-19°00'10.87"(2)	47°18'52.00"(2)	1319 (2)	-18°53'05.60"	6 377 235	4 090 865 (2)	4 435 471 (2)	-2 064 105 (2)
WLPQ	Wallops Island	FPQ-6	37°51'36.83"(2)	284°29'25.98"(2)	14(2)	37°40'26.17"	6 370 168	1 261 610 (2)	-4 881 606 (2)	3 893 236 (2)
WLPF		FPS-16	37°50'28.72"(2)	284°30'53.11"(2)	11(2)	37°39'18.17"	6 370 172	1 263 994 (2)	-4 882 319 (2)	3 891 576 (2)
VALT	Vandenberg AFB, Cal.	TPQ-18	34°39'57.62"(2)	239°25'7.80"(2)	108(2)	34°29'10.35"	6 371 395	-2 671 847 (2)	-4 521 239 (2)	3 607 533 (2)
GTC 3	NT & TF Greenbelt, Md.	USBS 30'	38°59'54.53"(2)	283°9'25.51"(2)	55 (2)	38°48'37.52"	6 369 795	-1 129 799 (2)	-4 833 203 (2)	3 992 241 (2)

(1) Uncertainties not available "(Dual)" indicates a common antenna, two receivers and two transmitters. Geodetic coordinates referenced to the Fischer Ellipsoid of 1960. The Geocentric Rectangular Coordinate system consists of a u-axis at the intersection of the earth's equatorial plane with the Greenwich meridian, a w-axis along the earth's rotational axis, and a v-axis such to complete a right-handed coordinate system.

(J) JPL derived coordinates.

(G) GSFC derived coordinates.

GSFC
DEB
3-11-70

MISTRAM APPLICATIONS WITH GEOS C

Prepared By:

N. Bush
Pan Am/RCA Engineering Planning and Analysis
Pan American World Airways, ASD

June 1970

For GEOS-II Review Conference at Goddard Space Center
22 - 24 June 1970

I. INTRODUCTION

The Missile Trajectory Measurement System (Mistram) is an accurate CW radar system that was designed to track cooperative targets such as missiles, aircraft or space vehicles. The current ETR Mistram configuration consists of two baseline stations (Valkaria, Fla. and Eleuthera) and seven rate vans (from Florida to Trinidad) usually called Mistram Rate Stations (MRS vans). For the GEOS-C study, the Mistram system is limited to the one baseline system at Valkaria (Mistram I) and three MRS vans (Grand Turk, Antigua and Trinidad).

The Valkaria (Mistram I) baseline station consists of a central site (with transmitting and receiving antennas) at the apex of a right triangle with two remote site receiving antennas located 10,000 and 100,000 feet, respectively, along each leg of this triangle. For the GEOS-C exercise only the 100,000 ft. baselines were used. The connections between the 100,000 ft. baselines and the central site are accomplished by microwave airlink. Figure 1 shows the Mistram I baseline geometry.

The MRS vans operate in a passive mode in conjunction with the active Mistram I station.

Thus, for this GEOS-C study the Mistram configuration consists of one transmitting station and three receiving stations at Valkaria along with one receiving station at each of the MRS van locations. At Mistram I, two X-band signals are transmitted to a transponder in the satellite. The transponder receives the signals, offsets them coherently in frequency and retransmits them to the receiving antennas. One of these signals is referred to as the "Continuous" signal which the active ground station compares to the transmitted reference signal in order to obtain phase-delay data from which the high quality ambiguous range information is obtained. The other transmitted signal which is called the "Calibrate" signal, in conjunction with the continuous channel, is

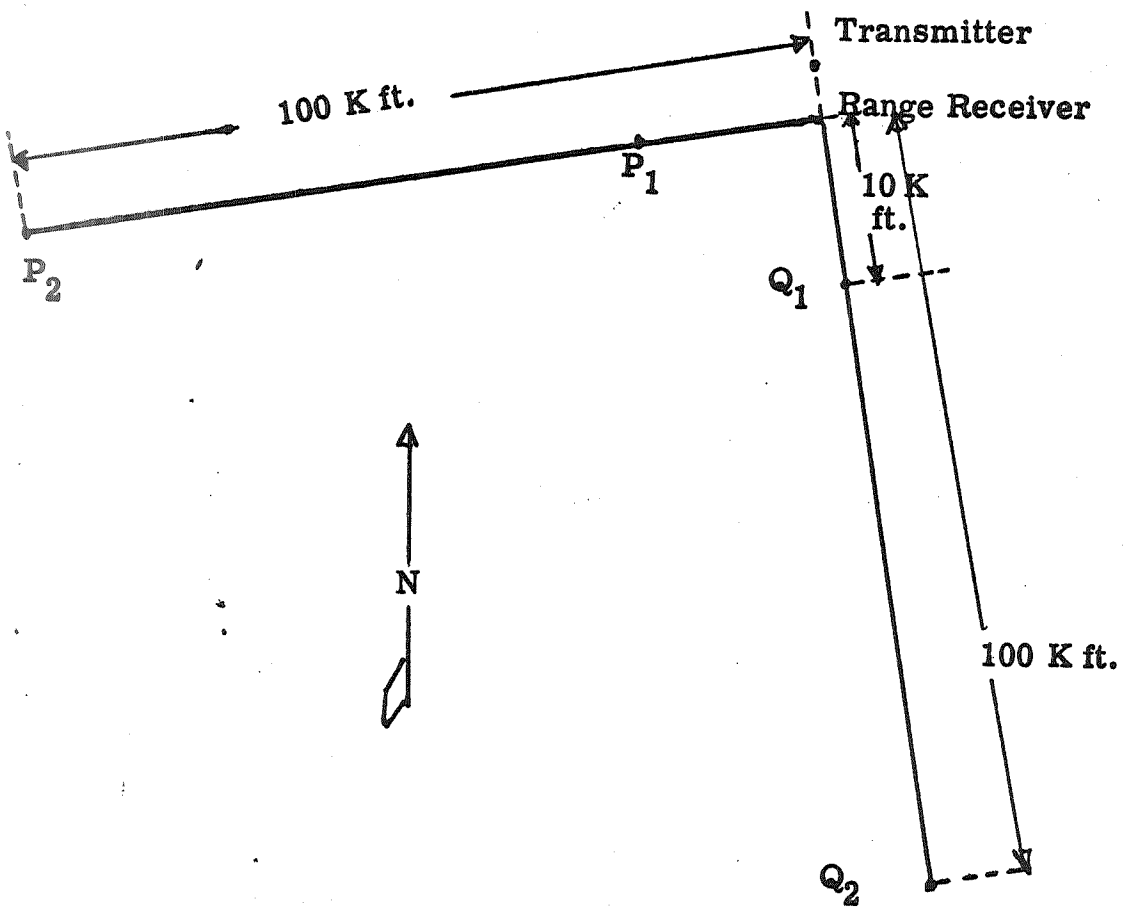

Figure 1. Mistram I Baseline Configuration (at Valkaria, Florida) .

used by the active station to periodically initialize the continuous data. By means of the calibrate channel an accurate Range Sum (RS) measurement is obtained at the central site, while accurate Range Difference (RD) measurements are obtained for the baseline sites. Since the passive MRS vans are not able to make a comparison of transmitted vs received phase (since the signal originates elsewhere) the measurements are subject to a rate bias error. The vans obtain an uninitialized range-sum measurement.

The Mistram I data is read out at 20 points/sec and can be transmitted to Cape Kennedy via microwave for real time computer processing (this is an invaluable procedure for obtaining range safety information for missile launches). The uninitialized or ambiguous MRS range-sum data is recorded on magnetic tape so that it can be combined with the Mistram I data in a Best Estimate of Trajectory Sense in order to obtain the correct initialization for each MRS van and the best estimate of trajectory (position and velocity).

Based on many years of Mistram operation with missiles, an accurate estimation of the random and systematic error sources is shown in Table 1. The error analysis for this report is based on the values shown in Table 1. Note that any improvements in the random or systematic uncertainties would, of course, imply better results than are shown in this study.

The purpose of this study is to determine how well the Mistram System (Mistram I and three MRS vans) can determine the radar altimeter bias from GEOS-C. It will be assumed that GEOS-C will be at a 20° inclination at approximately 600 nm. The accuracy of the Mistram System's capability to calibrate the radar altimeter is primarily a function of the error in the height coordinate of the orbit. The orbital accuracies are shown in the H, C, and L coordinate system where H is along the radius vector, C is the cross track coordinate and is perpendicular to the plane of the orbit and L is along the orbit (in track), see Figure 2. Our interests are in the H coordinate since it represents the height accuracy of the orbit.

TABLE 1

MISTRAM MEASUREMENT AND ERROR MODEL* UNCERTAINTIES

MISTRAM Meas. (m)	RANDOM ERROR POSITION s_{e_m} (ft)	RANDOM ERROR VELOCITY $s_{e_{\dot{m}}}$ (fps)	ZERO SET s_{a_1} (ft)	FREQ. BIAS s_{a_2} (fps)	TIMING s_{a_3} (μs)	SCALE FACTOR s_{a_4} (ppm)	REFRACTION s_{a_5}, a_6	SURVEY RELATIVE TO LAUNCH PAD s_x (meters)	s_y	s_z
MISTRAM I										
RS(A)	0.25	0.02	2.0	---	10	0.5	0.1	0.07	0.07	0.09
P_2	0.20	0.005	1.0	---	10	0.5	0.1	---	---	---
Q_2	0.20	0.005	1.0	---	10	0.5	0.1	---	---	---
MRS VANS										
GTK	0.25	0.02	10^6	.002	10	0.5	0.1	2.1	1.5	2.1
ANT	0.25	0.02	10^6	.002	10	0.5	0.1	3.7	2.7	3.4
TRIN	0.25	0.02	10^6	.002	10	0.5	0.1	6.1	6.7	4.6

* Mistram Error Model:

$$\Delta m = a_1 + a_2 t + a_3 \dot{m} + a_4 m + a_5 \csc E_1 \pm a_6 \csc E_2 + \text{survey} + e_m \ .$$

From: RCA Quarterly Accuracy Bulletin No. 33, 30 March 1970.
AFETR Geodetic Coordinates Manual, August 1969.

FIGURE 2: H, C, AND L COORDINATE SYSTEM

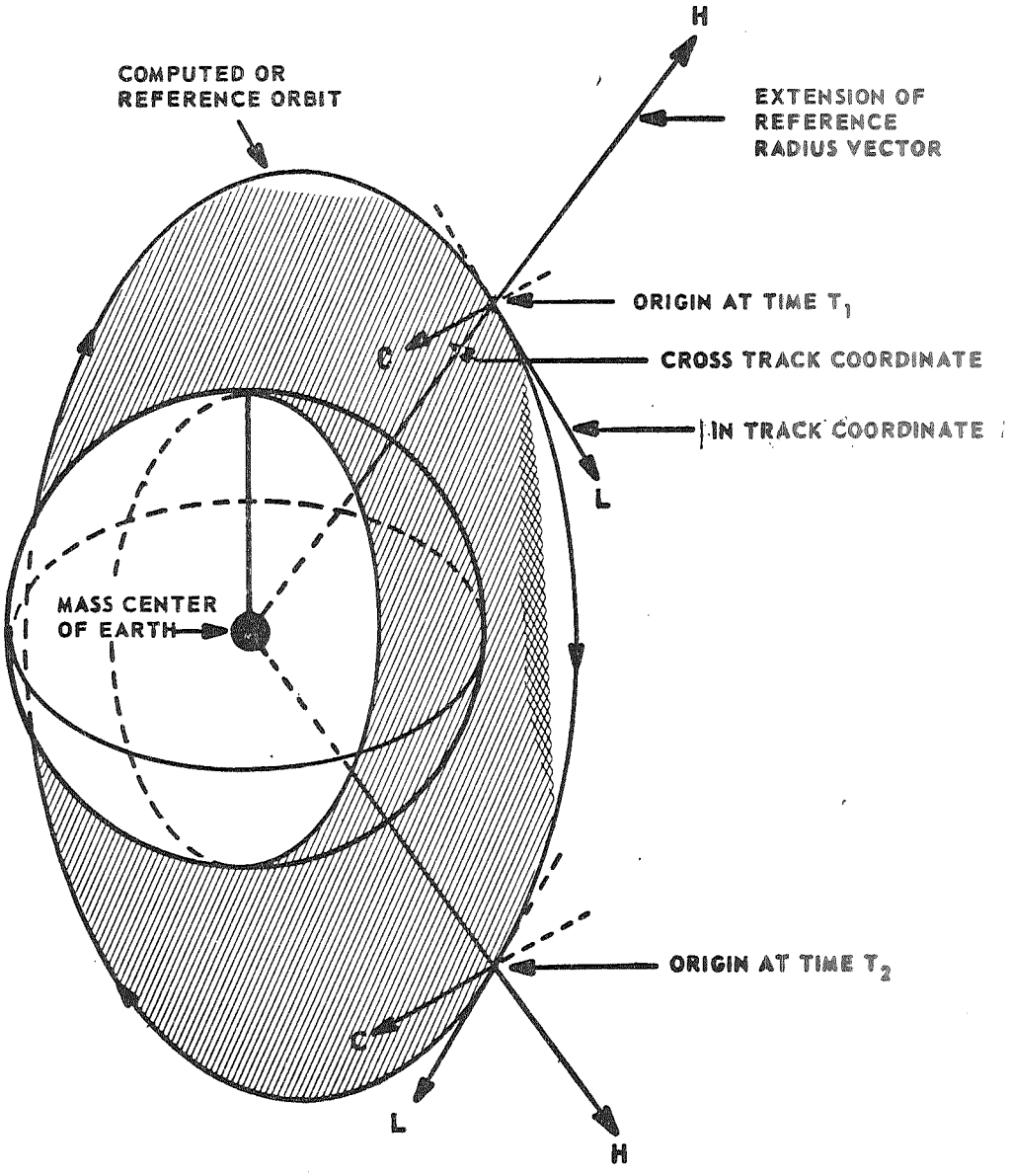

The orbital error analysis program used for this study is OREA [1] and is capable of computing the orbital error propagation with unmodeled effects.

II. EXPERIMENTAL STUDIES

All of the experimental studies were considered as short arc determinations with about 10 - 15 minutes of data. The only instrumentation used to determine the orbit is Mistram I (with 100,000 ft. baselines) and MRS vans at Grand Turk, Antigua and Trinidad. Unless otherwise indicated, the error propagations were accomplished with the uncertainties shown in Table 1. The following experimental situations were considered:

1. Mistram I with MRS sites at Grand Turk, Antigua and Trinidad.
2. Mistram I only.

One short arc was considered and the best height determinations are found between 70° and 80° West longitude. Note that Mistram I is about at 80° West longitude and 28° North latitude. The latitude of the orbit in this region ranged from 18.2° to 16.4° North latitude and covers about three minutes of data. For this particular portion of track the height uncertainty for Experimental Situation 1 is about 1.0 meter, while it is about 1.6 meters for Experimental Situation 2. That is, the three Mistram MRS vans essentially contribute to the solution in a way such that the height uncertainty can be reduced from 1.6 meters to 1.0 meter. Table 2 below shows the geodetic location of the Mistram MRS stations.

TABLE 2

Geodetic Locations Of Mistram Stations

	Latitude (North)	Longitude (West)	Height (meters)
Mistram I	27.96	-80.56	.7
Grand Turk	21.46	-71.13	28.5
Antigua	17.14	-61.79	49.4
Trinidad	10.74	-61.61	273.5

It would therefore be concluded that the Mistram system with MRS vans would offer the best height determination (1 meter) but that Mistram I alone may be perfectly satisfactory for the radar altimeter evaluation with determination of less than 2 meters for height determination.

REFERENCES

[1] Bush, N., Nicola, L., and Young, B. F., "OREA, Orbital Error Analysis Program," Pan Am Technical Memo No. 114, ETV-TM-70-61, Patrick AFB, Fla., January 1970.

GEOS-C RADAR ALTIMETER

John W. Bryan
Goddard Space Flight Center

ABSTRACT

A radar altimeter is planned for the GEOS-C geodetic satellite. The radar has not been designed. This paper presents a review of the ideas and requirements presented at the December 1969 Altimeter Conference as well as a sample design criteria for a radar to fulfill those requirements.

GEOS-C RADAR ALTIMETER

John W. Bryan
Goddard Space Flight Center

The radar altimeter is primarily concerned with transmitting to and receiving a backscatter return from the surface of the ocean. The character of the surface can vary widely, and the factors which affect it electromagnetic reflectivity are many. The most important factors are:

1. Surface roughness (sea state)
2. Transmitted wavelength
3. Incidence angle of the radiation with respect to the surface
4. Electromagnetic polarization
5. Wind velocity, i.e., wind direction and wind speed.

In principle these are usually summed up in a single term sigma zero (σ^0). Sigma zero is defined as the radar cross section per unit area of the reflecting surface. If it were possible to express the value of σ^0 in term of these parameters and obtain an accurate estimate of each of them, the most difficult part of the problem of sea definition by spaceborne radar would be solved.

The agreement between theory and some measurements appears to be good. The facet theory, as described by Katzin[1], appears to relate these parameters to the resulting σ^0. However Katzin did not establish all of the necessary formulation for converting σ^0 to each of the parameters. Using the radar of GEOS-C and visual observations of the radar illuminated area some of the necessary formulation will be derived.

The Oceanography Group at NRL are working under the direction of I. W. Fuller[4] ~~and~~ the value of σ^0 versus wave height. Mr. Fuller summed up their work on vertical incidence radiation both in the NRL pool under controlled conditions and at several of the "Texas Tower" type of sites. The curve of Figure 1 presents a summary of their findings on σ^0 versus wave height. Of particular interest was Mr. Fuller's statement that they plan to study reflectivity from various portions of the sea wave structure. This sort of information may be very useful when interpreting data from future more sophisticated satellite radars.

Professor Pierson[(2)] presented a theory at the December meeting which related return pulse shape to sea roughness. To verify this theory requires the leading edge of the return pulse be analyzed. In particular the onset of the typical ramp rise and the end of the rise. To supply data for this, the leading edge of the return will be sampled several times (perhaps 10) and this information transmitted to the ground. This particular study does not require an accurate orbit, but should be conducted in an area where the sea state, wind and wind direction are monitored. To gain meaningful data for oceanography, tests will be conducted in deep (greater than 16 fathoms) water. Since depths such as this do not occur close to shore, a ship will be required.

The topography of the sea surface is not only of interest to oceanography but also the Geodesy and Meteorology. It is of interest to Geodesy because the mean sea level surface reflects the structure of the earth's gravity field.

Since the oceans cover 70 percent of the earth's surface, an experimental determination of the mean sea level will provide a good measure of the over all geopotential. Satellites are the most stable platforms available for this type of measurement. At the proposed altitude of approximately 1000 km, satellite trajectories are quite smooth when compared to the features to be studied. With the present gravity models orbits are determinable to less than a meter.

The altimeter for this application would be a device to determine the vertical range from the satellite to mean sea level. This range is not known or determinable to a meter with present instrumentation and techniques. On board integration will be required to remove the ocean noise from the altitude determination.

The GEOS-C altimeter must establish both engineering feasibility and the scientific validity of the observations. To this end Dr. Weiffenbach[3] suggested that the altimeter experiment should be designed in two phases. The first is to make a series of measurements in a well observed area where sea state, weather, surface gravity, etc. can be determined. The second is to move out into the largest ocean area available and compare the altimeter observations with geopotential models determined through orbital dynamics.

Before the required characteristics of the radar can be defined the GEOS-C orbital parameters must be defined. The present desired parameters are shown in Chart I. The design is also constrained by the available spacecraft size, weight and power capabilities. The antenna is envisioned as approximately

60 centimeter diameter parabolic reflector. This results in a 4 degree beam width which is compatible with the spacecraft attitude stability. The antenna is to be placed on the bottom as earth facing side of the spacecraft. With this size antenna and an orbital height of 1000 km the system will be beam width limited. That is the trailing edge of the transmitted pulse reaches the reflecting surface before the leading edge crosses the beam edge. The physical constraints placed upon the altimeter design by the spacecraft are given in Chart II.

For a leading edge tracker and a one (1) meter resolution the pulse length should not exceed a few hundred nanoseconds. A design goal will be a 50 nanosecond pulse length with a 10 nanosecond resolution. A 50 nanosecond pulse in a pulse width limited system results in an interrogated area having a diameter of 7.8 km.

Using a 60 centimeter dish, a 3 centimeter wave length, a σ^0 of +6 dB, the 50 nanosecond pulse, a height of 1000 km and a 20 MHz bandwidth receiver, the required transmitter power is approximately 2 kw. This does not account for various losses in the system or transmission path anamolies. If a pulse compression (PC) system is considered the peak transmitter power may be reduced. This reduction in peak power may be estimated in that a pulse compression system trades peak power for pulse length on a one for one basis. However in designing a compression system care must be exercised in that the long transmitter pulse must not allow the interrogating area approach a beam width limited system. The pulse repetition frequency (prf) may have to be reduced

in a PC system to reduce the surface correlation effects. If these restraints are observed the resulting PC system should not affect the altitude determination and should actually increase the oceanographic capabilities.

The actual design of the altimeter has still not been accomplished. However a chart of minimum requirements is given in Chart III for a straight pulse system. When system losses and transmission path anamolies are considered the peak power should be increased by 10 dB. Using this radar and one second averaging to reduce ocean noise and thermal noise an acceptable resolution of one (1) meter should be achieved.

The averaging or integration times must be carefully selected. In the study of sea state a short averaging time is desirable, however for mean sea level measurements the averaging time must exceed the correlation time. For a static antenna the correlation time has been determined to be in the order of 10 milliseconds. The recommended times are: for sea state studies a 10 KHz prf and a 10 millisecond averaging time; for mean sea level studies a 1 KHz prf and a 500 millisecond averaging.

This coupled with the radar of Chart III should result in the desired scientific data.

REFERENCES

1. Katzin, M. "Backscattering from the Sea Surface" IRE Conv. Record 3, 1955.
2. Pierson, W. J. and Mehr, E. "The Effects of Winds and Swell on the Ranging Accuracy of a Radar Altimeter" Prepared for U. S. Naval Oceanographic Office contract N62306-70-A-0075 January 1970, presented at GSFC December 1969.
3. Weiffenbach, G. C. "The GEOS-C Radar Altimeter" presented at GSFC December 1969.
4. Fuller, I. W. and Myers, G. F. "NRL Nanosecond Radar σ^0 and Wave Height Measurements" presented at GSFC December 1969.

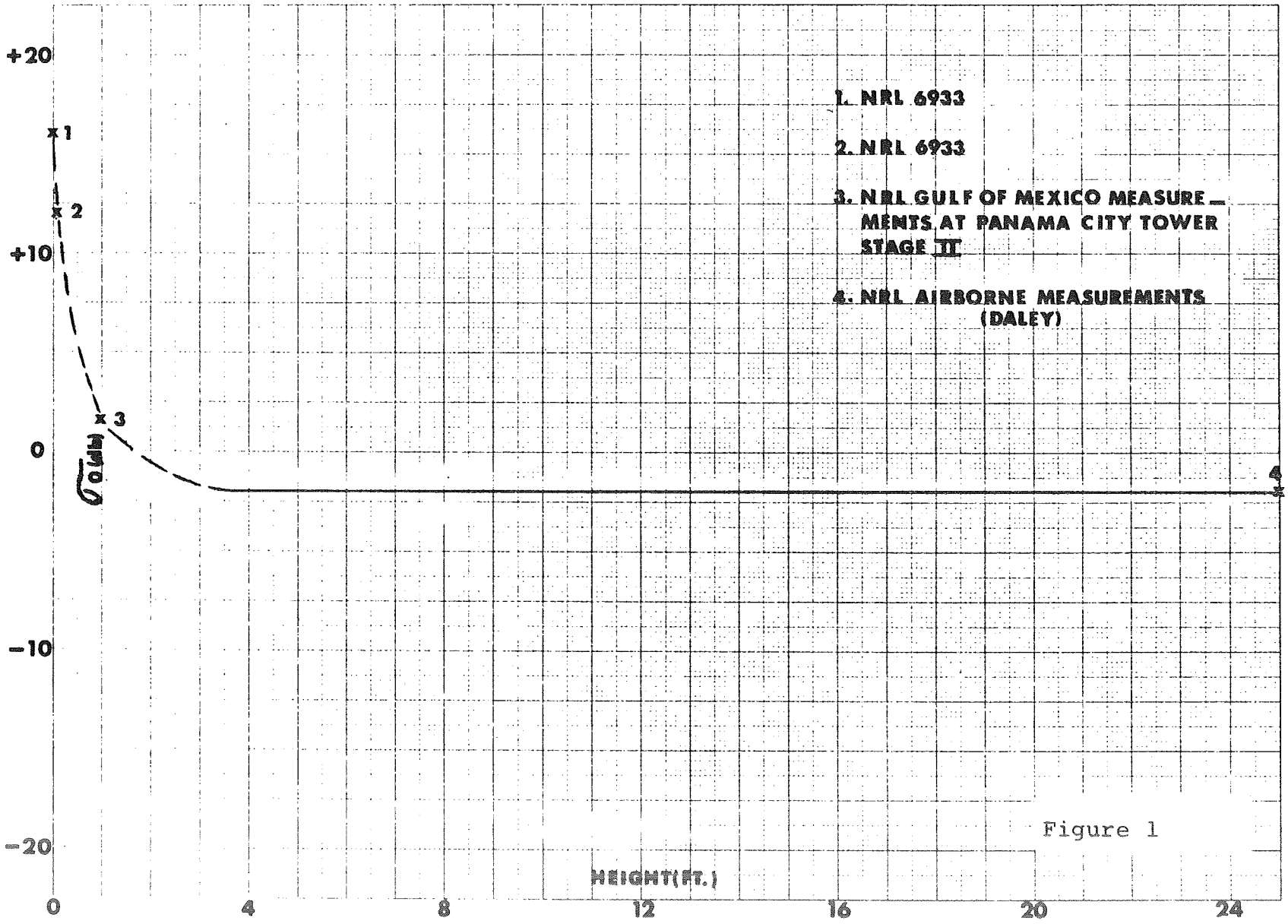
+20
+10
0
−10
−20
0
4
8
12
16
20
24
HEIGHT(FT.)
1
2
3
4
1. NRL 6933
2. NRL 6933
3. NRL GULF OF MEXICO MEASUREMENTS AT PANAMA CITY TOWER STAGE II
4. NRL AIRBORNE MEASUREMENTS (DALEY)

Figure 1

CHART I

Inclination	17^{o} - 22^{o}
Eccentricity	0.02
Perigee	700 - 900 km
Apogee	1000 - 1400 km

CHART II

INPUT POWER	50 WATTS MAX. SHORT PERIOD 10 WATTS CONTINUOUS
SIZE	1000 cm^3
WEIGHT	50 POUNDS MAX.
RESOLUTION (ALTIMETER)	1 METER
RESOLUTION (SYSTEM)	5 METERS

Chart 3

TRANSMITTER

Frequency	X-Band
Type	Pulse
Peak Pulse Power	1.0 KW Minimum
Pulse Length	50 MS
Pulse Repetition Rate	1.0 KHz

RECEIVER

Bandwidth	20 MHz
Noise Figure	8 dB
Detector	Square Law
Tracking	Split Gate

ANTENNA

Aperture	≈61 cm Diameter
Parabola or Array	
Beamwidth	≈4 Degrees
Gain	≈31 dB

NOTE: The above values are tentative and may be revised when the final specification is issued.